ADVANCING THE STERILE FILTRATION OF THERAPEUTIC VIRUSES

A MULTIFACETED APPROACH TOWARDS ADVANCING THE STERILE FILTRATION

OF THERAPEUTIC VIRUSES

By EVAN WRIGHT, B.Eng

A Thesis Submitted to the School of Graduate Studies in Partial Fulfilment of the Requirements

of the Degree Doctor of Philosophy

McMaster University DOCTOR OF PHILOSOPHY (2022) Hamilton, Ontario (Chemical Engineering)

TITLE: A multifaceted approach towards advancing the sterile filtration of therapeutic viruses

AUTHOR: Evan Wright, B. Eng. (University of Guelph)

SUPERVISOR: Dr. David R. Latulippe

NUMBER OF PAGES: xxiv, 197

Lay Abstract

While many people are aware that viruses can be used in medicine as vaccines, there are even more new and developing ways they can be used, such as in fighting cancer or treating previously uncurable diseases. However, testing of and patient access to these new treatments is often limited due to the challenges in producing and purifying enough of the virus. Viruses are highly complex and large relative to other products, and so many of the common methods and manufacturing processes which are standard in the industry need to be significantly adapted or improved to suit the production of viruses. This study investigates one step of the purification process, sterile filtration, and considers how a variety of factors from the materials used to the properties of the virus solution can be optimized to improve performance. With a deeper understanding of the sterile filtration process, recommendations can be made to help improve the production of future virus-based therapies.

Abstract

Therapeutic viruses are a class of biotherapeutic which have enabled new treatments and medical advances in the areas of vaccines, cancer treatment, gene therapy, and more. While many rapid advancements and novel products have been made in research labs and used in small scale trials, there are a multitude of technological and financial barriers to the large-scale manufacturing and commercialization of these products. Key among them are the complex unit operations involved in the purification of therapeutic viruses which often have low yields and high costs. Significant work has gone into optimizing unit operations including harvest and clarification, chromatography, and ultrafiltration, while the terminal sterile filtration step has largely been overlooked despite its crucial use in ensuring the final product is safe and free from any contaminating bioburden. Thus, this thesis seeks to address the gap and explore various aspects of process development and optimization in the sterile filtration of therapeutic viruses.

What constitutes a sterile filter is well defined by regulatory agencies such as the FDA and by accepted ASTM standards. However, few studies have characterized the fundamental mechanisms and membrane properties which govern how bacteria (specifically the standard validation organism, *Brevundimonas diminuta*) is retained during filtration. By comparing the bacteria retention of commercial membranes with various chemistries and pore size ratings the relative importance of adsorptive and size exclusion-based retention was explored. Applied pressure during filtration was also found to be a critical factor, theorized to be due to bacteria deformation resulting in passage through pore constrictions. Applying the insights gained to the sterile filtration of a therapeutic virus, it was demonstrated how effective sterile filtration could be

performed using a specific 0.45 µm rated membrane under low pressure filtration, resulting in improved virus recovery and throughput relative to the standard 0.22 µm rated membrane.

To better understand the factors which cause membrane fouling and loss of virus during sterile filtration, the effect of host cell impurities on filtration performance was investigated. Host cell DNA and protein were isolated using anion exchange chromatography and then spiked into a highly purified vesicular stomatitis virus preparation at controlled amounts in order to determine what effects the impurities would have alone and in combination. This revealed that small amounts of host cell protein are a major factor in both membrane fouling and reduced virus yield, and that there is a synergistic effect between the virus and the host cell protein adsorbing to the membrane surface.

Recognizing that the conventional phase-inversion polymeric membranes have many fundamental limitations such as high internal surface area and a broad pore size distribution which can contribute to poor performance, a novel ultrathin, isoporous, microfabricated silicon nitride membrane was tested for suitability as a sterile filter. Membranes with patterned circular and slit pores were characterized and compared using model solutions of polystyrene nanoparticles and bovine serum albumin. After validating that a membrane with 0.2 µm width slits was able to act as a sterile filter in accordance with ASTM standards, it was challenged with preparations of rhabdovirus Maraba and adenovirus. When compared against a conventional Durapore 0.22 µm membrane, the silicon nitride 0.2 µm slit membrane showed similar virus recovery and was unsuccessful in reducing the rate of fouling. While promising in some respects, further work is required to develop the technology and optimize it for biotherapeutic and virus filtration processes.

Throughout this work, a small supply of purified virus has imposed limitations on the number of experiments which could be performed, and this is a common issue encountered when performing small scale studies. In order to develop nanoparticle models more suited to represent the complexities of virus particles, a process was created through which nanoparticles could be fused together to create controlled amounts of particle doublets or larger aggregates, similar to how viruses can be prone to aggregation. Filtration performance of the fused particles was strongly dependent on the degree of aggregation, and fitting the filtration data to the standard fouling models revealed that the membrane fouling even resembled true virus solutions. This methodology could be readily applied by others to achieve simple, high throughput testing of sterile filtration membranes.

Acknowledgements

All of the research and writing in this thesis was only made possible by the amazing people surrounding me. I would like to extend my deepest thanks to my advisor Dr. David Latulippe for all the support, mentorship, and for the many opportunities to learn and grow. Many amazing collaborations, research opportunities and conferences would not have been possible without him. I would also like to acknowledge my supervisory committee members, Dr. Zeinab Hosseinidoust and Dr. Ravi Selvaganapathy for their valuable contributions and assistance. In addition, the entire Chemical Engineering department at McMaster University also deserves recognition, including the always helpful administrative and technical staff.

Financial support for this work was provided by the Natural Sciences and Engineering Research Council of Canada in the form of a Canada Graduate Scholarship and as a Discovery Grant, by the National Institute of Health as a Research Grant, by the "Alliance for Biotherapeutics Manufacturing Innovation," which is supported by the Ontario Research Fund, and finally by McMaster University in the form of a Dean's Excellence Award.

Many parts of this work involved a collaboration with the McMaster Immunology Department. I am grateful to Natasha Kazhdan, Maria Fe C. Media, Uma Sankar, and Fuan Wang for providing invaluable assistance with training, technical support, and design of experiments. Marcia Reid from the McMaster Electron Microscopy Facility and Liliana De Sousa from the McMaster Farncombe Metagenomics Facility also provided support and enabled crucial parts of this research. I would also like to recognize James Roussie, Dr James McGrath, and the entire team

at Simpore Inc. for their collaboration and the opportunity to help develop some of their amazing technologies.

The entire Latulippe research group has been a warm and welcoming home for me, with fruitful discussions, fun times, and cherished memories that will not be forgotten. The fellowship from everyone around me helped keep me motivated and moving forward. I am incredibly grateful to have worked closely with Reza Pazouki, Dr Shabnam Shoaebargh, and Dr Karina Kawka, who all provided invaluable assistance and contributed directly to many of my research projects. I am also fortunate enough to have worked with many amazing undergraduate students. Matthew, Eric, Christina, Alex, and Sarah all contributed more than I ever would have expected, and I wish you all the best in your future endeavors.

Last but not least, I would like to thank my parents Harold and Lori for their love, support, and encouragement throughout this long process and for all of my life. A special thank you to my significant other, Taryn MacDonald for always providing a happy smile, endless love, and for putting up with the many times where my focus was solely dedicated to viruses and membranes.

Table of Contents

List of Figures

List of Tables

List of Acronyms, Abbreviations and Symbols

Acronyms and Abbreviation

AAV	Adeno-associated virus
AEX	Anion Exchange Chromatography
ASTM	American Society for Testing and Materials
ATCC	American Type Culture Collection
BDL	Below Detection Limit
BSA	Bovine Serum Albumin
CA	Cellulose Acetate
CAR-T	Chimeric Antigen Receptor T cell
CFU	Colony Forming Unit
cGMP	Current Good Manufacturing Practices
DNA	Deoxyribonucleic Acid
DI	Deionized
DUV	Deep Ultraviolet
DLS	Dynamic Light Scattering
DMEM	Dulbecco's Modified Eagle Medium
EDTA	Ethylenediaminetetraacetic acid
EMA	European Medicines Agency
FBS	Fetal Bovine Serum
FDA	Food and Drug Administration
FIB	Focused Ion Beam

GFP	Green Fluorescent Protein
GMP	Good Manufacturing Practices
HA	Hemagglutinin
HCDNA	Host Cell Deoxyribonucleic Acid
HCP	Host Cell Protein
HEK	Human embryonic kidney
HEPES	N-2-hydroxyethylpiperazine-N-2-ethane sulfonic acid
HIC	Hydrophobic Interaction Chromatography
HPV	Human Papilloma Virus
ID	Inner Diameter
LC-MS	Liquid Chromatography–Mass Spectrometry
LFMC	Lateral Flow Membrane Chromatography
MMFC	Multi-channel Microfluidic Flow Control
MPN	Micro Porous Silicon Nitride
MOI	Multiplicity of Infection
MSN	Micro Slit Silicon Nitride
N/A	Not Applicable
PBS	Phosphate Buffered Saline
PCR	Polymerase Chain Reaction
PEG	Poly(ethylene glycol)
PES	Polyethersulfone
PFU	Plaque Forming Unit
PVDF	Polyvinylidene Fluoride

RNA	Ribonucleic acid
RPM	Revolutions Per Minute
SDS-PAGE	Sodium Dodecyl Sulfate–Polyacrylamide Gel Electrophoresis
SEC	Size Exclusion Chromatography
SEM	Scanning Electron Microscopy
SG	Sucrose Gradient
SLB	Saline Lactose Broth
SSE	Sum of Squared Error
TE	Tris Ethylenediaminetetraacetic acid
TMP	Transmembrane Pressure
TSB	Tryptic Soy Broth
UV	Ultraviolet
VSV	Vesicular Stomatitis Virus
WHO	World Health Organization

Symbol	Meaning	Units
J	Flux	m s^{-1}
P	Pressure	Pa
μ	Fluid viscosity	Pa s
R_m	Resistance of membrane	m^{-1}
R_f	Resistance of deposited fouling	m^{-1}
α	Specific resistance of cake deposit	m kg^{-1}
m_p	Mass of particles in the cake	kg
A_m	Membrane area	m^2
ε	Void fraction	-
ρ_p	Particle density	kg m^{-3}
d_p	Particle diameter	m
τ	Aggregation half time	s
r	Radius	m
W	Stability ratio	-
T	Temperature	°K
φ	Solids fraction	-
v	Volumetric Throughput	m^3
$Vmax$	Maximum volumetric throughput	m^3
Q	Volumetric flow rate	m^3 s^{-1}
t	Time	s
K_b	Complete blocking rate constant	s^{-1}
K_s	Standard blocking rate constant	m^{-1}
K_i	Intermediate blocking rate constant	m^{-1}
K_c	Cake blocking rate constant	s m^{-2}

Declaration of Academic Achievement

This Ph.D. thesis has been prepared as a sandwich thesis containing work previously published or in preparation for publishing, as listed below:

- Chapter 3 is adapted from the manuscript "An Experimental Study of Bacteria Transmission Through Microfiltration Membranes Reveals the Potential of Enhancing the Yield of Therapeutic Viruses in Downstream Processing" which is currently in preparation for journal submission. Experiments were primarily carried out by me, with assistance from A. Jucan and under the supervision of D.R. Latulippe.

- Chapter 4 is adapted from the paper "Evaluation of Host Cell Impurity Effects on the Performance of Sterile Filtration Processes for Therapeutic Viruses". *Membranes* 2022, 12(4): 359. https://doi.org/10.3390/membranes12040359. Experiments were primarily carried out by me, with assistance from K. Kawka in optimizing and performing chromatography methods and under the supervision of both M.F.C. Medina. and D.R. Latulippe

- Chapter 5 is partially adapted from the paper "Development of isoporous microslit silicon nitride membranes for sterile filtration applications". *Biotechnology and Bioengineering* 2020, 117(3): 879-885. https://doi.org/10.1002/bit.27240. Experiments involving bacteria or virus filtration were carried out by me, and some experiments involving membrane characterization and nanoparticle filtration were carried out by me with assistance from M. Csordas under the supervision of D.R. Latulippe. J.J. Miller, A.R. Gosselin and J.A. Carter were responsible for the fabrication of the silicon nitride membranes and partially carried out characterization experiments under the supervision of J.L. McGrath and J.A. Roussie.

- Chapter 6 is adapted from the manuscript "Fused Nanoparticles as Model Virus Aggregates for Membrane Filtration" which is currently in preparation for journal submission. Experiments were primarily carried out by me, with assistance from C. Hassey and under the supervision of D.R. Latulippe.

Chapter 1

Introduction

1. Introduction

1.1. Therapeutic Viruses

As early as the 15th century, there are records of physicians attempting to induce immunity to smallpox through the inhalation of dried crusts from smallpox lesions – what is now seen as the earliest attempt at immunization[1]. Long before germ theory, the discovery or viruses, and modern medicine, viruses (knowingly or not) were finding applications as therapeutic tools in medicine. Later, through a series of discoveries, the exact nature of viruses was elucidated. In the early 20th century, a "filterable agent" implicated in human and animal disease was discovered, plaques were identified growing on cell cultures, and with the electron microscope virus particles were directly visualized[2]. Growing alongside modern medicine, viruses have been used as therapeutic agents for vaccinations to a wide range of diseases, as a vector for gene therapy, and as oncolytic agents for the treatment of cancer, which all will be the focus of the work presented here. However many other novel and highly valuable applications of viruses in medicine and biotechnology exist, including phage therapy for treating bacterial infections[3], as a drug delivery agent[4] or imaging contrast agent[5], and as a scaffold for tissue engineering[6].

1.1.1. Vaccines

Vaccines are credited with saving an estimated 2-3 million lives each year and can be considered one of the most significant medical advances in improving human longevity[7]. As numerous advancements have been made in immunology and biotechnology, vaccinations have enabled the eradication of smallpox and have resulted in significant reduction in measles, pertussis, polio, and other diseases[7]. In 1974 the World Health Organization set the goal to reach every child in the world with vaccines for diphtheria, pertussis, tetanus, poliomyelitis, measles, and

tuberculosis by 1990. To date, this has not been reached, showing that worldwide access to vaccines and the mass production of cost effective vaccines is still an issue[7]. Furthermore, the development of novel approaches to vaccination and new diseases to be treated continues to push the development of technologies to produce vaccines.

While vaccines can provide protection against a wide range of pathogens including bacteria, fungi, parasites, and viruses, only the technologies and applications relevant to viruses will be discussed here.

The physiological mechanisms behind vaccination are well established, and involves the introduction of a foreign antigen to the body, which through various pathways activates the immune system and leads to an adaptive immune response specific to the introduced agent[1]. The two major components of the adaptive immune system are T-cells (cell mediated immunity) and B-cells (humoral and antibody mediated immunity). Through various cascading immune pathways, a response to the antigen produces short-term protection against the vaccine antigen through antibody production and $CD8^+$ effector cells, plus long term future protection against the vaccine antigen through B memory cells and $CD8^+$ memory cells[8]. Depending on the strength of the memory B-cell production, this may even enable life-long protection from any future infection[7].

Live, or live-attenuated viruses were the first forms of vaccines to be used, and continue to be used to this day in applications such as the varicella vaccine[9]. Introduction of live virus to the patient poses a risk of infection and illness, and so viruses must be weakened or attenuated first to

a point where they no longer pose a risk, but still trigger an immune response in the patient and produce the desired vaccination effect. One common method of producing attenuated vaccines involves passaging the virus through an abnormal host. This could be a living organism, such as the first polio vaccine being passaged in mice, or in-vitro cell culture such as rotavirus vaccine being passaged in Vero (African green monkey kidney) cells[10]. Replication inside of non-human host cells induces adaptation to that medium, resulting in loss of or modification of key genes responsible for infecting humans[9]. However, there is a risk that the adaptations and mutations can on very rare occasion make the virus into a more virulent form and cause a strong illness once administered[9]. In addition, it is possible for the adaptations to be lost if the virus is able to being replicating again inside human cells, for example an attenuated poliovirus vaccine replicating in the human intestine and re-developing virulence, leading to cases of paralysis after vaccination[11].

Through the use of chemicals, heat, or radiation, live viruses can be inactivated to the point of no longer causing illness but still being recognized by the immune system and generating an immune response[9]. For example, a typical protocol may involve incubating the virus with 0.01% formaldehyde[12]. While this method does provide increased assurance against unintended replication and infection, it has been shown that the long-term immunity from inactivated virus can be lower than that from attenuated virus. With a measles vaccine, a single does of attenuated virus produced a robust long term immunity while an inactivated virus required three doses and still produced shorter lasting protection against future infection[13].

Another option for non-infectious and non-replication competent vaccines is to only use subunits or isolated proteins of the target virus which are sufficient to stimulate the immune system

and create protection against future infection by the virus they were derived from. For example, the influenza virus can be broken apart using detergents and the viral hemagglutinin (HA) protein can be isolated to serve as the vaccine antigen[14]. The HA protein is a surface protein on the influenza virus which is critical for attachment to host cells, and so an immune response directed at the specific protein will still be effective against infection by the influenza virus.

Enabled by advances in biotechnology and the revolution of genetic engineering, virus proteins can also be produced and purified in a system entirely separate from any original or infectious virus. Through various genetic engineering techniques, the genes required to express viral proteins can be inserted into yeast, animal, or insect cell culture[10]. The synthesis of hepatitis B surface proteins in yeast lead to the production of the first recombinant vaccine[15] and the development of novel vaccines such of the human papilloma virus (HPV) vaccine was possible due to the production of the HPV L1 and L2 proteins in yeast[16].

Some of the most recent advances in vaccine technology are recombinant vaccine vectors. A well known base virus, such as an adenovirus, vaccinia virus, or rhabdovirus, can be genetically modified such that it expresses the proteins of the vaccine target[7]. The ideal final product will maintain the low infectivity and ability to replicate of the base virus but will lead to an immune response against the vaccine target. The first vaccine based on this live virus vector technology was only just approved by the FDA in 2019[17], and consists of a recombinant vesicular stomatitis virus (VSV) which expresses the surface glycoprotein of the Ebola virus and results in strong immunity against the native Ebola virus[18]. VSV is a promising platform for a wide range of vaccine

vector products, with ongoing research and clinical trials for HIV[19], Zika virus[20], SARS-CoV-2[21], Influenza[22], and more.

1.1.2. Gene Therapy

A wide range of diseases result from underlying genetic defects in the patient, such as hemophilia, macular degeneration, and sickle cell disease[23]. Thus, a long sought-after goal in medicine has been a mechanism through which missing or defective genes in the patient could be replaced. While liposomes, polymers, and peptides can be used to deliver genetic material to the patient's cells, taking advantage of the natural ability of viruses to deliver their genetic material into host cells is the most common approach to gene therapy[24].

The virus vector will be defined by three criteria: the protein capsid or envelope, the genetic package of interest to be expressed in the target cells, and the regulatory genes of the virus that control genetic expression[23]. An ideal virus vector must be able to transport large therapeutic genes, have a high transduction efficiency, should not be immunogenic, pathogenic, or cause inflammation, and be able to target specific cells[24]. Meeting all these criteria is the challenge faced by virus vector gene therapy products.

Gene therapy can be applied *in vivo*, where the virus vector is administered directly to the patient to replace missing genes, or *ex vivo*, where cells from the patient are isolated, transfected, and then returned to the body. Hepatocytes from the liver, stem cells and from bone marrow, T cell lymphocytes from blood, and retinal photoreceptors from the eye have all been the focus of this method[25]. Chimeric antigen receptor T cell (CAR-T) therapy is an *ex vivo* gene therapy which

has received considerable attention for the ability to treat various forms of cancer. T cells are isolated from the patient and reprogrammed with the transgene allowing the immune cells to identify cellular markers for cancer, and after administration help build and immune response against and directly kill cancer cells[26].

To date, only a handful of gene therapy virus vectors have been approved by the FDA or EMA. Glybera, an adeno-associated virus based vector for the treatment of lipoprotein lipase deficiency marked the first gene therapy product approved by the EMA in 2012, followed by Luxturna, an adeno-associated virus vector for the treatment of retinal dystrophy approved by the FDA in 2017. Also in 2017, the first CAR-T cell therapy, Kymriah, used for the treatment of acute lymphoblastic lymphoma and non-Hodgkin lymphoma was approved[23]. Currently, adenovirus, adeno-associated virus, and lentivirus have been the focus of the large majority of research due to their well understood nature and suitability to gene therapy, making up over 90% of all viruses used in clinical trials[24].

1.1.3. Oncolytic Viruses

The ability of a coincidental virus infection to result in the regression of cancer was first observed as early as the 19th century. Case notes would describe a patient with advanced leukemia which would go into remission after an influenza infection, or a child with leukemia which regressed after a chickenpox infection[2]. Even though the entire concept of viruses as we understand them today was not established, doctors had noticed a connection between natural infectious disease and the regression of cancer. In more modern medical settings, regression of leukemia[27] and lymphoma[28] has been associated with a natural measles infection.

It is now understood than cancerous cells are fundamentally more vulnerable to infection due to defects in signalling pathways used to detect and eliminate viral infection, changes in the cell response to stress, and abnormalities in homeostasis mechanisms[29]. Protein kinase R is a critical factor which combats intracellular viral infections, and may be absent in cancer cells. Similarly, toll like receptors, a surface and intracellular cell element which stimulates interferon release and immune response, may be absent or downregulated in cancer cells[30]. Furthermore, cell surface receptors which facilitate viral entry into the cell may be upregulated in cancer cells, leading to viruses having a higher selectivity for cancer cells over healthy cells. For example, various melanoma and carcinomas overexpress the CD46 surface receptor, which the measles virus uses for cell entry[31]. This vulnerability will lead to viral infection and replication, and potentially lysis of the cancer cells through the stimulation of apoptosis, necrosis or autophagy pathways. Upon lysis of the cell, the release of tumor associated antigens will then aid the immune system in recognizing and targeting the cancer via the release of cytokines, danger associated molecular patterns, and the activation of T cells[29]. These two main mechanisms, replication within and subsequent lysis of tumor cells and enhancement of systemic immune response are the methods through which antitumor activity is mediated by oncolytic viruses. The relative contribution of the two mechanisms will vary depending on the nature of the virus[29]. Oncolytic virus may also incorporate some aspects of gene therapy, through the insertion of genes which produce immune stimulating or anti-cancer factors. In many cases, oncolytic viruses are used in tandem with traditional cancer treatments, including radiation, chemotherapy, and immunotherapy where they show a synergistic effect and greatly improve patient outcomes[29]

Imlygic (T-VEC), a herpes simplex virus for the treatment of melanoma, was the first oncolytic virus to be approved by the FDA in 2015. A specific strain of herpes virus, HSV-JS1, was selected for a strong innate oncolytic activity. To increase safety, the virus was attenuated through the deletion of genes encoding specific virulence factors, keeping the ability to replicate in malignant cells but not in normal cells. In addition, genes encoding a macrophage stimulating factor were added to the virus, allowing the virus to promote an innate anti-tumor immune response[32]. Rigvir, an unmodified echovirus (picornavirus) was approved for use as a treatment for melanoma in Latvia, Georgia, and Armenia, while Oncorine, an attenuated adenovirus was approved in China for the treatment of head and neck cancer[33]. To date no other oncolytic viruses have been approved by the FDA, however as of 2021 over 70 clinical trials are ongoing[34]. Adenovirus and herpes simplex viruses make up the majority of viruses used in these clinical trials, with reovirus, Vaccinia virus, Newcastle disease virus, and others also used[34].

1.2. Manufacturing of Therapeutic Viruses

To supply these viral therapeutic products, the ability to generate large amounts of virus is required. Production is generally divided into two main streams, an upstream side where host cells are expanded and infected to replicate the virus, and a downstream side where the virus is purified. On the upstream side, all therapeutic viruses are by nature produced in a biological culture system ranging from simpler systems such as fertilized chicken eggs for the production of influenza vaccines[12] to highly complex bioreactors. While animal cell lines (specifically mammalian cells) are often the host for a majority of therapeutic viruses, some other cell lines may used in specific scenarios, such as insect cells with a baculovirus helper system for the production of adeno-associated viruses[35], or bacteria for the production of bacteriophage[36]. Mammalian cells require

highly specific growth conditions, and culture supplements such as serum proteins[37] and viral transfection enhancers[38] are often added. While significant research continues to be done in optimizing the conditions for cell growth, virus replication, and bioreactor design[39–41], the upstream side of virus manufacturing will not be the focus of this work.

Following upstream processing, a series of downstream unit operations are implemented in order to purify the virus product. While the exact unit operations are variable, the process will generally involve a clarification step to remove bulk debris and turbidity, a purification step to eliminate the majority of impurities, a polishing step to eliminate any final small amount of impurities and formulate the product, and a sterile filtration step before the product is vialed. The design of these operations is motivated by the goals of creating a product which is safe, potent, and stable.

An overview of four different downstream purification processes used in the production of Lentivirus is shown in Figure 1.1. While each process contains a majority of the same core steps, the exact implementation and order is highly variable, demonstrating the complexity of downstream processing. Process A involves the use of high speed centrifugation, which is able to produce a highly pure end product[42], however it is not a scalable technology for the production of very large batches[43]. Process A is also unique in that it does not involve a terminal sterile filtration unit operation, instead operating the entire process aseptically and testing each batch for sterility before use[42]. Process B uses the same main unit operation as C and D, however the Benzonase® treatment is moved to an intermediate step after chromatography and concentration. While no specific justification for this was given[44], the reduced residual DNA concentration and overall

volume at this point in the process would allow for significantly less of the Benzonase® enzyme to be used, saving significant costs[43]. Process C is unique in using a size exclusion chromatography process for formulating the final product, implemented to provide extra clearance of contaminating DNA and increase product purity[45]. Finally process D reorganized the final steps, with sterile filtration occurring right before concentration and diafiltration, as the authors found this improved the overall recovery of virus[46]. The design of any downstream purification process will require significant optimizing and a strong knowledge of all the different unit operations which are available.
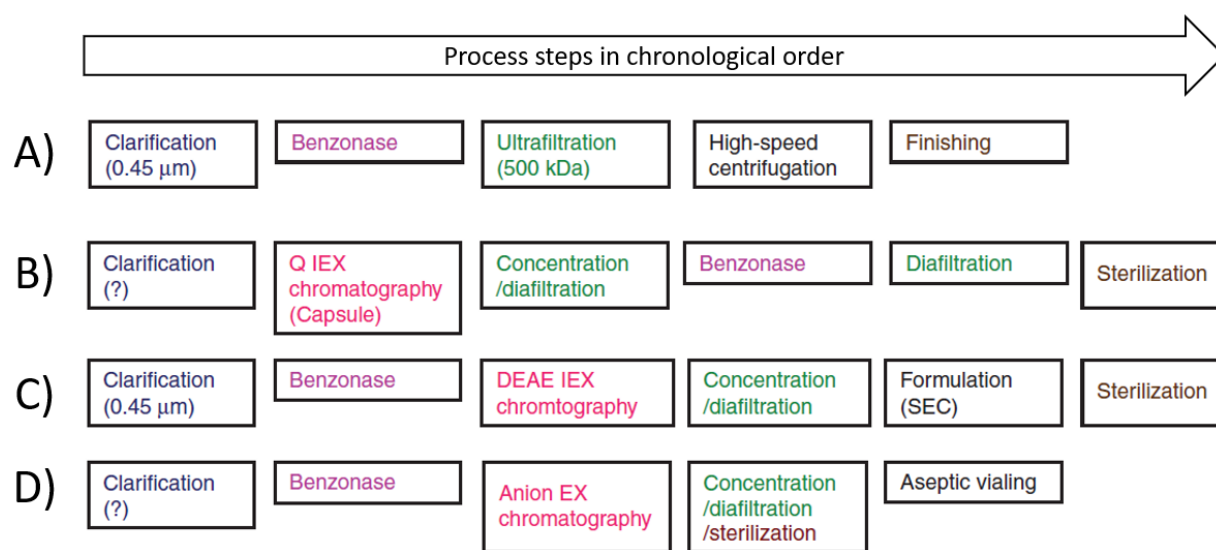
Figure 1.1: Main downstream processing steps involved in the large-scale production of Lentivirus for clinical purposes. Reprinted and adapted from Merten *et al.*[47] under Creative Commons license.

1.2.1. Physicochemical Properties of Therapeutic Viruses

Any purification unit operation will exploit a difference in one or more physicochemical properties between the virus and the impurities in solution to achieve separation. Within the

incredibly diverse nature of viruses, a wide range of properties can be found (Table 1.1) which will

influence how the virus particles are produced and purified.

Table 1.1: Overview of some physicochemical properties for select therapeutic viruses

Virus	Morphology	Size (nm)	Envelope	Isoelectric Point
Adenovirus	Icosahedral	70-90[48]	No	4.5
Adeno-associated virus	Icosahedral	20-25	No	5.9
Baculovirus	Rod	D: 30-60 L: 250-300	Yes	5.4
Echovirus	Icosahedral	30	No	5.6[49]
Hepatitis A virus	Icosahedral	30	No	2.8
Herpes simplex virus	Spherical	180-200	Yes	4.9[50]
Influenza virus	Spherical	80-120	Yes	5.3
Lentivirus	Spherical	80-130	Yes	N/D
Measles virus	Pleomorphic	100-300[51]	Yes	6.8[51]
Newcastle disease virus	Spherical	100-500[52]	Yes	5.7[52]
Rabies virus	Bullet	D:75-80 L: 100-300	Yes	7.0
Vesicular stomatitis virus	Bullet	D: 70 L: 200[53]	Yes	4.0[54]
Reovirus	Icosahedral	85[55]	No	3.8[49]
Vaccinia virus	Brick	D: 250 L: 350	Yes	5.0

Data from Wolff *et al.*[56] unless otherwise noted
D: diameter, L: length, N/D: data not found

The size of therapeutic virus particles can vary from as small as 20 nm for adeno-associated

virus, to as large as 250 by 350 nm for vaccinia virus[56]. Some viruses may have a tight size

distribution, with adenovirus particles ranging from 70 to 90 nm in diameter[48], while others can

have a large variability in size, with Newcastle disease virus particle being anywhere from 100 too

500 nm in diameter, even having some filamentous forms smaller than 100 nm[52]. Within a

complete process for the production of biopharmaceuticals, it is common for there to be anywhere

from 10 to 20 membrane based separation steps[57], the majority of which are sized based separation. Unit operations such as clarification, ultrafiltration, diafiltration, and sterile filtration all rely on membranes with a given pore size or size cut-off, therefore optimization of these unit operation will be highly dependent on the virus in question. As discussed further in subsequent sections, some operations such as sterile filtration with 0.22 µm rated membranes are simply not feasible with larger viruses, such as vaccinia virus and measles virus[51].

The isoelectric point of the virus represents the solution pH at which the virus particle will have neutral charge; below the isoelectric point the virus will be negatively charged and above it the virus will be positively charged. In addition to charge contributions from the virus surface (envelope or capsid), the charge of internal components including genetic material and proteins will influence the overall isoelectric point[49]. Isoelectric point is a key consideration for separation processes based on relative charge, namely ion exchange chromatography[43]. Long term stability of the virus and the potential for aggregation will also be influenced by isoelectric point and surface charge. Aggregates are more likely to form when the virus is at a pH near the isoelectric point[58], and so proper formulation of buffer solutions used during downstream processing is required to prevent aggregation.

The presence of a viral envelope adds significant complexity to the virus. The envelope consists of a lipid bilayer derived from the host cell with additional viral proteins and glycoproteins incorporated into the structure, and can be prone to variations from cholesterol levels, temperature, culture medium, and other factors[59]. As the outer layer of the virus, the envelope will influence characteristics such as surface charge and hydrophobicity[43], and will determine surface interactions

and binding (intended or unintended) during purification unit operations. The envelope of the virus is also sensitive to damage from shear forces, foaming, and pressure changes[47,59,60], therefore more gentle processing is often required for enveloped viruses during unit operations such as ultrafiltration, which is known to generate high shear forces.

1.2.2. Safety and Regulatory Considerations

The end result of the upstream processing stage and virus culture process is a complex mixture of the target virus, whole cells and cell debris, additives, media components, helper viruses, and more. This introduces a wide range of complications and safety considerations that may not be present in traditional synthetic pharmaceutical products. As with any pharmaceutical entity, therapeutic viruses require approval by regulatory agencies such as the United States Food and Drug Administration (FDA) and the European Medicines Agency (EMA) to ensure that they are both safe and effective. Varying with the exact nature of the product, a wide range of specifications for a final product must be met, with some potential criteria detailed in Table 1.2.

Table 1.2: Sample of quality and safety specifications for therapeutic virus products[61–63]

Attribute	Specification
Process related impurities	Host cell protein
	Host cell DNA
	Helper viruses or plasmids
	Media components (e.g. fetal bovine serum)
	Enzymes (e.g. endonuclease)
	Leachables and extractables
Product related impurities	Aggregates
	Inactive, degraded or improperly assembled variants
Biological contamination	Bacterial sterility
	Mycoplasma
	Adventitious viruses
	Endotoxins
Product quantity	Mass

	Potency/ infectivity/ transducing units (cell or animal based tests)
	Particle count
Product identity	Verified with appropriate assay (e.g. PCR, SDS-PAGE)
General characteristics	Color
	Turbidity/ Clarity
	pH
	Osmolarity

Impurities derived from the host cells (host cell protein and DNA) are often of greatest concern and can have the most stringent safety requirements. Limits for host cell DNA are set based on a theoretical risk calculation of the oncogenicity of DNA impurities. Continuous host cell lines can be derived from mammalian tumor cells and so the presence of oncogenic genes which could be administered to patients are of utmost concern, with over 200 currently known oncogenes identified in various host cell species[64,65]. Based on probabilistic models and risk calculations, it has been shown that a safety factor of 1.2×10^{10} results from 1 ng host cell DNA that has been enzymatically degraded to a median 450 base pairs[65]. From this and other calculations performed by agencies such as the World Health Organization, the current regulations specify that host cell DNA should be limited to sequences shorter than 200 base pairs and the total host cell DNA content should be less that 10 ng/dose[66]. This can represent a level of purity where the selectivity for the viral DNA relative to impurity DNA must be on the order of magnitude of 10^5 or greater[67], presenting a significant challenge in downstream purification.

Host cell protein impurity limits are not always so strictly defined, and are instead evaluated on a case-by-case basis given risks associated with immunogenicity, inflammation, enzymatic activity, or anaphylactic shock[66]. The use of *in vivo* animal testing or *in vitro* immunoassay tests can be used to assess the safety of protein impurities and general immunotoxicity effects[68]. For monoclonal antibody therapeutics, a much more mature area of

biotherapeutics, the limit of host cell protein is typically considered to be 100ng/mg product[68], a very rigorous requirement which approaches the limit of detection of many technologies used for protein quantification. With typical monoclonal antibody doses ranging from 0.1 to 10 mg[69], this is equivalent to a per dose limit of 10 to 1000 ng of host cell protein. For therapeutic virus products, no strict limits have been set and the protein impurity content will vary from product to product and the case-by-case approach is taken. For example, two different adenovirus-based SARS-CoV-2 vaccines, ChAdOx1 nCoV-19 (AstraZeneca) and Ad26.COV2.S (Johnson & Johnson) were found to have host cell protein content of at least 19.1 and 0.04 µg per dose respectively[70], highlighting how there is a wide range of acceptable host cell protein content in therapeutic viruses preparations. From other published GMP production processes typical host cell protein content can be seen, with 7.9 µg/dose[71] host cell protein in an oncolytic adenovirus and 0.42 µg/dose[72] host cell protein in a recombinant HPV vaccine.

Product related impurities such as aggerates, empty or partially empty virus capsids, and misassembled virus particles must also be considered. While not inherently problematic, these inactive forms of the virus lack infectivity or an ability to deliver genetic material properly, and so in applications such as gene therapy they provide no effective benefit. An excess of inactive forms can render the product more immunogenic, increasing the chances of side effects in the patient or antiviral immune response[66,73]. In large doses, inactive forms of the virus may even compete for binding sites on the host cells, lowering the overall transduction efficiency[67]. In some cases, empty forms of the virus can make up as much as 98% of the total particle count[74], and so they must be removed or have their content reduced. While no strict limits have been set, as a guideline the total particle to infectious particle ratio should not exceed 30 in the final product[71].

Contamination of final products by any biological organisms (fungi, bacteria, viruses) can have deleterious effects on patients, given that therapeutic virus products are most often administered through injection directly into tissue and that patients may already be in a weakened state and unable to fight off infection. Thus, great care must be taken to ensure products are not contaminated. In the broader pharmaceutical industry, sterilization using heat or irradiation are common[75], however this is not applicable to therapeutic virus products (excluding some subunit vaccines) due to their sensitivity and need to remain biologically active. Thus, sterility must be ensured using other methods validated to remove contaminating organisms. For removal of bacteria and larger organisms, sterility is typically ensured by passing the product through a microfiltration membrane validated to fully retain a challenge test of 10^7 *Brevundimonas diminuta* bacteria per cm^2 of membrane area[75,76]. When sterile filtration is not feasible, the alternative is complete aseptic processing, which is achieved by having the entire production take place in a closed, Grade A cleanroom environment, along with directly testing each final batch of product for sterility[47,75].

Not all contaminating organisms can simply be removed through sterile filtration. Mycoplasma, which are known to pass through most filtration membranes[77] are a common source of contamination is pharmaceutical preparations[78]. Thus, mycoplasma must be specifically tested for in the final product through culture assays in broth or agar, or PCR based methods[42,79]. Contaminating viruses are a particular challenge, as membrane filtration with a small enough pore size membrane to retain viruses (known as virus filtration[57]) would also retain the therapeutic virus product. Thus, other methods such as chromatography can be validated for viral clearance[80].

Testing the final product for contaminating viruses using PCR is also common[62,79]. Throughout the entire production process, validation of environmental controls, use of high level cleanrooms, appropriate sterilization of containers and equipment, and automated processing in sterile environments should be implemented to reduce risk of contamination[81].

1.2.3. Downstream Processing and Purification

Highly intensive downstream processing is required to achieve product purity standards, and it is recognized as a major bottleneck in the production of therapeutic viruses[43,51,59]. The challenge is how to achieve the aforementioned safety and purity criteria with cost effective and industrially scalable methods that provide a high recovery of the virus product. To date, overall recovery during downstream processing can be as low as 20-30%[42,60], and so new technologies and processes to improve recovery are highly desirable.

1.2.3.1. Harvest and Clarification

The first step in downstream processing will be heavily influenced by the nature of the bioreactor bulk. Many viruses are intra-cellular and must first be released through a lysis step. Addition of a strong detergent is the commonly accepted method, as it is simple, scalable, and cost effective, however downstream removal of the detergent from the end product must be confirmed. Furthermore, it has been shown that detergents such as Triton™ X-100 can stabilize virus particles, preventing further degradation or aggregations during subsequent downstream processing[82]. However, many detergents (including Triton™ X-100) are already or soon to be restricted by regulatory agencies due to environmental effects and potential for endocrine disruption, and so alternate detergents such as polysorbate-20 (Tween-20) have been investigated[71]. The use of shear

force in hollow fiber tangential flow filtration as a method to disrupt cells has been studied[83], however the implementation can be difficult as damage to the virus particles from shear force must also be prevented. Regardless of the method used, cell lysis introduces a large amount of host cell impurities into the bioreactor bulk, rendering further downstream processing more complex. For enveloped viruses, such as rhabdovirus, lentivirus and influenza which are secreted by the host cell, no further processing is required, and gentle processing is ideal so that the majority of the cells remain intact and release less debris into solution.

At this stage, a suitable clarification step will remove the majority of cell debris and large aggregates while preparing the solution for further purification. Clarification using microfiltration, either in a dead-end or tangential flow setup, is commonly implemented using membranes with a 0.22 to 1 µm pore size. In an adenovirus purification process, an 0.8 µm pore size tangential flow filtration operation has been shown to recover 98% of virus particles while significantly reducing turbidity[82]. In a lentivirus purification process, a dead end filtration process using a 0.45 µm membrane was able to recover close to 100% of virus particles while removing upwards of 25% DNA and 65% protein[60]. Depth filtration (designed to trap contaminants within its structure as opposed to on a surface layer) is an alternative for highly turbid solutions which contain large amounts of debris, and has been successfully implemented to increase recovery by three fold relative to conventional membranes in an adenovirus purification process[84]. The use of filter aids such as diatomaceous earth can also be considered to further improve filtration performance in some cases[85].

Host cell DNA is a particular concern at this stage as it can increase the viscosity of the bioreactor bulk, rendering further processing more difficult[43]. In addition, to meet regulatory requirements the size of the DNA chains must be reduced. Therefore, the majority of downstream purification processes perform a treatment step with endonuclease enzyme to degrade DNA. This can be performed directly in the bioreactor bulk before clarification, or in a standalone reactor after clarification[86]. The enzyme must then be removed in subsequent downstream purification as it is considered a process related impurity. As an alternative, DNA can be selectively precipitated using cationic detergents and polymers. Coupled with clarification, this can remove up to 99% of DNA[87], however this does not address the regulatory requirement of DNA chain length.

1.2.3.2. Chromatography

Chromatography is widely used in downstream processing and is one of the scalable unit operations which can separate virus particles from process and product impurities to the strict limits required by regulatory agencies. Chromatographic separation is driven by viruses and impurities carried in a liquid phase having different physicochemical interactions with a stationary or solid phase. Operated in a "bind and elute" mode, most of the impurities will pass through the stationary phase without interacting, while the virus and some impurities will bind to the stationary phase. Through a step or gradient change in a property of the liquid phase (ionic strength, pH, chaotropic salts, solvents) the virus and remaining impurities can be selectively eluted from the stationary phase[43]. The stationary phase can take on various structures or arrangements: packed beds, monoliths, and membrane adsorbers are all commonly used[43]. Packed beds of porous particles are the most traditional chromatography media, however it suffers from significant disadvantages for the purification of viruses. Porous particles fundamentally depend on diffusion

as the dominant transport mechanism, and given the large size of many virus particles, they are unable to effectively diffuse into the pores[88]. For the smallest virus particles, such as adeno-associated virus and parvovirus, effective purification with resin media is possible[89,90] as they are small enough to effectively diffuse into and interact with the resin pores. Monolith and membrane adsorbers instead consist of a single block or membrane of solid matrix with a highly interconnected macroporous structure, with a pore size ranging from 0.2 to 6 µm, through which the virus particles are transported by convective flux[88]. Monoliths and membranes can present challenges, being prone to clogging and possessing an overall lower binding capacity than traditional resins[43], however they have still emerged as a promising technology for the chromatographic purification of virus particles[86].

Beyond the three main substrate structures, chromatography media uses a variety of surface chemistries and ligands to selectively bind and elute the virus particles. Common chromatographic modes include ion exchange, affinity, hydrophobic interaction, and size exclusion, which respectively take advantage of differences in isoelectric point, binding to functional groups, hydrophobicity, and particle size to achieve seapration[43]. Applying chromatography to purify virus particles and remove impurities, high degrees of separation can be achieved. For example, in the purification of adeno-associated virus using hydrophobic interaction membrane chromatography (phenyl ligand), a virus recovery of greater than 90% is achieved, while eliminating more than 80% of DNA and 90% of protein impurities[91]. Each chromatography mode separates the virus from impurities based on a given physicochemical property, and so by including multiple stages of chromatographic separation using different modes (orthogonal separation), even higher degrees of purity can be obtained. Using anion exchange chromatography resin (quaternary amine)

followed by size exclusion chromatography in the purification of adenovirus, an overall recovery of 61% was achieved with 99.9% and 97% of host cell protein and DNA being eliminated[71]. Chromatography is also one of the few methods which is able to separate genome containing and empty (infectious and non-infectious) virus particles, due to slight differences in isoelectric point caused by the presence of DNA[66,67].

1.2.3.3. Ultrafiltration

Ultrafiltration can be used to achieve multiple objectives in downstream purification with the ability to remove impurities, concentrate the virus, and perform buffer exchange. Ultrafiltration is a pressure driven filtration processes which uses membranes with defined molecular weight cut-offs, typically ranging from 1 to 1000 kDa[92]. Ultrafiltration membranes are designed to reject the product of interest (virus particles) while allowing water and impurities to cross to the permeate side of the membrane. When operated in a tangential flow configuration with recirculation, the retained volume and level of impurities is reduced with each pass by the membrane, allowing for high levels of purification and concentration to be reached. Simultaneously, the medium the virus is suspended in can be exchanged by adding a new medium to replace volume lost to the permeate, in a process known as diafiltration[43,92].

Careful selection of the membrane molecular weight cut-off must be taken such that the virus particle is fully retained and the impurities are able to fully transmit with minimal buildup (fouling) on the membrane surface. Due to this, larger viruses such as lentivirus are highly amenable to purification through ultrafiltration, with recoveries as high as 100% and clearance of protein and DNA over 90% achieved with a 300 kDa cut-off membrane[60]. In the purification of an adenovirus,

a 750 kDa cut-off membrane was able to recover 100% of adenovirus particles while clearing 66% of DNA and 86% of protein impurities[93]. Smaller viruses, such as adeno-associated virus, can be concentrated or diafiltered using membranes with molecular weight cut-offs below 100 kDa, however this will also retain a high degree of impurities and is not an effective purification step[66]. Regardless of the choice in unit operations for purification, at least one final ultrafiltration or diafiltration step will typically be required in order to exchange the virus into a buffer solution intended for long term stability and safe administration.

1.2.3.4. Sterile Filtration

Sterile filtration is typically the terminal unit operation in downstream processing and involves dead-end filtration through a microfiltration membrane validated to completely retain any contaminating bacteria. In almost all cases this step is performed using a polymeric membrane with a 0.22 µm pore size rating which retains the bacteria through size exclusion and adsorption effects[94]. However, because of the large size of many virus particles and their complex surface chemistry (Table 1.1), it is possible for the therapeutic virus product to simultaneously be retained by the sterile filter membrane. *B. diminuta*, the bacteria used to validate sterile filtration membranes, has a minimal dimension of 0.3-0.4 µm[75,94], while large virus particles can be greater than 0.1 µm in size, thus sterile filtration demands a very difficult separation, requiring complete retention of the bacteria and complete transmission of the virus.

Within small scale clinical and larger scale GMP production processes for therapeutic viruses, losses during sterile filtration are commonly reported (Table 1.3). Recoveries up to 100% are reported for adenovirus, while lentivirus and other viruses consistently experience significant

losses, with only 40% of the product being recovered in the worst case. Despite how critical such losses are to the efficiency of the overall production process, sterile filtration has received little attention relative to the other downstream processing unit operations. In many cases, authors who report on complete downstream purification processes, and even state that they are producing a "final product", neglect to consider a sterile filtration step or provide other assurances of aseptic processing and sterility[84,95–97]. Of note, few historical reports could be found detailing the recovery of virus vaccine products after sterile filtration. This may partially be due to research at the time not reporting recovery for individual unit operations[98] or due to some work utilizing 0.45 µm rated filters before the 0.22 µm standard had been fully adopted[99].

Table 1.3: Overview of sterile filtration recoveries for various therapeutic viruses from clinical or GMP production processes. Process 1/Process 2 shows sterile filtration recoveries resulting from different downstream purification unit operations before sterile filtration. Membrane material and trade name are listed only when provided in the original publication.

Virus	Membrane	Recovery (%)	Reference
Adenovirus	0.22 µm PVDF Millipore Millex	Process 1: 57 Process 2: 97	[48]
	0.2 µm cellulose acetate Sarstedt Filtropur S	99	[82]
	0.6/0.2 µm PES Cytiva Ulta Prime CG	100	[71]
	0.22 µm PVDF Millipore Millex	85	[100]
Influenza virus	0.22 µm	Process 1: 49 Process 2: 71	[12]
Lentivirus	0.22 µm	Process 1: ~50 Process 2: ~75	[44]
	0.22 µm	50-70	[60]
	0.22 µm PES Pall Acrodisc	70	[59]
Rotavirus	0.22 µm	62	[101]
Vesicular stomatitis virus	0.45/0.22 µm cellulose acetate Satrorius Sartoban	40-50	[102]

To date, little work has been done to optimize the sterile filtration process or to investigate the fundamental causes behind these high losses of virus during sterile filtration. Many authors only report recovery values for a single type of sterile filtration membrane (Table 1.3) and do not discuss any membrane selection or optimization of process conditions. Even when the authors identify that different downstream purification processes leading up to sterile filtration can result in drastically different recovery, the cause of this is not explained in detail or explored further. In recent studies specifically investigating the sterile filtration of viruses, Shoaebargh *et al.* first identified the importance of membrane structure, demonstrating how multi-layered or asymmetric membranes provided a higher recovery, with recoveries of a Maraba rhabdovirus ranging from 5 to 21 %[103]. Further work then investigated how additives in solution such as polymers or proteins could improve virus recovery, attributed to blocking adsorption to the membrane surface and potentially reducing aggregation of the virus, with recoveries ranging from 11 to 54 %. Taylor *et al.* explored the sterile filtration of a cytomegalovirus using a wide range of membrane materials and structures, again demonstrating improved performance by asymmetric and multi-layered membranes, with recoveries drastically ranging from 10 to 80 %[104].

Studies from other areas of application, such as wastewater treatment, have investigated the interaction of viruses with microfiltration membranes. Using a series of viruses with different sizes, it has been shown that as the size of the virus particle increases, retention also increases[105]. Adsorption of the virus to the membrane surface plays a significant role in retention, with studies showing that hydrophobic interactions are a dominant mechanism[106–108] and that electrostatic repulsion (pH above virus isoelectric point, low salt concentration to prevent shielding) reduces adsorption[106]. Additional components in solution, such as surfactants, can reduce adsorption and

retention[107] while organic material and proteins can increase adsorption[109]. While these conclusions should be taken into consideration, the approach taken in wastewater treatment differs greatly from downstream bioprocessing and may limit the applicability of results. Wastewater treatments seeks to maximize virus retention, often uses membranes not suited for bioprocessing (high background adsorption, incompatible materials and solution components) and use virus solutions multiple orders of magnitude less concentrated.

1.3. Objectives and Thesis Outline

Sterile filtration of therapeutic viruses can result in significant losses, contributing to the overall inefficiency of downstream purification, with recent studies on the economics of therapeutic virus production identifying sterile filtration as a significant increase to cost[101] and the largest contributor to overall cost[110]. Significantly more work is required to better understand the fundamental mechanisms leading to loss of virus during sterile filtration and to develop methods by which recovery can be improved. This thesis aims to explore a variety of approaches towards improving sterile filtration, taking into consideration bacteria retention and regulatory compliance, properties of the virus and other solution components, and the membrane material and structure.

Chapter 2 provides a brief overview of membrane filtration, detailing the principles of operation and mechanisms of action, methods of data analysis and commonly applied models, and available membrane materials and structures.

Chapter 3 investigates how sterile filtration membranes are validated using *B. diminuta* and explores the mechanisms and membrane properties through which the bacteria is retained. Despite

how critical *B. diminuta* is to validating sterile filtration membranes, little work has been done to date testing how it is retained by a wide variety of commercial membranes under varying conditions. Of particular interest, we sought to determine if there were possible conditions under which larger pore size membranes not typically rated for sterile filtration (e.g. 0.45 µm membranes) could completely retain a *B. diminuta* challenge test in accordance with regulatory standards. A large series of bacteria filtration experiments were performed, comparing various membrane chemistries, pore size ratings, and the effect of applied pressure during filtration. Using select 0.45 and 0.22 µm membrane, sterile filtration experiments with a vesicular stomatitis virus were then performed. In essence, this chapter seeks to better understand why 0.22 µm membranes are typically required for sterile filtration, if this requirement can be relaxed to 0.45 µm membranes under the appropriate conditions, and what impact this could have on the sterile filtration of therapeutic viruses.

Chapter 4 demonstrates what effect small amount of residual host cell DNA and protein impurities can have on the sterile filtration performance of a vesicular stomatitis virus. As discussed in Chapter 1.2.2, while host cell impurities must be removed during downstream processing to ensure product safety, small amounts can remain in solution. While previous work has connected residual DNA with increased virus aggregation and reduced sterile filtration recovery[48], there has been no work investigating the effects of residual protein, either alone or in combination with residual DNA. Host cell protein and DNA were selectively isolated and then spiked back into a pure virus preparation either alone or in combination, and the effect on sterile filtration recovery and membrane fouling was observed. Further experiments specifically measured virus adsorption to the membrane in the presence of impurities.

Chapter 5 evaluates microfabricated isoporous silicon nitride membranes for suitability as sterile filters. Standard polymeric membranes have a broad pore size distribution, with some 0.22 µm rated membranes having pores as small as 0.05 µm[111] which can theoretically lead to the entrapment of larger virus particles. Thus, isoporous microfabricated membrane are an attractive technology to potentially improve sterile filtration performance. In collaboration with the research group at Simpore Inc., a variety of membranes were manufactured for testing, including a first of its kind 0.2 µm isoporous slit pore silicon nitride membrane. The effect of membrane pore size and geometry (circular pore vs. slit) on filtration performance was characterized using simple model solutions on nanoparticles and bovine serum albumin. The silicon nitride membranes were challenged with *B. diminuta* to validate their ability to act as a sterile filter, then tested in the sterile filtration performance of two different therapeutic viruses.

Chapter 6 presents a technique for fabricating model virus particles using polystyrene nanoparticles. While nanoparticles have commonly been used to model virus particles in filtration studies[104,112], they have lacked the ability to represent some aspect of virus solutions, such as the presence of aggregates. To address this, a tunable and consistent process was designed for producing nanoparticle with a distribution of doublets, triplets, and larger aggregates. Filtration tests using standard 0.22 and 0.45 µm membranes were performed, and the results were analyzed using standard pore blockage and Vmax models. The similarity of results to the sterile filtration of viruses is discussed.

1.4. References

1. Clem AS. Fundamentals of Vaccine Immunology. *J Glob Infect Dis*. 2011;3(1):73-78. doi:10.4103/0974-777X.77299

2. Kelly E, Russell SJ. History of Oncolytic Viruses: Genesis to Genetic Engineering. *Mol Ther*. 2007;15(4):651-659. doi:10.1038/sj.mt.6300108

3. Lin DM, Koskella B, Lin HC. Phage therapy: An alternative to antibiotics in the age of multi-drug resistance. *World J Gastrointest Pharmacol Ther*. 2017;8(3):162-173. doi:10.4292/wjgpt.v8.i3.162

4. Ma Y, Nolte RJM, Cornelissen JJLM. Virus-based nanocarriers for drug delivery. *Adv Drug Deliv Rev*. 2012;64(9):811-825. doi:10.1016/j.addr.2012.01.005

5. Shukla S, Steinmetz NF. Virus-based nanomaterials as positron emission tomography and magnetic resonance contrast agents: from technology development to translational medicine. *WIREs Nanomedicine Nanobiotechnology*. 2015;7(5):708-721. doi:10.1002/wnan.1335

6. Zhao X, Lin Y, Wang Q. Virus-based scaffolds for tissue engineering applications. *Wiley Interdiscip Rev Nanomed Nanobiotechnol*. 2015;7(4):534-547. doi:10.1002/wnan.1327

7. Pollard AJ, Bijker EM. A guide to vaccinology: from basic principles to new developments. *Nat Rev Immunol*. 2021;21(2):83-100. doi:10.1038/s41577-020-00479-7

8. Pulendran B, Ahmed R. Immunological mechanisms of vaccination. *Nat Immunol*. 2011;12(6):509-517.

9. Hajj Hussein I, Chams N, Chams S, et al. Vaccines Through Centuries: Major Cornerstones of Global Health. *Front Public Health*. 2015;3. Accessed June 16, 2022. https://www.frontiersin.org/article/10.3389/fpubh.2015.00269

10. Plotkin S. History of vaccination. *Proc Natl Acad Sci U S A*. 2014;111(34):12283-12287. doi:10.1073/pnas.1400472111

11. Baicus A. History of polio vaccination. *World J Virol*. 2012;1(4):108-114. doi:10.5501/wjv.v1.i4.108

12. Kon TC, Onu A, Berbecila L, et al. Influenza Vaccine Manufacturing: Effect of Inactivation, Splitting and Site of Manufacturing. Comparison of Influenza Vaccine Production Processes. Krammer F, ed. *PLOS ONE*. 2016;11(3):e0150700. doi:10.1371/journal.pone.0150700

13. Griffin DE. Measles Vaccine. *Viral Immunol*. 2018;31(2):86-95. doi:10.1089/vim.2017.0143

14. Cate TR, Couch RB, Kasel JA, Six HR. Clinical trials of monovalent influenza A/New Jersey/76 virus vaccines in adults: reactogenicity, antibody response, and antibody persistence. *J Infect Dis*. 1977;136 Suppl:S450-455. doi:10.1093/infdis/136.supplement_3.s450

15. Valenzuela P, Medina A, Rutter WJ, Ammerer G, Hall BD. Synthesis and assembly of hepatitis B virus surface antigen particles in yeast. *Nature*. 1982;298(5872):347-350. doi:10.1038/298347a0

16. McNeil C. Who Invented the VLP Cervical Cancer Vaccines? *JNCI J Natl Cancer Inst*. 2006;98(7):433. doi:10.1093/jnci/djj144

17. Munis AM, Bentley EM, Takeuchi Y. A tool with many applications: vesicular stomatitis virus in research and medicine. *Expert Opin Biol Ther*. 2020;20(10):1187-1201. doi:10.1080/14712598.2020.1787981

18. Regules JA, Beigel JH, Paolino KM, et al. A Recombinant Vesicular Stomatitis Virus Ebola Vaccine. *N Engl J Med*. 2017;376(4):330-341. doi:10.1056/NEJMoa1414216

19. Racine T, Kobinger GP, Arts EJ. Development of an HIV vaccine using a vesicular stomatitis virus vector expressing designer HIV-1 envelope glycoproteins to enhance humoral responses. *AIDS Res Ther*. 2017;14(1):55. doi:10.1186/s12981-017-0179-2

20. Shi X, Hu J, Guo J, Wu C, Xiong S, Dong C. A Vesicular Stomatitis Virus-Based Vaccine Carrying Zika Virus Capsid Protein Protects Mice from Viral Infection. *Virol Sin*. 2019;34(1):106-110. doi:10.1007/s12250-019-00083-7

21. O'Donnell KL, Clancy CS, Griffin AJ, et al. Optimization of Single-Dose VSV-Based COVID-19 Vaccination in Hamsters. *Front Immunol*. 2022;12. Accessed June 29, 2022. https://www.frontiersin.org/article/10.3389/fimmu.2021.788235

22. Haglund K, Leiner I, Kerksiek K, Buonocore L, Pamer E, Rose JK. High-level primary CD8(+) T-cell response to human immunodeficiency virus type 1 gag and env generated by vaccination with recombinant vesicular stomatitis viruses. *J Virol*. 2002;76(6):2730-2738. doi:10.1128/jvi.76.6.2730-2738.2002

23. Bulcha JT, Wang Y, Ma H, Tai PWL, Gao G. Viral vector platforms within the gene therapy landscape. *Signal Transduct Target Ther*. 2021;6(1):1-24. doi:10.1038/s41392-021-00487-6

24. Goswami R, Subramanian G, Silayeva L, et al. Gene Therapy Leaves a Vicious Cycle. *Front Oncol*. 2019;9. Accessed July 14, 2022. https://www.frontiersin.org/articles/10.3389/fonc.2019.00297

25. Naldini L. Gene therapy returns to centre stage. *Nature*. 2015;526(7573):351-360. doi:10.1038/nature15818

26. Ruella M, Kenderian SS. Next-Generation Chimeric Antigen Receptor T-Cell Therapy: Going off the Shelf. *BioDrugs*. 2017;31(6):473-481. doi:10.1007/s40259-017-0247-0

27. Pasquinucci G. Possible effect of measles on leukaemia. *Lancet Lond Engl*. 1971;1(7690):136. doi:10.1016/s0140-6736(71)90869-5

28. Bluming AZ, Ziegler JL. Regression of Burkitt's lymphoma in association with measles infection. *Lancet Lond Engl*. 1971;2(7715):105-106. doi:10.1016/s0140-6736(71)92086-1

29. Kaufman HL, Kohlhapp FJ, Zloza A. Oncolytic viruses: a new class of immunotherapy drugs. *Nat Rev Drug Discov*. 2015;14(9):642-662. doi:10.1038/nrd4663

30. Hanahan D, Weinberg RA. Hallmarks of Cancer: The Next Generation. *Cell*. 2011;144(5):646-674. doi:10.1016/j.cell.2011.02.013

31. Dhiman N, Jacobson RM, Poland GA. Measles virus receptors: SLAM and CD46. *Rev Med Virol*. 2004;14(4):217-229. doi:10.1002/rmv.430

32. Pol J, Kroemer G, Galluzzi L. First oncolytic virus approved for melanoma immunotherapy. *OncoImmunology*. 2016;5(1):e1115641. doi:10.1080/2162402X.2015.1115641

33. Russell L, Peng KW. The emerging role of oncolytic virus therapy against cancer. *Chin Clin Oncol*. 2018;7(2):16-16. doi:10.21037/cco.2018.04.04

34. Abd-Aziz N, Poh CL. Development of oncolytic viruses for cancer therapy. *Transl Res*. 2021;237:98-123. doi:10.1016/j.trsl.2021.04.008

35. Chahal PS, Aucoin MG, Kamen A. Primary recovery and chromatographic purification of adeno-associated virus type 2 produced by baculovirus/insect cell system. *J Virol Methods*. 2007;139(1):61-70. doi:10.1016/j.jviromet.2006.09.011

36. Hwang YJ, Myung H. Engineered Bacteriophage T7 as a Potent Anticancer Agent in vivo. *Front Microbiol*. 2020;11:491001. doi:10.3389/fmicb.2020.491001

37. Yuk IH, Lin GB, Ju H, et al. A serum-free Vero production platform for a chimeric virus vaccine candidate. *Cytotechnology*. 2006;51(3):183-192. doi:10.1007/s10616-006-9030-7

38. Cervera L, Fuenmayor J, González-Domínguez I, Gutiérrez-Granados S, Segura MM, Gòdia F. Selection and optimization of transfection enhancer additives for increased virus-like particle production in HEK293 suspension cell cultures. *Appl Microbiol Biotechnol*. 2015;99(23):9935-9949. doi:10.1007/s00253-015-6842-4

39. Rathore AS, Agarwal H, Sharma AK, Pathak M, Muthukumar S. Continuous processing for production of biopharmaceuticals. *Prep Biochem Biotechnol*. 2015;45(8):836-849. doi:10.1080/10826068.2014.985834

40. Butler M. Animal cell cultures: recent achievements and perspectives in the production of biopharmaceuticals. *Appl Microbiol Biotechnol*. 2005;68(3):283-291. doi:10.1007/s00253-005-1980-8

41. Kiesslich S, Kamen AA. Vero cell upstream bioprocess development for the production of viral vectors and vaccines. *Biotechnol Adv*. 2020;44:107608. doi:10.1016/j.biotechadv.2020.107608

42. Ausubel LJ, Hall C, Sharma A, et al. Production of CGMP-Grade Lentiviral Vectors. *BioProcess Int*. 2012;10(2):32-43.

43. Nestola P, Peixoto C, Silva RRJS, Alves PM, Mota JPB, Carrondo MJT. Improved virus purification processes for vaccines and gene therapy: Improved Virus Purification Processes for Vaccines. *Biotechnol Bioeng*. 2015;112(5):843-857. doi:10.1002/bit.25545

44. Dropulić B, Slepushkin V, Chang N, et al. Large-scale Purification of a Lentiviral Vector by Size Exclusion Chromatography or Mustang Q Ion Exchange Capsule. Published online 2003. doi:10.12665/J25.DROPULIC

45. Merten OW, Charrier S, Laroudie N, et al. Large-scale manufacture and characterization of a lentiviral vector produced for clinical ex vivo gene therapy application. *Hum Gene Ther*. 2011;22(3):343-356. doi:10.1089/hum.2010.060

46. Truran R, Buckley R, Radcliffe P, Miskin J, Mitrophanous K. Virus purification. Published online December 31, 2009. Accessed March 15, 2021. https://patents.google.com/patent/US20090325284A1/en

47. Merten OW, Hebben M, Bovolenta C. Production of lentiviral vectors. *Mol Ther - Methods Clin Dev*. 2016;3:16017. doi:10.1038/mtm.2016.17

48. Konz JO, Lee AL, Lewis JA, Sagar SL. Development of a Purification Process for Adenovirus: Controlling Virus Aggregation to Improve the Clearance of Host Cell DNA. *Biotechnol Prog*. 2005;21(2):466-472. doi:10.1021/bp049644r

49. Michen B, Graule T. Isoelectric points of viruses. *J Appl Microbiol*. 2010;109(2):388-397. doi:10.1111/j.1365-2672.2010.04663.x

50. Olofsson S. Isoelectric focusing of herpes simplex virus. *Arch Virol*. 1975;49(2):93-98. doi:10.1007/BF01317529

51. Loewe D, Dieken H, Grein TA, Weidner T, Salzig D, Czermak P. Opportunities to debottleneck the downstream processing of the oncolytic measles virus. *Crit Rev Biotechnol*. 2020;40(2):247-264. doi:10.1080/07388551.2019.1709794

52. Yusoff K, Tan WS. Newcastle disease virus: macromolecules and opportunities. *Avian Pathol J WVPA*. 2001;30(5):439-455. doi:10.1080/03079450120078626

53. Ge P, Tsao J, Schein S, Green TJ, Luo M, Zhou ZH. Cryo-EM Model of the Bullet-Shaped Vesicular Stomatitis Virus. *Science*. 2010;327(5966):689-693. doi:10.1126/science.1181766

54. Schloemer RH, Wagner RR. Cellular adsorption function of the sialoglycoprotein of vesicular stomatitis virus and its neuraminic acid. *J Virol*. 1975;15(4):882-893. doi:10.1128/jvi.15.4.882-893.1975

55. Eledge MR, Zita MD, Boehme KW. Reovirus: Friend and Foe. *Curr Clin Microbiol Rep*. 2019;6(3):132-138. doi:10.1007/s40588-019-00121-8

56. Wolff MW, Reichl U. Downstream processing of cell culture-derived virus particles. *Expert Rev Vaccines*. 2011;10(10):1451-1475. doi:10.1586/erv.11.111

57. Zydney AL. New developments in membranes for bioprocessing – A review. *J Membr Sci*. 2021;620:118804. doi:10.1016/j.memsci.2020.118804

58. Gerba CP, Betancourt WQ. Viral Aggregation: Impact on Virus Behavior in the Environment. *Environ Sci Technol*. 2017;51(13):7318-7325. doi:10.1021/acs.est.6b05835

59. Bandeira V, Peixoto C, Rodrigues AF, et al. Downstream Processing of Lentiviral Vectors: Releasing Bottlenecks. *Hum Gene Ther Methods*. 2012;23(4):255-263. doi:10.1089/hgtb.2012.059

60. Valkama AJ, Oruetxebarria I, Lipponen EM, et al. Development of Large-Scale Downstream Processing for Lentiviral Vectors. *Mol Ther - Methods Clin Dev*. 2020;17:717-730. doi:10.1016/j.omtm.2020.03.025

61. FDA. *Viral Safety Evaluation of Biotechnology Products Derived From Cell Lines of Human or Animal Origin*. Center for Drug Evaluation and Research, Food and Drug Administration; 1998.

62. FDA. *Test Procedures and Acceptance Criteria for Biotechnological/Biological Products*. Center for Drug Evaluation and Research, Food and Drug Administration; 1999.

63. FDA. *Chemistry, Manufacturing, and Control (CMC) Information for Human Gene Therapy Investigational New Drug Applications (INDs)*. Center for Drug Evaluation and Research, Food and Drug Administration; 2020.

64. Zhou Y, Ma BG, Zhang HY. Human oncogene tissue-specific expression level significantly correlates with sequence compositional features. *FEBS Lett*. 2007;581(22):4361-4365. doi:10.1016/j.febslet.2007.08.018

65. Yang H, Zhang L, Galinski M. A probabilistic model for risk assessment of residual host cell DNA in biological products. *Vaccine*. 2010;28(19):3308-3311. doi:10.1016/j.vaccine.2010.02.099

66. Hebben M. Downstream bioprocessing of AAV vectors: industrial challenges & regulatory requirements. *Cell Gene Ther Insights*. 2018;4(2):131-146. doi:10.18609/cgti.2018.016

67. Wright J. Product-Related Impurities in Clinical-Grade Recombinant AAV Vectors: Characterization and Risk Assessment. *Biomedicines*. 2014;2(1):80-97. doi:10.3390/biomedicines2010080

68. Bracewell DG, Smith V, Delahaye M, Smales CM. Analytics of host cell proteins (HCPs): lessons from biopharmaceutical mAb analysis for Gene therapy products. *Curr Opin Biotechnol*. 2021;71:98-104. doi:10.1016/j.copbio.2021.06.026

69. Weinberg WC, Frazier-Jessen MR, Wu WJ, et al. Development and regulation of monoclonal antibody products: Challenges and opportunities. *Cancer Metastasis Rev*. 2005;24(4):569-584. doi:10.1007/s10555-005-6196-y

70. Michalik S, Siegerist F, Palankar R, et al. Comparative analysis of ChAdOx1 nCoV-19 and Ad26.COV2.S SARS-CoV-2 vector vaccines. *Haematologica*. 2022;107(4):947-957. doi:10.3324/haematol.2021.280154

71. Moleirinho MG, Rosa S, Carrondo MJT, et al. Clinical-Grade Oncolytic Adenovirus Purification Using Polysorbate 20 as an Alternative for Cell Lysis. *Curr Gene Ther*. 2018;18(6):366-374. doi:10.2174/1566523218666181109141257

72. Jorritsma-Smit A, van Zanten CJ, Schoemaker J, et al. GMP manufacturing of Vvax001, a therapeutic anti-HPV vaccine based on recombinant viral particles. *Eur J Pharm Sci*. 2020;143:105096. doi:10.1016/j.ejps.2019.105096

73. Flotte TR. Empty Adeno-Associated Virus Capsids: Contaminant or Natural Decoy? *Hum Gene Ther*. 2017;28(2):147-148. doi:10.1089/hum.2017.29039.trf

74. Wang D, Tai PWL, Gao G. Adeno-associated virus vector as a platform for gene therapy delivery. *Nat Rev Drug Discov*. 2019;18(5):358-378. doi:10.1038/s41573-019-0012-9

75. FDA. *Sterile Drug Products Produced by Aseptic Processing — Current Good Manufacturing Practice*. Center for Drug Evaluation and Research, Food and Drug Administration; 2004.

76. ASTM. *F838-20: Standard Test Method for Determining Bacterial Retention of Membrane Filters Utilized for Liquid Filtration*. American Society for Testing and Materials; 2020. Accessed November 29, 2021. https://www.astm.org/f0838-20.html

77. Helling A, König H, Seiler F, Berkholz R, Thom V, Polakovic M. Retention of Acholeplasma laidlawii by Sterile Filtration Membranes: Effect of Cultivation Medium and Filtration Temperature. *PDA J Pharm Sci Technol*. 2018;72(3):264-277. doi:10.5731/pdajpst.2017.008102

78. Sundaram S, Auriemma M, Howard G, Brandwein H, Leo F. Application of membrane filtration for removal of diminutive bioburden organisms in pharmaceutical products and processes. *PDA J Pharm Sci Technol*. 1999;53(4):186-201.

79. Ausubel LJ, Meseck M, Derecho I, et al. Current good manufacturing practice production of an oncolytic recombinant vesicular stomatitis viral vector for cancer treatment. *Hum Gene Ther*. 2011;22(4):489-497. doi:10.1089/hum.2010.159

80. Adams B, Bak H, Tustian AD. Moving from the bench towards a large scale, industrial platform process for adeno-associated viral vector purification. *Biotechnol Bioeng*. 2020;117(10):3199-3211. doi:10.1002/bit.27472

81. Agalloco JP. Aseptic Processing: A Review of Current Industry Practice. *Pharm Technol*. 2004;28(10). Accessed July 13, 2022. https://www.pharmtech.com/view/aseptic-processing-review-current-industry-practice

82. Peixoto C, Ferreira TB, Sousa MFQ, Carrondo MJT, Alves PM. Towards purification of adenoviral vectors based on membrane technology. *Biotechnol Prog*. 2008;24(6):1290-1296. doi:10.1002/btpr.25

83. Subramanian S, Altaras GM, Chen J, Hughes BS, Zhou W, Altaras NE. Pilot-scale adenovirus seed production through concurrent virus release and concentration by hollow fiber filtration. *Biotechnol Prog*. 2005;21(3):851-859. doi:10.1021/bp049561a

84. Fernandes P, Peixoto C, Santiago VM, Kremer EJ, Coroadinha AS, Alves PM. Bioprocess development for canine adenovirus type 2 vectors. *Gene Ther*. 2013;20(4):353-360. doi:10.1038/gt.2012.52

85. Thomassen YE, van 't Oever AG, Vinke M, et al. Scale-down of the inactivated polio vaccine production process. *Biotechnol Bioeng*. 2013;110(5):1354-1365. doi:10.1002/bit.24798

86. Moleirinho MG, Silva RJS, Alves PM, Carrondo MJT, Peixoto C. Current challenges in biotherapeutic particles manufacturing. *Expert Opin Biol Ther*. 2020;20(5):451-465. doi:10.1080/14712598.2020.1693541

87. Goerke AR, To BCS, Lee AL, Sagar SL, Konz JO. Development of a novel adenovirus purification process utilizing selective precipitation of cellular DNA. *Biotechnol Bioeng*. 2005;91(1):12-21. doi:10.1002/bit.20406

88. Orr V, Zhong L, Moo-Young M, Chou CP. Recent advances in bioprocessing application of membrane chromatography. *Biotechnol Adv*. 2013;31(4):450-465. doi:10.1016/j.biotechadv.2013.01.007

89. Nass SA, Mattingly MA, Woodcock DA, et al. Universal Method for the Purification of Recombinant AAV Vectors of Differing Serotypes. *Mol Ther Methods Clin Dev*. 2018;9:33-46. doi:10.1016/j.omtm.2017.12.004

90. Smith RH, Yang L, Kotin RM. Chromatography-based purification of adeno-associated virus. *Methods Mol Biol Clifton NJ*. 2008;434:37-54. doi:10.1007/978-1-60327-248-3_4

91. McNally DJ, Piras BA, Willis CM, Lockey TD, Meagher MM. Development and Optimization of a Hydrophobic Interaction Chromatography-Based Method of AAV Harvest, Capture, and Recovery. *Mol Ther - Methods Clin Dev*. 2020;19:275-284. doi:10.1016/j.omtm.2020.09.015

92. van Reis R, Zydney A. Bioprocess membrane technology. *J Membr Sci*. 2007;297(1):16-50. doi:10.1016/j.memsci.2007.02.045

93. Nestola P, Martins DL, Peixoto C, et al. Evaluation of Novel Large Cut-Off Ultrafiltration Membranes for Adenovirus Serotype 5 (Ad5) Concentration. Rito-Palomares M, ed. *PLoS ONE*. 2014;9(12):e115802. doi:10.1371/journal.pone.0115802

94. Meltzer TH, Jornitz MW. The Sterilizing Filter and Its Pore Size Rating. *Am Pharm Rev*. 2003;6:6.

95. Peixoto C, Sousa MFQ, Silva AC, Carrondo MJT, Alves PM. Downstream processing of triple layered rotavirus like particles. *J Biotechnol*. 2007;127(3):452-461. doi:10.1016/j.jbiotec.2006.08.002

96. Kamen A, Henry O. Development and optimization of an adenovirus production process. *J Gene Med*. 2004;6(S1):S184-S192. doi:10.1002/jgm.503

97. Tomono T, Hirai Y, Okada H, et al. Ultracentrifugation-free chromatography-mediated large-scale purification of recombinant adeno-associated virus serotype 1 (rAAV1). *Mol Ther Methods Clin Dev*. 2016;3:15058. doi:10.1038/mtm.2015.58

98. Väänänen P, Vaheri A. Large-scale purification of rubella virus and preparation of an experimental split rubella virus vaccine. *Appl Microbiol*. 1971;22(3):255-259. doi:10.1128/am.22.3.255-259.1971

99. Reimer CB, Baker RS, vanFrank RM, Newlin TE, Cline GB, Anderson NG. Purification of Large Quantities of Influenza Virus by Density Gradient Centrifugation. *J Virol*. 1967;1(6):1207-1216.

100. Green AP, Huang JJ, Scott MO, et al. A new scalable method for the purification of recombinant adenovirus vectors. *Hum Gene Ther*. 2002;13(16):1921-1934. doi:10.1089/10430340260355338

101. Hamidi A, Hoeksema F, Velthof P, et al. Developing a manufacturing process to deliver a cost effective and stable liquid human rotavirus vaccine. *Vaccine*. 2021;39(15):2048-2059. doi:10.1016/j.vaccine.2021.03.033

102. Cutler MW, Kang Y, Ouattara AA, Syvertsen KE. Purification processes for isolating purified vesicular stomatitis virus from cell culture. Published online March 6, 2008. Accessed March 15, 2021. https://patents.google.com/patent/WO2007123961A3/en

103. Shoaebargh S, Gough I, Fe Medina M, et al. Sterile filtration of oncolytic viruses: An analysis of effects of membrane morphology on fouling and product recovery. *J Membr Sci*. 2018;548:239-246. doi:10.1016/j.memsci.2017.11.022

104. Taylor N, Ma W, Kristopeit A, Wang S, Zydney AL. Evaluation of a sterile filtration process for viral vaccines using a model nanoparticle suspension. *Biotechnol Bioeng*. 2021;118(1):106-115. doi:10.1002/bit.27554

105. Oshima KH, Evans-Strickfaden TT, Highsmith AK, Ades EW. The Use of a Microporous Polyvinylidene Fluoride (PVDF) Membrane Filter to Separate Contaminating Viral Particles from Biologically Important Proteins. *Biologicals*. 1996;24(2):137-145. doi:10.1006/biol.1996.0018

106.   van Voorthuizen EM, Ashbolt NJ, Schäfer AI. Role of hydrophobic and electrostatic interactions for initial enteric virus retention by MF membranes. *J Membr Sci*. 2001;194(1):69-79. doi:10.1016/S0376-7388(01)00522-1

107.   Farrah SR. Chemical Factors Influencing Adsorption of Bacteriophage MS2 to Membrane Filterst. *Appl Environ Microbiol*. 1982;43:5.

108.   Lukasik J, Scott TM, Andryshak D, Farrah SR. Influence of Salts on Virus Adsorption to Microporous Filters. *Appl Environ Microbiol*. 2000;66(7):2914-2920. doi:10.1128/AEM.66.7.2914-2920.2000

109.   Huang H, Young TA, Schwab KJ, Jacangelo JG. Mechanisms of virus removal from secondary wastewater effluent by low pressure membrane filtration. *J Membr Sci*. 2012;409-410:1-8. doi:10.1016/j.memsci.2011.12.050

110.   Comisel RM, Kara B, Fiesser FH, Farid SS. Lentiviral vector bioprocess economics for cell and gene therapy commercialization. *Biochem Eng J*. 2021;167:107868. doi:10.1016/j.bej.2020.107868

111.   Taylor N, Ma WJ, Kristopeit A, Wang S ching, Zydney AL. Retention characteristics of sterile filters – Effect of pore size and structure. *J Membr Sci*. 2021;635:119436. doi:10.1016/j.memsci.2021.119436

112.   Pazouki M, Noelle Wilton A, Latulippe DR. An experimental study on sterile filtration of fluorescently labeled nanoparticles – the importance of surfactant concentration. *Sep Purif Technol*. 2019;218:217-226. doi:10.1016/j.seppur.2019.02.038

Chapter 2

Filtration Fundamentals

2. Filtration Fundamentals

In broad terms, filtration is a pressure driven separation process in which a feed solution is forced through a porous medium (or membrane), on which suspended solids or particles from the feed are captured. Various modes of filtration can be distinguished. In dead end filtration, the fluid flows normal to the membrane surface with all fluid passing through the membrane. Stirred cell filtration is similar to dead end filtration, but with added agitation from an impeller or stir bar. Finally there is cross flow filtration, where the fluid flows tangential to the membrane surface and only a portion of the fluid passes through the membrane[1]. The driving force for filtration will typically be supplied as a constant pressure source (e.g. pressurized reservoir, hydrostatic pressure, vacuum) or a constant flux source (syringe pump, peristaltic pump).

Flux through the membrane during pressure driven filtration can be derived from the Hagen-Poiseuille equation[2]:

$$J = \frac{\varepsilon\, d_p^2\, P}{8\, \mu\, \tau\, L} \tag{1}$$

The Hagen-Poiseuille equation assumes a series of uniform, cylindrical pores with infinitely thin walls, which is a large abstraction from the true structure of many membranes as discussed in Section 1.2. Despite this, the model has been shown to be accurate for the predicting the flux through a variety of membranes[3,4]. Accounting for factors such as the membrane porosity ε and membrane tortuosity τ can aid in representing some of the non-ideal forms of many membranes. From this equation, key factors which influence flux through the membrane are the applied pressure P, the membrane pore size d_p, and the membrane thickness L. To achieve the highest throughput, using a thinner membrane, with a larger pore size, at a higher operating pressure is ideal, however there are many trade-offs with real world considerations.

Flux through the membrane can also be represented using a flow resistance term[2]:

$$J = \frac{P}{\mu \left(R_m + R_f\right)} \tag{2}$$

Here, the resistance to flow from the membrane is given by R_m, while R_f represents additional resistance to flow contributed by the buildup of captured particles on or inside the membrane, also know as membrane fouling. As filtration progresses and more particulate is captured by the membrane, the fouling will continue to build and increase the overall resistance to flow. From Equation 2, if the pressure is kept constant and the overall membrane resistance is increased over the course of filtration, this will result in a decrease in flux, or for a constant flux source the reverse will occur, with an increase in pressure. This results in the classic pressure and flux curves as shown in Figure 1. These curves are highly indicative of filtration performance as the relative rate of pressure increase or flux decline is directly related to the degree of membrane fouling. Further discussion on this subject is provided in the next section.
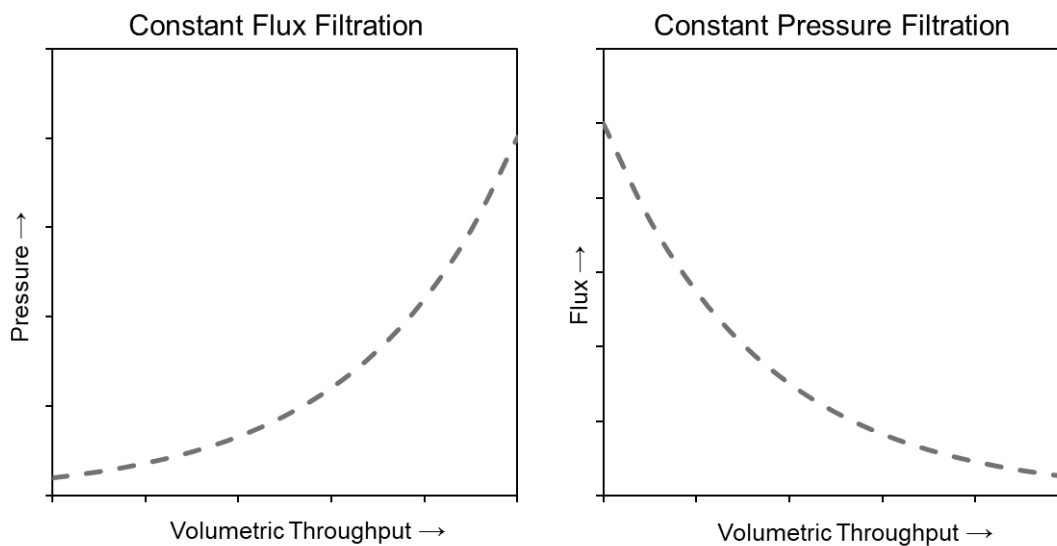
Figure 2.1: Graphical representation of the effect of fouling on filtration performance. As filtration progresses and fouling occurs, a constant flux filtration system will experience an increase in pressure, while a constant pressure system will experience a decline in flux.

Particle capture and fouling of the membrane primarily occurs through two phenomena. The first is sieving, where the pore size of the membrane is small enough that it physically restricts the passage of the suspended particles in solution. Filtration membranes are classified based on their pore sizes, as it largely determines what type of particles or solutes the membrane will be able to reject[5]:

- Nanofiltration membranes – Pore size of 10 to 1 nm. Can retain small molecules, sugars, or dyes.

- Ultrafiltration membranes – Pore size of 100 nm to 10 nm. Effective at retaining viruses, proteins, or large polymers

- Microfiltration membranes – Pore size of 10 µm to 0.1 µm. Effective at retaining large particulate and aggregates, suspended solids, yeast, or bacteria.

Given Equation 1, the class of membrane and pore size must be carefully selected such that the pores are small enough that the particles of interest are fully retained, but not smaller than necessary so that the highest possible throughput can be obtained. Due to the pore size distribution present in most polymeric membranes, the particle sieving of a membrane will never be a perfectly sharp cut-off where particles above the pore size are fully retained and particle below the pore size are fully transmitted; the selectivity of a membranes will decrease with increasing pore size distribution[6].

The other mechanism for particle capture is adsorption to the membrane. When a particle is transported to the surface or pore wall of a membrane, a resulting balance between attractive and repulsive forces will determine if the particle adsorbs to the surface. A variety of theories have been proposed to describe the forces involved, including DLVO theory[7], xDLVO theory[8] and thermodynamic minimization of Gibbs free energy[9]. Strong particle-membrane interaction will allow for the formation of a monolayer on the membrane surface with potentially minimal fouling, while further particle-particle interaction will lead to greater buildup of the fouling layer[1,10].

2.1. Modeling of Membrane Fouling

Understanding the flux or pressure profiles which occur due to fouling during filtration can give insights into how the foulant material is mechanistically interacting with the membrane. Various models of membrane filtration have been developed which rely on different mechanisms of pore blockage in order to describe how pressure will increase or flux will decrease with increased throughput during filtration[2,11].
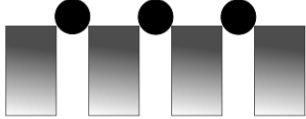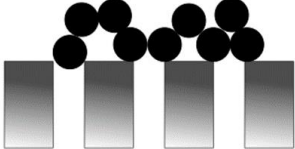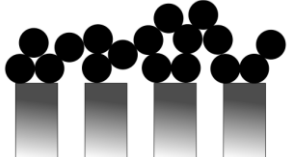
Experimental data can be fit to these models in order to determine which mechanism of membrane fouling is likely occurring. Derivation of the models follows the characteristic equation[11]

$$\frac{dP}{dv} = K \, P^n \tag{3}$$

Where n is a filtration constant that characterizes the mode of fouling, with $n = 0$ for cake filtration, $n = 1$ for intermediate blocking, $n = 3/2$ for standard blocking, and $n = 2$ for complete blocking. The resistance coefficient K will depend on the properties of the feed solution, membrane, and operating conditions, with a different coefficient for each mode of fouling[11].

Stochastic and mechanistic models of fouling have also been derived and matched to the various modes of fouling originating from Equation 3[11]. The resulting fouling models for both constant pressure and constant flux filtration are given in Table 4. Complete blocking occurs when particles larger than the pores deposit directly on top of the pores, entirely blocking them and preventing any flow. Standard blocking occurs with particles smaller than the membrane pore size being trapped within the membrane structure, slowly narrowing the pore width as the fouling layer grows. Intermediate blocking occurs with large particles partially seal pores and partially bridge pores. Finally, Cake filtration occurs when a layer of particles is formed on the membrane surface which neither blocks or enters the pores.

Table 2.1: Review of pore blocking models, giving the equations for both constant flux and constant pressure models and showing an idealized graphical representation of the fouling occurring on a membrane.

Blocking Model	Constant Pressure Equation	Constant Flux Equation	Graphical Representation
Complete Blocking	$J = J_0 - K_b V$	$P = \dfrac{P_0}{1 - \dfrac{K_b}{J_0} V}$	
Standard Blocking	$J = J_0 \left(1 - \dfrac{K_s}{2} V\right)^2$	$P = \dfrac{P_0}{\left(1 - \dfrac{K_s}{2} V\right)^2}$	
Intermediate Blocking	$J = J_0 * e^{-K_i V}$	$P = P_0 * e^{K_i V}$	
Cake Filtration	$J = \dfrac{J_0}{J_0 K_c V + 1}$	$P = P_0 (K_c J_0 V + 1)$	

These models have been successfully applied to investigate the fouling of membranes by a wide variety of substances, including proteins[12], viruses[13], polymers[14] and nanoparticles[15]. However, these models represent an idealized interaction between the particles and the membrane which may not capture the true fouling behavior. Thus, improved models have been developed where the fouling occurs in distinct stages each fit to different a different model[16] or where models are combined and multiple mechanism of fouling occur simultaneously[17,18].

2.2. Membrane Materials and Structures

The large majority of membranes currently employed in filtration operations are polymeric membranes with a complex polydisperse inner structure (Figure 2.1). Isotropic, or symmetric, membranes have a uniform pore structure throughout the depth of the membrane. In the filtration of particles larger than the membrane pore size, particles are primarily captured directly on the membrane surface, while the filtration of particles smaller than the membrane pore size will result in particle capture distributed throughout the membrane structure[19]. Anisotropic, or asymmetric, membranes have a pore structure that varies throughout the depth of the membrane. Typically filtration will be operated with the larger pore size side of the membrane placed on the upstream side, resulting in a prefilter effect where the bulk of particle capture can occur before the smallest pores are reached[20]. Finally, composite, or multi-layer, membranes consist or two or more district layers with varying properties and each having their own pore size. Membranes may be designed with this form for structural reasons, such as ultrafiltration membranes having a thin active layer with a tight pore size on top and a thicker, larger pore size support layer beneath to provide mechanical strength[19]. For example, the selective layer of a PES 500 kDa ultrafiltration membrane was found to be only 0.5 µm thick, while the entire membrane was greater than 35 µm thick[21]
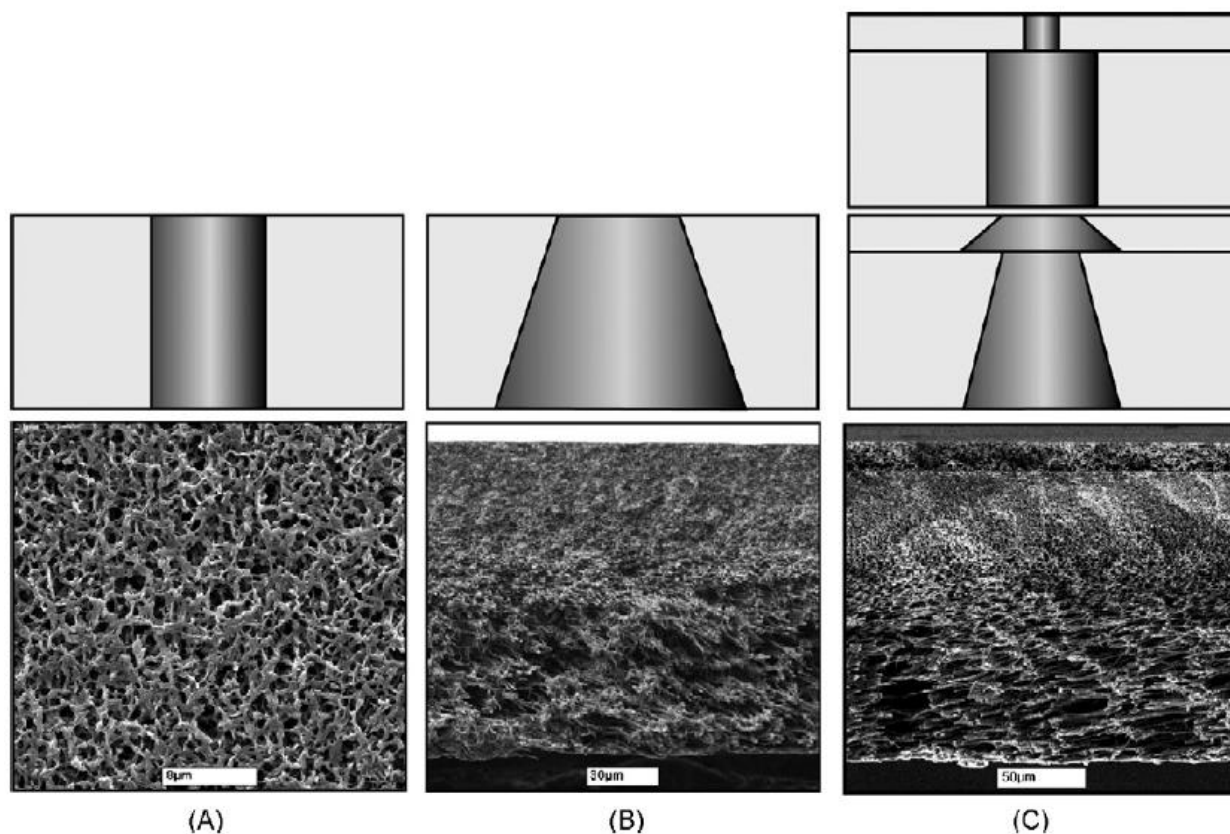
Figure 2.2: Variety of structures available for membrane filtration technology. Top images provide a graphic representation of how pore size changes with depth through the membrane while bottom images are SEM image of actual membrane structures. Membranes shown are (A) Isotropic (symmetric), (B) Anisotropic (asymmetric) and (C) Composite (multi-layer). Reprinted with permission from Reis *et al.*[19].

These polydisperse membranes can be described with a certain pore size (e.g 0.22 or 0.45 μm), however it is important to recognize that this is only a nominal designation; the actual membrane structure will consist of pores covering a wide range of sizes. Typically the pore size distribution is represented using a log-normal probability density function[22,23] with the smallest and largest pores potentially spanning more than an entire order of magnitude[24]. For example, a 20 nm nominal pore size PVDF membrane was found to have an actual average pore size of 44 nm with the smallest and largest pores being 4 nm and 100 nm respectively. Similarly, a 0.22 μm

nominal pore size membrane was found to have an average pore size of 0.33 µm and with the smallest and largest pores being 0.06 µm and 6 µm respectively[25], an incredibly broad range of pore sizes. These measurements are achieved using mercury intrusion porosimetry, however the method has been criticized due to the high intrusion pressures which can alter pore structures and distort results[19]. Other techniques such as liquid-liquid displacement or gas displacement porosimetry have been described, and selection of the measurement technique can change the measured average pore sized from 0.23 to 0.41 µm for a nominal 0.2 µm membrane[24], demonstrating how variable the measurements can be.

The broad pore size distribution in membranes is a consequence of how the membranes are fabricated. Common polymeric membranes are fabricated from materials such as PES, PVDF, CA and PAN using a phase inversion technique. Beginning with a homogeneous polymer solution, the solution is demixed (through the introduction of solvent, evaporation of solvent heating, etc.) into a polymer rich and polymer lean phases with solidification of the polymer rich phase solidifying to form the membrane solid matrix and the polymer lean phase forming the membrane pore void space[26]. This process is driven by thermodynamic and kinetic aspects, with randomness behind the patterning of solids and voids leading to a disordered structure and pore size distribution. Alternate methods for the formation of polymeric membranes include interfacial polymerization, stretching, and electrospinning[27]. One technique of note is track etching, as it allows for the formation of highly controlled pores with a very uniform pore size. In this method a polymer film is irradiated with heavy ions, leading to the formation of damaged tracks which can be subsequently exposed to an etching solution to dissolve the damaged ion track and expand the pores[28].The resulting membranes is isoporous, having a uniform pore size with straight channel pores. However, track

etched membranes have low porosity and a relatively large thickness, leading to low hydraulic permeability and limited applications.

Membranes are not solely limited to polymeric materials, and many inorganic membranes fabricated from metallic or ceramic material exist. Ceramic and metallic membranes made of silver, alumina, titania, zirconia or glass can be fabricated by sintering of powders, with the resulting in a polydisperse membrane pore size controlled by the particle size of the powder used for sintering[29]. These membranes have the advantage of high chemical and thermal stability, allowing them to be used in extreme applications or to be cleaned with harsh conditions between uses. Other techniques such as foaming, electrospinning, and casting can also be applied to the formation of inorganic membranes[30]. Some techniques of particular interest are anodization, de-alloying, and microfabrication which all allow for the creation of isoporous membranes. Through the application of electrochemistry principles, thick oxide layers can be grown on metals such as aluminum or titanium. These oxide layers can self assemble into honeycomb or circular structures with pore diameters ranging from 4 to 200 nm[31]. In de-alloying, a eutectic alloy such as NiAl-Cr is directionally solidified to create rod-like phase boundaries. The rod-phase can then be selectively etched to leave behind circular pores[32]. Finally, microfabrication techniques such as deep reactive ion etching[33] or photolithography[34] can also be used to create isoporous membranes, with the unique advantage of also being able to design the pore geometry, as further discussed in Chapter 5.

2.3. References

1. Bowen WR, Jenner F. Theoretical descriptions of membrane filtration of colloids and fine particles: An assessment and review. *Adv Colloid Interface Sci*. 1995;56:141-200. doi:10.1016/0001-8686(94)00232-2

2. Field R. Fundamentals of Fouling. In: *Membrane Technology*. John Wiley & Sons, Ltd; 2010:1-23. doi:10.1002/9783527631407.ch1

3. Yoon SH, Lee S, Yeom IT. Experimental verification of pressure drop models in hollow fiber membrane. *J Membr Sci*. 2008;310(1):7-12. doi:10.1016/j.memsci.2007.11.048

4. Du X, Wang Z, Chao L. A combined model for describing the trans-membrane pressure (P) variation in constant flux dead-end microfiltration (MF) process. *J Environ Chem Eng*. 2022;10(1):107076. doi:10.1016/j.jece.2021.107076

5. Ripperger S, Gösele W, Alt C, Loewe T. Filtration, 1. Fundamentals. In: *Ullmann's Encyclopedia of Industrial Chemistry*. John Wiley & Sons, Ltd; 2013:1-38. doi:10.1002/14356007.b02_10.pub3

6. Kanani DM, Fissell WH, Roy S, Dubnisheva A, Fleischman A, Zydney AL. Permeability - Selectivity Analysis for Ultrafiltration: Effect of Pore Geometry. *J Membr Sci*. 2010;349(1-2):405. doi:10.1016/j.memsci.2009.12.003

7. Redman JA, Walker SL, Elimelech M. Bacterial Adhesion and Transport in Porous Media: Role of the Secondary Energy Minimum. *Environ Sci Technol*. 2004;38(6):1777-1785. doi:10.1021/es034887l

8. Sun C, Zhang N, Li F, et al. Quantitative Analysis of Membrane Fouling Mechanisms Involved in Microfiltration of Humic Acid–Protein Mixtures at Different Solution Conditions. *Water*. 2018;10(10):1306. doi:10.3390/w10101306

9. He M, Gao K, Zhou L, et al. Zwitterionic materials for antifouling membrane surface construction. *Acta Biomater*. 2016;40:142-152. doi:10.1016/j.actbio.2016.03.038

10. Belfort G, Davis RH, Zydney AL. The behavior of suspensions and macromolecular solutions in crossflow microfiltration. *J Membr Sci*. 1994;96(1):1-58. doi:10.1016/0376-7388(94)00119-7

11. Iritani E. A Review on Modeling of Pore-Blocking Behaviors of Membranes During Pressurized Membrane Filtration. *Dry Technol*. 2013;31(2):146-162. doi:10.1080/07373937.2012.683123

12. Hlavacek M, Bouchet F. Constant flowrate blocking laws and an example of their application to dead-end microfiltration of protein solutions. *J Membr Sci*. 1993;82(3):285-295. doi:10.1016/0376-7388(93)85193-Z

13. Shoaebargh S, Gough I, Fe Medina M, et al. Sterile filtration of oncolytic viruses: An analysis of effects of membrane morphology on fouling and product recovery. *J Membr Sci*. 2018;548:239-246. doi:10.1016/j.memsci.2017.11.022

14. Vela MCV, Blanco SÁ, García JL, Rodríguez EB. Analysis of membrane pore blocking models applied to the ultrafiltration of PEG. *Sep Purif Technol*. 2008;62(3):489-498. doi:10.1016/j.seppur.2008.02.028

15. Warkiani ME, Wicaksana F, Fane AG, Gong HQ. Investigation of membrane fouling at the microscale using isopore filters. *Microfluid Nanofluidics*. 2015;19(2):307-315. doi:10.1007/s10404-014-1538-0

16. Hwang KJ, Lin TT. Effect of morphology of polymeric membrane on the performance of cross-flow microfiltration. *J Membr Sci*. 2002;199(1):41-52. doi:10.1016/S0376-7388(01)00675-5

17. Bolton G, LaCasse D, Kuriyel R. Combined models of membrane fouling: Development and application to microfiltration and ultrafiltration of biological fluids. *J Membr Sci*. 2006;277(1):75-84. doi:10.1016/j.memsci.2004.12.053

18. Duclos-Orsello C, Li W, Ho CC. A three mechanism model to describe fouling of microfiltration membranes. *J Membr Sci*. 2006;280(1):856-866. doi:10.1016/j.memsci.2006.03.005

19. van Reis R, Zydney A. Bioprocess membrane technology. *J Membr Sci*. 2007;297(1):16-50. doi:10.1016/j.memsci.2007.02.045

20. Ho CC, Zydney AL. Effect of membrane morphology on the initial rate of protein fouling during microfiltration. *J Membr Sci*. Published online 1999:15.

21. Roberge H, Moreau P, Couallier E, Abellan P. Determination of the key structural factors affecting permeability and selectivity of PAN and PES polymeric filtration membranes using 3D FIB/SEM. *J Membr Sci*. 2022;653:120530. doi:10.1016/j.memsci.2022.120530

22. Zydney AL, Aimar P, Meireles M, Pimbley JM, Belfort G. Use of the log-normal probability density function to analyze membrane pore size distributions: functional forms and discrepancies. *J Membr Sci*. 1994;91(3):293-298. doi:10.1016/0376-7388(94)80090-1

23. Lee JK, Liu BYH. A filtration model of microporous membrane filters in liquids. *KSME J*. 1994;8(1):78-87. doi:10.1007/BF02953246

24. Bottino A, Capannelli G, Petit-bon P, Cao N, Pegoraro M, Zoia G. Pore Size and Pore-Size Distribution in Microfiltration Membranes. *Sep Sci Technol*. 1991;26(10-11):1315-1327. doi:10.1080/01496399108050534

25. Taylor N, Ma W, Kristopeit A, Wang S, Zydney AL. Evaluation of a sterile filtration process for viral vaccines using a model nanoparticle suspension. *Biotechnol Bioeng*. 2021;118(1):106-115. doi:10.1002/bit.27554

26. Hołda AK, Vankelecom IFJ. Understanding and guiding the phase inversion process for synthesis of solvent resistant nanofiltration membranes. *J Appl Polym Sci*. 2015;132(27). doi:10.1002/app.42130

27. Lalia BS, Kochkodan V, Hashaikeh R, Hilal N. A review on membrane fabrication: Structure, properties and performance relationship. *Desalination*. 2013;326:77-95. doi:10.1016/j.desal.2013.06.016

28. Tan X, Rodrigue D. A Review on Porous Polymeric Membrane Preparation. Part I: Production Techniques with Polysulfone and Poly (Vinylidene Fluoride). *Polymers*. 2019;11(7):1160. doi:10.3390/polym11071160

29. Kayvani Fard A, McKay G, Buekenhoudt A, et al. Inorganic Membranes: Preparation and Application for Water Treatment and Desalination. *Mater Basel Switz*. 2018;11(1):E74. doi:10.3390/ma11010074

30. Zhu B, Duke M, Dumée LF, et al. Short Review on Porous Metal Membranes—Fabrication, Commercial Products, and Applications. *Membranes*. 2018;8(3):83. doi:10.3390/membranes8030083

31. Warkiani ME, Bhagat AAS, Khoo BL, et al. Isoporous Micro/Nanoengineered Membranes. *ACS Nano*. 2013;7(3):1882-1904. doi:10.1021/nn305616k

32. Desorbo W, Cline HE. Metal Membranes with Uniform Submicron-Size Pores. *J Appl Phys*. 1970;41(5):2099-2105. doi:10.1063/1.1659171

33. Kim S, Feinberg B, Kant R, et al. Diffusive Silicon Nanopore Membranes for Hemodialysis Applications. *PLOS ONE*. 2016;11(7):e0159526. doi:10.1371/journal.pone.0159526

34. Rijn CJM van, Veldhuis GJ, Kuiper S. Nanosieves with microsystem technology for microfiltration applications. *Nanotechnology*. 1998;9(4):343-345. doi:10.1088/0957-4484/9/4/007

Chapter 3

An Experimental Study of Bacteria Transmission

Through Microfiltration Membranes Reveals the Potential

of Enhancing the Yield of Therapeutic Viruses in

Downstream Processing

3. An Experimental Study of Bacteria Transmission Through Microfiltration Membranes Reveals the Potential of Enhancing the Yield of Therapeutic Viruses in Downstream Processing

Evan Wright, Alexandra Jucan, David R. Latulippe

Prepared for journal submission

3.1. Abstract

Effective sterile filtration using commercial polymeric membranes is an ongoing issue in the downstream purification of virus vector products due to the inherent challenge in both ensuring retention of contaminating bacteria while also maximizing yield of the virus. Bacteria retention is validated using a challenge test with *Brevundimonas diminuta* bacteria, however there is little detail available characterizing how membrane and process properties influence retention of this bacteria. Furthermore, parallel testing of bacteria retention and virus product transmission is often not investigated, and there is the opportunity to use this approach in order to develop improved sterile filtration processes. To this end, the present study compares the performance of nine commercial microfiltration membranes with different chemistries (PES, PVDF, cellulose acetate) and pore size ratings (0.2, 0.45, 0.8 µm) in filtration experiments with *B. diminuta*. For 0.45 µm membranes specifically, applied pressure was critical in determining bacteria retention, and for some 0.45 µm membranes at appropriately low operating pressures (< 34 kPa) the bacteria were even completely retained, demonstrating effective sterile filtration. Using a rhabdovirus-based vector, the performance of 0.22 and 0.45 µm membranes was then compared, highlighting how the yield could be improved from 61% to 84%. Characterization of the membrane physicochemical

properties (zeta potential, surface structure) showed a complex relationship between membrane structure and function with poor correlation to performance, indicating that further investigation is required. The results from this work provide important insights into bacteria transmission through microfiltration membranes and a novel direction for optimizing the sterile filtration of viral vector products.

3.2. Introduction

Cell and virus gene therapies are a highly promising platform for the treatment and even cure of a myriad of diseases[1]. However, high manufacturing costs, consistent production, and product safety are all barriers to further adoption of these technologies. Manufacturing of virus therapy products involves a complex series of upstream and downstream bioprocessing unit operations[2], which can include the sterile filtration step for bioburden reduction and as a safeguard to ensure sterility of the final product[3]. A wide range of commercially available 0.22 µm rated polymeric membranes are able to perform this operation, and the implementation is generally straightforward for conventional small molecule pharmaceuticals. However, issues with low throughput and retention of valuable product can be encountered for many types of biopharmaceuticals such as highly concentrated antibody solutions[4], exosomes[5], glycoconjugate vaccines[6], and especially virus particles[7–9]. Loss of product from the sterile filtration step in addition to material costs has even been found to be one of the largest contributors to the high per dose costs of a particular virus therapy[10].

For these products, their particle size (anywhere from 15 nm for antibodies to 200 nm and larger for virus particles) relative to the 0.22 µm pore size is often a critical factor which leads to

issues during sterile filtration. Despite this, the 0.22 µm pore size is seen as a necessity to achieve the required function of ensuring product sterility. When polymeric membrane filters were first introduced, the 0.45 µm rated membranes were originally assumed to be able to retain all bacteria, however, this changed in the 1960's with the identification of *Pseudomonas diminuta* (now *Brevundimonas diminuta*), and the requirement for sterile filtration was shifted to the 0.22 µm designation[11]. The *B. diminuta* bacteria has since been seen as the gold standard for testing and validating sterile filtration membranes. Starting in 1987, the FDA stated that a sterilizing filter is specifically defined based on the ability to retain a minimum of 10^7 *B. diminuta* per cm^2 of membrane area[12] with the common methodology for this challenge test defined by ATM F838[13]. From this, the ability to act as a sterile filter is not necessarily limited to a nominal pore size but is based on an applied challenge test; the 0.22 µm pore size is not a strict necessity.

Despite the importance of sterile filtration and the ability of a membrane to retain *B. diminuta*, there is a lack of fundamental studies documenting how the bacteria transmits through membranes with different pore sizes and properties. In the existing literature, there are brief reports showing that *B. diminuta* can be fully retained by 0.45 µm rated membranes[14,15], which would be a highly desirable implementation given the previously described issues in the sterile filtration of biotherapeutics using 0.22 µm rated membranes. Other existing studies are often performed from a theoretical perspective, using isoporous[16,17] or custom-made (non-commercial) membranes[18–20] to investigate the fundamentals of how bacteria transmit through membranes. While these studies have presented many useful conclusions on the importance of media composition and temperature [19], the effect of flow interruptions[20], and most importantly the effect of applied pressure during

filtration[21], these is still a lack of available information on how and if certain commercial membrane retain *B. diminuta* under different conditions.

To address this, the present study compares how membrane material, pore size, and applied pressure during filtration influences the retention of *B. diminuta* by commercial microfiltration membranes, with a focus on the 0.45 µm pore size. Using a small-scale microfiltration setup and following the protocols identified in ASTM F838, we have performed over 110 individual filtration experiments in order to characterize the transmission of *B. diminuta* through nine different commercial membranes with different chemistries (PES, PVDF, cellulose acetate), pore size ratings (0.2, 0.45, 0.8 µm), and manufacturers. The membranes are then further characterized by measuring surface zeta potential in both standard electrolyte and the ASTM specified solution and by imaging the membrane surfaces using scanning electron microscopy to link filtration performance to membrane physicochemical properties.

To extend the insights gained from the *B. diminuta* retention testing, a practical challenge test was performed comparing the sterile filtration of a virus vector through specific 0.22 and 0.45 µm rated membranes. Specifically, a vesicular stomatitis virus (VSV) was chosen due to it's unique bullet shape and large size[22], its use as a viral vector in vaccine and gene therapies[23], and past results which have shown losses during sterile filtration[8,24].

Filter validation through bacteria retention testing and optimization of filter performance through application specific testing is rarely if ever connected in experimental work. By taking a holistic

approach to this problem and investigating the two properties in tandem, new insights can be gained into the selection of membranes and the optimization of downstream processing.

3.3. Materials and Methods

3.3.1. Membrane Selection and Characterization

Millipore Durapore PVDF (0.22 µm GVWP, 0.45 µm HVLP), Millipore Express PLUS PES (0.22 µm GPWP, 0.45 µm HPWP), Sartorius PES (0.22 µm 15407, 0.45 µm 15406), and Sartorius CA (0.22 µm 11107, 0.45 µm 11106, 0.8 µm 11104) were used in this study. All membranes are hydrophilic, considered low protein binding by the manufacturers, and all 0.22 µm rated membranes are recommended for sterile filtration. Membranes were either purchased with a 13 mm diameter or manually cut to that size using a hollow punch. All membranes were housed in a polycarbonate assembly (Cole-Parmer) with an effective 0.5 cm^2 of filtration area. When performing filtration studies with *B. diminuta* or VSV, all fittings, tubing, and membranes were sterilized in an autoclave at 121 °C for 30 minutes before use.

Zeta potential of the various membranes was measured using the streaming potential method using a Surpass 3 instrument (Anton Parr). A pair of 2 x 1 cm samples of membrane were fitted into the adjustable gap cell of the instrument, and a gap distance of 100 ± 10 µm was maintained for all the trials. A full characterization of the zeta potential over a pH range of 3 to 11 was performed using 1mM KCl as the electrolyte and using 0.05 M NaOH or 0.05 M HCl to adjust the pH within ±0.1 of the target value. Beginning at a pH of 3, the pH was increased in increments of 1 unit up to 11, then decreased back down to 3 with a zeta potential measurement performed at each step. A measurement consisted of three individual observations recorded by the Surpass

instrument. A second set of zeta potential measurements were performed for each membrane using SLB as the electrolyte with no pH adjustments.

To image the membrane surface pore structures, scanning electron microscopy was used. Portions of the various membranes were cut using a razor blade and mounted on specimen stubs using carbon tape and nickel paste, then sputter coated with gold (Polaron E5100). The images were obtained using a Vega II LSU (Tescan) instrument at 20 kV and a magnification ranging from 1000 to 10,000 x. The complete set of SEM images obtained in this study are shown in Figure S3.6 and Figure S3.7.

3.3.2. Filtration Experiments

Small scale constant pressure filtration tests were performed in triplicate using an Elveflow OB1 MK3 multi-channel microfluidic flow control (MMFC) system. The pressure controller was supplied with compressed nitrogen at approximately 410 kPa, while the applied pressure in three parallel reservoirs (15 mL Falcon tubes, VWR) was controlled using a computer interface (Elveflow SI 2.6.1). The reservoirs were connected to the membrane assemblies using approximately 10 cm of 1/16" ID Masterflex silicone tubing (Cole-Parmer) and luer lock fittings (McMaster Carr). Prior to any filtration experiments, the reservoirs were filled with approximately 10 mL of sterile solution without bacteria or virus (SLB or formulation buffer respectively) and set to 210 kPa. The throughput of each membrane was observed and compared to previous results in order to check the membrane integrity and ensure the membrane was fully wet. All filtration experiments were performed inside of a Class II Type A2 biosafety cabinet.

3.3.3. Preparation and Analysis of Brevundimonas diminuta

Lactose broth was prepared by suspending 1.3g of dry media in 100mL of water. Saline lactose broth (SLB) was then prepared by suspending 7.6g of NaCl in 970mL of water followed by adding 30 mL of lactose broth. Tryptic soy broth (TSB) and tryptic soy agar were prepared following manufacturer's instructions. All media was autoclaved at 121 °C for 30 minutes before use (Tuttnauer 3850E).

Brevumondias diminuta ATCC® 19146 was purchased from Microbiologics in the lyophilized Kwik-Stik™ format. The *B. diminuta* was plated onto tryptic soy agar and allowed to grow for 48 hours at 30°C, at which point a colony was picked and transferred into 5mL of tryptic soy broth. After incubation for another 24 hours at 30°C with no shaking, a 0.5 mL aliquot was mixed with 0.5 mL of 50% glycerol and stored at -80°C as the master stock. Another aliquot was taken and used for 18S rRNA Sanger sequencing, performed by the Mobix Lab at McMaster University. The sample was boiled for 15 minutes followed by amplification of the 16S gene using 8f(5'AGAGTTTGATCCTGGCTCAG) and 926r(5'CCGTCAATTCCTTTRAGTTT) primers and subsequent purification of the 16S gene (PureLink PCR Purification Kit, Invitrogen) for DNA sequencing. The results were checked using the BLAST database (National Institute of Health) and showed a 99% conformity with *Brevumondias diminuta* ATCC® 19146.

To prepare an active *B. diminuta* culture, 5mL of TSB was inoculated with a scraping from the master stock, and incubated for 24 hours at 30°C. 20 µl of the culture was diluted into 5 mL of SLB and incubated for an additional for 24 hours at 30°C. For the bacteria challenge filtration tests, the prepared *B. diminuta* was further diluted in SLB to a final volume of 40 mL, then the

three parallel reservoirs were each filled with 12 mL of the solution with a bacteria concentration ranging from 6.8 to 7.6 log CFU/mL (average 7.3±0.3 log CFU/mL), ensuring that the minimum 10^7 CFU/cm^2 (7 log CFU/cm^2) challenge as specified by the ASTM standard[13] was exceeded. The pressure in each of the reservoir was set to the required level using the MMFC, and 10 mL of filtrate from the 3 replicate membranes was collected in individual 15 mL tubes. All 0.22 µm rated membranes were initially tested at 210 kPa (30 PSI) to confirm their ability to act as sterile filters. Then, to investigate the effect of applied pressure on filtration performance, all 0.45 µm and 0.8 µm membranes were tested over a range of 3.4 to 100 kPa (0.5 to 15 PSI). Following each filtration experiment, the *B. diminuta* concentration in each of the triplicate filtrate samples was assessed using a colony forming unit (CFU) count, where 0.1 mL of serially diluted solution was placed onto tryptic soy agar (MilliporeSigma) in triplicate, which was then incubated for 48 hours at 30°C followed by the manually counting colonies visible to the naked eye. In addition, to confirm the complete absence of *B. diminuta* in the filtrate, a membrane detection method was used. The full volume filtrate was passed through a separate analytical membrane (Durapore 0.45 µm) designed to capture any remaining bacteria, which was then removed from the housing and placed directly onto agar. Following an incubation for 48 hours at 30°C, if no growth on the membrane was observed then the solution was deemed to be sterile and not contain any *B. diminuta*. Final bacteria concentrated is reported as the log$_{10}$ value of the counted CFU/mL. The complete data set of all feed and filtrate *B. diminuta* concentrations from this work is available as Table S1.

To investigate potential interactions of the *B. diminuta* cells with the membrane surface, the zeta potential of *B. diminuta* was measured. A culture of *B. diminuta* in SLB was prepared, then triplicate samples of the bacteria suspension were measured using a folded capillary cell

(DTS1070, Malvern Instruments) in a Zetasizer Nano ZSP (Malvern Instruments). The bacteria refractive index was set to 1.38 based on the value used in pervious work[19].

The cell size of *B. diminuta* was determined using scanning electron microscopy measurements. A solution of *B. diminuta* was prepared identically to the filtration challenge test, with a 24 hour culture in TSB and a 24 hour incubation in SLB. The bacteria solution was then further diluted 100 fold in SLB. The bacteria cells were then captured on a silicon nitride membrane with 0.2 µm slit pores by actively filtering 500 µl of solution through the 0.036 cm^2 surface area membrane. See Chapter 5 for more details on the membrane and filtration process. The membrane with captured bacteria was then gently washed with ultrapure water (Millipore MilliQ) and was then treated with a solution of 2% glutaraldehyde in cacodylate buffer for 30 minutes. A series of exchanges of increasing ethanol concentration (25, 50, 70, 95, 100 %) were performed, with a 10 minute incubation at each step. The membrane was then loaded into a Leica EMCPD 300 critical point dryer, where the ethanol was exchanged with critical point CO_2 over 20 drying cycles. The dried membrane was mounted on a stub, sputter coated, and imaged as previously described for the microfiltration membranes. ImageJ software was used to measure the cell size of B. *dimunta* from the SEM images, with 50 cells measured over 5 different locations on the membrane surface.

3.3.4. Preparation and Analysis of Vesicular Stomatitis Virus

A batch of VSV was prepared using conventional viral culture methodologies and purified using hydrophobic interaction chromatography for further use in sterile filtration testing. VSV was propagated inside Vero cells (both provided by Robert E. Fitzhenry Vector Laboratory at

McMaster University), and infected supernatant was collected and clarified using centrifugation. Clarified supernatant containing VSV was loaded onto a Sartobind Phenyl Nano 3mL capsule (Sartorius) operated on an NGC chromatography system (Biorad) and eluted using a step change in ammonium sulfate concentration. The eluted fraction containing purified VSV was dialyzed (Slide-a-Lyser G2,10 kDa cut-off, Thermo-Fisher) against a buffer solution to stabilize the virus (Formulation buffer; 150 mM NaCl, 4% sucrose, 10 mM HEPES, pH 7.4) and stored at -80 °C. See Chapter 4 for further details on the production and purification of VSV.

To assess the transmission of virus through the membranes, the reservoirs were filled with 7 mL of VSV solution with a titer of $9.3\pm3\times10^8$ PFU/mL. 0.22 and 0.45 µm Sartorius PES membranes were specifically compared at a pressure of 34 kPa, based on results showing complete retention of *B. diminuta* (demonstrated effective sterile filtration) by the 0.45 µm membrane at this pressure. The pressure in each of the reservoirs was set using the MMFC and 5 mL of filtrate from the three replicate membranes was collected. Virus titer of the feed and triplicate filtrate samples was assessed as plaque forming units per mL (PFU/mL) using a standard plaque assay. Vero cells were seeded into a 6-well plate (Corning) and infected with 100 µl of serially diluted samples in triplicate. An agarose overlay was applied, and after a 24-hour incubation the cells were fixed with 3.7% formaldehyde and stained with 0.1% crystal violet solution. Plaques visible to the naked eye were manually counted.

3.4. Results and Discussion

3.4.1. Measurement of *B. diminuta* Cell Size

The size of *B. diminuta* cells are known to vary based on culture conditions, with nutrient availability and temperature[19] or agitation[25] influencing the cell size. When in a nutrient deficient environment, some bacteria adapt by decreasing their cell size and reducing activity[26], and a high ionic strength medium is also known to reduce cell size through osmotic effects[27]. Validation of sterile filtration using *B. diminuta* is meant to present a worst case scenario, and therefore the culture and solution conditions are optimized to minimize cell size and increase the likelihood of the bacteria passing through a membrane. The additional step of transferring the cells to SLB and incubating for 24 hours before filtration will theoretically shrink the size of the cells. The average size of *B. diminuta* cells adapted to the SLB medium has been reported as 0.4×1 µm[28] from scanning electron microscopy, while the FDA and ASTM standard describe the *B. diminuta* cell size as being $0.3\text{-}0.4 \times 0.6\text{-}1$ µm in size[12,13]. In order to validate that the size of cultured *B. diminuta* cells used in this work are within the expected size range, the size of individual cells were measured from SEM images (Figure 3.1). The cells were prepared using a critical point drying method, a method for dehydrating and preserving cells with minimal distortion to their size and structure[29]. From the SEM images, the *B. diminuta* cells were measured to have an average width of 0.38 ± 0.04 µm and a length of 0.95 ± 0.1 µm, within the expected values for the cell size. Of note, the smallest cell measured was only 0.29×0.68 µm, representing the smallest particle a sterile filter must be able to retain.
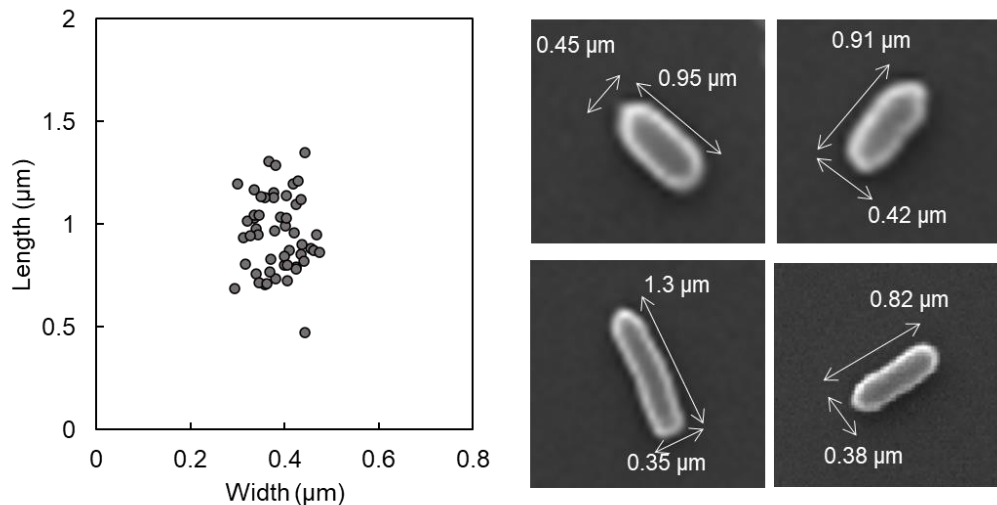
Figure 3.1: Measurement of *B. diminuta* cell size from SEM images. Cells were captured on a silicon nitride membrane surface and fixed using glutaraldehyde followed by critical point drying. Data from 50 total measured cells is given, with representative measurements also shown as an example.

3.4.2. Effect of Membrane Pore Size

First, different pore size Sartorius CA membranes were compared, with Figure 3.2 showing the results of this experiment. Figure 3.2A shows the results of the *B. diminuta* filtration tests, presenting the bacteria filtrate concentration following filtration at pressures ranging from 3.4 to 100 kPa for 0.22, 0.45, and 0.8 µm pore size membranes. For example, when the 0.45 µm CA membrane was tested in triplicate at 100 kPa, filtrate concentrations of 3.4 ± 0.3, 4.3 ± 0.2, 4.7 ± 0.3 log CFU/mL were measured. As the pressure was reduced to 69 and 34 kPa, the amount of bacteria in the filtrate was significantly reduced, then at 14 kPa and below all filtration tests resulted in sterile filtrate with no detectable *B. diminuta*. For the 0.45 µm membrane, there was a clear link between applied pressure and bacteria transmission. When the 0.22 µm membrane was tested at 100 kPa, no bacteria were detected in the filtrate, as expected of a commercial sterile filter. Finally, the 0.8 µm membrane was tested from 3.4 to 100 kPa and had no statistical

difference in the transmission between pressures ($p<0.05$) with an overall average filtrate concentration of 6.4 ± 0.3 log CFU/mL. From the SEM images in Figure 3.2B, it can clearly be seen how the membranes have progressively larger pore sizes and more open structures as the nominal pore sizes increases. While the trend in size is clear, the observable pores are also all significantly larger than the nominal size. It is well known that polymeric membranes have a broad pore size distribution, and that the stated pore size is a nominal label and not necessarily reflective of a size cut-off[30] and studies on some of the same membranes used in this study have shown that measured pore sizes can cover an entire order of magnitude with the mean pore size being almost double the nominal pore size[31]. Thus, the insights that can be gained from the SEM images are limited, but it nevertheless shows the relative trend between pore size and bacteria retention.
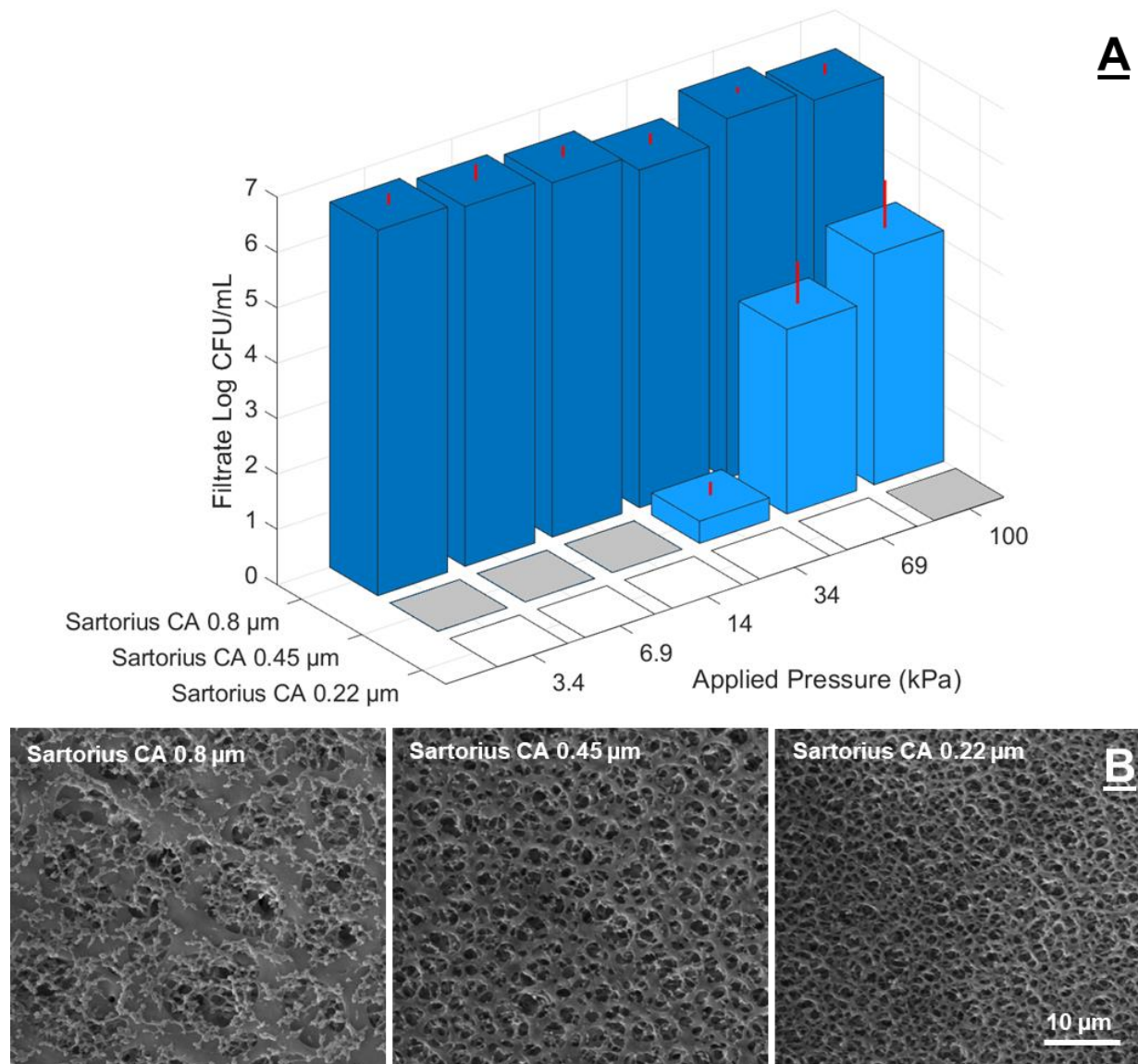
Figure 3.2: A) Filtrate *B. diminuta* concentrations after challenging 0.8, 0.45, and 0.22 µm pore size cellulose acetate (CA) membranes with a feed of 7.3±0.3 log CFU/mL over a range of pressures from 3.4 to 100 kPa. Data is from triplicate experiments and is reported as the log CFU/mL geometric mean ± the standard deviation (shown by red lines) of the log transformed data. Flat grey areas indicate that no *B. diminuta* was detected in the filtrate and that sterility was achieved, while areas with white squares were not tested. B) Scanning electron microscopy images of the 0.22, 0.45, and 0.8 µm Sartorius CA membranes, showing the pore structure of the membrane surface.

At the 0.45 µm pore size, the applied pressure had a clear effect on bacteria retention, with increasing applied pressure decreasing bacteria retention. It is important to note that the 0.45 µm

CA membrane fully retained the *B. diminuta* at up to 14 kPa. Given that the filtration test was performed in accordance with typical industry and ASTM standards for validating a sterile filter, this would indicate that the 0.45 µm Sartorius CA membrane can act as a sterile filter when operated below 14 kPa.

3.4.3. Effect of Membrane Material and Structure

To expand on this result, three other commercial 0.45 µm membranes were also tested for *B. diminuta* retention over the 3.4 to 100 kPa range. In addition to the 0.45 µm membranes, 0.22 µm versions of each membrane were tested, and each fully retained the *B. diminuta* at up to 200 kPa. Figure 3.3A shows that the various 0.45 µm membranes had greatly different performance in their ability to retain *B. diminuta* at low pressures. At 3.4 kPa, three of the four membranes tested were able to completely retain the *B. diminuta*, with only the Durapore membrane showing significant transmission. Then as the pressure was increased, the other membranes all reached a breakthrough point, below which the membranes could be considered to act as sterile filters and above which *B. diminuta* would pass through the membrane. The highest pressure that the Express PLUS, Sartorius CA, and Sartorius PES 0.45 µm membranes fully retain the *B. diminuta* was 6.9, 14, and 34 kPa respectively, and these points are highlighted on Figure 3.3 by the asterisks. All 0.45 µm membranes also showed a trend of increase transmission with increasing pressure. These membranes possess significantly different morphologies as shown in Figure 3.3B, with the visible pores on the membrane surface being vastly different between membranes. However, there was no clear relation between the surface pore structure and the bacteria retention. For example, the Sartorius PES 0.45 µm fully retained the bacteria at a higher pressure than the Sartorius CA 0.45 µm, however from the SEM image it also appears to have larger pores. From the pure water flux

measurements performed at 210 kPa for each membrane, average flux values were 0.92, 1.3, 0.88, and 1.2 mL min^{-1} cm^{-2}, and no trend between flux and bacteria retention was observed. While a previous trend between observed pore size and bacteria retention was found (Figure 3.2), this is not applicable when comparing membranes of the same nominal pores size.
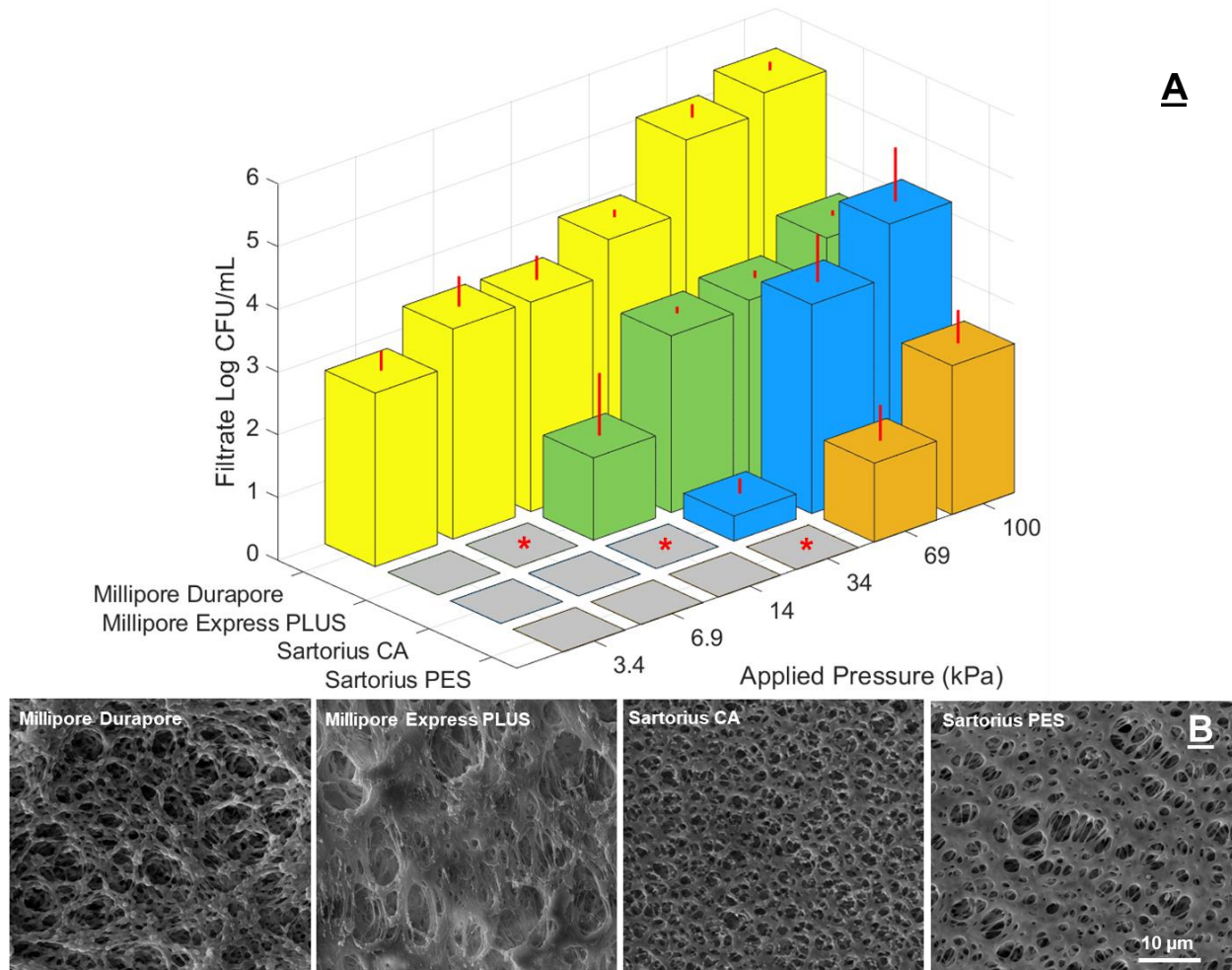
Figure 3.3: A) Filtrate *B. diminuta* concentrations after challenging various 0.45 µm membranes with a feed of 7.3±0.3 log CFU/mL over a range of pressures from 3.4 to 100 kPa. Data is from triplicate experiments and is reported as the log CFU/mL geometric mean ± the standard deviation (shown by red lines) of the log transformed data. Flat grey areas indicate that no *B. diminuta* was detected in the filtrate and that sterility was achieved. Areas marked with an asterisk indicate the highest pressure condition at which each membrane fully retained the bacteria. B) Scanning electron microscopy images of the 0.45 µm membranes, showing the pore structure of the membrane surface

From the experiments with 0.45 µm membranes, the importance of applied pressure during filtration is clear. The common theory to explain this phenomena is that bacteria deform under pressure and can be forced through pores that may be smaller than the size of the bacteria cell; Gram negative bacteria such as *B. diminuta* lack a thick outer peptidoglycan layer, and so they act as flexible particles during filtration[16–18,21]. This effect of increasing pressure resulting in increased transmission was only seen at the 0.45 µm pore size. Applied pressure up to 200 kPa did not affect the 0.22 µm membranes, pressure had a significant effect on the 0.45 µm membranes, and no effect was seen for the 0.8 µm membrane. This is in line with behavior expect from the approximately 0.4 × 1 µm cells (Figure 3.1), where at this size range the bacteria cell approaches the nominal 0.45 µm pore size and could potentially be retained through sieving by the membrane.

In addition to size-exclusion based retention based on pore size selection, adsorption of bacteria to the membrane likely plays a role. While the membranes are all considered low protein binding or low adsorption by the manufacturers, some level of adsorption is still possible. Even for hydrophilic membranes with very large pore sizes, when challenged with a high concentration of bacteria some retention through adsorption is observed[32]. To assess the role of adsorption in the performance of these membranes, filtration of *B. diminuta* through specific membranes was repeated with the addition of 0.1% Tween™ 20 to the solution. Tween™ 20 is a surfactant which can change the surface charge of a surface, prevent electrostatic interactions, and also provides a steric hinderance[33] all resulting in a reduced level of adsorption. The four 0.22 µm were first tested at 200 kPa with the added 0.1% Tween™ 20, and all membranes still completely retained the *B. diminuta*, resulting in sterile filtrate. Next, the Express 0.45 µm, Sartorius CA 0.45 µm, and

Sartorius PES 0.45 µm were tested at 6.9, 14, and 34 kPa respectively with the added surfactant. These conditions were selected as the highest pressures where complete retention of *B. diminuta* had previously been demonstrated with each membrane (indicated by asterisks in Figure 3.3). The Express 0.45 and Sartorius CA 0.45 maintained their performance in the presence of 0.1% Tween™ 20 and fully retained the *B. diminuta*, while the Sartorius PES 0.45 µm allowed 1.8 ± 0.4 log CFU/mL to pass through. The addition of surfactant decreased the performance of the Sartorius 0.45 µm PES membrane, indicating that adsorption is involved in the ability to retain bacteria. It is unclear if adsorption is a significant factor in only the Sartorius PES membrane performance, or if a decrease in performance experienced by the other membranes was simply not significant enough to be observed. Regardless, if considering the 0.45 µm membranes as sterile filters, the impact of solution components is a critical criterion. Proper evaluation of sterile filtration performance should be performed in a medium resembling the final product as opposed to simple buffer or saline, as per FDA guidelines[12].

3.4.4. Membrane Zeta Potential

As an additional approach to characterize the 0.45 µm membranes used in this study, the zeta potential in both SLB and a standard 1 mM KCl electrolyte over a pH range of 3 to 11 was measured (Figure 3.4). An increase in ionic strength is known to lower the magnitude of the zeta potential, while varying the species of ion can influence the zeta potential due to differences in ion mobility[34] and so a large difference in ionic strength between the two electrolyte solutions was expected. Membrane zeta potential values reported in literature are highly variable, with zeta potential values for a Durapore 0.22 µm membrane measured using the Surpass 3 instrument, streaming potential method, and 1mM KCl electrolyte solution being reported as both -23 mV[35]

and -38 mV[36] at approximately pH 9, while this work measured the zeta potential to be -21 mV at that pH (Figure S3.8). Furthermore, other work has found that the zeta potential of the Durapore 0.22 µm membrane was much lower magnitude at low pH (i.e pH below 4)[36] compared to the results presented here. It was observed that membranes made of the same material (Millipore Express and Sartorius PES) had distinctly different values. Comparing membranes with varying pore sizes and the same material (Figure S3.8), the difference in zeta potential was either relatively small, up to 5 mV depending on the pH (Millipore Express and Durapore), or not a significant difference (Sartorius PES and Sartorius CA). Furthermore, the zeta potential of *B. diminuta* in SLB was measured and found to be -3.9 ± 0.6 mV. Previously reported values for the zeta potential of *B. diminuta* include -3.8 mV measured in 150 mM NaCl, pH 5.5 (same salt and ionic strength as SLB)[16] and -1.9 ± 0.2 mV measured in 20 mM sodium phosphate buffer, pH 7.1[19], which are similar to the value obtained in this study. Generally, for hydrophilic surfaces larger negative zeta potentials will better repel negatively charged bacteria[37,38], but despite this no correlation was observed between membrane zeta potential and bacteria retention. Previous work has found that when testing a variety of bacteria with different surface charges, there was no correlation with transmission through a single membrane[16]. The present study shows that for a variety of membranes with different surface charges, there is no correlation with the transmission of a single bacteria, further confirming that the ability of bacteria to be retained by a membrane is not related to surface charge properties. Therefore, any interactions between the bacteria and the membrane surface in this situation are likely driven by Van der Waals or hydrophobic forces, however further work would be required to verify this.
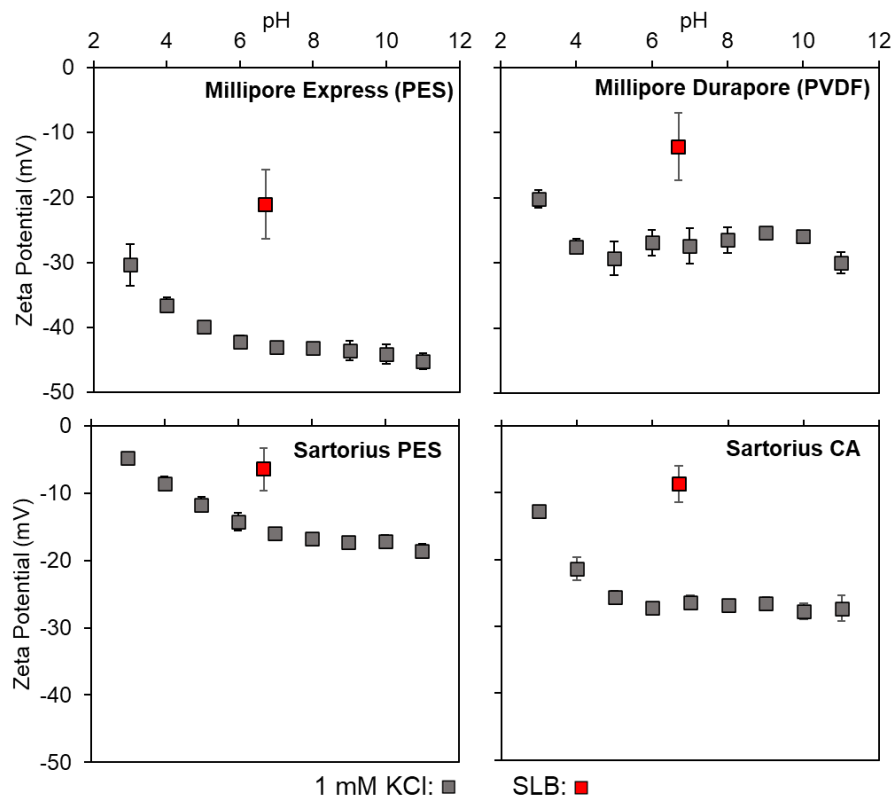
Figure 3.4: Zeta potential of the various 0.45 µm membranes, measured over a pH range of 3 to 11 in 1 mM KCl, and measured in the experimentally relevant saline lactose broth (SLB; ionic strength 150 mM, pH 6.9).

3.4.5. Sterile filtration of VSV

The data presented here has demonstrated how in the appropriate low-pressure conditions, certain 0.45 µm membranes are able to completely retain a challenge test of *B. diminuta* under the same methodology used to validate sterile filters. While further work is required to add robustness to this claim, such as testing lot-to-lot variance between membranes, it is nonetheless a worthwhile contribution given the need to improve the sterile filtration of certain biotherapeutics where 0.22 µm sterile filtration can result in considerable losses. To demonstrate this, the filtration and recovery of VSV through both a 0.22 and 0.45 µm membrane was compared. The Sartorius 0.45 µm CA membrane was specifically chosen for this test, as it was able to fully retain the *B. diminuta*

at the highest pressure of 34 kPa. As shown in Figure 3.5, from a starting titer of $9.3 \pm 3 \times 10^8$ PFU/mL, the filtrate of the 0.22 and 0.45 µm membranes contained $5.5 \pm 2 \times 10^8$ and $7.8 \pm 2 \times 10^8$ PFU/mL respectively. This is equivalent to a filtration recovery (ratio of titer in the filtrate to titer in the feed) of $61 \pm 10\%$ and $84 \pm 20\%$ for the 0.22 and 0.45 µm membranes. The loss of virus titer is statistically significant for the 0.22 µm membrane ($p<0.01$) while it is not significant for the 0.45 µm membrane ($p>0.1$). In addition, filtration of VSV through the 0.22 µm membrane occurred at an approximate average flux of 12 mL min^{-1} cm^{-2} which improved to 26 mL min^{-1} cm^{-2} for the 0.45 µm membrane. Filtration of the VSV was significantly improved when comparing the Sartorius 0.45 µm CA membrane to a conventional sterile filter Sartorius 0.22 µm CA membrane in terms of both the product yield and throughput. This demonstrates that sterile filtration with 0.45 µm membranes could be applied to increase the recovery of difficult to sterile filter virus. Lentivirus, an increasingly popular platform for gene therapy applications, is notorious for low recovery during 0.22 µm sterile filtration[9]. Furthermore, some viruses such as measles virus[39] and vaccinia virus[40] are simply too large for sterile filtration with 0.22 µm rated membranes to be feasible
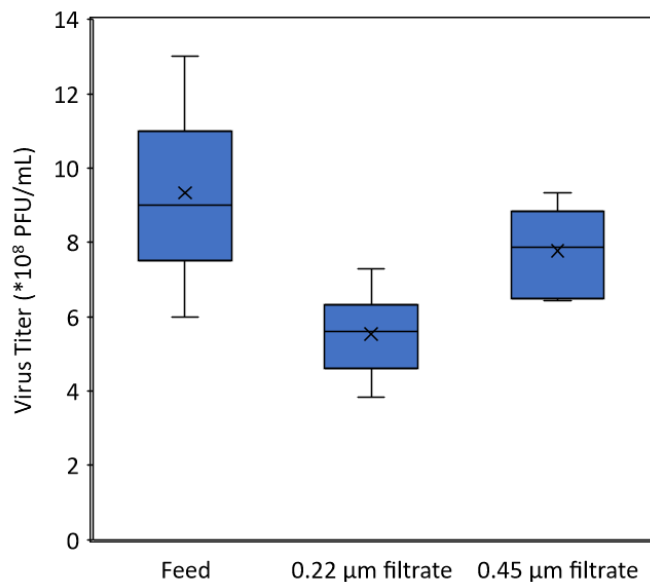
Figure 3.5: VSV titer in the feed and filtrate after triplicate filtration experiments through either a 0.22 or 0.45 µm Sartorius PES membrane at 34 kPa. Box and whisker plot depicts the interquartile range with the shaded area, the horizontal lines represent the median, the cross mark represent the mean and the whiskers extending from the boxes show the maximum and minimum values measured.

3.5. Conclusions

This study provides valuable data on the *B. diminuta* retention properties of a wide range of commercial membranes with varying physical and chemical properties. It has been shown that specific 0.45 µm rated membranes are able to fully retain a *B. diminuta* challenge test of a minimum 10^7 CFU/cm^2 of membrane area, performed in accordance with ASTM F838, when filtration is performed under low pressure. Retention varied greatly between membranes, with the most effective membrane being the Sartorius PES 0.45 µm which retained the *B. diminuta* at up to 34 kPa. For all 0.45 µm membranes, and not for any 0.22 or 0.8 µm membranes, a clear trend was observed between increased pressure and decreased bacteria retention. Additional testing was performed with the surfactant Tween™ 20 added to the feed solution, and this resulted in a decrease in bacteria retention. Results show that pore size is the dominant factor for determining retention,

indicating that size exclusion is the main mechanism by which the bacteria are retained, however the results with added surfactant show that adsorption does also play some role. Specific membrane properties such as the surface pore size (as observed using SEM imaging) and surface zeta potential were not corelated to bacteria retention; membranes with similar values often performed differently and there were no clear overall trends with bacteria retention.

Given that specific 0.45 µm membranes under the appropriate conditions were able to fully retain the *B. diminuta* challenge, they can theoretically act as sterile filters. To highlight the importance of this outcome, a direct comparison of the sterile filtration performance of a therapeutic virus through both 0.22 and 0.45 µm membranes was compared. In terms of product recovery, the 0.22 µm membrane resulted in a significant loss of the virus, while the 0.45 µm membrane had no significant difference in virus titer between the feed and filtrate. For biotherapeutic products with large particles sizes, many traditional 0.22 µm membranes are not an ideal technology for sterile filtration due to product losses. This work has demonstrated that using larger pore size membranes may be a viable alternative and that virus recovery can be improved while still meeting the required bacteria retention characteristics. This could also indicate the need for a new generation of membrane technologies which are tuned to an intermediate pore size designation which is better designed to maximize the transmission of larger biotherapeutic particles.

3.6. References

1. Alhakamy NA, Curiel DT, Berkland CJ. The era of gene therapy: From preclinical development to clinical application. *Drug Discov Today*. 2021;26(7):1602-1619. doi:10.1016/j.drudis.2021.03.021

2. Moleirinho MG, Silva RJS, Alves PM, Carrondo MJT, Peixoto C. Current challenges in biotherapeutic particles manufacturing. *Expert Opin Biol Ther*. 2020;20(5):451-465. doi:10.1080/14712598.2020.1693541

3. Zydney AL. New developments in membranes for bioprocessing – A review. *J Membr Sci*. 2021;620:118804. doi:10.1016/j.memsci.2020.118804

4. Allmendinger A, Mueller R, Huwyler J, Mahler HC, Fischer S. Sterile Filtration of Highly Concentrated Protein Formulations: Impact of Protein Concentration, Formulation Composition, and Filter Material. *J Pharm Sci*. 2015;104(10):3319-3329. doi:10.1002/jps.24561

5. Yamashita T, Takahashi Y, Nishikawa M, Takakura Y. Effect of exosome isolation methods on physicochemical properties of exosomes and clearance of exosomes from the blood circulation. *Eur J Pharm Biopharm*. 2016;98:1-8. doi:10.1016/j.ejpb.2015.10.017

6. Emami P, Fallahianbijan F, Dinse E, et al. Fouling Behavior during Sterile Filtration of Different Glycoconjugate Serotypes Used in Conjugate Vaccines. *Pharm Res*. 2021;38(1):155-163. doi:10.1007/s11095-020-02983-w

7. Taylor N, Ma W, Kristopeit A, Wang S, Zydney AL. Evaluation of a sterile filtration process for viral vaccines using a model nanoparticle suspension. *Biotechnol Bioeng*. 2021;118(1):106-115. doi:10.1002/bit.27554

8. Shoaebargh S, Gough I, Fe Medina M, et al. Sterile filtration of oncolytic viruses: An analysis of effects of membrane morphology on fouling and product recovery. *J Membr Sci*. 2018;548:239-246. doi:10.1016/j.memsci.2017.11.022

9. Valkama AJ, Oruetxebarria I, Lipponen EM, et al. Development of Large-Scale Downstream Processing for Lentiviral Vectors. *Mol Ther - Methods Clin Dev*. 2020;17:717-730. doi:10.1016/j.omtm.2020.03.025

10. Comisel RM, Kara B, Fiesser FH, Farid SS. Lentiviral vector bioprocess economics for cell and gene therapy commercialization. *Biochem Eng J*. 2021;167:107868. doi:10.1016/j.bej.2020.107868

11. Meltzer TH, Jornitz MW. The Sterilizing Filter and Its Pore Size Rating. *Am Pharm Rev*. 2003;6:6.

12. FDA. *Sterile Drug Products Produced by Aseptic Processing — Current Good Manufacturing Practice*. Center for Drug Evaluation and Research, Food and Drug Administration; 2004.

13. ASTM. *F838-20: Standard Test Method for Determining Bacterial Retention of Membrane Filters Utilized for Liquid Filtration*. American Society for Testing and Materials; 2020. Accessed November 29, 2021. https://www.astm.org/f0838-20.html

14. Tanny GB, Strong DK, Presswood WG, Meltzer TH. Adsorptive retention of Pseudomonas diminuta by membrane filters. *J Parenter Drug Assoc*. 1979;33(1):40-91.

15. Trotter AM, Thoma P, Rodrigues P. The Usefulness of 0.45 µm Rated Filter Membranes. *Pharm Technol*. 2002;26(4). Accessed April 7, 2022. https://www.pharmtech.com/view/usefulness-045-181m150rated-filter-membranes

16. Lebleu N, Roques C, Aimar P, Causserand C. Role of the cell-wall structure in the retention of bacteria by microfiltration membranes. *J Membr Sci*. 2009;326(1):178-185. doi:10.1016/j.memsci.2008.09.049

17. Wang Y, Hammes F, Düggelin M, Egli T. Influence of Size, Shape, and Flexibility on Bacterial Passage through Micropore Membrane Filters. *Environ Sci Technol*. 2008;42(17):6749-6754. doi:10.1021/es800720n

18. Helling A, Kubicka A, Schaap IAT, et al. Passage of soft pathogens through microfiltration membranes scales with transmembrane pressure. *J Membr Sci*. 2017;522:292-302. doi:10.1016/j.memsci.2016.08.016

19. Helling A, König H, Seiler F, Berkholz R, Thom V, Polakovic M. Retention of Acholeplasma laidlawii by Sterile Filtration Membranes: Effect of Cultivation Medium and Filtration Temperature. *PDA J Pharm Sci Technol*. 2018;72(3):264-277. doi:10.5731/pdajpst.2017.008102

20. Helling A, Grote C, Büning D, et al. Influence of flow alterations on bacteria retention during microfiltration. *J Membr Sci*. 2019;575:147-159. doi:10.1016/j.memsci.2019.01.021

21. Gaveau A, Coetsier C, Roques C, Bacchin P, Dague E, Causserand C. Bacteria transfer by deformation through microfiltration membrane. *J Membr Sci*. 2017;523:446-455. doi:10.1016/j.memsci.2016.10.023

22. Ge P, Tsao J, Schein S, Green TJ, Luo M, Zhou ZH. Cryo-EM Model of the Bullet-Shaped Vesicular Stomatitis Virus. *Science*. 2010;327(5966):689-693. doi:10.1126/science.1181766

23. Munis AM, Bentley EM, Takeuchi Y. A tool with many applications: vesicular stomatitis virus in research and medicine. *Expert Opin Biol Ther*. 2020;20(10):1187-1201. doi:10.1080/14712598.2020.1787981

24. Wright E, Kawka K, Medina MFC, Latulippe DR. Evaluation of Host Cell Impurity Effects on the Performance of Sterile Filtration Processes for Therapeutic Viruses. *Membranes*. 2022;12(4):359. doi:10.3390/membranes12040359

25. Lee SH, Lee SS, Kim CW. Changes in the cell size of Brevundimonas diminuta using different growth agitation rates. *PDA J Pharm Sci Technol*. 2002;56(2):99-108.

26. Kjelleberg S, Hermansson M. Starvation-induced effects on bacterial surface characteristics. *Appl Environ Microbiol*. 1984;48(3):497-503. doi:10.1128/aem.48.3.497-503.1984

27. Baldwin WW, Sheu MJ, Bankston PW, Woldringh CL. Changes in buoyant density and cell size of Escherichia coli in response to osmotic shocks. *J Bacteriol*. 1988;170(1):452-455. doi:10.1128/jb.170.1.452-455.1988

28. Lee A, McVey J, Faustino P, et al. Use of Hydrogenophaga pseudoflava Penetration To Quantitatively Assess the Impact of Filtration Parameters for 0.2-Micrometer-Pore-Size Filters. *Appl Environ Microbiol*. 2010;76(3):695-700. doi:10.1128/AEM.01825-09

29. Czerwińska-Główka D, Krukiewicz K. Guidelines for a Morphometric Analysis of Prokaryotic and Eukaryotic Cells by Scanning Electron Microscopy. *Cells*. 2021;10(12):3304. doi:10.3390/cells10123304

30. Meltzer TH, Jornitz MW. The Sterilizing Filter and Its Pore Size Rating. *Am Pharm Rev*. 2003;6:6.

31. Taylor N, Ma WJ, Kristopeit A, Wang S ching, Zydney AL. Retention characteristics of sterile filters – Effect of pore size and structure. *J Membr Sci*. 2021;635:119436. doi:10.1016/j.memsci.2021.119436

32. Bobbitt JA, Betts RP. The removal of bacteria from solutions by membrane filtration. *J Microbiol Methods*. 1992;16(3):215-220. doi:10.1016/0167-7012(92)90006-P

33. Zhong H, Liu G, Jiang Y, et al. Transport of bacteria in porous media and its enhancement by surfactants for bioaugmentation: A review. *Biotechnol Adv*. 2017;35(4):490-504. doi:10.1016/j.biotechadv.2017.03.009

34. Burns DB, Zydney AL. Buffer effects on the zeta potential of ultrafiltration membranes. *J. Mem. Sci*. 20001;172(1-2):39-48.

35. Ladner DA, Steele M, Weir A, Hristovski K, Westerhoff P. Functionalized nanoparticle interactions with polymeric membranes. *J. Haz. Matl*. 2012 15;211:288-95.

36. Nguyen MN, Loulergue P, Karpel N, Teychene B. Electron beam irradiation of polyvinylidene fluoride/polyvinylpyrrolidone ultrafiltration membrane in presence of zwitterions molecules evaluation of filtration performances. *Rad. Phys. Chem*. 2019:1(159):101-110.

37. Oh JK, Yegin Y, Yang F, et al. The influence of surface chemistry on the kinetics and thermodynamics of bacterial adhesion. *Sci Rep*. 2018;8(1):17247. doi:10.1038/s41598-018-35343-1

38. Redman JA, Walker SL, Elimelech M. Bacterial Adhesion and Transport in Porous Media: Role of the Secondary Energy Minimum. *Environ Sci Technol*. 2004;38(6):1777-1785. doi:10.1021/es034887l

39. Loewe D, Dieken H, Grein TA, Weidner T, Salzig D, Czermak P. Opportunities to debottleneck the downstream processing of the oncolytic measles virus. *Crit Rev Biotechnol*. 2020;40(2):247-264. doi:10.1080/07388551.2019.1709794

40. Tang VA, Renner TM, Varette O, et al. Single-particle characterization of oncolytic vaccinia virus by flow virometry. *Vaccine*. 2016;34(42):5082-5089. doi:10.1016/j.vaccine.2016.08.074

3.7. Acknowledgements

3.8. Supplementary Material

Table S3.1: *B. diminuta* feed and filtrate concentration for all filtration experiments performed in this work. Data is reported as average ± standard deviation, with N/D signifying that no bacteria were detected in the filtrate.

Membrane	Pressure (kPa)	Feed (CFU/mL)	Filtrate (CFU/mL)		
			Test 1	Test 2	Test 3
Durapore 0.22 µm	210	$1.0 \pm 0.3 \times 10^7$	N/D	N/D	N/D
Express 0.22 µm		$2.0 \pm 0.7 \times 10^7$	N/D	N/D	N/D
Sartorius CA 0.22 µm		$1.6 \pm 0.5 \times 10^7$	N/D	N/D	N/D
Sartorius PES 0.22 µm		$1.0 \pm 0.5 \times 10^7$	N/D	N/D	N/D
Durapore 0.45 µm	3.4	$1.5 \pm 0.2 \times 10^7$	$1.1 \pm 0.3 \times 10^3$	$8.5 \pm 0.5 \times 10^2$	$8.5 \pm 0.6 \times 10^2$
	6.9	$1.3 \pm 0.3 \times 10^7$	$3.1 \pm 1 \times 10^3$	$6.8 \pm 0.9 \times 10^3$	$6.8 \pm 0.7 \times 10^3$
	14	$7.7 \pm 0.2 \times 10^6$	$2.4 \pm 1 \times 10^3$	$2.7 \pm 0.2 \times 10^3$	$3.3 \pm 0.3 \times 10^3$
	34	$2.4 \pm 0.7 \times 10^7$	$6.4 \pm 2 \times 10^3$	$8.4 \pm 2 \times 10^3$	$4.0 \pm 1.3 \times 10^3$
	69	$4.8 \pm 0.8 \times 10^7$	$9.6 \pm 1 \times 10^4$	$2.1 \pm 0.5 \times 10^5$	$7.1 \pm 0.9 \times 10^4$

Membrane					
	100	$3.5 \pm 0.7 \times 10^7$	$2.2 \pm 0.6 \times 10^5$	$1.8 \pm 0.4 \times 10^5$	$3.2 \pm 0.5 \times 10^5$
Express 0.45 µm	3.4	$2.1 \pm 0.3 \times 10^7$	N/D	N/D	N/D
	6.9	$1.7 \pm 0.6 \times 10^7$	N/D	N/D	N/D
	14	$2.4 \pm 0.7 \times 10^7$	$1.3 \pm 0.6 \times 10^1$	$3.2 \pm 0.4 \times 10^2$	$3.3 \pm 0.6 \times 10^1$
	34	$3.6 \pm 0.4 \times 10^7$	$5.4 \pm 1 \times 10^2$	$8.6 \pm 0.5 \times 10^2$	$6.4 \pm 1 \times 10^2$
	69	$2.1 \pm 0.4 \times 10^7$	$1.1 \pm 0.06 \times 10^3$	$1.4 \pm 0.2 \times 10^3$	$6.4 \pm 0.1 \times 10^2$
	100	$3.7 \pm 0.6 \times 10^7$	$2.7 \pm 0.5 \times 10^3$	$3.7 \pm 0.4 \times 10^3$	$3.5 \pm 0.7 \times 10^3$
Sartorius CA 0.45 µm	3.4	$2.8 \pm 0.8 \times 10^7$	N/D	N/D	N/D
	6.9	$1.4 \pm 0.1 \times 10^7$	N/D	N/D	N/D
	14	$1.3 \pm 0.7 \times 10^7$	N/D	N/D	N/D
	34	$2.9 \pm 0.3 \times 10^7$	2.1 ± 1	7.0 ± 3	1.8 ± 0.5
	69	$1.2 \pm 0.6 \times 10^7$	$1.2 \pm 0.2 \times 10^3$	$2.7 \pm 1 \times 10^3$	$2.8 \pm 0.4 \times 10^3$
	100	$1.3 \pm 0.7 \times 10^7$	$2.6 \pm 1 \times 10^3$	$2.4 \pm 1 \times 10^4$	$5.2 \pm 0.4 \times 10^4$
Sartorius PES 0.45 µm	3.4	$1.77 \pm 1 \times 10^7$	N/D	N/D	N/D
	6.9	$1.4 \pm 0.9 \times 10^7$	N/D	N/D	N/D
	14	$1.2 \pm 0.4 \times 10^7$	N/D	N/D	N/D
	34	$2.0 \pm 1 \times 10^7$	N/D	N/D	N/D
	69	$3.6 \pm 0.7 \times 10^7$	$2.0 \pm 1 \times 10^1$	$1.3 \pm 0.6 \times 10^1$	$6.7 \pm 3 \times 10^1$
	100	$3.6 \pm 0.6 \times 10^7$	$2.9 \pm 0.7 \times 10^2$	$4.0 \pm 2 \times 10^2$	$6.7 \pm 2 \times 10^2$
Sartorius CA 0.8 µm	3.4	$3.1 \pm 0.3 \times 10^7$	$6.3 \pm 2 \times 10^6$	$4.0 \pm 1 \times 10^6$	$6 \pm 1 \times 10^6$
	6.9	$2.6 \pm 0.8 \times 10^7$	$3.7 \pm 1 \times 10^6$	$3.7 \pm 2 \times 10^6$	$3.4 \pm 2 \times 10^6$
	14	$1.3 \pm 0.2 \times 10^7$	$4.3 \pm 0.7 \times 10^6$	$2.7 \pm 0.9 \times 10^6$	$1.7 \pm 0.5 \times 10^6$
	34	$6.7 \pm 2 \times 10^6$	$1.1 \pm 0.2 \times 10^6$	$1.3 \pm 0.5 \times 10^6$	$1.1 \pm 0.4 \times 10^6$
	69	$1.5 \pm 0.2 \times 10^7$	$3.7 \pm 0.8 \times 10^6$	$3.3 \pm 0.4 \times 10^6$	$4.0 \pm 0.8 \times 10^6$
	100	$2.4 \pm 0.6 \times 10^7$	$1.5 \pm 0.3 \times 10^6$	$3.0 \pm 0.4 \times 10^6$	$2.4 \pm 0.5 \times 10^6$

Table S3.2: *B. diminuta* feed and filtrate concentration for filtration experiments comparing the effect of added surfactant in solution. Data is reported as average ± standard deviation, with N/D signifying that no bacteria were detected in the filtrate. Results without added surfactant are repeated from Table S1 for ease of comparison.

Membrane	Pressure (kPa)	Surfactant	Feed (CFU/mL)	Filtrate (CFU/mL)		
				Test 1	Test 2	Test 3
Express 0.45	6.9	N/A	$1.7 \pm 0.6 \times 10^7$	N/D	N/D	N/D
		0.1% Tween 20	$2.6 \pm 0.9 \times 10^7$	N/D	N/D	N/D
Sartorius CA 0.45 µm	14	N/A	$1.3 \pm 0.7 \times 10^7$	N/D	N/D	N/D
		0.1% Tween 20	$1.3 \pm 1 \times 10^7$	N/D	N/D	N/D
Sartorius PES 0.45 µm	34	N/A	$2.0 \pm 1 \times 10^7$	N/D	N/D	N/D
		0.1% Tween 20	$1.2 \pm 1 \times 10^7$	$4.7 \pm 2 \times 10^1$	$2.6 \pm 0.5 \times 10^2$	$2.7 \pm 1 \times 10^1$
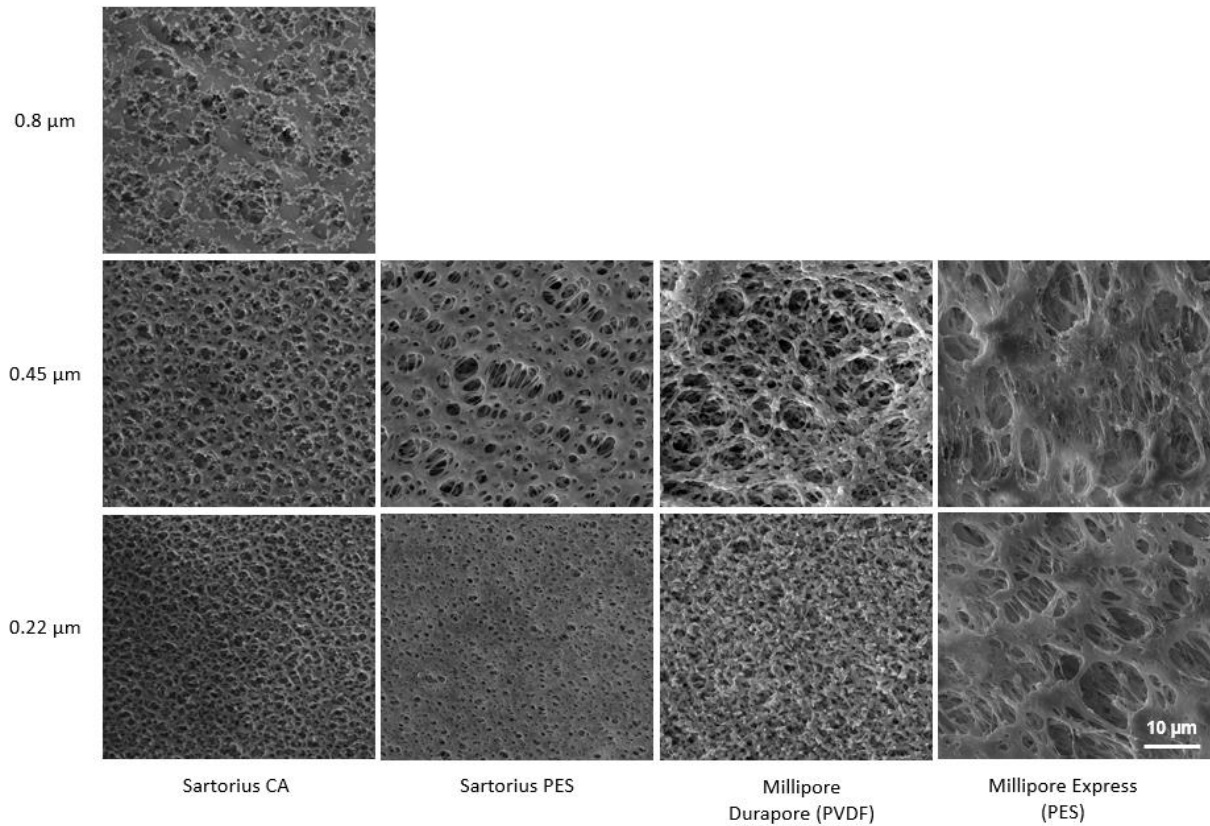
Figure S3.6: Scanning electron microscopy images of all membrane used in this study, highlighting the pore structure on the surface of the membrane. Images obtained at 5000 × magnification.
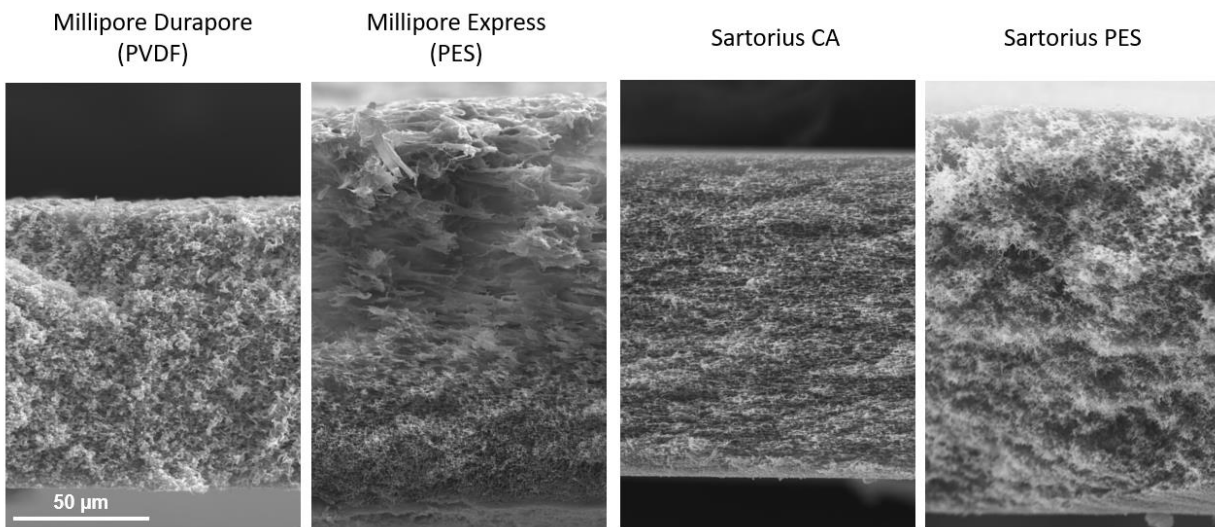
Figure S3.7: Cross section scanning electron microscopy images of the 0.45 µm membrane used in this study. Images obtained at $1000 \times$ magnification
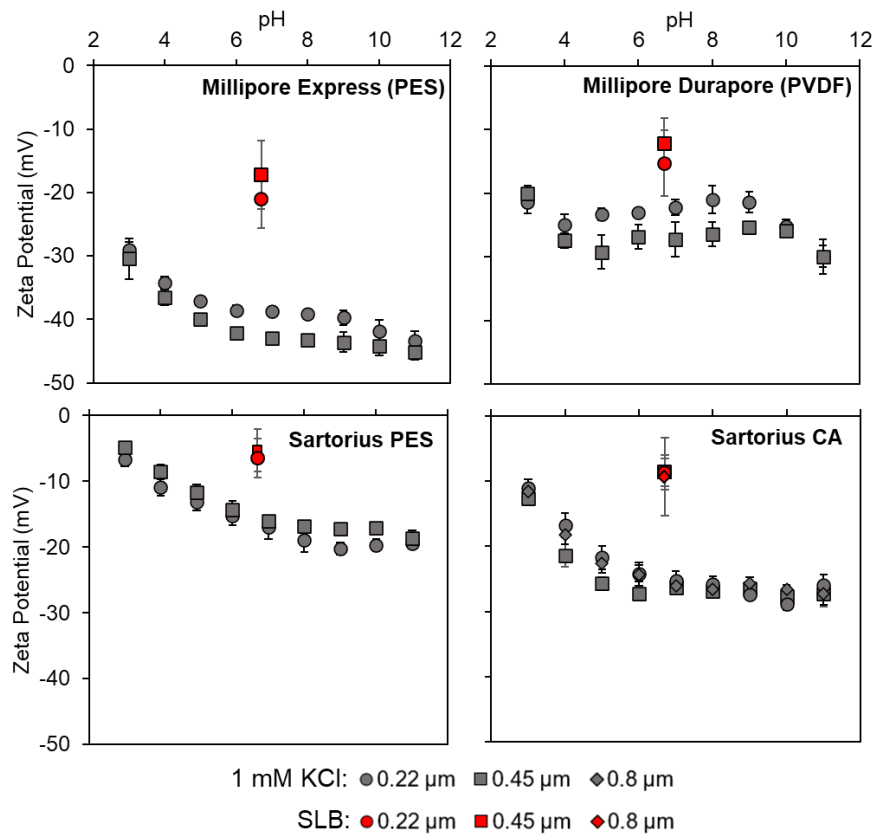
Figure S3.8: Zeta potential of all membranes used in this study, measured over a pH range of 3 to 11 in 1 mM KCl, and measured in the experimentally relevant saline lactose broth (SLB; ionic strength 150 mM, pH 6.9).

Chapter 4

Investigating the Effects of Residual Host Cell Impurities on the Sterile Filtration Performance of a Therapeutic Virus

4. Investigating the Effects of Residual Host Cell Impurities on the Sterile Filtration Performance of a Therapeutic Virus

Evan Wright, Karina Kawka, Maria Fe C. Medina, David R. Latulippe

4.1. Abstract

Efficient downstream processing represents a significant challenge in the rapidly developing field of therapeutic viruses. While it is known that the terminal sterile filtration step can be a major cause of product loss, there is little known about the effect of host cell impurities (DNA and protein) on filtration performance. In this study, fractions of relatively pure Vero host cell protein and DNA were isolated and then spiked them into a highly pure preparation of vesicular stomatitis virus (VSV). The spiked virus solutions were then sterile filtered using two commercially available microfiltration membranes. Using a combination of transmembrane pressure measurements, virus recovery measurements, and post-filtration microscopy images of the microfiltration membranes, it is demonstrated how host cell protein content plays a major role in both membrane fouling and virus losses during sterile filtration. This effect was consistent across both tested membranes and was also observed in static adsorption experiments. The results presented in this work indicate that an "isolate and spike" methodology is valuable for those interested in better understanding and optimizing a downstream purification process for therapeutic viruses.

4.2. Introduction

Therapeutic viruses are an important and rapidly developing class of biotherapeutics, with applications ranging from cancer treatment[1–3] to novel vaccines[4]. As of 2017, 38% of new therapeutics approved by the FDA were biologics-based[5], and this number is expected to continue to grow in the future. Thus, researchers have been increasingly focusing on developing efficient and scalable methods to manufacture therapeutic virus. Many advances have been made in upstream processing in recent years, such as the development of novel cell lines[6] or new bioreactor designs[7]; as a result, bottlenecking in the production process has shifted to downstream processing steps[8,9], which can represent up to 70% of the overall manufacturing costs[9]. Fortunately, progress in various areas of downstream purification, including harvest and clarification, chromatography, and ultrafiltration[11], has helped to relieve this bottleneck.

The terminal sterile filtration step, which is required by regulatory agencies to ensure that the final product is free of any bacterial bioburden[12], is an often-overlooked component of the downstream purification train. While sterile filtration is not an issue in many cases, some studies have reported high losses for lentivirus[8], influenza virus[13], enterovirus[14], and rhabdovirus[15] during this process. In situations where significant virus loss occurs during sterile filtration, alternative strategies can be applied, such as the aseptic processing of a virus[16] or reorganizing the downstream processing train[17], however this is not desirable due to cost and complexity. For some larger viruses, such as herpes virus (~200 nm)[18] or vaccinia virus (~250 nm)[19], sterile filtration is particularly challenging due to their size being similar to the rated pore size of sterile filtration membranes (0.22 µm). In all these cases, it is critical to understand the factors that influence the sterile filtration of viruses, as doing so is key to minimizing losses.

Clarification is a common membrane microfiltration unit operation which as been thoroughly studied[20], however key considerations such as relative virus and impurity content, degree of fouling experienced during filtration, and solution components render it significantly different from sterile filtration. Similarly, many studies have investigated the removal or retention of viruses using ultrafiltration membranes[21–23], but few have examined the filtration of viruses with respect to maximizing transmission and throughput. Some factors that are known to influence the sterile filtration of viruses include the presence of aggregates[24,25], the membrane material and structure[15], and the solution conditions[26]. In general, two mechanisms govern the retention of viruses by the membrane: size exclusion and adsorption. As the ratio between the virus particle size and the membrane pore size decreases, it becomes more difficult for the virus to transmit through the membrane and more likely that it will be retained[27,28]. For effective sterile filtration, a 0.22 µm pore size rating is required based on challenge tests with *Brevundimonas diminuta*[29], however selection of different membrane structures (i.e. symmetric vs asymmetric, pore geometry) can still influence particle retention and membrane fouling[30,31]. In addition, viruses may also adsorb directly to the membrane through a combination of electrostatic and hydrophobic effects; this is influenced by membrane chemistry, the pH and ionic strength of the solution, and the presence of any additives or other components in solution[26,32,33]. For biopharmaceutical applications, virus formulation buffers are often precisely optimized in order to maximize virus stability[34,35], which leaves little room for modifications aimed at improving filtration performance.

One modification that can be made to improve the filtration process is to minimize the amount of residual protein and DNA impurities. DNA impurities can originate from host cells in

the culture system, or if applicable, helper components such as other viruses or plasmids[36]; similarly, protein impurities are derived from host cells or are present in culture media components (i.e., fetal bovine serum)[36]. Guidelines relating to these impurities are typically strict and evaluated on a case-by-case basis[37], depending on the risks they pose. Particular concerns relating to product safety include the oncogenicity of residual DNA and the immunogenicity of residual proteins[36,38]. Although impurities are typically removed during downstream processing prior to sterile filtration, some small residual amounts can remain. This can be problematic, as small residual amounts of DNA have been shown to mediate aggregation in adenovirus and lead to reduced recovery after sterile filtration[24,25]. Beyond this, to our knowledge, no other prior work has investigated how small amounts of residual host cell impurities affect the sterile filtration performance of therapeutic viruses.

Studies using monoclonal antibodies have shown that numerous species of host cell proteins are still present in final formulations, even after downstream purification[39,40]. These residual proteins are a diverse population that possess a range of molecular weights, isoelectric points, and hydrophilicities[41], as well as specific properties, such as charge, structure, and reactivity, that have all been shown to influence membrane fouling[42]. Furthermore, studies in related areas have shown that residual DNA can mediate the aggregation of proteins, thus leading to membrane fouling[43], and that protein aggregates can form nucleation sites on membranes, which contributes to further fouling[44,45].

It is therefore possible that residual host cell proteins and DNA, either alone or in combination, may play a role in membrane fouling during the sterile filtration of therapeutic

viruses. The present study consists of a series of small-scale sterile filtration tests using viruses prepared with a defined amount of host cell protein and DNA impurities. These conditions were achieved by first producing a highly pure virus batch via sucrose gradient (SG) ultracentrifugation, and then spiking host cell protein or DNA into the virus preparation at a consistent level. The overall filtration performance was then assessed by monitoring the changes in transmembrane pressure (indicative of fouling) during filtration and measuring the amount of virus recovered after filtration. Since sucrose gradient ultracentrifugation cannot be scaled up for large-scale manufacturing[9,46], hydrophobic interaction membrane chromatography (HIC) was used as an alternative approach for purifying a batch of virus and comparing the performance of sterile filtration on these samples. Static adsorption studies were subsequently performed to develop a more in-depth understanding of the interactions between the virus, the impurities, and the membrane. Vesicular stomatitis virus (VSV), a type of rhabdovirus, was selected as a model therapeutic virus for this study for its potential as an oncolytic virus[47] and as it possesses a bullet shape geometry with a relatively large size of ~70 nm in width and ~200 nm in length[48], which may present an additional challenge for typical sterile filters with a pore size of 0.22 µm.

There is a need to improve current manufacturing protocols to maximize virus recovery during 0.22 µm filtration, and an investigation of the influence of host cell impurities on filtration performance will contribute to optimizing therapeutic virus downstream processing and enabling greater production of many next-generation biopharmaceuticals.

4.3. Materials and Methods

4.3.1. Production of VSV and Isolated Host Cell Impurities

A series of purification techniques were used to produce two sub-batches of VSV, one purified via sucrose gradient ultracentrifugation (SG VSV) and another purified via HIC (HIC VSV). Isolated host cell protein (HCP) and host cell DNA (HCDNA) were also prepared from Vero cell lysates. Figure 4.1 shows a schematic of the different methodologies employed.
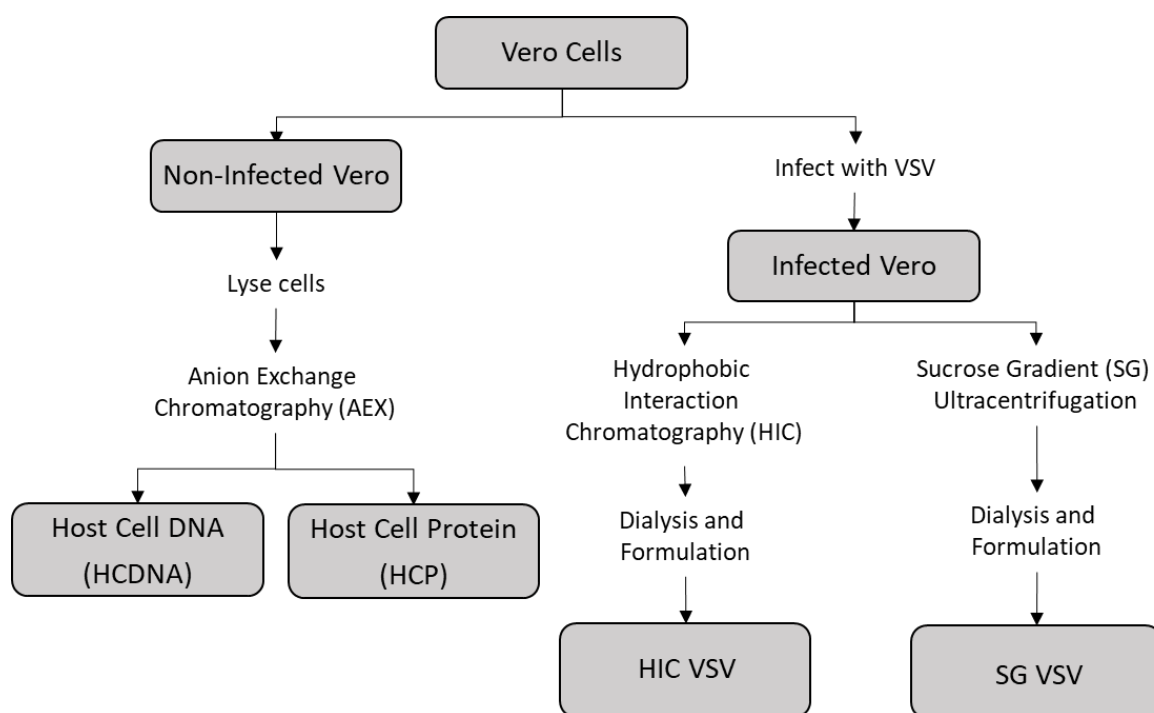
Figure 4.1: Outline of process used to isolate host cell impurities (HCDNA and HCP) and prepare sub-batches of VSV purified via sucrose gradient ultracentrifugation (SG VSV) and hydrophobic interaction chromatography (HIC VSV).

The Vero cells (ATCC CCL-81) used in this work were provided by the Robert E. Fitzhenry Vector Laboratory at McMaster University and were cultured using Dulbecco's Modified Eagle Medium (DMEM) supplemented with 10% fetal bovine serum (FBS) and 1% L-glutamine (Gibco). The cells were maintained in $150\,cm^2$ cell-culture flasks (Corning), which were

incubated at 37 °C with 5% CO_2 and passaged every 3-4 days. To expand the cells to produce uninfected Vero or VSV cultures, 15 cm diameter tissue-culture-treated dishes (Corning) were seeded at an approximate density of 5×10^5 cells/cm^2 and grown to confluence. The Vero cells were spit into new plates at a 1:2 ratio and were incubated for 24 hours. After this time, the media was removed, the cells were washed with phosphate buffered saline (PBS), and new FBS-free DMEM was added, followed by the addition of 1 mL of VSV (Indiana strain, recombinant expressing GFP[49], provided by the Robert E. Fitzhenry Vector Laboratory) at a multiplicity of infection (MOI) of 0.1. The cells were then allowed to incubate for another 24 hours, after which the cell supernatant containing virus was harvested.

The cell supernatant was portioned into 50 mL tubes, centrifuged (Beckman Coulter Allegra 6R) at 1400 ×g and 4°C for 15 minutes to pellet any cell debris, collected, and then clarified via 0.45 µm bottle top vacuum filtration (Nalgene Rapid Flow). To prevent virus aggregation, a 0.5 M EDTA (Gibco) solution (pH 8.0) was added at a ratio of 1:25. To prepare the SG VSV samples, the filtrate containing the virus was then centrifuged (Beckman Coulter Avanti J-25i) using a JLA-10.500 rotor (Beckman Coulter) at 12,200 ×g and 4 °C for 90 min to pellet the virus. The resultant supernatant was then discarded, and the virus pellet was resuspended in 1 mL of PBS). A sucrose (BioShop) gradient was created by layering 0.5 mL of 75% sucrose, 4 mL of 40% sucrose, and 4 mL of 3% sucrose in an ultracentrifuge tube (Beckman Coulter Ultra-Clear 13.2 mL) from which a linear gradient was created using a Gradient Master 108 (BioComp Instruments). Next, 1 mL of resuspended virus was placed on top of the linear sucrose gradient and ultracentrifuged using a SW41 rotor (Beckman Coulter) at 70,800 ×g and 4°C for 30 min. The purified virus was visible as a single band (approximately one third of the way down the gradient)

and was collected by puncturing the side of the tube with a syringe needle. The collected virus was then dialyzed (Slide-a-Lyser G2, 10 kDa cut-off, Thermo-Fisher) against formulation buffer (150 mM NaCl, 4% sucrose, 10 mM HEPES, pH 7.4) and further diluted to a final titer of approximately 2.4×10^8 PFU/mL. The final virus solution was then portioned into 7 mL aliquots and stored at -80°C until use.

A second sub-batch of VSV supernatant was purified using HIC, a method which has been shown to be highly effective in the purification of virus particles [50,51]. First, a Sartobind Phenyl Nano capsule (Sartorius) containing 3 mL of membrane was attached to an NGC medium-pressure liquid chromatography system (BioRad). Next, virus-containing supernatant was prepared and clarified according to the above-described procedure, then mixed with buffer containing 10 mM HEPES and 3.6 M ammonium sulfate (Sigma). The final solution consisted of 19% buffer and 81% virus supernatant, with an ammonium sulfate concentration of 700 mM and a pH of 7.4. The Nano capsule was equilibrated with 10 membrane volumes of equilibration buffer (10 mM HEPES, 4% sucrose, 700 mM ammonium sulfate, pH 7.4) at a flow rate of 9 mL/min, which was maintained throughout the experiment. Following equilibration, 10 mL of the prepared sample was applied to the capsule using the sample pump, followed by a wash step with 10 membrane volumes (30 mL) of equilibration buffer to remove any unbound impurities. Finally, the virus was eluted from the membrane via a single step change to an ammonium sulfate free buffer solution (i.e. 10 mM HEPES, 4% sucrose, pH 7.4). During the run, conductivity and UV absorbance at both 260 nm and 280 nm were continuously monitored. The 6 mL fraction containing the largest portion of virus was collected, dialyzed against formulation buffer (as described above), and stored in aliquots of approximately 7 mL at -80 °C.

Isolated host cell impurities were produced using a non-infected Vero cell culture. Confluent cells were detached from a 150 cm^2 cell-culture flask, resuspended in 10 mL of low ionic strength buffer (Buffer A, 10 mM HEPES pH 7.4, 4% sucrose), and centrifuged at 1400 ×g for 15 minutes in order to pellet the cells. The supernatant was then discarded, and the cell pellet was subjected to a 3× freeze-thaw process consisting of a cold bath in 95% ethanol and dry ice and a warm bath at 37 °C. Following the freeze-thaw process, the lysed cell pellet was diluted in another 10 mL of Buffer A, centrifuged at for 15 minutes to pellet any cell debris, and the supernatant was collected. Host cell protein and DNA were purified from this mixture using an adapted version of a previously documented method[52] and a laterally-fed membrane chromatography (LFMC) device containing 1 mL of Sartobind Q membrane (Sartorius), which is a strong anion-exchange membrane. Briefly, the membrane was first equilibrated with Buffer A, and the cell lysate was then loaded onto it using a 5 mL loop. A wash step with Buffer A was applied after loading the sample to wash any unbound material. Next, a stepwise elution profile was applied by mixing proportions of Buffer B (10 mM HEPES pH 7.4, 4% sucrose, 2 M NaCl) and Buffer A to generate steps of 450 mM, 600 mM, and 800 mM NaCl. These steps had the purpose to elute protein, a mixture of protein and DNA, and DNA, respectively. From previous experiments, a 2-step elution proved insufficient for effectively separating pure host cell protein and DNA, and therefore the 3-step elution process was necessary to remove any protein and DNA co-eluting at similar intermediate ionic strengths. In each step, 6 membrane volumes (6 mL) were eluted and collected in 3 fractions of 2 mL. A constant flow rate of 5 mL/min was used throughout the process. During the run, conductivity and UV absorbance at both 260 nm and 280 nm were continuously monitored.

4.3.2. Sterile Filtration

Sterile filtration experiments were performed on a small-scale constant flux system, with flow being driven using a syringe pump (Harvard Apparatus PhD Ultra) with a 10 mL syringe (Becton-Dickinson). During operation, a digital pressure transducer (Omega PX409) was used to measure the transmembrane pressure (TMP) relative to the atmospheric pressure. The resultant data was normalized against the starting TMP value (TMP_0) to account for variance in membrane permeability and was averaged over a 0.25 mL interval to reduce the effect of noise and oscillations introduced by the syringe pump. Silicone tubing (Cole-Parmer Masterflex L/S 14) was used to connect the syringe to a cross junction, which was also connected to the pressure transducer and a polycarbonate membrane housing (Cole Parmer) with 0.5 cm^2 of effective filtration. All tubing connections were secured using polypropylene Luer-lock fittings (McMaster-Carr). This study used either hydrophilic polyvinylidene fluoride (PVDF, Millipore Sigma, Durapore) membranes or hydrophilic polyether sulfone (PES, Millipore Sigma, Millipore Express PLUS) membranes, both of which are designed for the sterile filtration of protein or other biological solutions and have a rated pore size of 0.22 µm. It is worth noting that the PES membrane has an asymmetric pore structure, with pores being more open on the upstream side of the membrane, while the PVDF membrane is symmetric and has a consistent pore size throughout the depth of the membrane. SEM images of the membrane top, bottom, and cross section are shown in Figure S4.8. All fittings, tubing, and membranes were sterilized in an autoclave at 121 °C for 30 minutes before use.

The assembled system was first pre-wet using a syringe loaded with formulation buffer and then the membrane permeability was determined by measuring the transmembrane pressure at

various volumetric flow rates ranging from 0.1-10 mL/min. A 7 mL aliquot of VSV was thawed and, if necessary, spiked with host cell protein and/or DNA. For tests using bovine serum albumin (BSA, BioShop) as the spiking impurity, a 1 mg/mL stock solution was prepared in formulation buffer and then spiked into the VSV. The VSV solution was incubated at 37 °C for 1 hour to allow any potential interactions between the virus and impurities to take place. The VSV solution was then loaded into a new syringe, which was then connected to the pump and the pre-wet tubing and membrane system. A total of 5 mL of VSV solution were then passed through the membrane at a flow rate of 0.15 mL min^{-1} (flux of 0.3 mL min^{-1} cm^{-2}). Next, the filtrate and remaining feed solution in the syringe were collected and saved at -80°C for future analysis. Finally, the membrane was removed from the polycarbonate membrane holder, gently washed in Milli-Q water, and fixed in 1% glutaraldehyde for 30 minutes. All experiments were performed in duplicate using identical conditions, with all reported data representing the average of the two tests unless otherwise mentioned.

4.3.3. Static Adsorption

A 7 mL aliquot of VSV was thawed and further divided into 0.5 mL samples. Each 0.5 mL sample was placed into a separate 1.5 mL Eppendorf tubes and then spiked with impurities as described above. An individual membrane (1.33 cm^2 surface area) was cut into small pieces using a razor, and the different VSV solutions were then incubated for 1 hour at room temperature on an orbital shaker at approximately 60 RPM. Concurrently, spiked VSV solutions with no added membrane pieces were prepared and incubated as a control. The resultant supernatant of each solution was collected and stored at -80°C for future analysis.

4.3.4. Assays

DNA concentration was measured using a Quant-iT PicoGreen dsDNA Kit (Invitrogen) in accordance with the manufacturer's instructions. In brief, a 10 µl aliquot of each sample was diluted in 40 µl of TE buffer, which was then mixed with 50 µl of working reagent in a half-area black 96-well microplate (Perkin Elmer), followed by incubation for 5 minutes in a light-free environment. The fluorescence of the samples was measured at 520 nm emission and 480 nm excitation using a SpectraMax i3 (Molecular Devices) plate reader, and the DNA concentration was calculated in relation to a 1-1000 ng/mL Lambda DNA (Roche) calibration curve.

Protein concentration was measured using a Micro BCA Protein Assay Kit (Thermo Scientific) in accordance with the manufacturer's instructions. In brief, a 100 µl aliquot of each sample was mixed with 100 µl of working reagent in a clear 96-well microplate (Corning) and incubated at 37 °C for 2 hours. The absorbance of the samples was measured at 562 nm using a plate reader, and the protein concentration was calculated relative to a 1-40 µg/mL BSA (Thermo Scientific) calibration curve. If necessary, the samples were serially diluted prior to measurement.

VSV titer was measured using a plaque assay. Vero cells were cultured using the above-described method and seeded into a 6-well plate (Corning) at approximately 6×10^5 cells per well and incubated for 24 hours. Virus samples were serially diluted 10-fold into supplemented DMEM, which was followed by the addition of 100 µl to each well (2 dilution levels, each in triplicate). The infected wells were incubated for 1 hour at 37 °C and 5% CO_2, with manual rocking every 15 minutes. An agarose overlay solution consisting of 0.5% agarose and 10% FBS in DMEM was prepared and kept warm at 40°C; 2 mL of this overlay solution was added to each well and allowed

to solidify before incubating for another 24 hours. After this incubation period, the cells were fixed for 1 hour at room temperature by adding 1 mL of 3.7% formaldehyde to each well. The agarose plugs were then manually removed from the wells and the fixed cells were stained by adding 1 mL of 0.1 % crystal violet in 20 % ethanol to each well for 10 minutes. Excess crystal violet stain was aspirated, and the wells were then washed under a gentle stream of water. Finally, the visible plaques (transparent spots on the cell layer) were counted in order to calculate the number of plaque-forming units per mL (PFU/mL) accounting for the dilution factor.

DNA fragment length was determined using an automated electrophoresis platform (Agilent TapeStation, Genomic DNA ScreenTape, Agilent Genomic DNA Reagents). Specifically, the DNA strand length analysis consisted of a comparison of the DNA from the unpurified Vero cell lysate and the AEX chromatography-purified DNA that was used in the spiking experiments. The DNA was prepared for analysis by first concentrating it approximately 30-fold and then buffer exchanging it into 10 mM Tris-HCl, pH 8.5, 0.1 mM EDTA using a Genomic DNA Clean & Concentrator spin column kit (Zymo Research) as per the manufacturer's instructions.

Protein size analysis was performed using SDS-PAGE gel and Coomassie Blue staining. As with the DNA strand length analysis, the protein size analysis compared protein from the unpurified Vero cell lysate and the AEX chromatography-purified protein used in the spiking experiments. 10 µg of each protein sample were mixed 1:1 with Laemmli sample buffer (Biorad) and heated in boiling water for 2 minutes, followed by separation on 8-16% acrylamide tris-glycine gel (Mini-PROETAN, Bio-Rad). An 8 to 260 kDa ladder (Chameleon Duo Pre-Stained Protein

Ladder, LI-COR Biosciences) was included as a reference. After separation, the gel was gently washed for 10 minutes in deionized water water, followed by staining with Coomassie Blue (0.02% Coomassie Brilliant Blue G-250, 10% ammonium phosphate, 20% methanol, 2% phosphoric acid). The gel was incubated for 2 hours in the staining solution with gentle shaking, then rinsed with deionized water, de-stained for 10 minutes in 20% methanol, and finally imaged using a ChemiDoc MP (Biorad) gel-imaging system.

4.3.5. Scanning Electron Microscopy

Segments were cut out of fixed membranes using a razor and mounted onto specimen stubs with carbon tape. The samples were then sputter coated (Polaron E5100) with gold for 60 s under vacuum conditions at a current of 20 mA; this resulted in the application of a layer approximately 24 nm thick. The samples were then imaged using a Vega II LSU (Tescan) instrument operating at an acceleration voltage of 20 kV.

4.4. Results and Discussion

4.4.1. Production of Purified VSV Batches and Host Cell Impurities

VSV was first purified via hydrophobic interaction chromatography (HIC). The solution conditions were selected to ensure that the VSV was selectively bound to the membrane, and that impurities were washed away (appearing as the first peak in the chromatogram shown in Figure S4.9). The VSV was then eluted through a step change to buffer without ammonium sulfate resulting in the second peak in the chromatogram. HIC purification combined with dialysis buffer exchange enabled the removal of 99.7% of the protein and 90.7% of the DNA from the VSV solution. Similarly, the purification of VSV via sucrose gradient (SG) ultracentrifugation and

dialysis buffer exchange resulted in 99.95% protein and a minimum of 99.6% DNA removal. No

DNA was detected and the minimal 1.24 µg/mL of protein is likely due to the viral proteins

themselves, given previously measured values of PFU/µg protein[53] Finally, AEX membrane

chromatography was employed to isolate host cell protein and DNA. As previously demonstrated,

this method is highly effective for separating biological components[52]. After cell lysate containing

host cell proteins and DNA were applied to the membrane under low ionic strength, the different

components were selectively eluted by increasing the ionic strength in a stepwise fashion. As

shown in Figure S4.10, a step to 450 mM eluted a solution largely consisting of pure host cell

protein, with a concentration of 941 µg/mL. While there was still a small amount of residual DNA

in the protein elution, the relative concentration was not high enough to not cause a significant

change in the DNA concentration when creating the VSV samples spiked with protein. An

intermediate step to 600 mM resulted in the elution of a mixture of protein and DNA, while a third

step to 800 mM generated a highly pure host cell DNA solution (Figure S4.10) with a concentration

of 397 ng/mL and no detectable protein. The compositions of the different eluted fractions are

summarized in Table S4.2. To investigate how AEX chromatography purification affected the

properties of the host cell protein and DNA, size analysis of the two biomolecules was conducted

using electrophoretic separation. An Agilent TapeStation kit was used to generate a profile of the

DNA fragment size distribution, while SDS-PAGE and Coomassie Blue staining were used to

separate and visualize the major protein bands. Vero cell lysate DNA consisted of a minor peak at

2400 bp and a large, broad peak from approximately 5000 bp to 50,000+ bp (Figure 4.2). While

the minor peak was eliminated following AEX purification, the major broad peak was largely

retained. The purified DNA likely consisted of a distribution of large genomic DNA fragments.

Both the protein from cell lysate and the purified protein produced numerous protein bands over a

wide range of sizes. Some of these bands were maintained after AEX purification, while some were lost, and some appear to have been concentrated. While the exact protein population shifted during purification, the purified host cell protein still contained many different proteins. In other downstream processing studies, impurities for spiking have been prepared via anion exchange chromatography[54], microfiltration and diafiltration[55], flow-through from protein A chromatography[40], and simply directly spiking culture supernatant[56]. The methods described here are advantageous as the DNA and protein impurities have been individually isolated, allowing for their effects to be discriminated and studied individually.
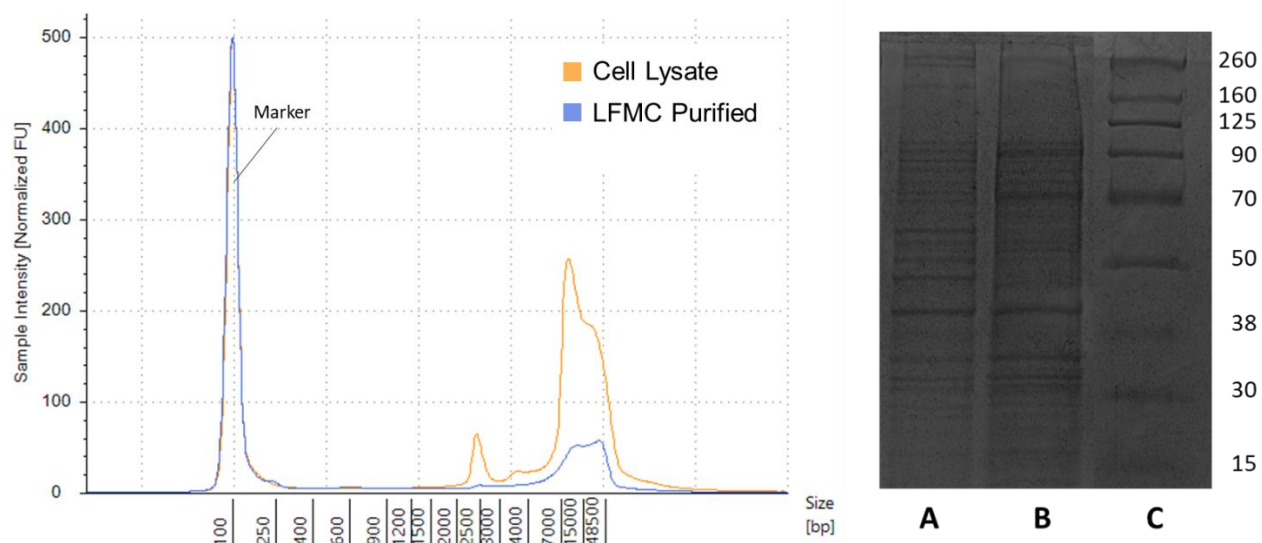
Figure 4.2: Effect of AEX chromatography purification on the size distribution of Vero host cell DNA and protein. Left) Electropherogram comparing the strand length of host cell DNA from crude cell lysate and DNA purified using AEX chromatography. Right) SDS-PAGE separation of A—Host cell protein from crude cell lysate; B—Host cell protein purified using anion exchange LFMC; C—Protein size ladder (kDa).

The isolated host cell protein and host cell DNA were then spiked into the SG VSV, resulting in the different solutions summarized in Table 4.1. Since HIC VSV had a higher degree

of impurities compared with SG VSV, the impurity levels in the HIC VSV were used as targets when spiking the SG VSV with host cell protein and/or host cell DNA. In all cases, adding the isolated impurities resulted in a volume change of less than 5% and a less than 6% change in ionic strength. Furthermore, the addition of the impurities had no significant effect on the virus titer ($p > 0.05$).

Table 4.1**:** Measurements of virus titer, protein, and DNA concentrations for the various VSV solutions. Results are reported as average ± standard deviation, with BDL indicating a concentration below the assay detection limits and N/A indicating that no spiking was performed.

Starting Solution	VSV Titer (PFU/mL)	Spike	Protein (µg/mL)	DNA (ng/mL)
SG VSV	$2.4 \pm 0.4 \times 10^8$	N/A	1.24±0.88	BDL
		+HCDNA	1.26±0.58	24.6±1.4
		+HCP	24.8±4.2	BDL
		+HCDNA +HCP	23.2±3.5	23.2±1.1
HIC VSV	$2.2 \pm 0.2 \times 10^8$	N/A	24.5±5.2	20.7±0.75

4.4.2. Effect of Host Cell Impurities on Sterile Filtration

We sought to evaluate whether AEX chromatography-purified host cell impurities can be used as surrogates for host cell impurities co-purified with VSV batches, as this allowed us to examine which component of host cell impurities (protein or DNA) had the greatest effect on virus recovery and fouling during 0.22 µm filtration. After purifying VSV batches using the two above-described methods (HIC and SG), we found that the HIC VSV contained higher levels of impurities compared to the SG VSV (Table 4.1).

By measuring increases in TMP during filtration and comparing the results for the spiked SG VSV and HIC VSV, we can evaluate whether spiking isolated host cell protein and DNA into the SG VSV will produce a virus solution with similar filtration characteristics as HIC VSV. As

shown in Figure 4.3, the HIC VSV and the SG VSV spiked with host cell protein and DNA (SG VSV +HCP +HCDNA) exhibited comparable increases in TMP during filtration, along with similar virus recoveries of 49±18 and 46±11 % respectively. Replicate filtration tests were conducted to demonstrate the precision of process. Spiking the DNA and protein into the final solution resulted in performance that was comparable to co-purifying the impurities alongside the VSV. Furthermore, characterization of the DNA and protein impurities (Figure 4.2) demonstrates their significant complexity that would do be obtained using typical protein or DNA standards. Therefore, the spiking model was deemed to be appropriate for studying the effects of residual impurities. When comparing the HIC VSV to the protein- and DNA-spiked SG VSV, the exact composition of the host cell impurities must be considered. Host cell proteins are very diverse[41], and different clarification and purification methods are known to select for portions of that population[39,57]. Furthermore, AEX chromatography will inherently select for a population of host cell proteins that is more negatively charged. Despite this, the spiked impurities appear to facilitate similar filtration performance as impurities co-eluted with VSV during HIC purification. This and all following constant flux filtration tests were performed at 0.3 mL min^{-1} cm^{-2}. While this flow rate is relatively low, it is comparable to the rates used in other sterile filtration operations[58,59], and it minimizes flux-dependant fouling[30] and potential shear forces[60].
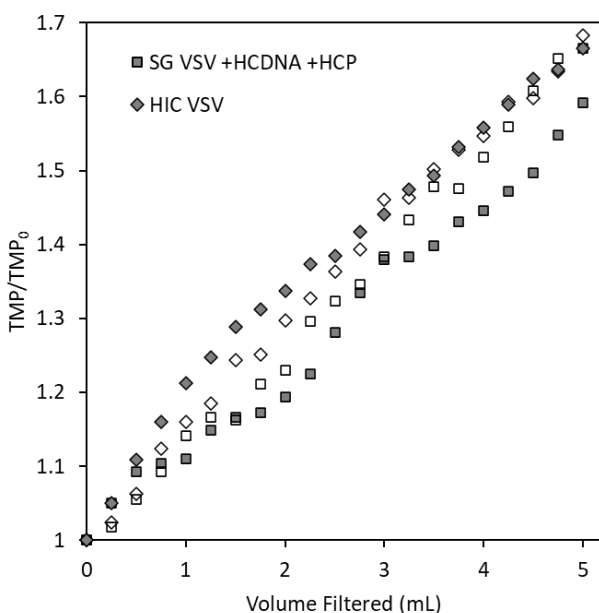
Figure 4.3: Change in transmembrane pressure (TMP), reported as the ratio of the measured TMP to the initial TMP, during the filtration of VSV through a PVDF 0.22 µm membrane at a constant flux of 0.3 mL min^{-1} cm^{-2}. VSV was purified via hydrophobic interaction chromatography (HIC VSV) or sucrose gradient (SG) ultracentrifugation. The SG VSV was then spiked with host cell protein and DNA (SG VSV +HCP +HCDNA) at amounts similar to those in the HIC VSV. Empty and open markers represent duplicate experiments under the same conditions.

Next, we wanted to investigate which impurity (protein or DNA) had a more detrimental effect during the filtration of VSV through 0.22 µm PES or PVDF membranes. As shown in Figure 4.4, there was a minimal increase in TMP during the filtration of SG VSV with both the PVDF and PES membranes. Similarly, when the SG VSV was spiked with DNA (SG VSV +HCDNA), only a very minor increase in TMP was observed for both membranes. Conversely, a noticeable change was observed (a 4-5 fold increase) when the SG VSV was spiked with protein (SG VSV +HCP); however, when the SG VSV was spiked with both protein and DNA (SG VSV +HCP +HCDNA), the increase in TMP did not significantly differ from spiking with protein alone. This indicates that, while DNA concentration does not appear to play a role in membrane fouling and TMP increase during filtration, protein concentration does have an effect. The comparison of the

two membranes revealed that the PVDF membrane was more susceptible to fouling, which is consistent with previous findings[15]. For both membranes, fouling increased linearly in relation to the volume filtered, thus theoretically implicating cake formation as the main fouling mechanism[61]. In cake filtration, particulate collects on the surface of the membrane, building up an external layer that resists fluid flow[61]. In the filtration of biological materials, the increase in TMP will typically follow an intermediate or standard pore blocking model[15,45,62,63] due to the adsorption and fouling of material within the membrane structure. This discrepancy could be due to the low volumes filtered and relatively mild fouling seen in these experiments, which do not allow for the observation of the full pattern of TMP increase.

No increase in TMP was observed when the VSV was spiked with BSA at a concentration comparable to HCP. BSA is commonly used as a model protein in fundamental studies of filtration theory[45,62] and in applied bioprocessing studies[23,30], as it provides an excellent analogue for how a generic protein might behave. In this study, however, BSA was proven to be a poor representation surrogate for host cell proteins. The absence of an increase in fouling with BSA indicates that the degree of membrane fouling is linked to specific qualities of the host cell proteins, rather than the presence of protein in general. In some cases, proteins in solutions such as beef extract[32], serum proteins[28], or BSA[64] have been specifically used to prevent adsorption to membranes and fouling during virus filtration, which further suggests that fouling is likely not caused by the general presence of protein in a solution. As a control, host cell DNA and host cell protein were spiked into formulation buffer and then filtered; these tests produced little to no increase in TMP. In other studies of protein microfiltration, the concentration and volume throughput required to achieve detectable fouling is orders of magnitude more than observed in this study[30,42]. These results

demonstrate that the fouling observed when VSV is spiked with host cell protein is not simply due to the host cell proteins themselves, but a combined interaction between the protein, the virus, and the membrane.
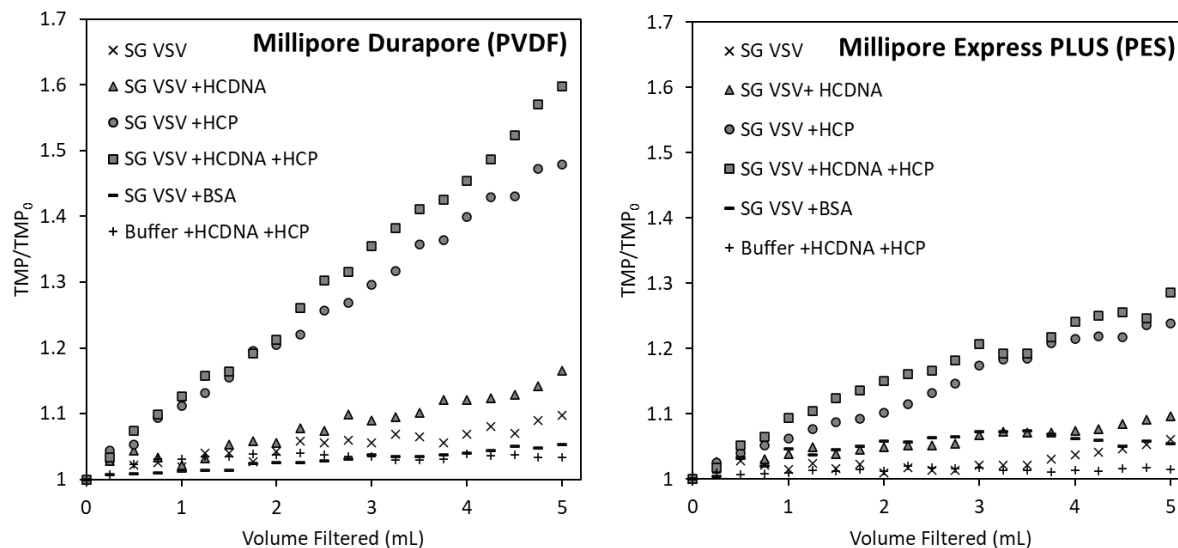
Figure 4.4: Change in transmembrane pressure (TMP), reported as the ratio of the measured TMP to the initial TMP, during the filtration of VSV. Sucrose-gradient-purified VSV (SG VSV) was spiked with host cell protein (HCP), host cell DNA (HCDNA), or both and then filtered. Two different membranes were compared: Millipore Durapore (PVDF) 0.22 µm, and Millipore Express PLUS (PES) 0.22 µm. Data points are the average of two filtration tests.

The effect of impurities can also be observed in the form of deposits on the PVDF membrane surface, as shown in the SEM images in Figure 4.5. As can be seen, minor fouling and build-up is present on the PVDF membrane (vs. the pristine membrane) after using it to filter SG VSV. The SG VSV spiked with host cell DNA gave a similar result. However, larger deposits can be seen following the filtrations of the SG VSV spiked with host cell protein; these deposits cover more area and clearly block some of the pores on the membrane surface. In contrast, no clear differences can be seen between the pristine PES membrane and the PES membranes that had been

used to filter the different VSV solutions. This difference may be due to the asymmetric structure of the PES membrane, which is more open at the top surface, as this may result in more material being trapped inside the membrane structure instead of on the surface. Asymmetric membranes are also known to be more resistant to fouling[31], which further explains the results in Figure 4.3, where less TMP increase was observed during the filtrations using the PES membrane than with those using the PVDF membrane.
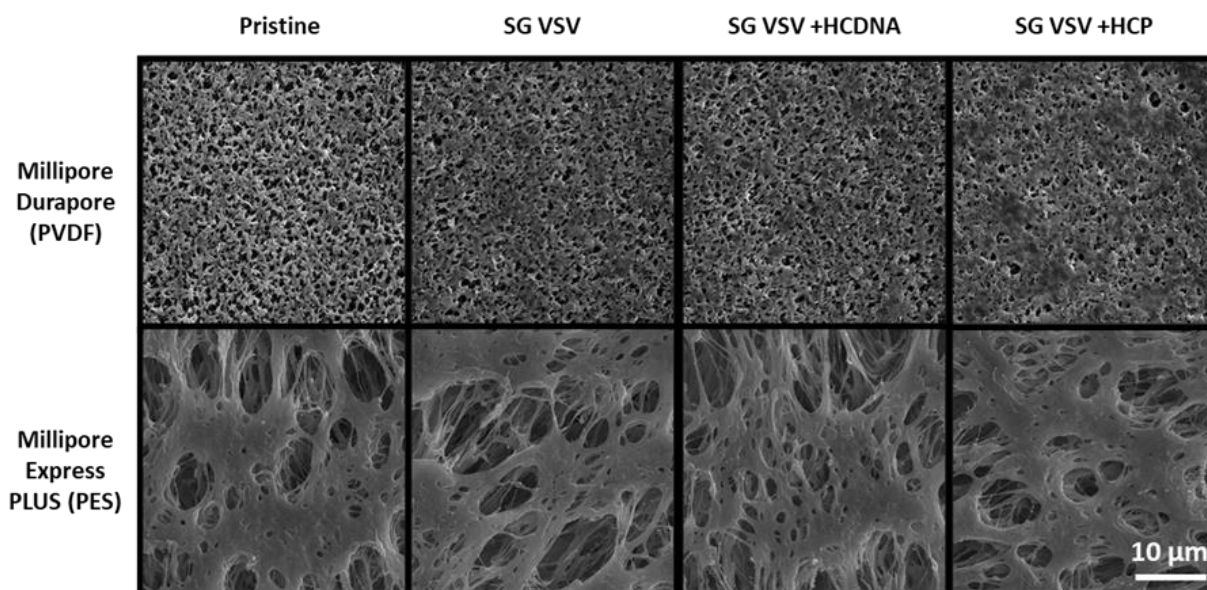
Figure 4.5: SEM images at 5000× magnification of Millipore Durapore (PVDF) 0.22 µm and Millipore Express PLUS (PES) 0.22 µm membranes in either pristine (unused) condition or after filtering sucrose gradient purified VSV (SG VSV) with added host cell DNA (HCDNA) or host cell protein (HCP).

The virus recovery (defined as the ratio of infectious particles in the filtrate to infectious particles in the feed) results for all the filtration tests are shown in Figure 4.6. There was no change in virus recovery between the SG VSV and the SG VSV spiked with host cell DNA for both tested membranes, with both having a relatively high recovery of approximately 85%. A comparison of the filtration tests with and without spiked host cell protein (regardless of the presence of DNA)

revealed a significant decrease in virus recovery (p<0.01). When host cell protein was spiked, the PES membrane provided significantly higher recovery than the PVDF membrane (p<0.05).

Recovery of protein was also measured for each filtration test, and no significant change in protein concentration was observed between the feed and the filtrate (Table S4.3). Even though the mass of the protein captured by the membranes was not significant, it is clear from these results that the presence of the host cell protein played an important role in determining how the VSV interacted with the membrane and the degree of fouling that was experienced.
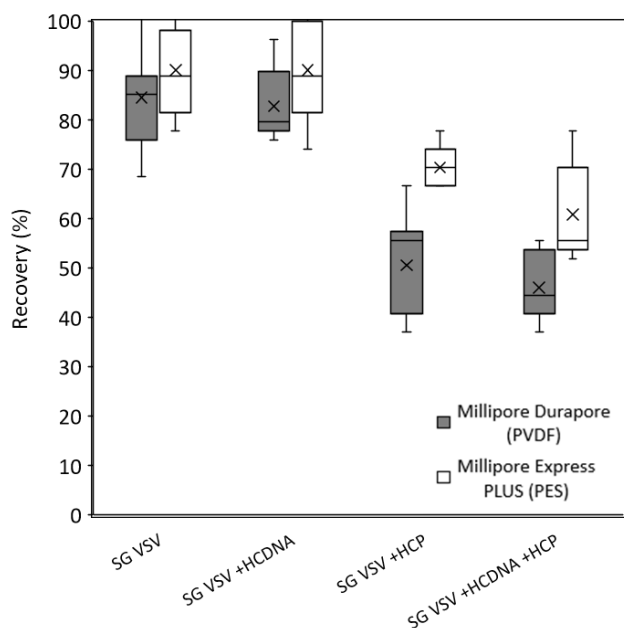
Figure 4.6: Box and whisker plot showing the recovery of VSV after filtration, calculated as the ratio of feed to filtrate titer. Sucrose-gradient-purified VSV (SG VSV) was spiked with host cell protein (HCP), host cell DNA (HC DNA), or both host cell protein and DNA prior to filtration. Two membranes are compared, Millipore Durapore (PVDF) 0.22 µm and Millipore Express PLUS (PES) 0.22 µm. The boxes depict the interquartile range, the horizontal lines represent the median, and the cross mark represent the mean. The whiskers extending from the boxes show the maximum and minimum values measured.

4.4.3. Adsorption of VSV, Host Cell Protein and DNA to Microfiltration Membranes

To better understand the interactions between VSV, host cell impurities and the microfiltration membranes, static adsorption tests were performed by incubating the various VSV solutions along with pieces of a membrane (Figure 4.7). When no additional spiked protein was present (SG VSV and SG VSV +HCDNA tests) little to no virus adsorbed to either membrane. However, a significant amount ($p<0.01$) of VSV adsorbed to the membrane in both conditions where the SG VSV was spiked with host cell protein (SG VSV +HCP and SG VSV +HCDNA +HCP)). This again shows the important role played by the host cell protein in determining how VSV will interact with the membranes; namely, VSV has a greater tendency to adsorb to the membrane when more host cell proteins are present in the solution. Loss during filtration can also likely be attributed to adsorption, rather than pore blockage by the host cell proteins. While the PVDF and PES membranes are both considered hydrophilic and low protein binding by their manufacturers, some level of protein adsorption is still observed, even under ideal conditions[65]; however, this can vary between manufacturers and membrane units. Adsorption can be mediated through either electrostatic or hydrophobic effects[26], while host cell proteins can have a wide range of charges and hydrophilicities[41]. Furthermore, the envelope of VSV is also known to have patches of variable charge and hydrophobicity[66]. Given this, it is certainly feasible that some sort of interaction is taking place, although a mechanistic explanation would require further investigation. Another explanation could be related to reactive groups on the host cell proteins. Studies examining membrane fouling via BSA have shown the critical role played by free thiol groups in this process[42]; notably, there are a wide range of functional proteins within the host cell protein population that may potentially possess similar reactive groups that could mediate fouling.
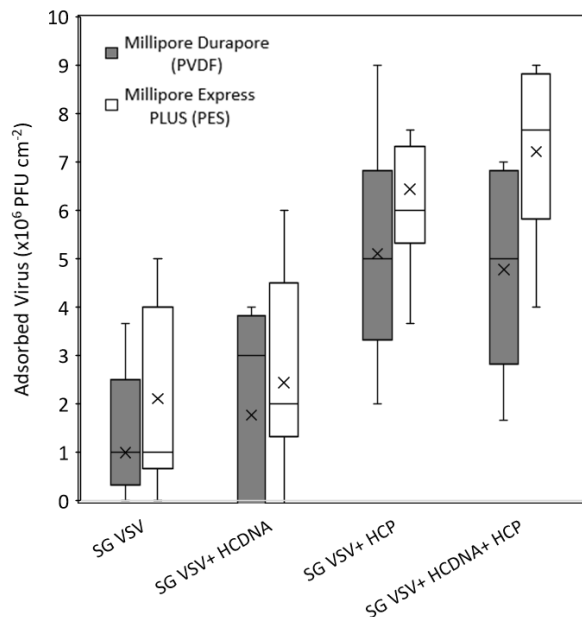
Figure 4.7: Box and whisker plot showing the static adsorption of sucrose-gradient-purified VSV (SG VSV) to Millipore Durapore (PVDF) 0.22 µm and Millipore Express PLUS (PES) 0.22 µm membranes in the presence of host cell protein (HCP), host cell DNA (HC DNA), or both. Data were calculated from plaque assays and adsorption experiments performed in triplicate. The boxes depict the interquartile range, the horizontal lines represent the median, and the cross marks represent the mean. The whiskers extending from the boxes show the maximum and minimum values measured.

4.5. Conclusions

Using measurements of TMP increase, virus recovery, and microscopy, we have shown how the presence of small amounts of host cell proteins increases membrane fouling during the sterile filtration of a virus solution. At the highest levels observed, spiking with approximately 25 µg/mL host cell protein resulted in a 4.8 times greater increase in TMP and a 34 % reduction in virus recovery. This effect is due, at least in part, to increased adsorption of the virus to the membrane in the presence of host cell proteins. Using static adsorption experiments it was shown that up to 5.1 times more virus adsorbed to the membrane when host cell protein was spiked into solution. Under the tested conditions, host cell DNA was not found to have a significant effect. It is theorized

that the population of host cell proteins contains unique key proteins that mediate adsorption due to specific properties, such as charge, hydrophobicity, or reactivity. However, further work is required to validate this claim. Furthermore, this paper also documented the development and validated a method of testing membrane fouling effects based on the isolation and subsequent spiking of host cell impurities. This method could be easily used by other researchers interested in the topic. Finally, this work can benefit manufacturers of therapeutic viruses who are experiencing issues with losses during sterile filtration, as it demonstrates that improving host cell protein removal in earlier downstream purification steps can enhance sterile filtration performance.

4.7. References

1. Ungerechts G, Bossow S, Leuchs B, et al. Moving oncolytic viruses into the clinic: clinical-grade production, purification, and characterization of diverse oncolytic viruses. *Mol Ther - Methods Clin Dev*. 2016;3:16018. doi:10.1038/mtm.2016.18

2. Reale A, Vitiello A, Conciatori V, Parolin C, Calistri A, Palù G. Perspectives on immunotherapy via oncolytic viruses. *Infect Agent Cancer*. 2019;14(1):5. doi:10.1186/s13027-018-0218-1

3. Russell L, Peng KW. The emerging role of oncolytic virus therapy against cancer. *Chin Clin Oncol*. 2018;7(2):16-16. doi:10.21037/cco.2018.04.04

4. Regules JA, Beigel JH, Paolino KM, et al. A Recombinant Vesicular Stomatitis Virus Ebola Vaccine. *N Engl J Med*. 2017;376(4):330-341. doi:10.1056/NEJMoa1414216

5. Kinch MS, Griesenauer RH. 2017 in review: FDA approvals of new molecular entities. *Drug Discov Today*. 2018;23(8):1469-1473. doi:10.1016/j.drudis.2018.05.011

6. Tomás HA, Rodrigues AF, Carrondo MJT, Coroadinha AS. LentiPro26: novel stable cell lines for constitutive lentiviral vector production. *Sci Rep*. 2018;8(1):5271. doi:10.1038/s41598-018-23593-y

7. Valkama AJ, Leinonen HM, Lipponen EM, et al. Optimization of lentiviral vector production for scale-up in fixed-bed bioreactor. *Gene Ther*. 2018;25(1):39-46. doi:10.1038/gt.2017.91

8. Bandeira V, Peixoto C, Rodrigues AF, et al. Downstream Processing of Lentiviral Vectors: Releasing Bottlenecks. *Hum Gene Ther Methods*. 2012;23(4):255-263. doi:10.1089/hgtb.2012.059

9. Nestola P, Peixoto C, Silva RRJS, Alves PM, Mota JPB, Carrondo MJT. Improved virus purification processes for vaccines and gene therapy: Improved Virus Purification Processes for Vaccines. *Biotechnol Bioeng*. 2015;112(5):843-857. doi:10.1002/bit.25545

10. Kramberger P, Urbas L, Štrancar A. Downstream processing and chromatography based analytical methods for production of vaccines, gene therapy vectors, and bacteriophages. *Hum Vaccines Immunother*. 2015;11(4):1010-1021. doi:10.1080/21645515.2015.1009817

11. Nestola P, Martins DL, Peixoto C, et al. Evaluation of Novel Large Cut-Off Ultrafiltration Membranes for Adenovirus Serotype 5 (Ad5) Concentration. Rito-Palomares M, ed. *PLoS ONE*. 2014;9(12):e115802. doi:10.1371/journal.pone.0115802

12. FDA. *Sterile Drug Products Produced by Aseptic Processing — Current Good Manufacturing Practice*. Center for Drug Evaluation and Research, Food and Drug Administration; 2004.

13. Kon TC, Onu A, Berbecila L, et al. Influenza Vaccine Manufacturing: Effect of Inactivation, Splitting and Site of Manufacturing. Comparison of Influenza Vaccine Production Processes. Krammer F, ed. *PLOS ONE*. 2016;11(3):e0150700. doi:10.1371/journal.pone.0150700

14. Chou AH, Liu CC, Chang CP, et al. Pilot Scale Production of Highly Efficacious and Stable Enterovirus 71 Vaccine Candidates. Guan Y, ed. *PLoS ONE*. 2012;7(4):e34834. doi:10.1371/journal.pone.0034834

15. Shoaebargh S, Gough I, Fe Medina M, et al. Sterile filtration of oncolytic viruses: An analysis of effects of membrane morphology on fouling and product recovery. *J Membr Sci*. 2018;548:239-246. doi:10.1016/j.memsci.2017.11.022

16. Ausubel LJ, Hall C, Sharma A, et al. Production of CGMP-Grade Lentiviral Vectors. *BioProcess Int*. 2012;10(2):32-43.

17. Truran R, Buckley R, Radcliffe P, Miskin J, Mitrophanous K. Virus purification. Published online December 31, 2009. Accessed March 15, 2021. https://patents.google.com/patent/US20090325284A1/en

18. Mundle ST, Hernandez H, Hamberger J, et al. High-Purity Preparation of HSV-2 Vaccine Candidate ACAM529 Is Immunogenic and Efficacious In Vivo. Sawtell NM, ed. *PLoS ONE*. 2013;8(2):e57224. doi:10.1371/journal.pone.0057224

19. Tang VA, Renner TM, Varette O, et al. Single-particle characterization of oncolytic vaccinia virus by flow virometry. *Vaccine*. 2016;34(42):5082-5089. doi:10.1016/j.vaccine.2016.08.074

20. Besnard L, Fabre V, Fettig M, et al. Clarification of vaccines: An overview of filter based technology trends and best practices. *Biotechnol Adv*. 2016;34(1):1-13. doi:10.1016/j.biotechadv.2015.11.005

21. Dishari SK, Micklin MR, Sung KJ, Zydney AL, Venkiteshwaran A, Earley JN. Effects of solution conditions on virus retention by the Viresolve® NFP filter. *Biotechnol Prog*. 2015;31(5):1280-1286. doi:https://doi.org/10.1002/btpr.2125

22. Arkhangelsky E, Gitis V. Effect of transmembrane pressure on rejection of viruses by ultrafiltration membranes. *Sep Purif Technol*. 2008;62(3):619-628. doi:10.1016/j.seppur.2008.03.013

23. Wickramasinghe SR, Stump ED, Grzenia DL, Husson SM, Pellegrino J. Understanding virus filtration membrane performance. *J Membr Sci*. 2010;365(1):160-169. doi:10.1016/j.memsci.2010.09.002

24. Konz JO, Lee AL, Lewis JA, Sagar SL. Development of a Purification Process for Adenovirus: Controlling Virus Aggregation to Improve the Clearance of Host Cell DNA. *Biotechnol Prog*. 2005;21(2):466-472. doi:10.1021/bp049644r

25. Wright JF, Le T, Prado J, et al. Identification of factors that contribute to recombinant AAV2 particle aggregation and methods to prevent its occurrence during vector purification and formulation. *Mol Ther*. 2005;12(1):171-178. doi:10.1016/j.ymthe.2005.02.021

26. van Voorthuizen EM, Ashbolt NJ, Schäfer AI. Role of hydrophobic and electrostatic interactions for initial enteric virus retention by MF membranes. *J Membr Sci*. 2001;194(1):69-79. doi:10.1016/S0376-7388(01)00522-1

27. Lee JK, Liu BYH. A filtration model of microporous membrane filters in liquids. *KSME J*. 1994;8(1):78-87. doi:10.1007/BF02953246

28. Cliver DO. Virus interactions with membrane filters. *Biotechnol Bioeng*. 1968;10(6):877-889. doi:10.1002/bit.260100612

29. Meltzer TH, Jornitz MW. The Sterilizing Filter and Its Pore Size Rating. *Am Pharm Rev*. 2003;6:6.

30. Loh S, Beuscher U, Poddar TK, et al. Interplay among membrane properties, protein properties and operating conditions on protein fouling during normal-flow microfiltration. *J Membr Sci*. 2009;332(1-2):93-103. doi:10.1016/j.memsci.2009.01.031

31. Ho CC, Zydney AL. Protein Fouling of Asymmetric and Composite Microfiltration Membranes. *Ind Eng Chem Res*. 2001;40(5):1412-1421. doi:10.1021/ie000810j

32. Mocé-Llivina L, Jofre J, Muniesa M. Comparison of polyvinylidene fluoride and polyether sulfone membranes in filtering viral suspensions. *J Virol Methods*. 2003;109(1):99-101. doi:10.1016/S0166-0934(03)00046-6

33. Lukasik J, Scott TM, Andryshak D, Farrah SR. Influence of Salts on Virus Adsorption to Microporous Filters. *Appl Environ Microbiol*. 2000;66(7):2914-2920. doi:10.1128/AEM.66.7.2914-2920.2000

34. Kissmann J, Ausar SF, Rudolph A, et al. Stabilization of measles virus for vaccine formulation. *Hum Vaccin*. 2008;4(5):350-359. doi:10.4161/hv.4.5.5863

35. Cruz PE, Silva AC, Roldao A, Carmo M, Carrondo MJT, Alves PM. Screening of Novel Excipients for Improving the Stability of Retroviral and Adenoviral Vectors. *Biotechnol Prog*. 2006;22(2):568-576. doi:10.1021/bp050294y

36. Wright J. Product-Related Impurities in Clinical-Grade Recombinant AAV Vectors: Characterization and Risk Assessment. *Biomedicines*. 2014;2(1):80-97. doi:10.3390/biomedicines2010080

37. Reiter K, Suzuki M, Olano LR, Narum DL. Host cell protein quantification of an optimized purification method by mass spectrometry. *J Pharm Biomed Anal*. 2019;174:650-654. doi:10.1016/j.jpba.2019.06.038

38. Hebben M. Downstream bioprocessing of AAV vectors: industrial challenges & regulatory requirements. *Cell Gene Ther Insights*. 2018;4(2):131-146. doi:10.18609/cgti.2018.016

39. Doneanu C, Xenopoulos A, Fadgen K, et al. Analysis of host-cell proteins in biotherapeutic proteins by comprehensive online two-dimensional liquid chromatography/mass spectrometry. *mAbs*. 2012;4(1):24-44. doi:10.4161/mabs.4.1.18748

40. Nogal B, Chhiba K, Emery JC. Select host cell proteins coelute with monoclonal antibodies in protein a chromatography. *Biotechnol Prog*. 2012;28(2):454-458. doi:10.1002/btpr.1514

41. Kornecki M, Mestmäcker F, Zobel-Roos S, Heikaus de Figueiredo L, Schlüter H, Strube J. Host Cell Proteins in Biologics Manufacturing: The Good, the Bad, and the Ugly. *Antibodies*. 2017;6(3):13. doi:10.3390/antib6030013

42. Kelly, Sean T. Z Andrew L. Protein fouling during microfiltration: Comparative behavior of different model proteins. *Biotechnol Bioeng*. 1997;55(1):11.

43. Higuchi A, Komuro A, Hirano K, et al. Permeation of γ-globulin through microporous membranes in the presence of trace DNA. *J Membr Sci*. Published online 2001:10.

44. Tracey EM, Davis RH. Protein Fouling of Track-Etched Polycarbonate Microfiltration Membranes. *J Colloid Interface Sci*. 1994;167(1):104-116. doi:10.1006/jcis.1994.1338

45. Kelly ST, Senyo Opong W, Zydney AL. The influence of protein aggregates on the fouling of microfiltration membranes during stirred cell filtration. *J Membr Sci*. 1993;80(1):175-187. doi:10.1016/0376-7388(93)85142-J

46. Moleirinho MG, Silva RJS, Alves PM, Carrondo MJT, Peixoto C. Current challenges in biotherapeutic particles manufacturing. *Expert Opin Biol Ther*. 2020;20(5):451-465. doi:10.1080/14712598.2020.1693541

47. Felt SA, Grdzelishvili VZ. Recent advances in vesicular stomatitis virus-based oncolytic virotherapy: a 5-year update. *J Gen Virol*. 2017;98(12):2895-2911. doi:10.1099/jgv.0.000980

48. Ge P, Tsao J, Schein S, Green TJ, Luo M, Zhou ZH. Cryo-EM Model of the Bullet-Shaped Vesicular Stomatitis Virus. *Science*. 2010;327(5966):689-693. doi:10.1126/science.1181766

49. van den Pol AN, Davis JN. Highly Attenuated Recombinant Vesicular Stomatitis Virus VSV-12'GFP Displays Immunogenic and Oncolytic Activity. *J Virol*. 2013;87(2):1019-1034. doi:10.1128/JVI.01106-12

50. Valkama AJ, Oruetxebarria I, Lipponen EM, et al. Development of Large-Scale Downstream Processing for Lentiviral Vectors. *Mol Ther - Methods Clin Dev*. 2020;17:717-730. doi:10.1016/j.omtm.2020.03.025

51. McNally DJ, Piras BA, Willis CM, Lockey TD, Meagher MM. Development and Optimization of a Hydrophobic Interaction Chromatography-Based Method of AAV Harvest, Capture, and Recovery. *Mol Ther - Methods Clin Dev*. 2020;19:275-284. doi:10.1016/j.omtm.2020.09.015

52. Kawka K, Wilton AN, Madadkar P, et al. Integrated development of enzymatic DNA digestion and membrane chromatography processes for the purification of therapeutic adenoviruses. *Sep Purif Technol*. 2021;254:117503. doi:10.1016/j.seppur.2020.117503

53. Moerdyk-Schauwecker M, Hwang SI, Grdzelishvili VZ. Analysis of virion associated host proteins in vesicular stomatitis virus using a proteomics approach. *Virol J*. 2009;6(1):166. doi:10.1186/1743-422X-6-166

54. Soderquist RG, Trumbo M, Hart RA, Zhang Q, Flynn GC. Development of advanced host cell protein enrichment and detection strategies to enable process relevant spike challenge studies. *Biotechnol Prog*. 2015;31(4):983-989. doi:10.1002/btpr.2114

55. Shukla AA, Jiang C, Ma J, Rubacha M, Flansburg L, Lee SS. Demonstration of Robust Host Cell Protein Clearance in Biopharmaceutical Downstream Processes. *Biotechnol Prog*. 2008;24(3):615-622. doi:10.1021/bp070396j

56. Tarrant RDR, Velez-Suberbie ML, Tait AS, Smales CM, Bracewell DG. Host cell protein adsorption characteristics during protein a chromatography. *Biotechnol Prog*. 2012;28(4):1037-1044. doi:10.1002/btpr.1581

57. Hogwood CEM, Tait AS, Koloteva-Levine N, Bracewell DG, Smales CM. The dynamics of the CHO host cell protein profile during clarification and protein A capture in a platform antibody purification process. *Biotechnol Bioeng*. 2013;110(1):240-251. doi:10.1002/bit.24607

58. Cutler MW, Kang Y, Ouattara AA, Syvertsen KE. Purification processes for isolating purified vesicular stomatitis virus from cell culture. Published online March 6, 2008. Accessed March 15, 2021. https://patents.google.com/patent/WO2007123961A3/en

59. Moleirinho MG, Rosa S, Carrondo MJT, et al. Clinical-Grade Oncolytic Adenovirus Purification Using Polysorbate 20 as an Alternative for Cell Lysis. *Curr Gene Ther*. 2018;18(6):366-374. doi:10.2174/1566523218666181109141257

60. Thomas CR, Geer D. Effects of shear on proteins in solution. *Biotechnol Lett*. 2011;33(3):443-456. doi:10.1007/s10529-010-0469-4

61. Iritani E. A Review on Modeling of Pore-Blocking Behaviors of Membranes During Pressurized Membrane Filtration. *Dry Technol*. 2013;31(2):146-162. doi:10.1080/07373937.2012.683123

62. Ho CC, Zydney AL. Effect of membrane morphology on the initial rate of protein fouling during microfiltration. *J Membr Sci*. Published online 1999:15.

63. Hlavacek M, Bouchet F. Constant flowrate blocking laws and an example of their application to dead-end microfiltration of protein solutions. *J Membr Sci*. 1993;82(3):285-295. doi:10.1016/0376-7388(93)85193-Z

64. Hahn RG, Hatlen JB, Kenny GE. Comparative Poliovirus Permeability of Silver, Polycarbonate, and Cellulose Membrane Filters. *Appl Microbiol*. 1970;19(2):317-320.

65. Mahler HC, Huber F, Kishore RSK, Reindl J, Rückert P, Müller R. Adsorption Behavior of a Surfactant and a Monoclonal Antibody to Sterilizing-Grade Filters. *J Pharm Sci*. 2010;99(6):2620-2627. doi:10.1002/jps.22045

66. Carneiro FA, Bianconi ML, Weissmüller G, Stauffer F, Da Poian AT. Membrane Recognition by Vesicular Stomatitis Virus Involves Enthalpy-Driven Protein-Lipid Interactions. *J Virol*. 2002;76(8):3756-3764. doi:10.1128/JVI.76.8.3756-3764.2002

4.8. Supplementary Material
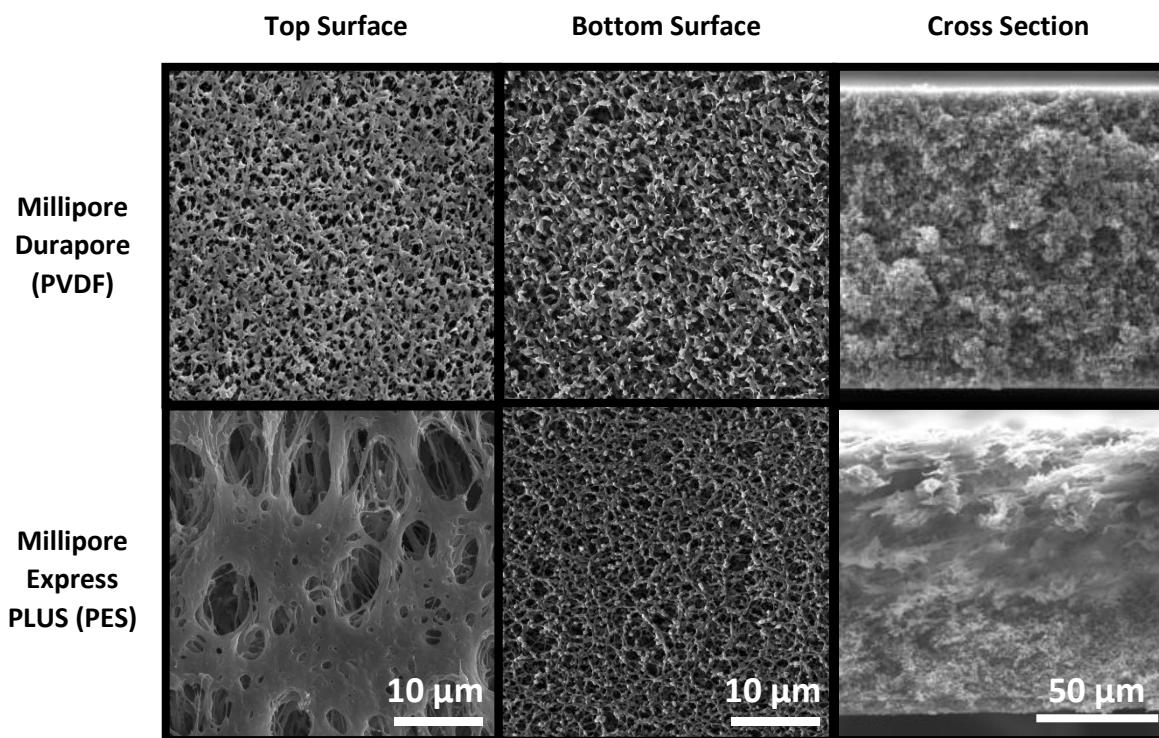
Figure S4.8: Additional SEM images of the Durapore PVDF 0.22 µm and Express PLUS PES 0.22 µm membranes showing the differences in structure between the top, bottom and cross section of the membranes. Top and bottom images taken at 5000x magnification and cross section images taken at 1000x magnification.
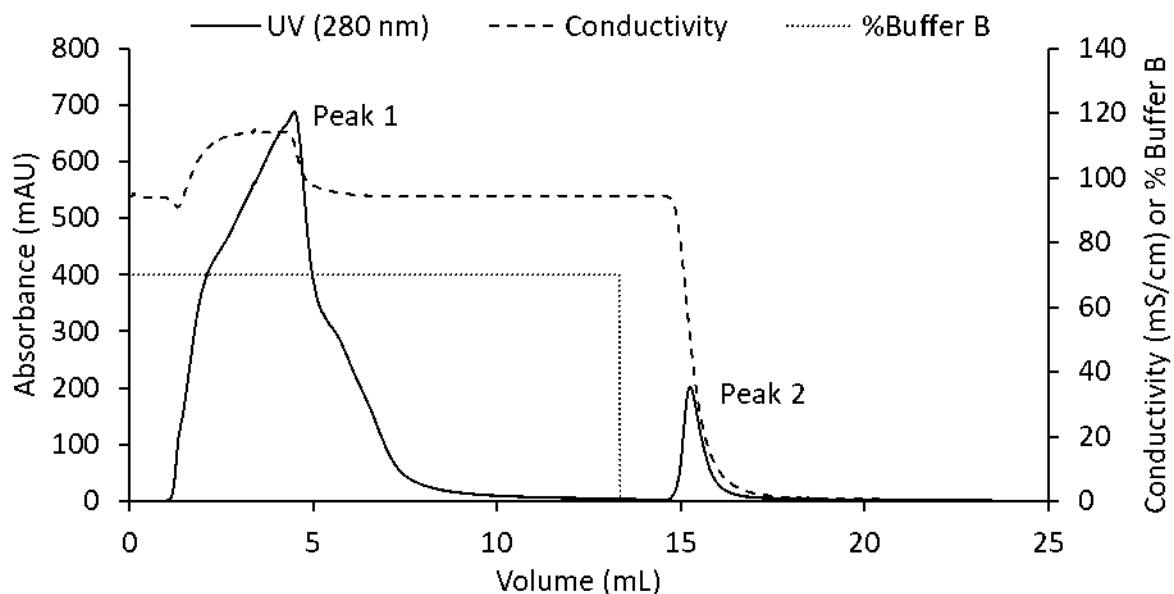
Figure S4.9: UV absorbance (at 280 nm) and conductivity profiles for the purification of VSV using hydrophobic interaction membrane chromatography (Sartobind Phenyl). Peak 1 corresponds to the fraction of the feed that did not bind to the membrane at the high-conductivity solution conditions (i.e. 100% Buffer B) associated with the loading step; Peak 2 corresponds to the fraction of the feed that eluted from the membrane at the low-conductivity solution conditions (i.e. 0% Buffer B). The 6 mL fraction of the eluted peak (i.e. hydrophobic interaction chromatography purified VSV (HIC VSV)) had a titer of $2.20 \pm 0.23 \times 10^8$ PFU/mL.
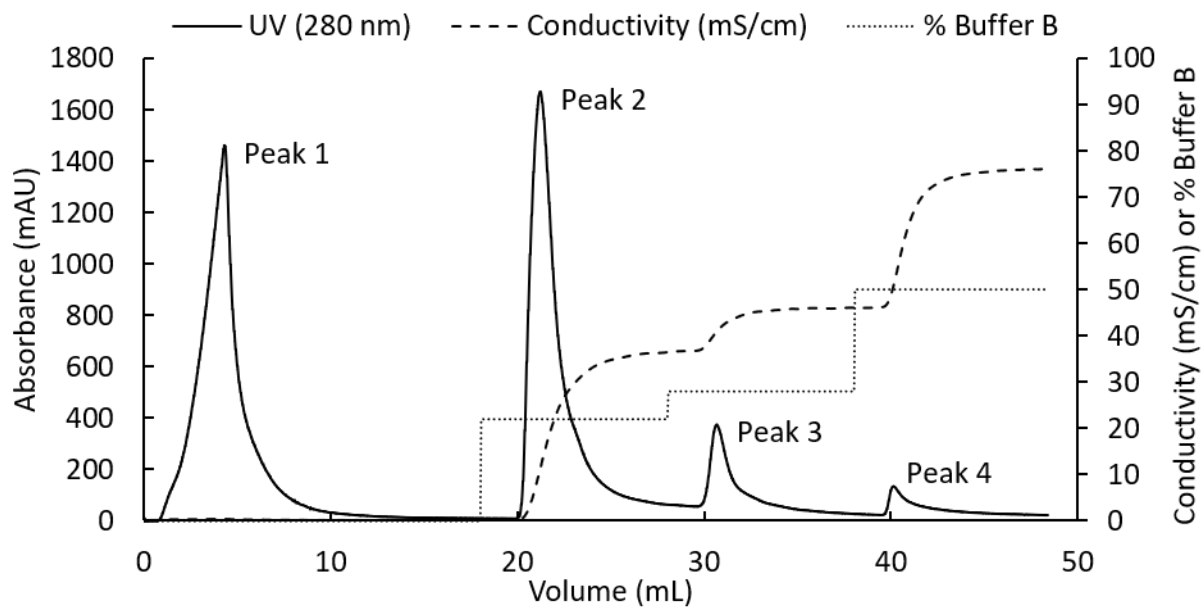
Figure S4.10: UV absorbance (at 280 nm) and conductivity profiles for the purification of host cell impurities using laterally-fed membrane chromatography with an anion exchange (Sartobind Q) membrane. Peak 1 corresponds to the fraction of the feed that did not bind to the membrane at the low-conductivity solution conditions (i.e. 0% Buffer B) associated with the loading step; Peak 2 corresponds to the fraction of the feed that eluted from the membrane at the solution conditions corresponding to 25% Buffer B (i.e. 75% Buffer A); Peak 3 corresponds to the fraction of the feed that eluted from the membrane at the solution conditions corresponding to 30% Buffer B (i.e. 70% Buffer A); Peak 4 corresponds to the fraction of the feed that eluted from the membrane at the solution conditions corresponding to 50% Buffer B (i.e. 50% Buffer A). As shown in Table S4.2., the fractions corresponding to Peaks 2 and 4 were used to spike in controlled amounts of host cell protein and host cell DNA respectively.

Table S4.2**:** Protein and DNA content (measured using a Micro BCA Protein Assay Kit and Quant-iT PicoGreen dsDNA Kit respectively) of the four elution peaks obtained for the purification of host cell impurities using laterally-fed membrane chromatography with an anion exchange (Sartobind Q) membrane. BDL indicates that the concentration was below the detection limit of the assay used.

	Protein (µg/mL)	DNA (ng/mL)
Peak 1	148	417
Peak 2 (HCP elution)	941	13.2
Peak 3	96.5	74.1
Peak 4 (HCDNA elution)	BDL	397

Table S4.3: Protein content of the feed and filtrate for VSV filtration experiments. Results reported as average ± standard deviation.

	Millipore Durapore (PVDF) 0.22 µm		Millipore Express PLUS (PES) 0.22 µm	
	Feed (µg/mL)	Filtrate (µg/mL)	Feed (µg/mL)	Filtrate (µg/mL)
SG VSV	1.50±0.63	1.58±0.64	0.97±0.68	1.14±0.47
SG VSV +HCDNA	1.12±0.42	1.03±0.88	1.39±0.32	0.94±0.57
SG VSV +HCP	27.5±3.1	25.5±2.4	22.1±1.8	23.1±2.8
SG VSV +HCDNA +HCP	24.7±1.1	23.9±2.0	23.6±2.5	23.5±2.1

Chapter 5

Application of Isoporous Microslit Silicon Nitride

Membranes for Sterile Filtration of Virus Vectors

5. Application of Isoporous Microslit Silicon Nitride Membranes for Sterile Filtration of Therapeutic Viruses

Evan Wright, Joshua J. Miller, Matthew Csordas, Andrew R. Gosselin, Jared A. Carter, James L McGrath, David R. Latulippe, James A. Roussie

5.1. Abstract

The widely used 0.22 µm polymer sterile filters were developed for small molecule and protein sterile filtration and in some cases are not well-suited for the production of large non-protein biological therapeutics due to their entrapment within the relatively thick and polydisperse polymer matrix, resulting in significant yield loss and production cost increases. Here, we report on the first-ever testing of isoporous sub-0.2 µm rectangular prism pores created using silicon micromachining to produce microslit silicon nitride (MSN) membranes. The very high porosity (~33%) and ultrathin nature (200 nm) of the 0.2 µm MSN membranes yielded performance properties (including hydraulic permeance, and nanoparticle sieving/fouling behavior) that were dramatically different than a traditional 0.2/0.22 µm polymer sterile filter. Testing of the membrane in a stirred cell demonstrated how stirring can be used to help reduce fouling on the membrane surface. The results from bacteria retention tests, conducted according to the guidance

of regulatory agencies, demonstrated that the 0.2 µm MSN membranes can completely retain a challenge test of bacteria, making this the first micromachined silicon membrane to be validated as a sterile filter. Applying the MSN membrane to the sterile filtration of therapeutic viruses and comparing the results with a conventional Durapore membrane a similar virus recovery was achieved indicating, improvements to the membrane must be made before it can be fully applied to industry relevant challenges. With further work, it is believed that the results and technologies presented in this work will find future utility in the production of biological therapeutics.

5.2. Introduction

Current Good Manufacturing Practice (cGMP) standards for the production of biological therapeutics rely on sterile filtration processes using microporous polymeric membranes to remove any potential bioburden in order to ensure the safety of the final formulation. Absent of aseptic production methods, the U.S. Food and Drug Administration (FDA) demands the incorporation of a final sterile filtration step to remove any potential microbial contaminants. The definition of a sterile filter is based on the retention of *Brevundimonas diminuta* (*B. diminuta*), a bacterium whose size is often reported in the range of 0.4 µm[1] to 0.8 µm under fully hydrated conditions[2]. Specifically, a membrane will achieve a 0.2 µm sterile filter designation according to the complete removal of *B. diminuta* when challenged with 10^7 *B. diminuta* per cm[2] of membrane surface area[3]. It is worth noting that this 0.2 µm designation is not strictly based on the pore size properties, but is known to depend on several interacting factors including the formulation conditions and operating pressure[4].

The use of sterile filtration membranes in the production of proteinaceous biological therapeutics is not a significant technical challenge due to the much smaller size of the therapeutic product relative to the typical membrane's pore size rating. However, recent advances in the development of larger (i.e., > 50 nm average diameter) bio-pharmaceutical products, such as extracellular vesicles, antibody-conjugated drug particles, and viruses, have created a significant challenge in downstream processing operations. Conventional polymer-based sterile filters often entrap these larger products because of their high internal surface area, tortuous path pores, and log-normal pore size distribution[5,6]. Consequently, sterile filtration of large therapeutics typically incurs significant yield loss and corresponding increase in related production costs. For instance, it has been shown that the recovery during sterile filtration of a therapeutic virus was less than 25% for four polymeric membranes from three different suppliers[7]. It has also been reported that the recovery of engineered extracellular vesicles for immunotherapy reached as low as 20% when using a conventional 0.22 µm pore size polymeric membrane[8]. Thus, there is a need for new membrane filtration technologies that are ideally suited for the downstream processing of large-sized biological therapeutics.

An attractive alternative to polymeric membranes are inorganic, microfabricated membranes. Typically fabricated using silicon as a base material and with techniques originally developed in the semiconductor industry, these membranes can be designed with isoporous and highly accurate patterned pores which provide precise control over their sieving behavior. To date, microfabricated filtration membranes have been used in applications including hemofiltration and dialysis[9], cell separations[10,11], food and beverage processing[12], and as a substrate or barrier for cell culture[13,14]. Using well-developed and conventional optical lithography techniques, construction

of inorganic membranes with a pore size in the range of 1 to 5 µm is possible[15]. With more advanced optical lithography techniques such as multiple exposure interference lithography, pore sizes down to 260 nm are achievable[16] however the fundamental limits imposed by the wavelength of light makes the fabrication of these smaller pores highly complex. In order to create pores on the nanometer scale (e.g. 1-100 nm) techniques such as ion track etching[17] or deep reactive ion etching[9] have been used. These techniques are slow and more cost intensive than optical lithography methods, limiting the manufacturing of products with these techniques.

With microfabrication, the pore structure and shape is not limited to simple circular pores; slit pores can be fabricated with multiple theoretical benefits to filtration performance. Slit pores are more resistant to blockage by large particulate completely occluding the pores[18,19] and are less likely to be bridged by small particles forming a fouling layer[20]. Furthermore, slit pores are highly tunable, with the width of the slit defining the overall sieving behavior while the length of the slit defines the overall permeance. Previous lab scale studies have been performed on membranes with slit widths either greater than 1 µm[18–20] or less than 30 nm[21,22], leaving a gap at the 0.2 µm size. To the best of our knowledge, no studies to date have reported on the use of a membrane with slit pore dimensions appropriate for sterile filtration applications.

Here, we report on the testing of various microfabricated membranes with circular or slit pores having critical dimensions (pore or slit width) of 0.2 µm or 0.5 µm. Membrane performance was initially characterized using a variety of tests including hydraulic permeability, nanoparticle sieving and fouling, and fouling by bovine serum albumin. These results were compared to a standard polymeric PVDF membrane (0.22 or 0.45 µm pore size) to highlight the benefits of the

microfabricated membranes. A challenge to the adoption of the membranes is the ability to scale up the technology. Therefore, we briefly demonstrate how multiple membrane can be integrated into an Amicon stirred cell and used to process larger volumes, with additional added benefits in preventing fouling due to the introduction of stirring. The 0.2 µm and 0.5 µm slit membrane were then further tested for suitability as a sterile filter in biopharmaceutical applications following the ASTM specified protocol[23] involving a challenge test of *B. diminuta* bacteria. Next, the 0.2 µm slit membrane was tested for transmission and fouling of two therapeutic viruses: a Maraba virus which has previously been shown to be very difficult to sterile filter with conventional polymeric membranes (low transmission and high fouling)[7] and an adenovirus which is typically not a challenge to sterile filter (high transmission and low fouling)[24,25]. This work represents the first step towards developing inorganic, microfabricated membranes for sterile filtration applications and an opportunity for the biopharmaceutical processing industry to move away from the polymeric phase inversion membranes which can present barriers to improving manufacturing processes.

5.3. Materials and Methods

5.3.1. Membranes and Filtration Tests

Microfabricated silicon nitride membranes were produced using a deep UV photolithography process (Figure 5.1A). Membrane pores were initially patterned on the frontside of a silicon wafer, within a low pressure chemical vapor-deposited silicon nitride layer on 150mm diameter, 310 µm thick, double-side polished silicon wafers (WaferPro Inc.). For the 0.2×10 µm slit features, deep UV (248 nm wavelength) photolithography (ASML PAS5500/300 C DUV 4X Reduction Stepper) was used to pattern the slits into 500 nm thick UV™ 210 DUV positive tone photoresist

(Microchemicals GmbH) and an underlying 60 nm thick DUV-42P antireflective coating (ARC; Brewer Science Inc.). The wafers were then developed with 726 MiF (Microchemicals GmbH) and the ARC was removed via etching (27 Pa, 50 W; 20 sccm O2, 20 sccm Ar; 75 s) using a MiniLock Etcher (Trion Technology Inc.). For the 0.5×50 μm and 1.0×50 μm slit features, conventional (365 nm wavelength) photolithography was used (ASML PAS5500/205 5X-Reduction Stepper) to pattern 1.2 μm thick AZ® MiR 701 positive tone photoresist (Microchemicals GmbH) and the patterned photoresist was developed in CD-26 (Microchemicals GmbH). Reactive ion etching (43 Pa, 150 W; 150 sccm He, 150 sccm SF6; 110–220 s) for slit feature transfer was performed using a LAM 490 Etcher (LAM Systems Inc.). To image the membrane surface structures, scanning electron microscopy was used. The membranes were and mounted on specimen stubs using carbon tape, then sputter coated with gold (Polaron E5100). The images were obtained using a Vega II LSU (Tescan) instrument at 20 kV and a magnification ranging from 1000 to 10,000 ×. ImageJ software (NIH) was used to verify the pore size of the silicon nitride membranes and to calculate their porosity.
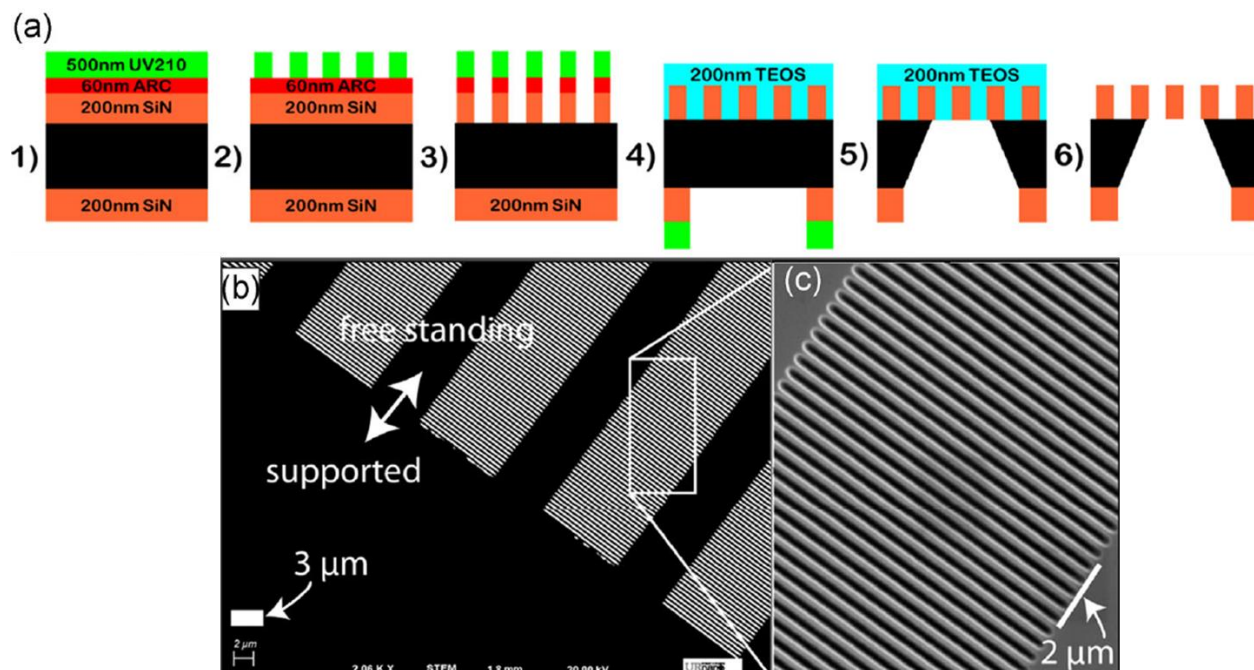
Figure 5.1: (A) Pictographic representation (not to scale) of process workflow steps for the 0.2 μm microslit silicon nitride (MSN) membrane. (B) Scanning electron micrograph (×2,060 magnification; 20 kV) of the resultant freestanding membranes. (C) Higher magnification micrograph (×12,000 magnification; 20 kV of a portion of the image from (B).

The final fabricated product is a 300 µm thick, 5.4 × 5.4 mm silicon chip with ultrathin windows of suspended membrane area (Figure 5.1B). The silicon nitride membranes were designed to have circular micropores (MPN) with a 0.5 µm pore diameter or to have microslits (MSN) with a 0.5 or 0.2 µm slit width (Figure 5.1C). The MPN 0.5 µm and MSN 0.5 µm membranes have a 400 nm thick suspended membrane area made up of three 0.7×0.3 mm windows (0.063 cm^2 surface area), while the MSN 0.2 µm membranes have a 200 nm thick suspended membrane area of four 0.3×3 mm windows (0.036 cm^2 surface area). For small scale filtration tests, the silicon nitride membranes were housed in a custom-built membrane holder (Figure 5.2). For comparable small scale filtration tests using a conventional polymeric membrane, Durapore (MilliporeSigma) 0.22 and 0.45 µm PVDF membranes were housed in a

polycarbonate assembly (Cole-Parmer) with an effective 0.5 cm^2 of filtration area. All filtration experiments were performed with this experimental setup unless otherwise stated.

Filtration experiments were performed under constant flux with an inline digital pressure transducer (Omega PX409) to record the transmembrane pressure (TMP) in real time. A syringe pump (Harvard Apparatus PhD 2000) and 10 mL syringe (Becton Dickenson) was used to supply the feed at the required flow rate (Figure 5.2). For filtration experiments with *B. diminuta,* Maraba virus, or adenovirus, all fittings, tubing, and the filtration module were autoclaved at 121 °C for 30 minutes before use (Tuttnauer 3850E). To begin a filtration experiment, the syringe was first filled with ultrapure water (Millipore MilliQ) and a series of fluxes ranging from 0.05 - 20 mL min^{-1} cm^{-2} were applied. The resulting change in TMP relative to the change in flux was used to calculate the membrane permeability and to check the membrane integrity by comparing the result to previous data. A syringe filled with buffer relevant to the test solution (described in their respective sections) was then loaded and 2-3 mL was passed to flush out the tubing and filtration module. All water and buffers were prefiltered through a 0.2 µm syringe filter to remove any potential contaminating particulate. A syringe of the test solution was then loaded and set to a constant flux of 0.8 mL min^{-1} cm^{-2} unless otherwise noted. Aliquots of the filtrate were collected throughout the filtration experiment and analyzed using their respective methods.
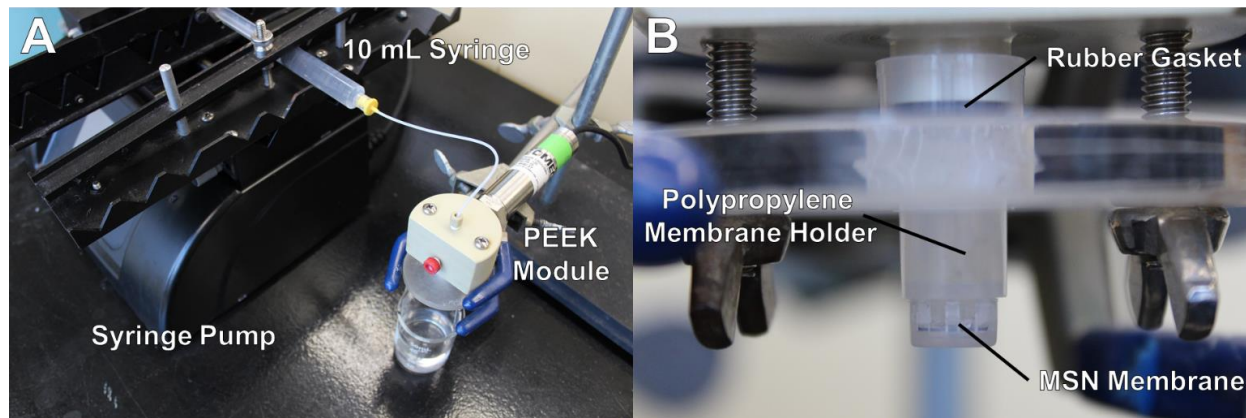
Figure 5.2: Pictures of the system used for the nanoparticle filtration and bacterial challenge tests. A) The PhD 2000 syringe pump (Harvard Apparatus) maintains a constant flow rate into a custom-made polyetheretherketone (PEEK) module. In order to measure the transmembrane pressure, the sensing port of a PX409 pressure transducer (Omega Engineering) was connected via a threaded port. B) A protrusion from the bottom of the PEEK module fits into the top of the membrane holder and is sealed by a rubber gasket. The membrane holder is sandwiched between the PEEK module and a polycarbonate plate to seal the membrane holder in place. For the select experiments conducted with the Durapore 0.22 µm PVDF membrane, the 13 mm membrane disc was inserted into a polycarbonate membrane holder (Cole-Parmer) and then attached to the bottom of the PEEK module.

In order to scale up the filtration experiments and to investigate the effect of stirring on filtration performance, the silicon nitride membranes were integrated into a 50 mL Amicon (MilliporeSigma) stirred cell. Six 0.5 µm MSN membranes (total 0.378 cm^2 effective surface area) were mounted in a 1.1 mm thick, 44.5 mm diameter polycarbonate disk (Figure 5.3A). This disk was inserted into the stirred cell and placed on a magnetic stir plate to control the rate of stirring. To perform constant flux filtration, a syringe pump was attached to the outlet of the Amicon and operated in withdraw mode to pull fluid through the membranes, with an inline pressure transducer recording the change in TMP over time (Figure 5.3B). Given that the transducer is placed downstream of the membrane, changes in transmembrane pressure are measured as negative pressure. For ease of interpretation, the TMP data is inverted. In addition, the height of water in the Amicon reservoir is not constant and the hydrostatic pressure will change during the filtration,

therefore the data has been adjusted to account for this factor. Flux during the Amicon filtration experiments was set at either 2.3 or 0.23 mL cm^{-2}·min^{-1}, while the rate of stirring was varied between 0 and 300 RPM.
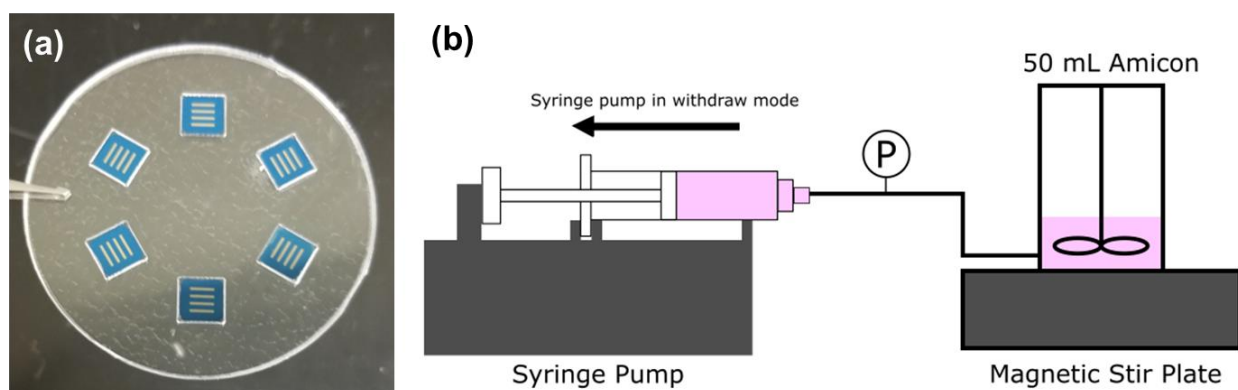
Figure 5.3: Adapting the MSN 0.5 µm membranes for a stirred cell format, by mounting six membranes in a polycarbonate disk. (B) Diagram of how constant flux filtration was performed in an Amicon stirred cell.

5.3.2. Nanoparticles and Protein Solutions

Stock solutions of fluorescent polystyrene nanoparticles with nominal diameters of 0.06, 0.18, 0.51, and 0.84 µm were purchased from Spherotech. Nanoparticles were diluted to a concentration of 0.003% (w/v) in a 0.1M carbonate buffer solution (Alfa Aesar), pH 9.4 with 0.01% (v/v) Tween™ 20. Using dynamic light scattering, these nanoparticles were verified to be monodisperse with average sizes near the reported nominal sizes (Figure 5.4). The prepared solutions were analyzed using a Zetasizer NanoZS (Malvern). Five measurements were made, each with a manually set 20 runs. Each nanoparticle solution was placed in an ultrasonic bath for 15 min immediately before it was used in a filtration test. Concentration of the nanoparticles in feed and filtrate solutions was measured by collecting aliquots in a black 96 well plate (Corning) and measuring the fluorescence intensity of the samples (Spark 10M, Tecan). The percent transmission

of the nanoparticles was then determined by taking the ratio of the fluorescence intensity of the filtrate and feed. In filtration experiments using the Amicon stirred cell system, a different selection of non-fluorescent 0.18 µm or 2.1 µm nanoparticles were used.
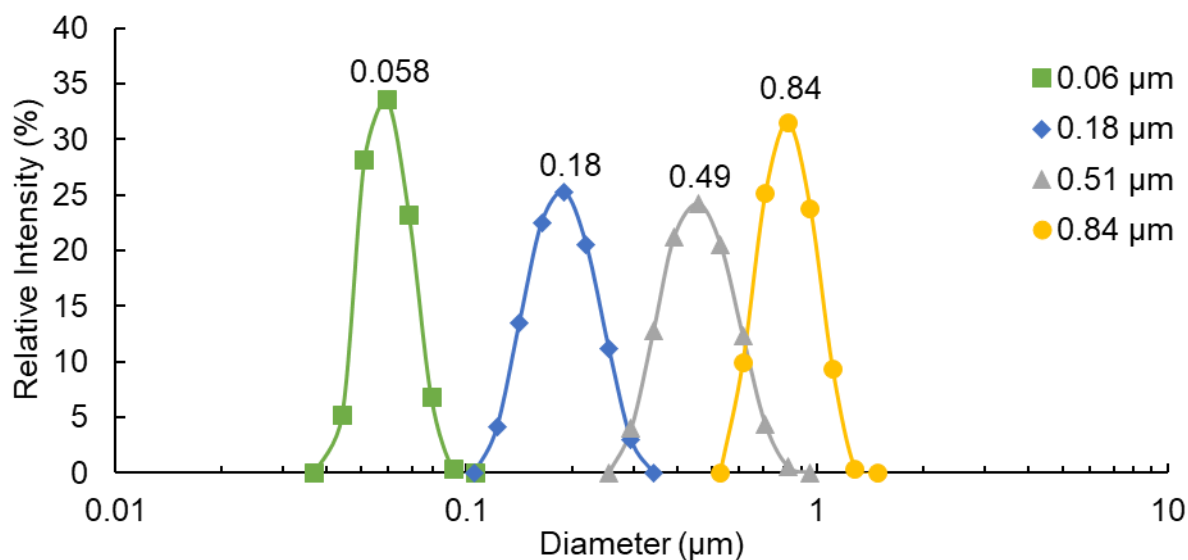
Figure 5.4: Dynamic light scattering results for the four polystyrene nanoparticles. The manufacturer's (Spherotech) reported average diameters are given in the legend. The measured average diameters (in µm) are shown above the corresponding intensity profiles for each polystyrene nanoparticle solution.

Lyophilized bovine serum albumin (BSA; Bioshop) was dissolved in 0.01 M Tris buffer, pH 7.5 to create a 0.1% (w/v) solution. After dissolving the BSA and before a filtration experiment, the solution was passed through a 0.2 µm syringe filter to remove any potential protein aggregates[26].

5.3.3. Preparation and Analysis of Brevundimonas diminuta

B. diminuta bacteria stocks and solutions for filtration were prepared as described in Chapter 3. The sterile filtration challenge with B. diminuta was performed similar to that described in

ASTM F838[23], following the previously mentioned filtration protocol but with the flux rate set to 2mL cm^{-2}·min^{-1} and a total of 6 mL cm^{-2} passed through the membrane. Along with the collected filtrate, a sample of the feed bacteria solution was assessed for *B. diminuta* concentration via triplicate analysis of the colony counts from a direct spread plate assay (incubation at 30°C for 2 days) on tryptic soy agar. Any plates that showed no colonies after 2 days were incubated for another 5 days and then checked again to confirm that no *B. diminuta* were present in the corresponding sample.

5.3.4. Preparation and Analysis of Rhabdovirus and Adenovirus

Rhabdovirus Maraba expressing green fluorescent protein was provided by the Ottawa Hospital Research Institute, prepared through a process of cell culture in roller bottles, harvest and clarification using depth filtration membranes, and purification using multiple ultrafiltration steps. A final diafiltration step exchanged the virus into formulation buffer consisting of 10 mM HEPES pH 7.4, 4% sucrose, and 150 mM NaCl. The virus stock and all collected filtrate samples were stored at -80 °C. The titer of the virus was determined using a 50% tissue culture infective dose (TCID$_{50}$) assay. Vero cells were grown in DMEM (supplemented with 8% FBS and 1% L-glutamine) to confluence in tissue culture treated 150cm^2 flasks (Corning) at 37°C and 5% CO$_2$. Confluent cells were detached using 0.1% trypsin and seeded into flat bottom 96 well plates (Corning) at 5×10^4 cells per well. After a 24-hour incubation, serially diluted virus was added to the wells. The virus was initially diluted 10-fold to approach the approximate expected TCID$_{50}$, then diluted 2-fold. For each dilution level, 100 µl of serially diluted virus was added to 8 wells. Following a 48 hour incubation, cytopathic effects (green fluorescence) was assessed using a

Typhoon Scanner (GE Healthcare). The infectious titer was then calculated using the Spearman-Karber method[27,28].

Adenovirus was grown and purified as previously described[29] to produced a virus stock for filtration tests. In brief, HEK 293 cells were propagated using the same method as the Vero cells above. HEK cells were expanded in culture flasks and resuspended in fresh media at a cell density of 5×10^5 cells/mL, then infected with adenovirus type-5 (provided by the McMaster Fitzhenry Vector Laboratory) at a multiplicity of infection of 5. After a 48 hour incubation, the infected cells were collected, pelleted through centrifugation, and then lysed using successive freeze-thaw cycles. The cell lysate was treated with Benzonase® endonuclease enzyme, then diluted with buffer and clarified using a 0.45 µm membrane filter. The clarified lysate was then purified using lateral flow anion exchange chromatography (process optimization described by Kawka *et al.*[29]) and finally dialyzed against formulation buffer (10 mM HEPES pH 7.4, 4% sucrose, and 150 mM NaCl). Analysis of virus titer was performed using a hexon immunostaining kit (Adeno-X Rapid Titer Kit, Clontech) following the manufacturer's protocol.

5.4. Results and Discussion

5.4.1. Membrane Characterization

The microfabricated silicon nitride membranes and the PVDF Durapore membranes were imaged using scanning electron microscopy (Figure 5.5). Measurements of the silicon nitride membranes show that the actual pore and slit dimensions of the MPN 0.5 µm, MSN 0.5 µm and MSN 0.2 µm membranes were 0.47±0.03 µm, 0.56±0.03 µm, and 0.18±0.01 µm respectively, and the membrane porosity was 8%, 12 % and 33% respectively. The deep UV photolithography

process used in fabrication allows for a highly precise pore size across the entire membrane surface. In comparison, the PVDF membranes fabricated using a polymer phase inversion process have a highly irregular surface structure with pores of varying sizes. This isoporous nature of the silicon nitride membrane theoretically allows for a very sharp cut-off in particle sieving[30].
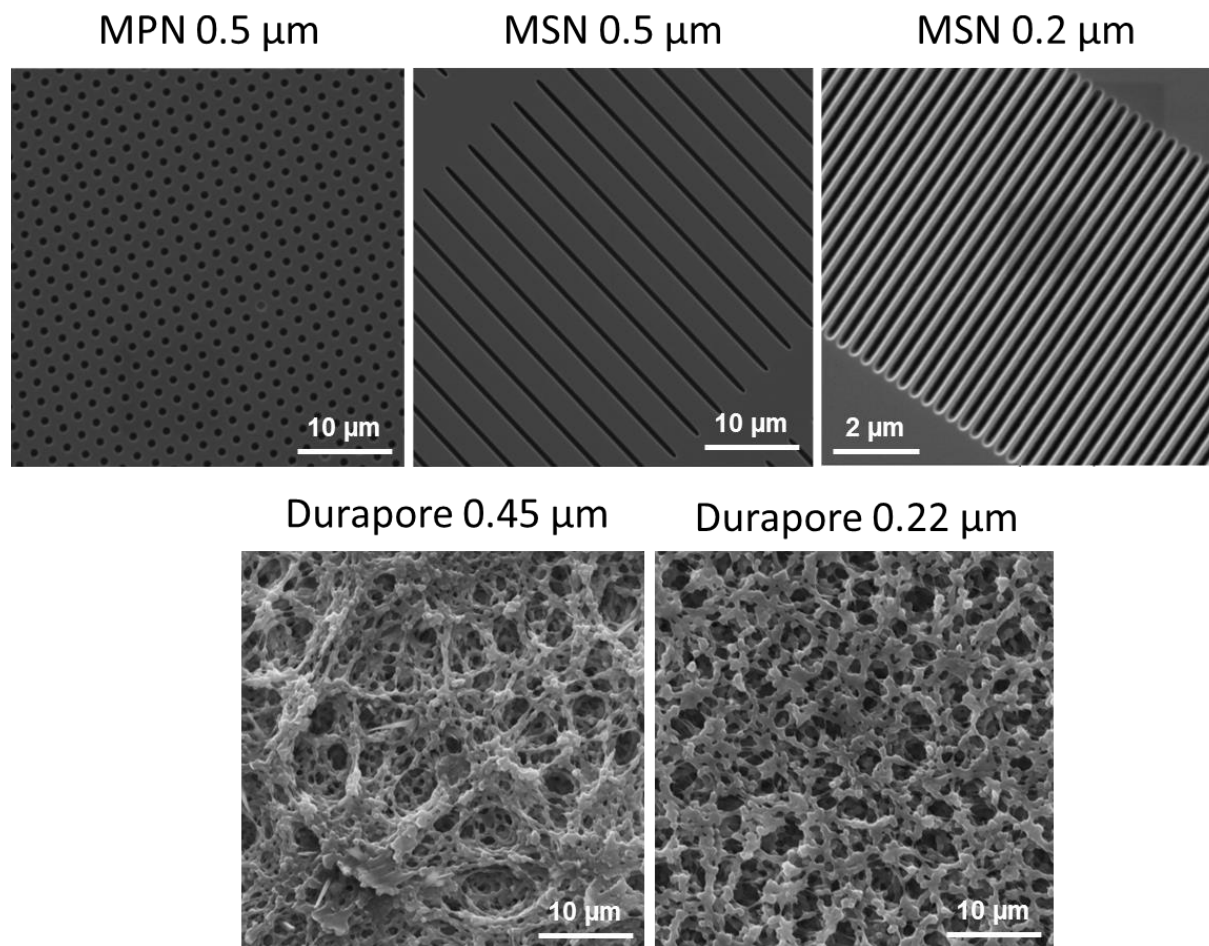
Figure 5.5: Scanning electron microscopy images of the silicon nitride and PVDF membranes used in this study. All images were obtained at 5,000 × magnification, except the MSN 0.2 µm membrane which was obtained at 20,000 × magnification to better show the smaller membrane slits.

The MSN 0.2 µm membrane has a thickness of only 0.2 µm, while the MSN 0.5 µm and MPN 0.5 µm membranes are 0.4 µm thick. In comparison, the Durapore membranes have an

average thickness of 125 µm. As shown in Figure 5.6, this large difference in thickness results in pure water hydraulic permeabilities which are orders of magnitude higher for the MSN and MPN membranes relative to the Durapore membranes. With higher permeability, fluid can be processed at higher flow rates or a lower pressures, potentially improving overall throughput. Comparing within the silicon nitride membranes, the MPN 0.5 µm membrane had approximately half the permeability of the MSN 0.5 µm membrane, due to the lower overall porosity, while the reduced slit width of the MSN 0.2 µm membrane also resulted in a lower permeability relative to the MSN 0.5 µm membrane. In addition to the pure water permeability, the gas permeability and membrane burst pressure were also assessed, with relevant methods and results detailed in Figures S5.14-S5.16). Contrary to the results from the hydraulic permeability, the gas permeability of the 0.2 µm slit membrane was greater than the 0.5 µm sit membrane due to the higher porosity playing a larger role in overall permeability than the slit width.
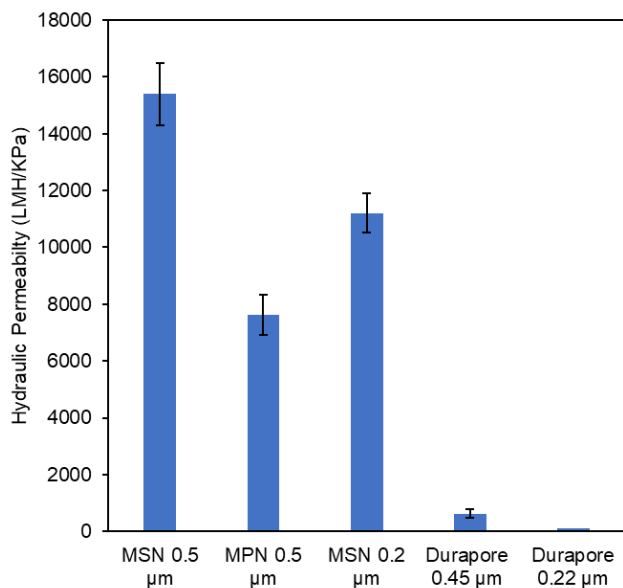
Figure 5.6: Hydraulic permeability (measured with pure water) of the silicon nitride (both microporous MPN and microslit MSN membranes) and PVDF Durapore membranes used in this study.

5.4.2. Small Scale Nanoparticle and Protein Filtration Studies

To assess the performance of the various membranes and to compare the effect of pore geometry (circular pores vs. slits), a series of filtration tests using standard model solutions were performed, measuring the transmembrane pressure change during filtration as an indication of membrane fouling (Figure 5.7). 0.84 µm diameter nanoparticles were selected as model particles likely to cause pore blockage in the 0.5 µm width slits or pores, where theoretically the slit membranes would experience less fouling. While a circular pore can be completely blocked by a spherical particle depositing on top of it, a slit will still allow for fluid flow around a particle trapped on the surface[18,19]. A small amount of surfactant (0.01% v/v Tween™ 20) was included in the nanoparticle solution to minimize the extent of nanoparticle–nanoparticle interactions and adsorption of nanoparticles to the membrane surface[31], allowing deposition of individual nanoparticles on the membrane surface to be the dominating factor in membrane fouling. For both membranes, the initial TMP was very low (<0.5 kPa) due to the incredible high permeability of the MPN and MSN 0.5 µm membranes. Comparing the rates of fouling between pore geometries, the experimental results did not show a significant difference in performance between the slit and circular pore membranes (Figure 5.7A). Both membranes fouled at a similar rate, and for both membranes the TMP increase was relatively linear with respect to throughput, indicating that cake formation was the dominant mode of fouling[32]. From this, it is likely that pore blockage (the expected mode of fouling) was not taking place for the MPN 0.5 µm membrane; the theorical scenario of one pore being blocked by a single particle depositing on top of it was not occurring. With both membranes experiencing cake fouling by the nanoparticles, there was no clear benefit to the slit pore geometry.

When a solution of 0.1% BSA was filtered through the MPN and MSN 0.5 µm membranes, a difference in performance between the pore geometries was observed (Figure 5.7B). Once again, both membranes had an incredibly low initial TMP, which then increased as fouling occurred. The rate of fouling observed with the slit membrane was significantly lower than the circular pore membranes. With small particles (i.e. proteins) significantly smaller than the pore size, fouling typically occurs following the pore constriction model, where proteins adsorb to the surface and a fouling layer slowly grows, gradually constricting the pore size, and eventually completely bridging and blocking the pore[18,26]. However, it has been shown that the high aspect ratio of slit pores leads to slower fouling, as both the initial deposition and growth of the fouling layer is only able to cover a small fraction of the slit at the edges[18]. The results observed comparing the fouling of the MPN and MSN 0.5 µm membranes matches this theory. Thus, the slit membranes have a clear advantage when filtering proteinaceous substances or those prone to adsorbing to the membrane surface, ideally making them more suited to the sterile filtration of therapeutic viruses.
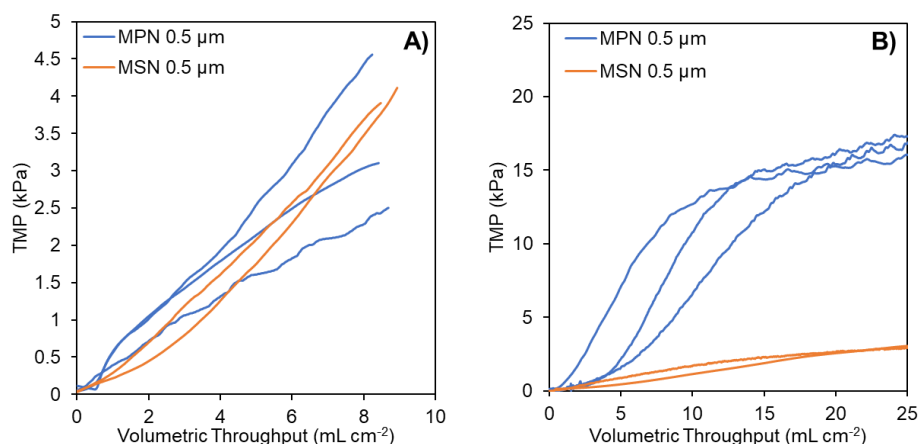
Figure 5.7: Comparison of 0.5 µm microporous (MPN) and microslit (MSN) silicon nitride membrane filtration performance. Membrane fouling by two model solutions was assessed through change in transmembrane pressure (TMP) during constant flux filtration. Lines in each panel show

the TMP profile for a single filtration experiment, with triplicate experiments performed for the MPN 0.5 µm membrane and duplicate experiments performed for the MSN 0.5 µm membrane. (A) Filtration of 0.003% (w/v) 0.84 µm polystyrene nanoparticles. (B) Filtration of 0.1% (w/v) bovine serum albumin.

With the advantages of the MSN slit structure demonstrated, the filtration performance was investigated in greater detail and compared to a conventional Durapore 0.22 µm membrane using solutions containing nanoparticles of varying sizes. Nominal diameters of 0.06, 0.18, 0.51, and 0.84 µm were chosen specifically to span the slit width dimension. Overall, the results were remarkably consistent across the triplicate testing. The TMP increase caused by each nanoparticle size when filtered through a MSN 0.2 µm membrane is shown in Figure 8A. The initial TMP was very low and is consistent with previous results. For the smallest nanoparticle (0.06 µm), there was no detectable increase in TMP during the entire duration of the constant flux filtration test. For the three other nanoparticles, although there was some variation between runs, overall the measured TMP profiles were fairly linear with respect to the total amount of filtrate throughput, again indicating the nanoparticles were fouling the membrane through the formation of a cake layer.
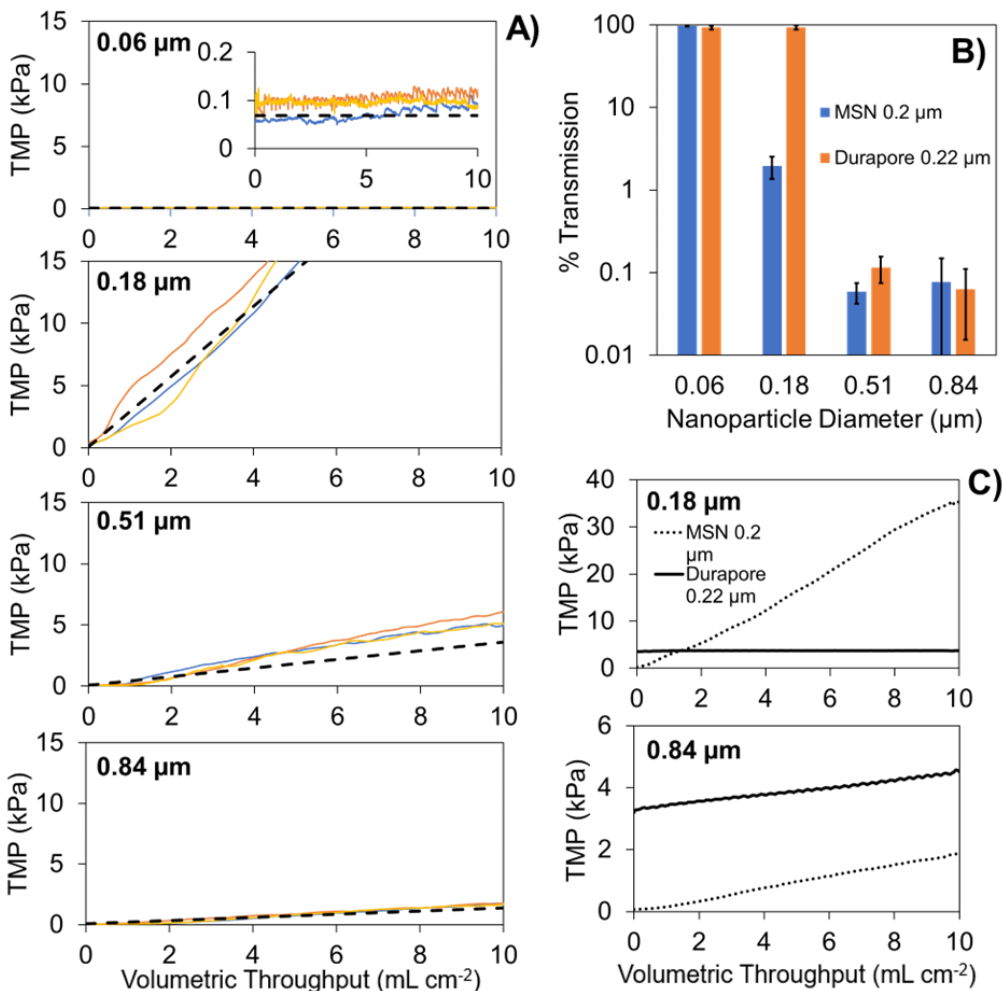
Figure 5.8: (A) Transmembrane pressure (TMP) profiles during constant flux filtration of polystyrene nanoparticle solutions through 0.2 μm microslit silicon nitride (MSN) membranes. The four panels correspond to the four reported sizes (0.06, 0.18, 0.51, and 0.84 μm) of polystyrene nanoparticles. The three solid colored lines within each panel correspond to the triplicate tests that were done for each size of polystyrene nanoparticle. The dashed black line within each panel corresponds to the predicted TMP profile due to formation of a cake layer on the surface of the membrane. (B) Percent transmission of polystyrene nanoparticles through the 0.2 μm MSN membranes and the 0.22 μm Durapore membrane, with error bars showing the standard deviation from triplicate experiments. (C) Comparison of TMP profiles for 0.2 μm MSN membranes and 0.22 μm Durapore membranes during constant flux filtration of solutions containing 0.18 or 0.84 μm polystyrene nanoparticles, with the lines showing the average TMP profile from triplicate testing of each membrane.

To validate the theory of a cake layer formation, all of the measured TMP profiles were compared against model predictions for the formation of a spherical particle cake layer on the membrane surface[32,33], following the equations:

$$J = \frac{\Delta P}{\mu\left(R_m + R_f\right)} \tag{4}$$

$$R_f = \frac{\alpha m_p}{A_m} \tag{5}$$

$$\alpha = \frac{180(1 - \varepsilon)}{\rho_p d_p^2 \varepsilon^3} \tag{6}$$

Where Equation 4 is used to calculate the changing TMP (ΔP) given a constant flux and an inherent membrane resistance R_m (calculated from earlier measurements of pure water flux) and an increasing fouling resistance R_f calculated from Equations 5 and 6. The experimental data showed a good agreement with the model (Figure 5.8A), supporting the theory of cake formation.

Analysis of nanoparticle amounts in the filtrate samples (as percentage of those in the corresponding feed sample) is shown in Figure 8B. The smallest 0.06 µm nanoparticles were essentially completely transmitted through both 0.2 µm MSN membranes (97 ± 2%) and conventional 0.22 µm Durapore membranes (92 ± 5%). The results for the 0.18 µm nanoparticles are particularly interesting. For the 0.2 µm MSN membrane, the transmission dropped sharply to 2.0 ± 0.6%, which is over 45-times lower than the corresponding result for the Durapore membrane (93 ± 5%). The low amount of 0.18 µm nanoparticles in the filtrate would suggest that a dense cake layer formed on the MSN membrane surface, rapidly leading to membrane fouling and an increase in TMP; this observation is in in good agreement with the TMP results in Figure 8A. Due to the incredibly consistent slit width of the MSN 0.2 µm membranes (measured width of

0.18±0.01 µm) the 0.18 µm particles were completely retained, whereas the polydisperse pore size of the Durapore 0.22 µm membrane likely did not allow it to retain particles with a size close to the nominal pore size. The experimental results for the Durapore membrane are in good agreement with those from a previous study of nanoparticle transmission through conventional 0.22 µm membranes[31]. While a very small amount of the 0.51 µm nanoparticles were seen in the filtrates from both MSN and Durapore membranes, this was likely due to a small amount of polydispersity in the nanoparticle size (Figure 5.4). A comparison of the TMP profiles for the two membranes (with two sizes of nanoparticles) is shown in Figure 8C. For the largest 0.84 µm nanoparticles, both membranes foul at a similar rate, however the MSN membranes maintained a lower TMP (Figure 5.8C). These results demonstrate the sharp selectivity of the MSN membrane, fully transmitting nanoparticles smaller than the slit width while fully retaining those larger than the slit width.

5.4.3. Stirred Cell Nanoparticle and Protein Filtration Studies

Due to the small size and surface area of the MSN and MPN membranes, a relatively low throughput and overall low filtrate volume (only 1-2 mL) is obtained during filtration. To scale up the filtration process, an alterative experimental setup using an Amicon stirred cell was designed. Furthermore, previous work using microfabricated membranes often implements cross flow filtration, where flow of fluid tangential to the membrane surface generates a shear force at the membrane surface that can prevent the deposition and buildup of particulate on the membrane[10,12,34,35]. Shear introduced by stirring may have a similar effect on improve filtration performance and reducing fouling. First, filtration of 0.18 µm nanoparticles through a disk of six MSN 0.5 µm membranes was tested. Given that the 0.18 µm nanoparticles are significantly smaller

than the 0.5 µm slit width, it is expected that little to no fouling should occur, as was seen with the 0.06 µm nanoparticles through the MSN 0.2 µm membrane. As shown in Figure 5.9A, only a small increase in TMP was measured throughout the filtration experiment. In addition, a filtrate volume of almost 20 mL was obtained demonstrating a significant increase in the overall throughput.
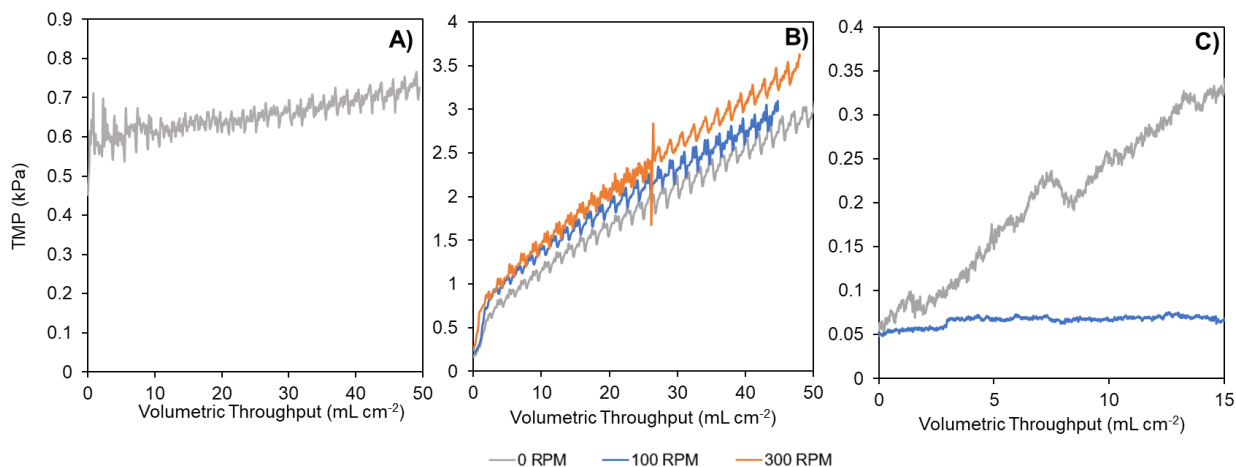
Figure 5.9: Influence of particle size and stirring on the change in TMP during the filtration of nanoparticles through a disk of six microslit silicon nitride membranes in an Amicon stirred cell. A) 0.18 µm nanoparticles at a constant flux of 2.3 mL cm^{-2}·min^{-1}. B) 2.1 µm particles at a constant flux of 2.3 mL cm^{-2}·min^{-1}. C) 2.1 µm particles at a constant flux of 0.23 mL cm^{-2}·min^{-1}

Next, filtration with 2.1 µm nanoparticles through the disk of MSN 0.5 µm membranes was tested. With particles significantly larger than the slit width, fouling is expected to occur and the effect of introducing stirring on the rate of fouling can be tested. At the original flux of 2.3 mL cm^{-2}·min^{-1} and with no stirring (0 RPM), a clear increase in TMP over the course filtration is seen (Figure 5.9B). When stirring was applied at either 100 RPM or 300 RPM, no clear difference in the rate of fouling was seen. A second set of filtration experiments was then attempted at a lower flux of only 0.23 mL cm^{-2}·min^{-1} (Figure 5.9C), where stirring at only 100 RPM appears to have completely prevented fouling of the membrane by the 2.1 µm nanoparticles. Stirring, or any fluid

flow parallel to the membrane surface, is able to prevent fouling due to shear and lift forces introduced at the membrane surface[36], and these forces are balanced against the drag force from the fluid flow normal to the membrane surface. It is likely that at the higher flux, the drag forces on the nanoparticles could not be overcome by the lift forces introduced through stirring, and therefore no effect from stirring was observed. Whereas at lower flux, lift forces from stirring were able to have a significant effect. This would mean that reduced fouling from stirring must be balanced against membrane flux, a common design criteria observed in cross flow operations[33].

Finally, the effect of stirring on fouling of the MSN 0.5 µm membranes by BSA was investigated. Beginning at the reduced flux rate of 0.23 mL cm^{-2}·min^{-1} stirring at 0 or 300 RPM was tested (Figure 5.10). This result appears to show that the stirring may have had a minor effect on the rate of fouling, with a longer delay until between the start of filtration and when the fouling buildup became detectable. Due to the significantly smaller particle size, proteins are less affected by shear and lift forces, and reduced fouling is often attributed to mixing of the boundary layer and reduction of a concentration polarization[33,36]. Further investigations are required to better understand the effects of stirring and the generated forces on the filtration performance of the MSN membranes.
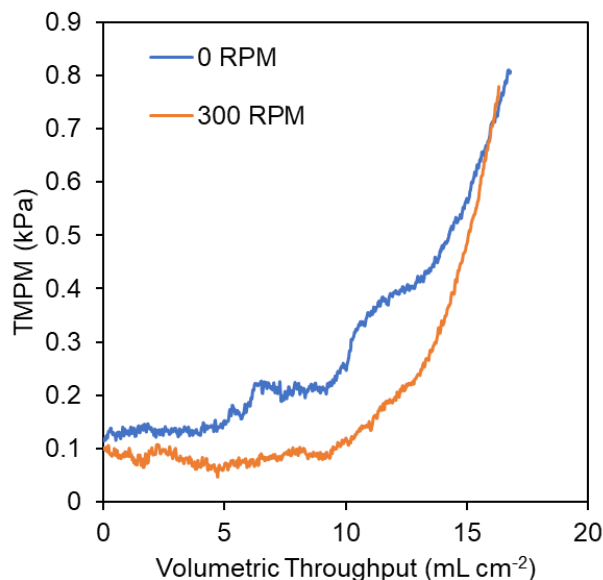
Figure 5.10: Change in TMP during the filtration of 0.1% BSA through a disk of six MSN 0.5 µm membranes at a constant flux of 0.23 mL cm^{-2}·min^{-1} in an Amicon stirred cell with stirring set to either 0 or 300 RPM.

5.4.4. Bacteria Filtration Studies

The MSN membranes have been shown to be resistant to fouling by proteins (relative to the MPN membranes), to have a sharp selectivity based on particle size, and to maintain a low TMP during filtration relative to conventional membranes; these factors should all make the membrane ideal for sterile filtration applications. To validate their sterile filtration functionality, both the MSN 0.2 and 0.5 µm membranes in the small scale format were tested by performing a challenge test with a solution of *B. diminuta* bacteria in accordance with the standard ASTM protocol[23]. As shown in Figure 5.11A, there was no detectable amount of B. diminuta in the filtrate samples from 0.2 µm MSN membranes. To the best of our knowledge, this result represents the first demonstration of sterile filtration using slit-shaped pores. To confirm the accuracy of our methods, we also evaluated the performance of a conventional 0.22 µm membrane (the same Durapore 0.22 µm membrane) in the same bacteria challenge test and found no detectable amount

of *B. diminuta* in the filtrate samples. For conventional polymer membranes, a combination of both sieving and adsorption phenomena is most often used to explain the bacterial removal mechanism[37]. Given the very high porosity and ultrathin nature of 0.2 μm MSN membranes, however, it is most likely that adsorption effects are negligible and that the bacterial removal capability occurs exclusively via sieving by the uniform slit pores. This hypothesis is supported by the filtration test results obtained with the 0.5 μm MSN membrane, which showed the permeation of high concentrations of *B. diminuta* into the corresponding filtrate samples. Given the proper operating conditions (e.g., low applied pressure) it is likely that an intermediate slit width dimension (i.e., between 0.2 and 0.5 μm) could be used and still achieve sterile filtration performance (i.e., no detectable amount of *B. diminuta* in the filtrate). As shown in Figures 5.11B–D, the TMP profiles for the *B. diminuta* challenge test were quite consistent across the triplicate tests that were done for each membrane (similar to results in Figure 5.8).
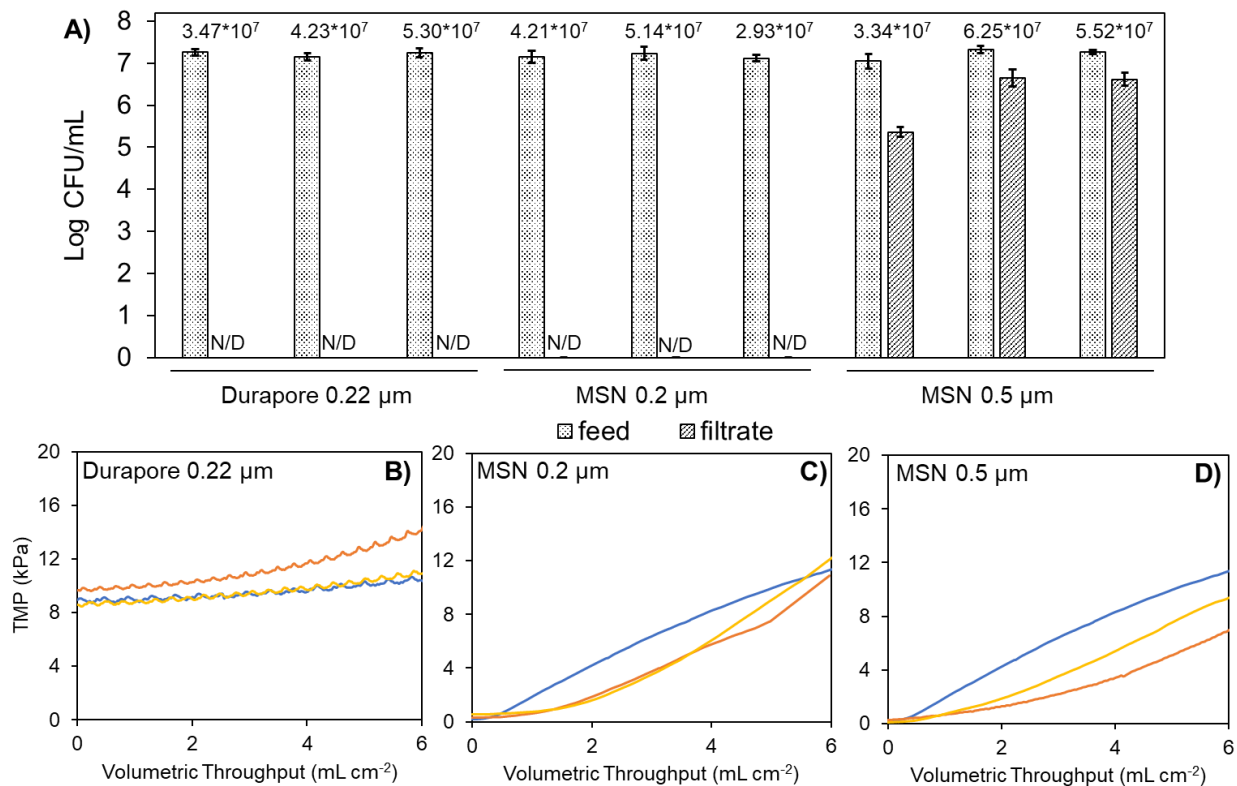
Figure 5.11: (A) Concentration of B. diminuta (expressed in colony forming units (CFU) per mL) in the feed and filtrate samples from filtration tests; the error bars correspond to the standard deviation from the triplicate plate count analysis that was done on each sample. The three sets of results for each membrane type correspond to the triplicate testing as shown in (B)–(D). The annotations for each pair of feed and filtrate sample indicate the total challenge amount of B. diminuta (CFU/cm^2). "N/D" is used to indicate those filtrate samples for which there was no detectable amount of B. diminuta. (B)–(D) Transmembrane pressure (TMP) profiles during constant flux filtration of B. diminuta solution through a Durapore 0.22 µm, MSN 0.2 µm and MSN 0.5 µm membrane. The three solid colored lines within each panel correspond to the triplicate testing that was done for each membrane.

5.4.5. Virus Filtration Studies

To test the MSN 0.2 µm membrane in a real sterile filtration application, two therapeutic virus solutions were filtered and assessed for performance through the transmission of the virus and the degree of membrane fouling. Performance was compared to a Durapore 0.22 µm membrane as a reference point for the existing conventional technologies. An oncolytic Maraba virus was selected as the first therapeutic virus to test, being a large challenge that conventional polymeric membranes

are unable to sterile filter efficiently given that previous work has shown poor recovery and high membrane fouling with a variety of polymeric membranes[7]. Furthermore, the virus is relatively large, being bullet shaped and 70×170 nm[7], which is relatively close to the 0.22 µm nominal pore size of sterile filters. Both the virus recovery and TMP profile for the filtration of Maraba virus through MSN 0.2 µm an Durapore 0.22 µm membranes are shown in Figure 5.12. The results show a very similar performance between membranes, with both membranes fouling rapidly and with very low recoveries of 7.8±5% and 6.5±4% respectively. The result for the Durapore 0.22 µm membrane closely matches previous work, where a 5% recovery was reported[7]. While the MSN membrane did initially start at a lower TMP, both membranes fouled so quicky that no overall lower TMP profile was achieved, as was observed in the nanoparticle tests. Previous work has studied the sterile filtration of Maraba virus in detail[7]. In this work, the resulting TMP profiles from constant flux filtration were fit to pore blocking models[32], and it was found that profiles best fit the standard or intermediate models[7]. This would indicate that the Maraba virus is fouling the interior of the pores or bridging the pores on top of the membrane[32]. In this work, the filtration of Maraba virus through the Durapore 0.22 µm membrane follows a similar pattern. However, the TMP profile for the MSN 0.2 µm membrane is largely linear, which as discussed in Section 5.4.2 is typically associated with cake filtration. This may indicate that the Maraba virus is acting as a large particle (similar to the nanoparticle filtration tests) building up a fouling layer on top of the membrane while not fully blocking or bridging the pores.
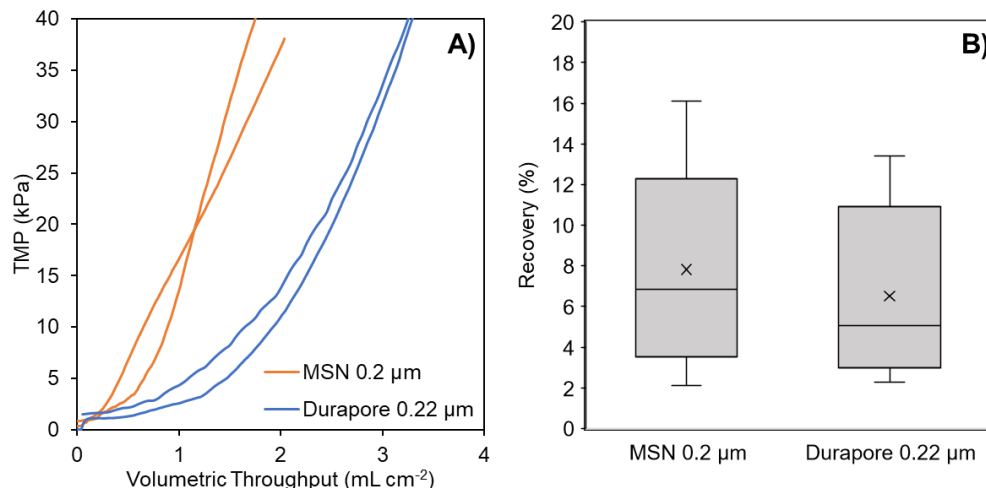
Figure 5.12: Change in transmembrane pressure (TMP) (A) and virus recovery (B) (calculated as the ratio of filtrate to feed titer) from the constant flux filtration of rhabdovirus Maraba through both microslit silicon nitride (MSN) 0.2 µm and Durapore 0.22 µm membranes. Solid colored lines in (A) correspond to TMP change during duplicate filtration experiments for both membranes. Boxes in (B) depict the interquartile range, the horizontal line represents the median, and the cross mark represents the mean. Whiskers extending from the boxes show the maximum and minimum values measured.

Next, a different type of virus was tested in a sterile filtration application. Adenovirus is commonly used in a variety of therapeutic applications and is an 80 nm icosahedral particle[25], with previous reports showing a recovery of greater than 90% after sterile filtration[24,25,38]. It was expected that Adenovirus would present less of a challenge for the MSN membrane and that less fouling during filtration would allow for the high permeability of the MSN to maintain an advantage over the Durapore membrane. While the TMP of the MSN membrane did initially start low (Figure 5.13) some degree of fouling was observed, whereas for the Durapore membrane there was no noticeable fouling. Both membranes achieved a high virus recovery of greater than 90%, however due to the fouling observed on the MSN membrane, it is expected that if a higher throughput was filtered that the recovery would begin to decrease.
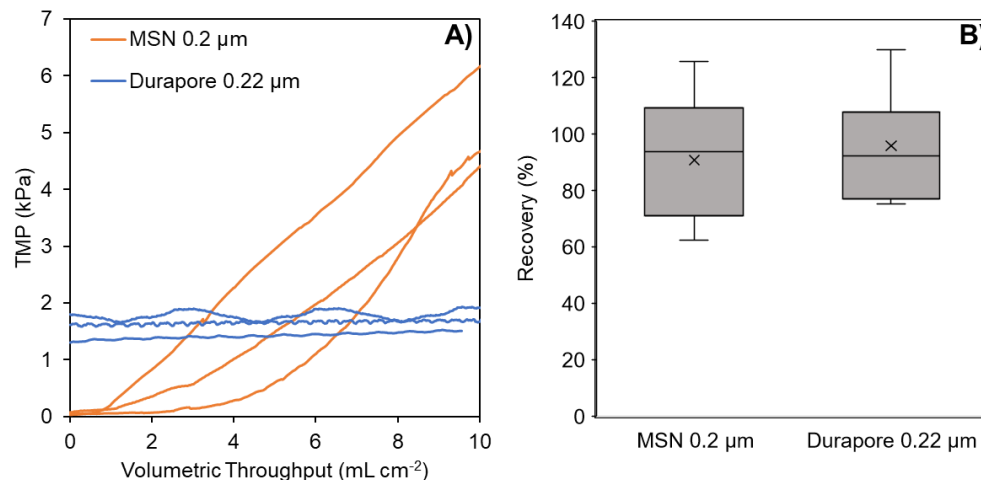
Figure 5.13: Change in transmembrane pressure (TMP) (A) and virus recovery (B) (calculated as the ratio of filtrate to feed titer) from the constant flux filtration of adenovirus through both microslit silicon nitride (MSN) 0.2 µm and Durapore 0.22 µm membranes. Solid colored lines in (A) correspond to TMP change during triplicate filtration experiments for both membranes. Boxes in (B) depict the interquartile range, the horizontal line represents the median, and the cross mark represents the mean. Whiskers extending from the boxes show the maximum and minimum values measured.

For both the adenovirus and Maraba virus, no clear improvement in filtration performance was observed when directly compared to a Durapore 0.22 µm membrane. It was theorized that the isoporous nature and thinness of the MSN membrane would prevent entrapment of virus within the membrane structure reducing fouling and loss of virus, however the results presented here show that there was no benefit to performance. While the MSN membrane does have the advantage of very high permeability as demonstrated in Figure 5.6, it is possible that the properties of the membrane also make it more sensitive to fouling. Previous work has shown the importance of pore interconnectivity in reducing fouling during membrane filtration[18,26,39,40], a property that the MSN membranes lack. Interconnected pores foul more slowly and result in less resistance to flow as the fluid can flow around the blockage as it passes through the membrane, whereas in with the straight-through pores of the MSN membranes once a pore is blocked that area of the membrane is rendered entirely inaccessible to flow. Furthermore, when particulate capture is concentrated in a single skin

layer, as it occurs on the surface of the MSN membrane, the degree of fouling and resistance to flow through the membrane is greater. Due to this phenomena, if both the MSN and Durapore membranes equally capture a material with a high propensity for fouling, such as large protein or virus aggregates, then it is possible that the resulting fouling could be more extreme for the MSN membrane.

One key advantage of isoporous microfabricated membranes is a smooth surface that is highly amenable to improved performance when operated in cross flow filtration. Initial investigations implementing the MSN membranes in a stirred cell format showed some promise and testing the filtration of virus solutions in this format is a clear next step, however significantly more work is required to better understand and optimize the process. Furthermore, the surface chemistry of the membrane could be improved to better prevent the adsorption of biological materials. Common approaches such as the grafting of PEG or zwitterionic molecules to a surface have been shown to reducing protein adsorption, and these methods are compatible with the silicon chemistry of the MSN membranes[41,42].

5.5. Conclusions

The results presented here are a promising first step towards the development of a new generation of membranes for biopharmaceutical processing, specifically sterile filtration of therapeutic viruses. Microfabricated silicon nitride membranes were shown to have a hydraulic permeability which is orders of magnitude greater than polymeric membranes, enabling higher throughput processing, while the isoporous and ultrathin nature of the membranes was theorized to give better selectivity of particles and result in a higher transmission of virus. Using model

nanoparticle and protein solutions, the filtration performance of MPN and MSN membranes was compared, with the slit pore membranes demonstrating a significantly lower degree of fouling by protein solutions, thus likely making them more appropriate for the filtration of biological solutions and the sterile filtration of therapeutic viruses. The MSN membrane was then integrated into a stirred cell filtration system, demonstrating the beneficial effects that stirring can have on reducing fouling from particle deposition on the membrane surface. Using the standard test organism *B. diminuta* and following the ASTM protocol, the MSN 0.2 µm membrane was validated to completely retain bacteria and act as a sterile filter. The MSN 0.2 µm membrane was then directly compared to a Durapore 0.22 µm membrane in the sterile filtration of both Maraba virus and adenovirus solutions. Despite the hypothesized benefits of the MSN membrane, a greater degree of fouling and similar virus recovery was seen when compared to the Durapore membrane. Future developments to the membrane surface chemistry and filtration configuration will likely provide large benefits to improving filtration performance and enable this technology to find use in the bioprocessing and sterile filtration of therapeutic viruses and other products.

5.6. Acknowledgements

form of a Summer Studentship Award (to MC). SiMPore Inc., a private company, participated in

this work and is commercializing the membrane material developed and used in the study.

5.7. References

1. Wang Y, Hammes F, Düggelin M, Egli T. Influence of Size, Shape, and Flexibility on Bacterial Passage through Micropore Membrane Filters. *Environ Sci Technol*. 2008;42(17):6749-6754. doi:10.1021/es800720n

2. Harp G, Cho SJ, Lester E, Rose D, Sabanyagam C, Ross SF. Microscopic Characterization of Brevundimonas diminuta in the Hydrated State. *PDA J Pharm Sci Technol*. 2015;69(3):355-365. doi:10.5731/pdajpst.2015.01045

3. FDA. *Viral Safety Evaluation of Biotechnology Products Derived From Cell Lines of Human or Animal Origin*. Center for Drug Evaluation and Research, Food and Drug Administration; 1998.

4. Meltzer TH, Jornitz MW. The Sterilizing Filter and Its Pore Size Rating. *Am Pharm Rev*. 2003;6:6.

5. Zydney AL, Aimar P, Meireles M, Pimbley JM, Belfort G. Use of the log-normal probability density function to analyze membrane pore size distributions: functional forms and discrepancies. *J Membr Sci*. 1994;91(3):293-298. doi:10.1016/0376-7388(94)80090-1

6. Lee JK, Liu BYH. A filtration model of microporous membrane filters in liquids. *KSME J*. 1994;8(1):78-87. doi:10.1007/BF02953246

7. Shoaebargh S, Gough I, Fe Medina M, et al. Sterile filtration of oncolytic viruses: An analysis of effects of membrane morphology on fouling and product recovery. *J Membr Sci*. 2018;548:239-246. doi:10.1016/j.memsci.2017.11.022

8. Lamparski HG, Metha-Damani A, Yao JY, et al. Production and characterization of clinical grade exosomes derived from dendritic cells. *J Immunol Methods*. 2002;270(2):211-226. doi:10.1016/S0022-1759(02)00330-7

9. Kim S, Feinberg B, Kant R, et al. Diffusive Silicon Nanopore Membranes for Hemodialysis Applications. *PLOS ONE*. 2016;11(7):e0159526. doi:10.1371/journal.pone.0159526

10. Kuiper S. Filtration of lager beer with microsieves: flux, permeate haze and in-line microscope observations. *J Membr Sci*. 2002;196(2):159-170. doi:10.1016/S0376-7388(01)00553-1

11. Ji HM, Samper V, Chen Y, Heng CK, Lim TM, Yobas L. Silicon-based microfilters for whole blood cell separation. *Biomed Microdevices*. 2008;10(2):251-257. doi:10.1007/s10544-007-9131-x

12. Carpintero-Tepole V, Brito-de la Fuente E, Martínez-González E, Torrestiana-Sánchez B. Microfiltration of concentrated milk protein dispersions: The role of pH and minerals on the performance of silicon nitride microsieves. *LWT - Food Sci Technol*. 2014;59(2):827-833. doi:10.1016/j.lwt.2014.06.057

13. Benavente JJM, Mogami H, Sakurai T, Sawada K. Evaluation of Silicon Nitride as a Substrate for Culture of PC12 Cells: An Interfacial Model for Functional Studies in Neurons. *PLOS ONE*. 2014;9(2):e90189. doi:10.1371/journal.pone.0090189

14. Carter RN, Casillo SM, Mazzocchi AR, DesOrmeaux JPS, Roussie JA, Gaborski TR. Ultrathin transparent membranes for cellular barrier and co-culture models. *Biofabrication*. 2017;9(1):015019. doi:10.1088/1758-5090/aa5ba7

15. van Rijn CJM, Elwenspoek MC. Microfiltration membrane sieve with silicon micromachining for industrial and biomedical applications. In: *Proceedings IEEE Micro Electro Mechanical Systems. 1995*. IEEE; 1995:83. doi:10.1109/MEMSYS.1995.472549

16. Rijn CJM van, Veldhuis GJ, Kuiper S. Nanosieves with microsystem technology for microfiltration applications. *Nanotechnology*. 1998;9(4):343-345. doi:10.1088/0957-4484/9/4/007

17. Vlassiouk I, Apel PY, Dmitriev SN, Healy K, Siwy ZS. Versatile ultrathin nanoporous silicon nitride membranes. *Proc Natl Acad Sci*. 2009;106(50):21039-21044. doi:10.1073/pnas.0911450106

18. Chandler M, Zydney A. Effects of membrane pore geometry on fouling behavior during yeast cell microfiltration. *J Membr Sci*. 2006;285(1-2):334-342. doi:10.1016/j.memsci.2006.09.002

19. Warkiani ME, Wicaksana F, Fane AG, Gong HQ. Investigation of membrane fouling at the microscale using isopore filters. *Microfluid Nanofluidics*. 2015;19(2):307-315. doi:10.1007/s10404-014-1538-0

20. Bromley AJ, Holdich RG, Cumming IW. Particulate fouling of surface microfilters with slotted and circular pore geometry. *J Membr Sci*. 2002;196(1):27-37. doi:10.1016/S0376-7388(01)00573-7

21. Fissell WH, Dubnisheva A, Eldridge AN, Fleischman AJ, Zydney AL, Roy S. High-Performance Silicon Nanopore Hemofiltration Membranes. *J Membr Sci*. 2009;326(1):58-63. doi:10.1016/j.memsci.2008.09.039

22. Kanani DM, Fissell WH, Roy S, Dubnisheva A, Fleischman A, Zydney AL. Permeability - Selectivity Analysis for Ultrafiltration: Effect of Pore Geometry. *J Membr Sci*. 2010;349(1-2):405. doi:10.1016/j.memsci.2009.12.003

23. ASTM. *F838-20: Standard Test Method for Determining Bacterial Retention of Membrane Filters Utilized for Liquid Filtration*. American Society for Testing and Materials; 2020. Accessed November 29, 2021. https://www.astm.org/f0838-20.html

24. Moleirinho MG, Rosa S, Carrondo MJT, et al. Clinical-Grade Oncolytic Adenovirus Purification Using Polysorbate 20 as an Alternative for Cell Lysis. *Curr Gene Ther*. 2018;18(6):366-374. doi:10.2174/1566523218666181109141257

25. Konz JO, Lee AL, Lewis JA, Sagar SL. Development of a Purification Process for Adenovirus: Controlling Virus Aggregation to Improve the Clearance of Host Cell DNA. *Biotechnol Prog*. 2005;21(2):466-472. doi:10.1021/bp049644r

26. Ho CC, Zydney AL. Effect of membrane morphology on the initial rate of protein fouling during microfiltration. *J Membr Sci*. Published online 1999:15.

27. Wang D, Soong SJ. Comparisons of titer estimation methods for multiplexed pneumococcal opsonophagocytic killing assay. *Comput Stat Data Anal*. 2008;52(11):5022-5032. doi:10.1016/j.csda.2008.04.025

28. Irwin JO. Statistical Method in Biological Assay. *Nature*. 1953;172(4386):925-926. doi:10.1038/172925a0

29. Kawka K, Madadkar P, Umatheva U, et al. Purification of therapeutic adenoviruses using laterally-fed membrane chromatography. *J Membr Sci*. 2019;579:351-358. doi:10.1016/j.memsci.2019.02.056

30. DesOrmeaux JPS, Winans JD, Wayson SE, et al. Nanoporous silicon nitride membranes fabricated from porous nanocrystalline silicon templates. *Nanoscale*. 2014;6(18):10798-10805. doi:10.1039/C4NR03070B

31. Pazouki M, Noelle Wilton A, Latulippe DR. An experimental study on sterile filtration of fluorescently labeled nanoparticles – the importance of surfactant concentration. *Sep Purif Technol*. 2019;218:217-226. doi:10.1016/j.seppur.2019.02.038

32. Iritani E. A Review on Modeling of Pore-Blocking Behaviors of Membranes During Pressurized Membrane Filtration. *Dry Technol*. 2013;31(2):146-162. doi:10.1080/07373937.2012.683123

33. Bowen WR, Jenner F. Theoretical descriptions of membrane filtration of colloids and fine particles: An assessment and review. *Adv Colloid Interface Sci*. 1995;56:141-200. doi:10.1016/0001-8686(94)00232-2

34. Gironès M, Lammertink RGH, Wessling M. Protein aggregate deposition and fouling reduction strategies with high-flux silicon nitride microsieves. *J Membr Sci*. 2006;273(1):68-76. doi:10.1016/j.memsci.2005.10.013

35. Ben Hassan I, Lafforgue C, Ellero C, Ayadi A, Schmitz P. Coupling of local visualization and numerical approach for particle microfiltration optimization. *Microsyst Technol*. 2015;21(3):509-517. doi:10.1007/s00542-013-1906-9

36. van Reis R, Zydney A. Bioprocess membrane technology. *J Membr Sci*. 2007;297(1):16-50. doi:10.1016/j.memsci.2007.02.045

37. Mittelman MW, Jornitz MW, Meltzer TH. Bacterial cell size and surface charge characteristics relevant to filter validation studies. *PDA J Pharm Sci Technol*. 1998;52(1):37-42.

38. Green AP, Huang JJ, Scott MO, et al. A new scalable method for the purification of recombinant adenovirus vectors. *Hum Gene Ther*. 2002;13(16):1921-1934. doi:10.1089/10430340260355338

39. Bacchin P, Derekx Q, Veyret D, Glucina K, Moulin P. Clogging of microporous channels networks: role of connectivity and tortuosity. *Microfluid Nanofluidics*. 2014;17(1):85-96. doi:10.1007/s10404-013-1288-4

40. Loh S, Beuscher U, Poddar TK, et al. Interplay among membrane properties, protein properties and operating conditions on protein fouling during normal-flow microfiltration. *J Membr Sci*. 2009;332(1-2):93-103. doi:10.1016/j.memsci.2009.01.031

41. Brault ND, Gao C, Xue H, et al. Ultra-low fouling and functionalizable zwitterionic coatings grafted onto SiO2 via a biomimetic adhesive group for sensing and detection in complex media. *Biosens Bioelectron*. 2010;25(10):2276-2282. doi:10.1016/j.bios.2010.03.012

42. Sharma S, Johnson RW, Desai TA. Ultrathin poly(ethylene glycol) films for silicon-based microdevices. *Appl Surf Sci*. 2003;206(1):218-229. doi:10.1016/S0169-4332(02)01220-5

5.8. Supplementary Material
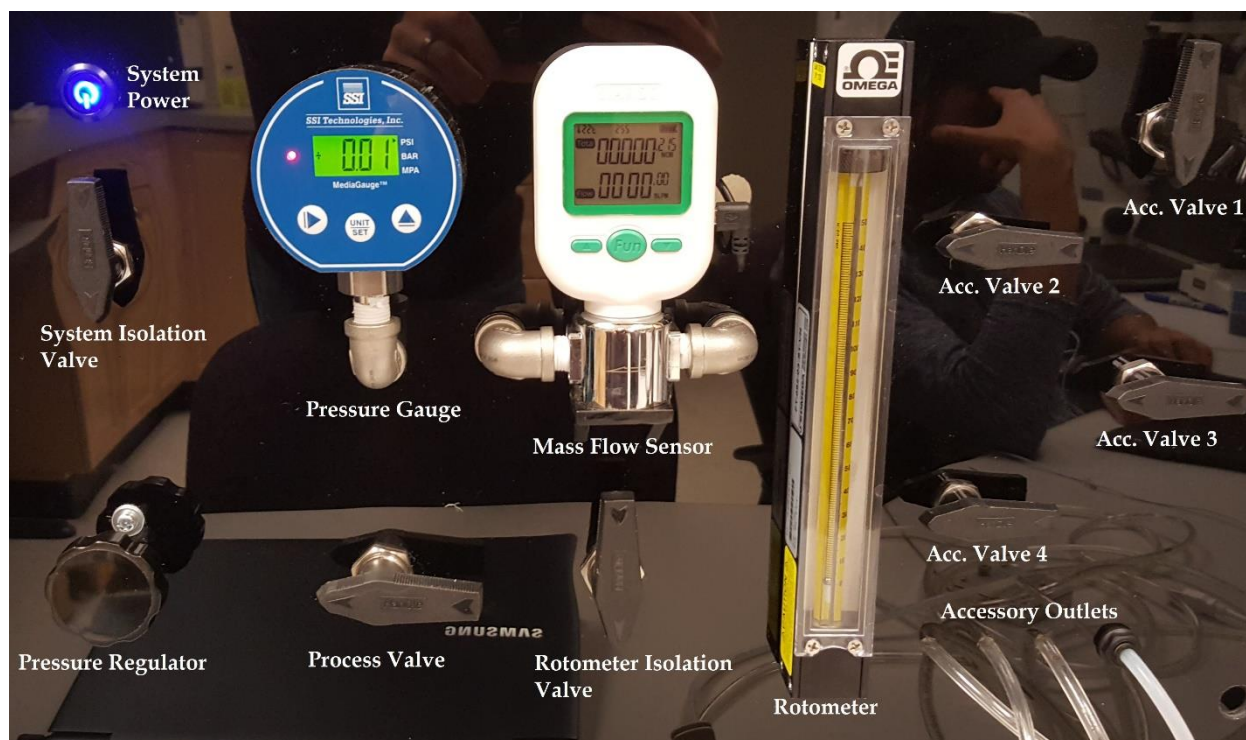
Figure S5.14. Picture of the custom-built pressure testing apparatus utilized for gas flow and differential pressure tolerance measurements reported in this work. This panel houses the main control elements used for metering a gas supply to one or more accessory lines in such a way that both the supply pressure (via the digital pressure gauge) and the volumetric gas flow (via either the ball rotameter or digital mass flow sensor) can be precisely measured.
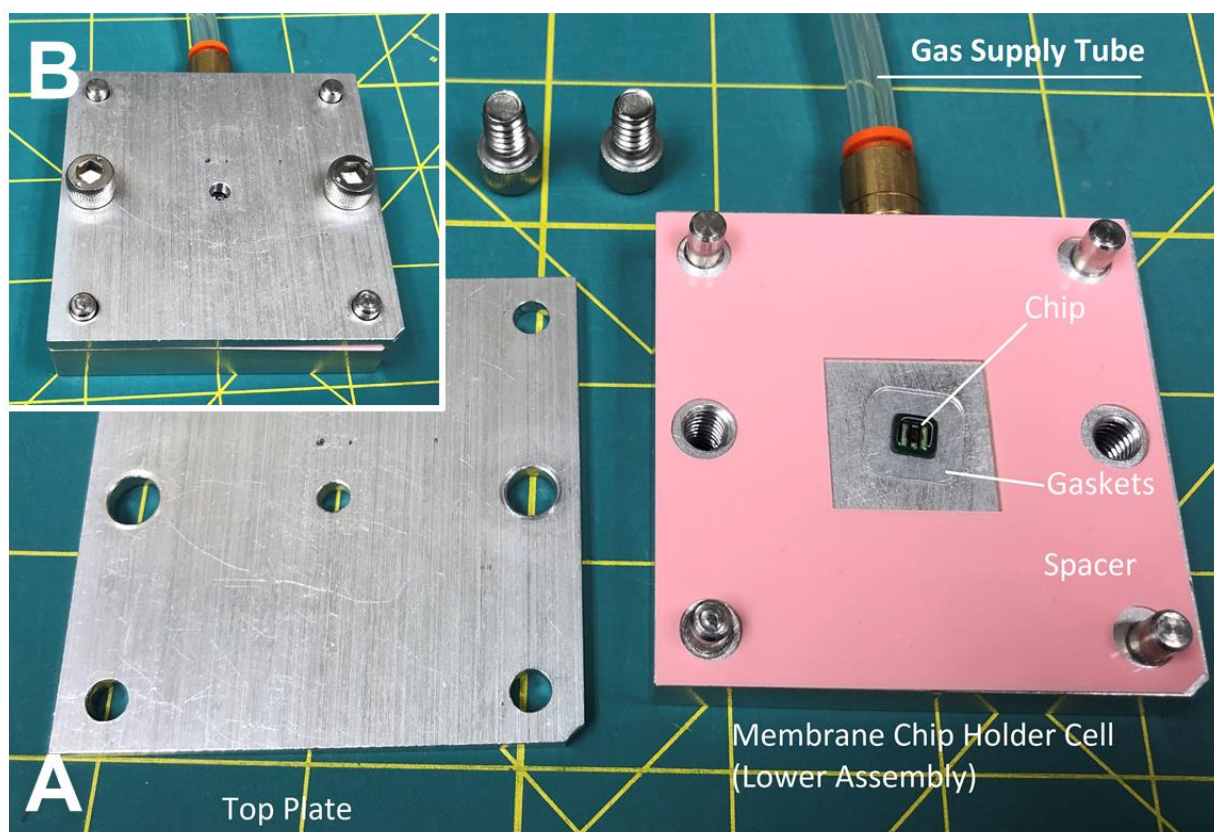
Figure S5.15: A) A machined pressure fixture used for placement and sealing of membrane chips above a gas supply orifice. This accessory was attached to the pressure regulation system in Figure S1 via ¼" OD Tygon tubing and used for all gas flow rate and differential pressure tolerance testing. Briefly; a membrane chip is placed between two 300 µm thick silicone gaskets, oversized to create a tight seal. The membrane chip-gasket assembly, is then placed over a machined orifice in the base of the holder cell and a 200 µm thick spacer layer (pink plastic sheet) is added to ensure uniform compression. B) The top plate is installed and secured by two socket-head cap screws to ensure a tight seal.
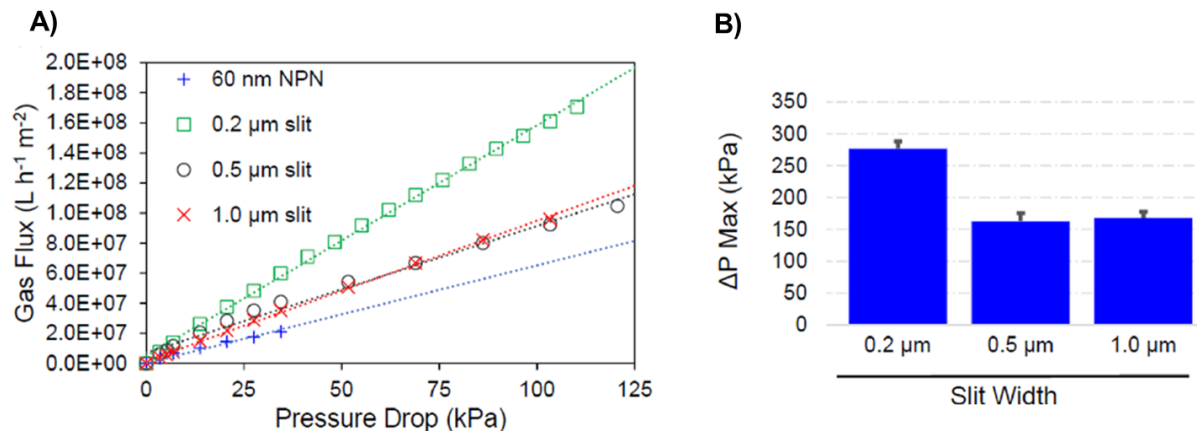
Figure S5.16: A) Nitrogen gas flux as a function of applied pressure for the three MSN membranes. each data point represents at least triplicate observations with average error <25% coefficient of variation. B) Maximum differential pressure tolerance (i.e. maximum pressure reached at membrane) for the three MSN membranes, with the error bars correspond to one standard deviation from the triplicate testing that was done for each membrane type.

Chapter 6

Fused Nanoparticles as Model Virus Aggregates for

Membrane Filtration

6. Fused Nanoparticles as Model Virus Aggregates for Membrane Filtration

Evan Wright, Christina Hassey, David R. Latulippe

Prepared for journal submission

6.1. Abstract

Nanoparticles are a ubiquitous part of separation and membrane science, used in a variety of ways for studying filtration performance and characterizing membranes. Of particular interest, nanoparticles can be used as approximate surrogates for virus particles which can present significant experimental complexity, low throughput testing, and safety concerns. However, many of the properties of nanoparticles are often overly simplified and this greatly limits their accuracy as surrogates for true virus particles; nanoparticles are often monodisperse, of uniform size, and have highly stable surfaces. Therefore, to create nanoparticles solutions with more complex properties, we show here how a "salting out – quenching – fusing" process can be used to create stable 0.19 µm nanoparticle aggregates. Our results show that the fabrication process is controllable and repeatable, and the distribution of aggregate sizes can be adjusted by modifying the experimental conditions. Basic constant pressure filtration tests using membranes with both 0.22 and 0.45 µm pore sizes were performed, demonstrating how the degree of aggregation relates to both the membrane fouling (measured as flux decline during filtration) and overall particle transmission through the membrane. Analysis of the constant pressure filtration data using pore blocking and Vmax models demonstrated how the fused nanoparticle filtration data can be related to the sterile filtration of therapeutic viruses. The fabrication technique and methodology presented

here can easily be used as a tool in future work to better model and study the filtration performance of complex solutions and as a simple method to investigate the potential performance of membranes in the sterile filtration of virus solutions.

6.2. Introduction

Nanoparticles have become a key tool in membrane science for applications such as evaluating pore size distribution in membranes[1–3], or as a test material for characterizing membrane fouling[4–7]. In filtration studies, nanoparticles have been compared with biological organisms such as yeast[8], bacteria[9], and in particular viruses[10–14]. This is of considerable interest due to safety concerns when working with viruses and due to the complexity in preparing, handling and interpreting results from experiments they are involved in. In areas such as biopharmaceutical processing and the purification of therapeutic viruses, simple nanoparticle surrogates to tests how viruses interact with membrane filters are highly valuable.

To date, nanoparticles used in filtration studies are largely monodisperse spheres made of inorganic materials such as polystyrene[11,14] gold[12,13] or silica[9]. While some studies have used a mixture of particle sizes[15], or alternate shapes such as rods[16,17], the current state of the art is lacking in ways to represent more complex particles during filtration experiments. This is of particular concern as viruses have many non-ideal properties that may not be reflected in simple nanoparticles which could have a large influence on filtration performance. Many viruses have non-spherical shapes, such as rhabdoviruses being bullet shaped[18], Vaccinia virus being brick shaped[19] and some viruses, such as respiratory syncytial virus, having various pleomorphic forms which can range from spherical to filamentous[20]. Furthermore, viruses have highly variable surface

properties, with charge and hydrophobicity varying between types of viruses and even depending on factors such as culture conditions[21]. Even within a single virus particle, there can be patches of varying surface properties[22] and these factors are all known to influence interactions with membrane filters[23,24]. Finally, virus particles are prone to aggregation based on a wide range of factors[25–27] and this aggregation is known to influence filtration performance[27–29], therefore treating them as monodisperse particles may often not be appropriate. Thus, it would be highly desirable to explore using nanoparticles with alternate and more complex structures in filtration studies to better reflect the properties of some viruses.

From areas of colloidal science and microfabrication, a wide variety of non-spherical or irregular nanoparticles have already been detailed in literature, including ellipsoids[30], half spheres[31], peanut shapes[32], rods[33], disks[34], rectangular prisms[35] and spheres with textured or patterned surfaces[36,37]. There is also the opportunity to create higher order structures such as packed clusters both small[38] and large[39], webs[40] and dimers[41,42]. However, many of these techniques require complex synthesis procedures and the use of microfluidics and/or microfabrication techniques, making them less suitable for widespread use. A simple and easy to perform method to fabricate aggregates or higher order colloidal structures would be highly valuable and could be applied to model virus aggregates during filtration studies. A suitable technique to achieve this is a "salting out – quenching – fusing" process as first introduced by Yake *et al.*[43,44] which creates controlled nanoparticle doublets and larger aggregates, which only requires commercially available functionalized polystyrene nanoparticles.

In this work, we demonstrate the repeatable and controllable nature by which higher order nanoparticle structures can be formed using the "salting out – quenching – fusing" process and extend the technique to how it can be used to create model feed solutions for membrane filtration tests. Basic filtration experiments using a commercial PES membrane at two different pore sizes (0.45 µm and 0.22 µm) were performed with the fused nanoparticle solutions in order to demonstrate how the filtration performance (membrane fouling and nanoparticle recovery) is influenced by the created aggregates. Analysis of the results using both pore blocking and Vmax models was then performed to demonstrate how the data obtained from the filtration of fused nanoparticles relates to the sterile filtration of virus particle and how the results can be practically applied.

6.3. Materials and Methods

6.3.1. Preparation of Fused Nanoparticles

The protocol used by Juluri *et al.* [45], optimized for the formation of doublet particles, was used as a starting point and was further optimized based on initial experimental results. In order to demonstrate the accuracy and flexibility of the process in producing different aggregate sizes, two different batches of fused nanoparticles were produced, one with a low fusing time and another with a high fusing time. The low fusing time was optimized for the formation of doublets and was targeted at 75% singlet particles remaining, while the high fusing time was optimized for 50% singlets particles remaining. To begin, 15 μL of carboxyl latex particles (Invitrogen, 4% w/v, mean diameter 0.19 μm) was added to 1.5 mL of 500 mM KCl solution in a glass vial and was gently swirled for 30 seconds or 120 seconds (low and high salting out time batches respectively) to ensure adequate mixing. The entire 1.5mL KCl-nanoparticle solution was then added to 150 mL

of DI water and this solution was autoclaved for 5 minutes at 120°C to fuse the particles and stabilise any aggregates. Following autoclaving, the solution was air-cooled to ambient temperature and centrifuged at 10,000 RPM for 2 hours to concentrate the fused particles. The resulting pellet was resuspended in 15mL of nanoparticle buffer (10mM phosphate buffer pH 7.4, 0.01%v/v Tween™ 20, 0.01% NaN_3). An overview of the complete process is shown in Figure S6.7. This process can be scaled or repeated as necessary, and multiple batches were pooled together to create one master solution (of both 75% singlet and 50% singlet nanoparticle solutions) used for all filtration tests described here.

As a control, a solution of unfused nanoparticles was also tested in the filtration experiments. Given that the fused nanoparticle solution is approximately 0.004% w/v (not accounting for any potential losses during production), to create the control solution the stock 4% w/v nanoparticle solution was simply diluted 1:1000 directly into the nanoparticle buffer.

In order to validate the salting out-quenching-fusing process, the nanoparticle solutions were imaged using scanning electron microscopy (SEM) and the fraction of each particle structure (singlets, doublets, triplets, quadruplets, and larger aggregates) was determined through manual counting. To prepare the solution for SEM imaging, a 1mL sample was centrifuged, the resulting pellet was collected then resuspended in deionized water, and a 10 µl drop was dried on a silicon wafer. The wafer was mounted on specimen carriers and the samples were sputter coated (Polaron E5100) with gold for 60 s under a current of 20 mA, depositing a layer of approximately 24 nm. The wafer was then imaged using SEM at 10,000 × magnification and the fraction of particle structures were manually counted in 10 different areas of each wafer.

6.3.2. Constant Pressure Filtration

A constant pressure filtration system was used to perform all filtration experiments. The pressure in a reservoir was controlled using an Elveflow OB1 MK3 multi-channel microfluidic flow control (MMFC) system. The OB1 MK3 pressure controller was supplied with compressed nitrogen at approximately 206 kPa (30 PSI), which was filtered prior to entering the unit. The pressure of the reservoir was controlled using a computer interface and was set to 6.89 kPa (1 PSI) for all constant pressure experiments. The pressurized reservoir was connected to a polycarbonate filter holder (Cole Parmer, 0.5 cm^2 of effective filtration area) using 15 cm of 1/16" ID Masterflex silicone tubing, and the appropriate Luer Lock fittings. A retort stand and clamp was used to position the filter holder in place above a glass beaker on a bench-top analytical balance.

Constant pressure experiments consisted of two phases: (1) a buffer pre-test, and (2) a nanoparticle solution filtration test. The membrane of interest was inserted in the polycarbonate membrane holder and wetted using the buffer solution by alternating between gentle forward and back flushing with a syringe. A new membrane was used for each constant pressure experiment. PES (Millipore Express PLUS) membranes with both 0.22 and 0.45 µm pore sizes were used. For the buffer pre-test, 15mL of the buffer solution was loaded into the reservoir. The reservoir was pressurized to 6.89 kPa and the weight of the filtrate was recorded at 30 second intervals until a cumulative filtrate weight of 10g was reached. The process was repeated at 13.8 and 27.6 kPa (2 and 4 PSI respectively), and with this data the permeability of the membrane could be calculated to ensure that it was within expected values. Next, for the nanoparticle filtration test, the reservoir was depressurized and filled with 15mL of nanoparticle solution. The reservoir was pressurized to

6.89 kPa and the first 1 mL was collected and discarded as the holdup volume inside the tubing and membrane holder. An empty beaker was then placed on the balance and the cumulative weight of the filtrate was recorded every 30 seconds until a weight of 10 g was reached. For the purpose of all calculations, the density of the feed and filtrate was assumed to be 1 g/mL. Using the measured filtrate weight, the filtrate flux during each 30 second interval was calculated.

Post-filtration samples of the feed and filtrate were measured using optical absorbance in order to assess the nanoparticle recovery, calculated as the ratio of filtrate to feed concentration. Triplicate 200 µl aliquots of both the feed and filtrate were transferred to a clear 96-well plate (Corning) and the optical absorbance was measured at 400 nm using a Spark 10M microplate reader (TECAN). Serial dilution of the stock nanoparticle solution followed by absorbance measurement was performed in order to ensure that a linear relationship between concentration and absorbance was valid for all measured samples.

6.4. Results and Discussion

6.4.1. Formation of Fused Particles

The "salting out – quenching – fusing" process is a series of steps which takes advantage of electrostatic repulsion by charged particles and how the repulsion can be shielded through the addition of charged ions to the solution. To begin, an electrostatically stable solution of polystyrene latex particles is salted out by adding a high concentration of potassium chloride and increasing the ionic strength of the solution. This reduces electrostatic repulsion between particles and allows them to aggregate through diffusion-controlled collisions and Van der Walls forces. After allowing the particles to aggregate for a predetermined amount of salting out time, the solution is quenched

by diluting it with a large volume of deionized water, reducing the ionic strength and halting any further aggregation. Finally, the particles are fused together by heating the solution above the glass transition temperature of polystyrene for a short time, creating particles which are permanently attached together. This process can be characterized by the Smoluchowski rapid flocculation estimate[43]:

$$\tau = \frac{\pi \mu r^3 W}{2kT\varphi} \tag{1}$$

Where τ is the estimated time for half of the singlet particles to aggregate. From this, there are multiple variables which can be tuned to achieve a desired result and control the degree of aggregation or size of higher order structures which are produced. For a given particle size, to achieve slower aggregation the ionic strength can be reduced (as this increases the stability ratio[46]) or the solids fraction can be decreased, while the opposite can be changed to speed up the aggregation. The original protocol[43] was optimized for the formation of doublets from approximately 2 µm particles, while other work has already adapted this technique for the formation of doublets from 0.2 µm nanoparticles[45]. As opposed to the simple estimate presented here, more complex mathematical models and calculations are available[47,48], however some degree of experimental optimization will likely still be required. Through experimental optimization, processes designed to create solutions with 75% singlet particles (30 second salting out time) and 50% singlet particles (120 second salting out time) were created.

Three different batches of both the nominal 75% singlet and 50% singlet solutions were assessed in order to show the reproducibility of the production process (Figure 6.1). The distribution of aggregate structures was calculated by manually counting SEM images, with representative SEM images given in Figure 6.2. Specifically, for the 75% singlet batches, 75.7%

of the particles found were defined as 'singlets', which refers to a single nanoparticle. 19.2% of the particles were defined as "doublets", which refers to two nanoparticles permanently fused together. The remaining 5.1% of particles were defined as "triplets", "quadruplets" and "larger aggregates", which refers to 3, 4, or more particles permanently fused together. For the 50% singlet batches, 52.4% of particles were singlets, 23.5% were doublets, 17.5 % were triplets, and 6.5% were quadruplets or larger aggregates. Between the 75% singlet and 50% singlet solutions, there were significantly less singlets and significantly more triplets and quadruplets (p<0.01) with no significant change in the number of doublets or larger aggregates. By precisely controlling the fusing time during the production process, the distribution of aggregate structures can be controlled, and once a procedure is established, it is reliable and repeatable.
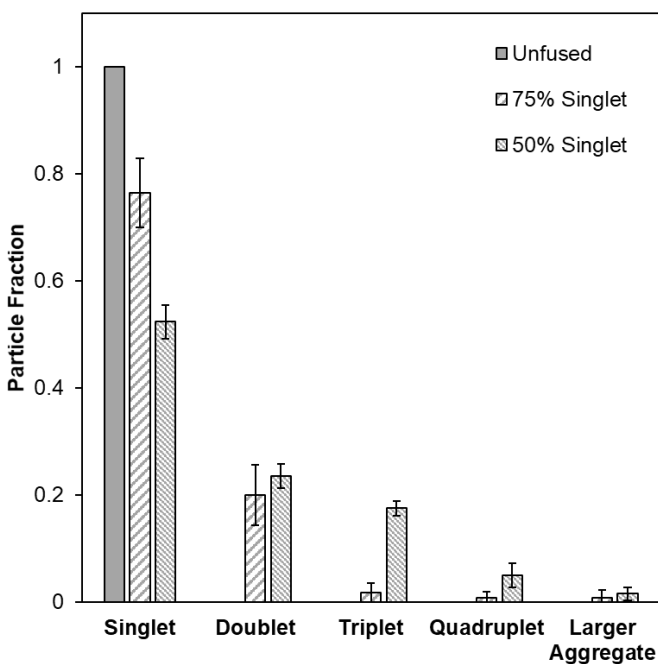
Figure 6.1: Fraction of aggregate structures in the nanoparticle solutions for both the nominal 75% singlet solution created with the low aggregation time (30 second salting out step) and the 50% singlet solution created with the high aggregation time (120 second salting out step). Bars show the average and standard deviation of 3 batches.
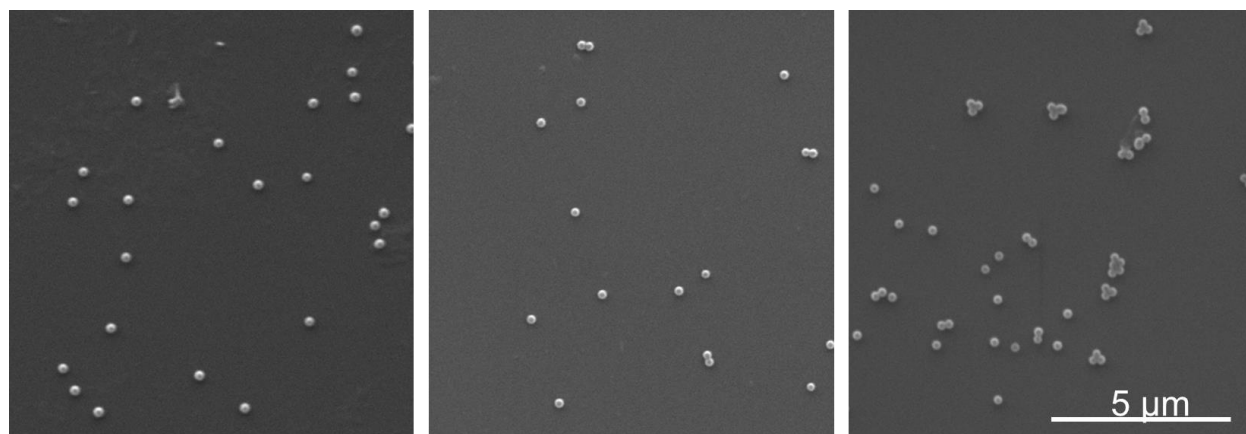
Figure 6.2: Representative images of the nanoparticle solutions using scanning electron microscopy at 10 kX magnification. The nanoparticles as received from the manufacturer (left), the 75% singlet solution created with the low aggregation (30 second salting out) time (middle) and the 50% singlet solution created with the high aggregation (120 second salting out) time (right) are shown. The original nanoparticles are clearly unaggregated and of uniform size, while the 75% singlet solution contains a small number of doublets and the 50% singlet solution contains a larger number of doublets, triplets, and some larger aggregates.

For the protocol presented here, the estimated aggregation time (τ) is approximately 9 seconds, however an actual aggregation time of 120 seconds was required in order to achieve 50% of the initial singlet particles aggregating. This discrepancy is likely due to variance in the stability ratio (W) or insufficient ionic strength to achieve a stability ratio of 1 as assumed. Small changes in ionic strength can cause large changes in the stability ratio[46] and there may be other minor repulsive forces preventing the ideal interaction from occurring. A large underestimation in the aggregation time was also reported in previous work[45].

6.4.2. Filtration of Nanoparticle Solutions

The permeability of the 0.22 and 0.45 PES membranes was measured to be 0.549±0.062 and 0.929±0.11 (mL min^{-1} cm^{-2} kPa^{-1}) respectively. Figure 6.3 shows the flux decline during filtration of a control solution of unfused particles, the 75% singlet solution, and the 50% singlet solution

all using both PES 0.22 µm and 0.45 µm membranes. When the unfused particles were filtered through both membranes a relatively steady flux was maintained, indicating that little to no fouling of the membrane or retention of the nanoparticles was occurring. This is supported by the post-filtration recovery of the nanoparticles as shown in Figure 6.4, given that greater than 90% recovery was seen for both membranes. While the average recovery was lower for the 0.22 µm membrane than the 0.45 µm (90.7% vs 97.2%) there was no statistical significance to that difference (p>0.1). Due to the inclusion of the surfactant Tween™ 20 in the buffer solution, adsorption of nanoparticles to the membrane should be largely inhibited[49] and any particle retention or membrane fouling should be due to a size exclusion or sieving effect. The nominal 0.22 µm rating is often unrelated to the actual dimensions of the pores[50] and it has been shown that other PES 0.22 µm rated membranes can have an average pore size as large as 0.43 µm[51] therefore the transmission of a 0.19 µm nanoparticle through the 0.22 µm membrane is not an unexpected result. Previous work has shown that some 0.22 µm rated membranes can even exhibit high transmission of particles as large as 0.3 µm[15].
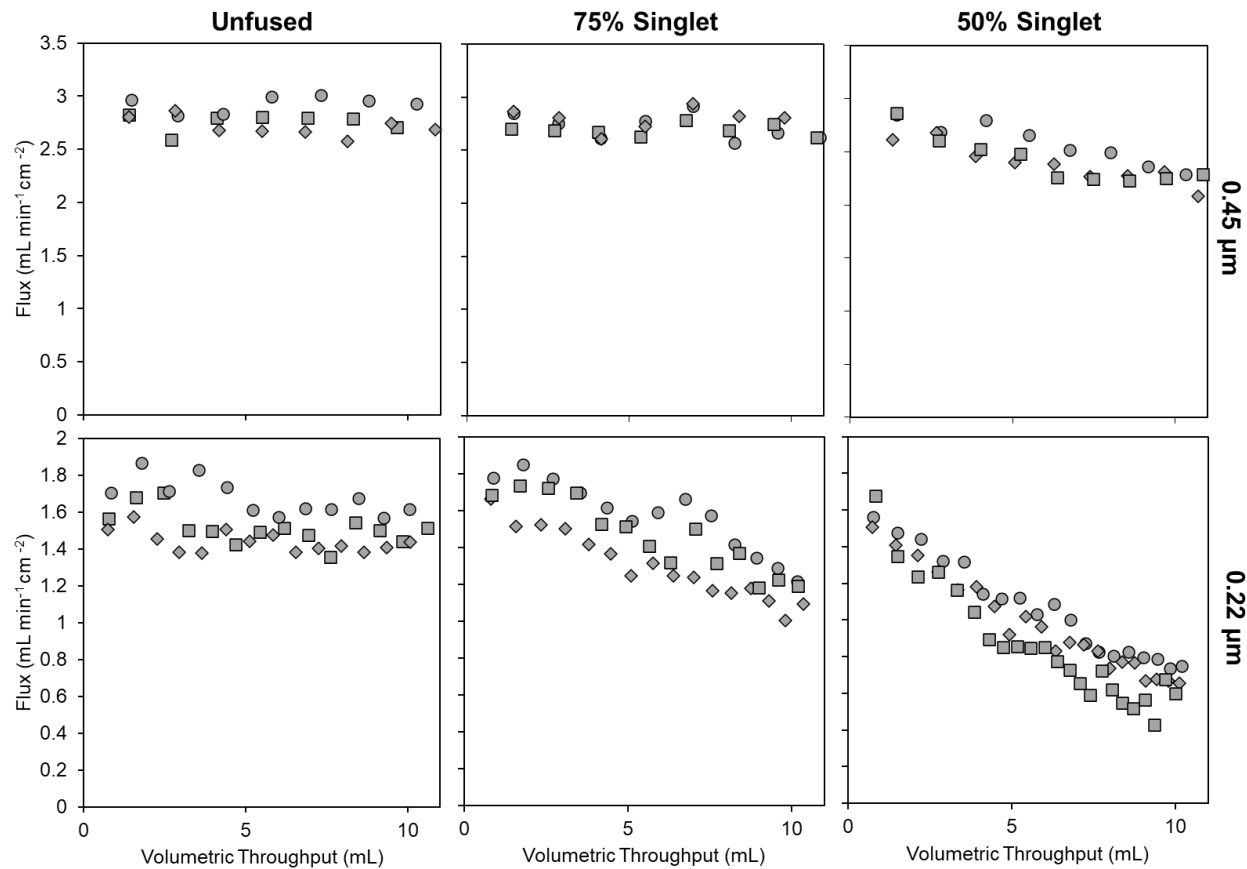
Figure 6.3: Flux decline during constant pressure filtration at 6.89 kPa for solutions of unfused nanoparticles, the 75% singlet solution created with the low aggregation time (30 second incubation step), and the 50% singlet solution created with the high aggregation time (120 second incubation step), all filtered using both 0.22 µm and 0.45 µm PES membranes. Triplicate experiments are shown using the different symbols in each panel.
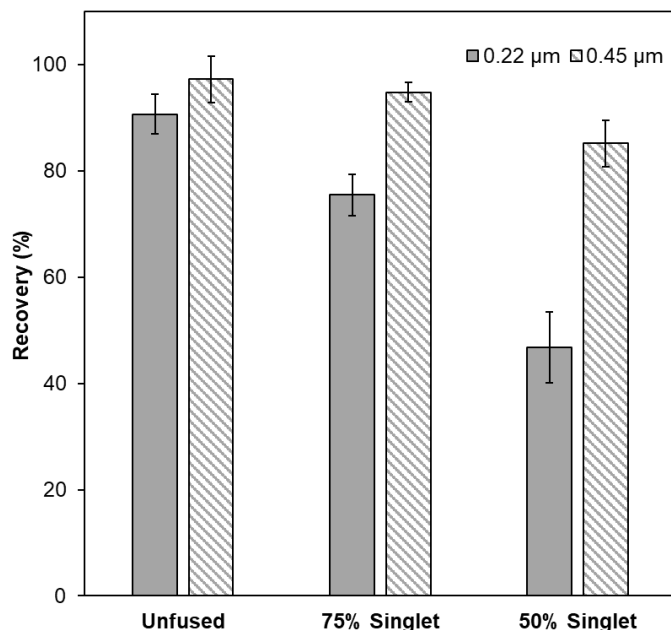
Figure 6.4: Recovery (measured as the ratio of filtrate to feed optical absorbance) of the unfused, 75% singlet (30 second incubation step), and 50% singlet (120 second incubation step) nanoparticles solutions after constant pressure filtration at 6.89 kPa through either a 0.22 or 0.45 µm PES membrane. Data is shown as the average of triplicate experiments, with error bars showing the standard deviation.

When the 75% singlet solution (which is largely comprised of singlet particles with some doublet particles) was filtered, a flux decline was seen for the 0.22 µm membrane (Figure 6.3) along with a corresponding decrease in recovery (Figure 6.4). It is theorized that the portion of doublets in the solution are large enough to block the 0.22 µm membrane pores, and once pore blockage begins to occur further fouling may happen due to cake buildup. Conversely for the 0.45 µm membrane, the doublet particles are still able to full transmit through the membrane without fouling the membrane at all.

Finally, when the 50% singlet solution (which contains singlets and a moderate amount of both doublets and triplets) was filtered, an even more severe flux decline was seen for the 0.22 µm

membrane (Figure 6.3) due to the presence of the triplet nanoparticles and less of the overall particles being able to pass through the membrane, leading to fouling. Again, a corresponding decrease in recovery was also seen (Figure 6.4). Now that triplets and larger aggregates have been created in the solution, some minor fouling and a decrease in flux was even seen for the 0.45 µm membrane.

As the fusing time of the nanoparticles increases, the degree of aggregation increases, and a corresponding flux decline during filtration and decrease in recovery is seen. The 0.22 µm membrane was very sensitive to any aggregation and the presence of nanoparticle doublets in solution, while no change in the performance of the 0.45 µm membrane was seen until a significant number of triplets and larger aggregates were produced. Total particle transmission through the 0.22 µm membrane was roughly proportional to the amount of singlet particles in solution, while transmission through the 0.45 µm membrane was comparable to the number of doublets and singlets, indicating that the ability of a membrane to transmit or retain aggregates of different sizes is related to the pore size of the membrane.

It is well known that the presence of aggregates can lead to increased membrane fouling and reduced transmission through the membrane in general filtration theory[52] and for virus particles during sterile filtration through 0.22 µm membranes in particular[27–29,53]. This reflects what has been demonstrated here, with the model aggregate nanoparticles resulting in reduced transmission and increased membrane fouling.

6.4.3. Analysis of Results Using Pore Blocking and Vmax Models

To better understand how results with the fused nanoparticles relate to the sterile filtration of viruses, the flux decline data from Figure 6.3 for the filtration of the 50 % singlet nanoparticle solution through the 0.22 µm membrane was compared against models for membrane fouling. Fitting data from other nanoparticle solutions or membranes was not attempted as significant flux decline during filtration is required for the distinction between the different models to be significant. These different models each relate to different mechanisms of fouling and how pores become blocked during filtration, and describe the pattern of flux decline during constant pressure filtration[54]. Each model relies on a blocking constant K_n which varies with the properties of the feed solution and membrane. The complete blocking model is based on particles being retained on the membrane surface and entirely occluding the membrane pores:

$$J = J_0 - K_b v \tag{7}$$

The standard blocking model is based on particles accumulating on the inside of pores, growing, and constricting the pores:

$$J = J_0 \left(1 - \frac{K_s}{2} v \right)^2 \tag{8}$$

The intermediate blocking model is based on a combination of pores being directly blocked by particles and the following buildup of particles on top of that layer:

$$J = J_0 \exp(-K_i v) \tag{9}$$

Finally the cake formation model is based on the formation of a packed bed of particles on top of the membrane surface:

$$J = \frac{J_0}{J_0 K_c v + 1} \tag{10}$$

By fitting the flux decline data during constant pressure filtration to the various models, the model which best describes the mechanism of fouling which is occurring during filtration can be identified. To perform the model fitting, the blocking constants K_n in each equation were varied such that the sum of squared error (SSE) between the model prediction $\overline{J_t}$ and the measured data J_i was minimized:

$$SSE = \sum_{i=1}^{n}(J_i - \overline{J_t})^2 \qquad (11)$$

The best model was then selected based on the lowest overall SSE.

Flux decline data from the triplicate experiments for the filtration of 50% singlet particles through the 0.22 µm membrane were each fit to the four blocking models, with an example of each blocking model fit to one set of flux decline data shown in Figure 6.5. The SSE and blocking constants for the triplicate data is given in 6.1. While there was not a large distinction between the models, for each of the filtration experiments the data was best fit to the intermediate blocking model (Equation 9), with the standard blocking model also closely fitting (Equation 8). The extent of fouling and flux decline in these experiments was relatively minor, and so it is possible that longer filtration experiments with a higher degree of fouling would have provided data to which the model fits would have been more distinct. With the intermediate model being the best fit, this would indicate that the fused particles are being trapped by the membrane and directly blocking the membrane pores, with some particle-particle interaction and buildup of multiple particles over the same area. While spherical particles significantly larger than the membrane pore size would be expected to follow the cake filtration model[17,55,56], it is possible that when the particle size closely matches the pore size, a direct pore blockage is more likely. Previous work examining the filtration of 0.3 µm nanoparticles through 0.22 µm sterile filtration membranes similarly showed membrane

fouling profiles that did not match the cake filtration model[15]. Given that virus particles have been shown to foul sterile filtration membranes following the intermediate model[53], the fused nanoparticles appear to behave similarly to virus particles in how they interact with the membrane pores and foul the membrane.
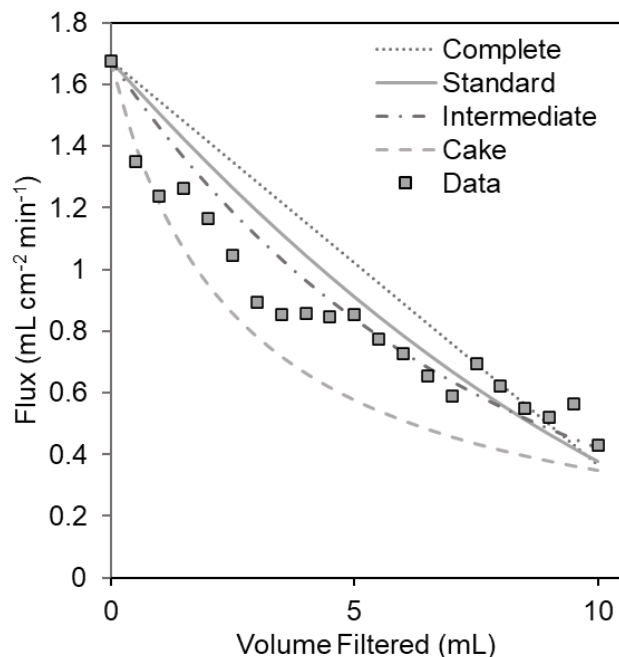
Figure 6.5: Graphical comparison of best fit curve for the four pore blocking models to the flux decline data from the constant pressure filtration of 50% singlet (120 second salting out step) fused nanoparticles through a PES 0.22 μm membrane. Data and curve fitting shown for one of three replicate experiments.

Table 6.1: Sum of squared error (SSE) from fitting pore blocking models to the triplicate flux decline data from the filtration of 50% singlet (120 second salting out step) fused nanoparticles through a PES 0.22 μm membrane. Calculated blocking constants (K_i) also shown. Data is given as average ± standard deviation.

Blocking Model	SSE	Blocking Constant (K_i)
Complete	0.66 ± 0.3	0.11 ± 0.02
Standard	0.23 ± 0.2	0.088 ± 0.01
Intermediate	0.13 ± 0.1	0.11 ± 0.03

Cake	0.86 ± 0.2	0.18 ± 0.04

With this similarity between the fused nanoparticles and viruses, the collected data from Figure 6.3 was examined in more detail for how the fused nanoparticles could be used as a screening tool and for how the results could be applied to select optimal membrane filters for a sterile filtration process. A common technique for scaling up and sizing membrane filters is to perform a small-scale filtration test and use that data to calculate the theoretical maximum throughput of the membrane before it becomes completely blocked, or the membrane Vmax value[57]. This method assumes that the membrane is fouled through pore constriction (the standard blocking model), and is known to overestimate or underestimate system capacity for feed solutions which foul primarily though other mechanisms[57]. Despite this, it is still considered the simplest and a typical first approach for screening membranes and assessing potential for scale up. This Vmax can be directly evaluated from filtration data using a plot of t/v as a function of t and is described by the equation[57]:

$$\frac{t}{v} = \frac{1}{Q_0} + \left(\frac{1}{Vmax}\right)t \tag{12}$$

Evaluating membranes using the Vmax model, as opposed to testing a membrane with large volumes until the actual capacity is reached in an experiment, is highly desirable as it can greatly accelerate testing and reduce the required volume. Using a fused nanoparticle solution as opposed to virus solution would serve to even further accelerate this process, and aid in screening the potentially dozens of commercially available sterile filters. As shown in Figure 6.6, average data from the triplicate constant pressure filtration of unfused, 75% singlet, and 50% singlet nanoparticles was plotted on a graph of t/v as a function of t. The slope of each data set is Vmax[-1], and from this average Vmax values of 20, 46 and 130 mL were calculated for the unfused, 75% singlet, and 50% singlet nanoparticle solutions respectively through the 0.22 µm PES membrane.

For the PES 0.45 µm membrane, only the 50 % singlet solution showed any measurable fouling or change in *t/v* over time, from which an average Vmax of 48 mL was calculated. This again demonstrates how the extent of nanoparticle aggregation can be used to tune the degree with which the final solution will foul a membrane during filtration. Given that the plotted data is highly linear, application of the Vmax model is still reasonable despite the assumption of a standard blocking model, even if it is not the best fit for the data as shown in Figure 6.5 and Table 6.1.
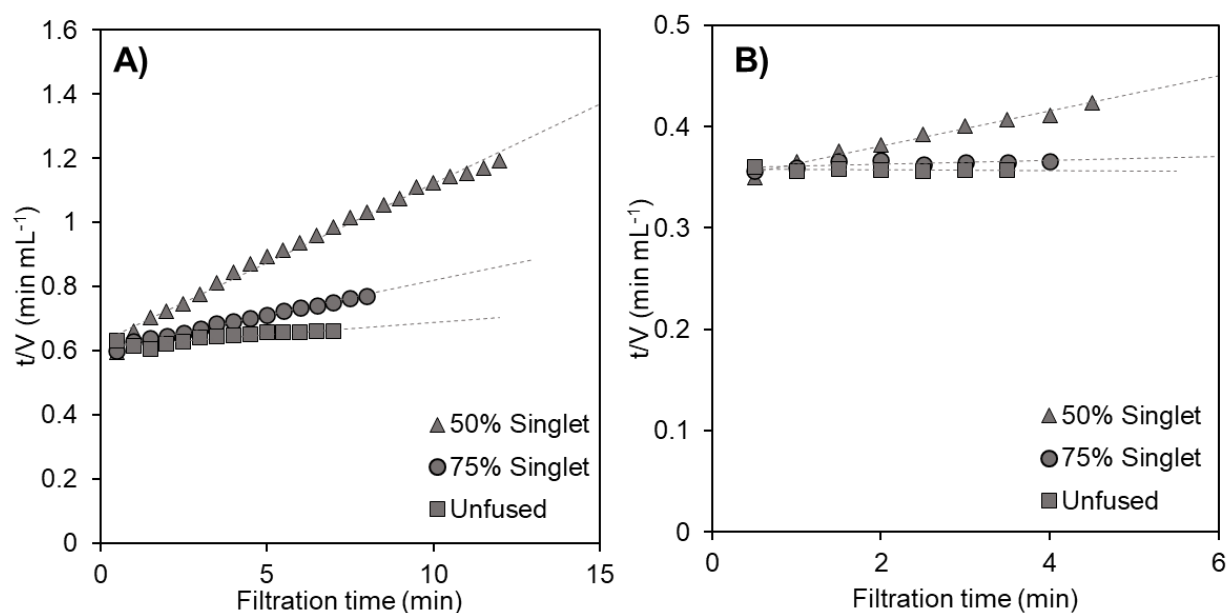
Figure 6.6: Average flux decay data from triplicate filtration experiments for 50% singlet (30 second salting out time), 75% singlet (120 second salting out time), and unfused nanoparticle solutions through either A) PES 0.22 µm membrane or B) PES 0.45 µm membrane. Data is plotted as filtrate volume over filtration time as a function of filtration time. Dashed lines represent linear regressions for each data set used for Vmax calculation.

Screening experiments using fused nanoparticles and Vmax analysis could potentially be used to evaluate sterile filters before performing in-depth experiments with actual virus solutions. In a recent study, Taylor *et al.*[15] evaluated 19 sterile filtration membranes to be used for a live attenuated virus vaccine by performing many filtration tests using actual virus solution. The results

clearly demonstrated that some membranes were not adequate for the application, fouling significantly faster than others. In such a situation, if the large number of membranes had initially been evaluated using simple nanoparticle solutions to eliminate some of the poor performing membranes, a significant amount of experimental time and valuable virus solution could have been saved for testing the membranes most likely to give the best performance.

6.5. Conclusions

The results presented here have demonstrated that the "salting out – quenching – fusing" process is a reliable method for fabricating controlled nanoparticle aggregates, and through both theoretical estimations and experimental optimization the final degree of aggregation can be tuned to a desired level. The fabrication process is consistent, scalable, and only requires readily available materials and simple laboratory equipment. Using 0.19 µm diameter polystyrene nanoparticles, solutions consisting of 100% singlet particles (unfused particles), 75% singlet particles, and 50% singlet particles were created and all filtered through both 0.22 and 0.45 µm PES membranes. A clear relationship was demonstrated between the degree of nanoparticle aggregation and the observed membrane fouling and particle transmission. Using pore blocking models, the data revealed that fused nanoparticles fouled the 0.22 µm PES membranes through the intermediate pore blocking model, similar to how true virus solutions behave. The data was then further analysed using the Vmax model to demonstrate how rapid fused nanoparticle filtration tests could be used to predict the filtration capacity of sterile filtration membranes.

This work provides a useful tool to others working in the area of membrane sciences, and specifically studying the filtration of biological organisms and viruses. More accurate model feed

solutions can be created which will better reflect realistic membrane performance with non-ideal solutions as opposed to simply using monodisperse and uniformly sized nanoparticles as is the standard methodology. In future work, these controlled aggregate models can be directly validated and through compared to aggregated and un-aggregated virus solutions, while other work to further improve the ability of nanoparticles to model viruses through surface functionalization (i.e. modification of surface charge and hydrophobicity) would be highly valuable.

6.6. Acknowledgements

6.7. References

1. Kosiol P, Hansmann B, Ulbricht M, Thom V. Determination of pore size distributions of virus filtration membranes using gold nanoparticles and their correlation with virus retention. *J Membr Sci*. 2017;533:289-301. doi:10.1016/j.memsci.2017.03.043

2. Duek A, Arkhangelsky E, Krush R, Brenner A, Gitis V. New and conventional pore size tests in virus-removing membranes. *Water Res*. 2012;46(8):2505-2514. doi:10.1016/j.watres.2011.12.058

3. DesOrmeaux JPS, Winans JD, Wayson SE, et al. Nanoporous silicon nitride membranes fabricated from porous nanocrystalline silicon templates. *Nanoscale*. 2014;6(18):10798-10805. doi:10.1039/C4NR03070B

4. Bromley AJ, Holdich RG, Cumming IW. Particulate fouling of surface microfilters with slotted and circular pore geometry. *J Membr Sci*. 2002;196(1):27-37. doi:10.1016/S0376-7388(01)00573-7

5. Ben Hassan I, Lafforgue C, Ellero C, Ayadi A, Schmitz P. Coupling of local visualization and numerical approach for particle microfiltration optimization. *Microsyst Technol*. 2015;21(3):509-517. doi:10.1007/s00542-013-1906-9

6. Winans JD, Smith KJP, Gaborski TR, Roussie JA, McGrath JL. Membrane capacity and fouling mechanisms for ultrathin nanomembranes in dead-end filtration. *J Membr Sci*. 2016;499:282-289. doi:10.1016/j.memsci.2015.10.053

7. Wright E, Miller JJ, Csordas M, et al. Development of isoporous microslit silicon nitride membranes for sterile filtration applications. *Biotechnol Bioeng*. 2020;117(3):879-885. doi:https://doi.org/10.1002/bit.27240

8. Kuiper S. Determination of particle-release conditions in microfiltration: a simple single-particle model tested on a model membrane. *J Membr Sci*. 2000;180(1):15-28. doi:10.1016/S0376-7388(00)00430-0

9. Baltus RE, Badireddy AR, Xu W, Chellam S. Analysis of Configurational Effects on Hindered Convection of Nonspherical Bacteria and Viruses across Microfiltration Membranes. *Ind Eng Chem Res*. 2009;48(5):2404-2413. doi:10.1021/ie800579e

10. Antony A, Blackbeard J, Angles M, Leslie G. Non-microbial indicators for monitoring virus removal by ultrafiltration membranes. *J Membr Sci*. 2014;454:193-199. doi:10.1016/j.memsci.2013.11.052

11. Fallahianbijan F, Giglia S, Carbrello C, Zydney AL. Use of fluorescently-labeled nanoparticles to study pore morphology and virus capture in virus filtration membranes. *J Membr Sci*. 2017;536:52-58. doi:10.1016/j.memsci.2017.04.066

12. Roberts PL, Feldman P, Crombie D, Walker C, Lowery K. Virus removal from factor IX by filtration: Validation of the integrity test and effect of manufacturing process conditions. *Biologicals*. 2010;38(2):303-310. doi:10.1016/j.biologicals.2009.12.006

13. Sekine S, Komuro M, Sohka T, Sato T. Integrity testing of Planova™ BioEX virus removal filters used in the manufacture of biological products. *Biologicals*. 2015;43(3):186-194. doi:10.1016/j.biologicals.2015.02.003

14. Pontius FW, Amy GL, Hernandez MT. Fluorescent microspheres as virion surrogates in low-pressure membrane studies. *J Membr Sci*. 2009;335(1-2):43-50. doi:10.1016/j.memsci.2009.02.026

15. Taylor N, Ma W, Kristopeit A, Wang S, Zydney AL. Evaluation of a sterile filtration process for viral vaccines using a model nanoparticle suspension. *Biotechnol Bioeng*. 2021;118(1):106-115. doi:10.1002/bit.27554

16. Agasanapura B, Baltus RE, Tanneru CT, Chellam S. Effect of electrostatic interactions on rejection of capsular and spherical particles from porous membranes: Theory and experiment. *J Colloid Interface Sci*. 2015;448:492-500. doi:10.1016/j.jcis.2015.02.016

17. Bourcier D, Féraud JP, Colson D, et al. Influence of particle size and shape properties on cake resistance and compressibility during pressure filtration. *Chem Eng Sci*. 2016;144:176-187. doi:10.1016/j.ces.2016.01.023

18. Ge P, Tsao J, Schein S, Green TJ, Luo M, Zhou ZH. Cryo-EM Model of the Bullet-Shaped Vesicular Stomatitis Virus. *Science*. 2010;327(5966):689-693. doi:10.1126/science.1181766

19. Roos N, Cyrklaff M, Cudmore S, Blasco R, Krijnse-Locker J, Griffiths G. A novel immunogold cryoelectron microscopic approach to investigate the structure of the intracellular and extracellular forms of vaccinia virus. *EMBO J*. 1996;15(10):2343-2355. doi:10.1002/j.1460-2075.1996.tb00590.x

20. Liljeroos L, Krzyzaniak MA, Helenius A, Butcher SJ. Architecture of respiratory syncytial virus revealed by electron cryotomography. *Proc Natl Acad Sci*. 2013;110(27):11133-11138. doi:10.1073/pnas.1309070110

21. Shi H, Tarabara VV. Charge, size distribution and hydrophobicity of viruses: Effect of propagation and purification methods. *J Virol Methods*. 2018;256:123-132. doi:10.1016/j.jviromet.2018.02.008

22. Carneiro FA, Bianconi ML, Weissmüller G, Stauffer F, Da Poian AT. Membrane Recognition by Vesicular Stomatitis Virus Involves Enthalpy-Driven Protein-Lipid Interactions. *J Virol*. 2002;76(8):3756-3764. doi:10.1128/JVI.76.8.3756-3764.2002

23. Armanious A, Aeppli M, Jacak R, et al. Viruses at Solid–Water Interfaces: A Systematic Assessment of Interactions Driving Adsorption. *Environ Sci Technol*. 2016;50(2):732-743. doi:10.1021/acs.est.5b04644

24. van Voorthuizen EM, Ashbolt NJ, Schäfer AI. Role of hydrophobic and electrostatic interactions for initial enteric virus retention by MF membranes. *J Membr Sci*. 2001;194(1):69-79. doi:10.1016/S0376-7388(01)00522-1

25. Gerba CP, Betancourt WQ. Viral Aggregation: Impact on Virus Behavior in the Environment. *Environ Sci Technol*. 2017;51(13):7318-7325. doi:10.1021/acs.est.6b05835

26. Floyd R, Sharp DG. Viral aggregation: buffer effects in the aggregation of poliovirus and reovirus at low and high pH. *Appl Environ Microbiol*. 1979;38(3):395-401. doi:10.1128/AEM.38.3.395-401.1979

27. Langlet J, Gaboriaud F, Duval JFL, Gantzer C. Aggregation and surface properties of F-specific RNA phages: Implication for membrane filtration processes. *Water Res*. 2008;42(10-11):2769-2777. doi:10.1016/j.watres.2008.02.007

28. Konz JO, Lee AL, Lewis JA, Sagar SL. Development of a Purification Process for Adenovirus: Controlling Virus Aggregation to Improve the Clearance of Host Cell DNA. *Biotechnol Prog*. 2005;21(2):466-472. doi:10.1021/bp049644r

29. Wright JF, Le T, Prado J, et al. Identification of factors that contribute to recombinant AAV2 particle aggregation and methods to prevent its occurrence during vector purification and formulation. *Mol Ther*. 2005;12(1):171-178. doi:10.1016/j.ymthe.2005.02.021

30. Sugimoto T, Itoh H, Mochida T. Shape Control of Monodisperse Hematite Particles by Organic Additives in the Gel–Sol System. *J Colloid Interface Sci*. 1998;205(1):42-52. doi:10.1006/jcis.1998.5588

31. Lan W, Li S, Xu J, Luo G. A one-step microfluidic approach for controllable preparation of nanoparticle-coated patchy microparticles. *Microfluid Nanofluidics*. 2012;13(3):491-498. doi:10.1007/s10404-012-0984-9

32. Lu Y, Yin Y, Xia Y. Three-Dimensional Photonic Crystals with Non-spherical Colloids as Building Blocks. *Adv Mater*. 2001;13(6):415-420. doi:https://doi.org/10.1002/1521-4095(200103)13:6<415::AID-ADMA415>3.0.CO;2-O

33. Mohraz A, Solomon MJ. Direct Visualization of Colloidal Rod Assembly by Confocal Microscopy. *Langmuir*. 2005;21(12):5298-5306. doi:10.1021/la046908a

34. Dendukuri D, Tsoi K, Hatton TA, Doyle PS. Controlled Synthesis of Nonspherical Microparticles Using Microfluidics. *Langmuir*. 2005;21(6):2113-2116. doi:10.1021/la047368k

35. Huang Y, Wu L, Chen X, Bai P, Kim DH. Synthesis of Anisotropic Concave Gold Nanocuboids with Distinctive Plasmonic Properties. *Chem Mater*. 2013;25(12):2470-2475. doi:10.1021/cm400765b

36. Zhang G, Wang D, Möhwald H. Decoration of Microspheres with Gold Nanodots—Giving Colloidal Spheres Valences. *Angew Chem*. 2005;117(47):7945-7948. doi:10.1002/ange.200502117

37. Zhang G, Wang D, Möhwald H. Patterning Microsphere Surfaces by Templating Colloidal Crystals. *Nano Lett*. 2005;5(1):143-146. doi:10.1021/nl048121a

38. Manoharan VN. Dense Packing and Symmetry in Small Clusters of Microspheres. *Science*. 2003;301(5632):483-487. doi:10.1126/science.1086189

39. Velev OD, Furusawa K, Nagayama K. Assembly of Latex Particles by Using Emulsion Droplets as Templates. 2. Ball-like and Composite Aggregates. *Langmuir*. 1996;12(10):2385-2391. doi:10.1021/la950679y

40. Mafuné F, Kohno J ya, Takeda Y, Kondow T. Nanoscale Soldering of Metal Nanoparticles for Construction of Higher-Order Structures. *J Am Chem Soc*. 2003;125(7):1686-1687. doi:10.1021/ja021250d

41. Yin Y, Lu Y, Xia Y. A Self-Assembly Approach to the Formation of Asymmetric Dimers from Monodispersed Spherical Colloids. *J Am Chem Soc*. 2001;123(4):771-772. doi:10.1021/ja0031873

42. Johnson PM, van Kats CM, van Blaaderen A. Synthesis of Colloidal Silica Dumbbells. *Langmuir*. 2005;21(24):11510-11517. doi:10.1021/la0518750

43. Yake AM, Panella RA, Snyder CE, Velegol D. Fabrication of Colloidal Doublets by a Salting Out−Quenching−Fusing Technique. *Langmuir*. 2006;22(22):9135-9141. doi:10.1021/la061339n

44. Velegol D, Yake AM, McDermott JJ. Particle doublets and n-mers and methods for fabrication thereof. Published online March 27, 2008. Accessed February 27, 2021. https://patents.google.com/patent/US20080072402/en

45. Juluri BK, Chaturvedi N, Hao Q, et al. Scalable Manufacturing of Plasmonic Nanodisk Dimers and Cusp Nanostructures Using Salting-out Quenching Method and Colloidal Lithography. *ACS Nano*. 2011;5(7):5838-5847. doi:10.1021/nn201595x

46. Behrens SH, Christl DI, Emmerzael R, Schurtenberger P, Borkovec M. Charging and Aggregation Properties of Carboxyl Latex Particles: Experiments versus DLVO Theory. *Langmuir*. 2000;16(6):2566-2575. doi:10.1021/la991154z

47. Higuchi WI, Okada R, Stelter GA, Lemberger AP. Kinetics of Rapid Aggregation in Suspensions. *J Pharm Sci*. 1963;52(1):49-54. doi:10.1002/jps.2600520110

48. Thomas DN, Judd SJ, Fawcett N. Flocculation modelling: a review. *Water Res*. 1999;33(7):1579-1592. doi:10.1016/S0043-1354(98)00392-3

49. Pazouki M, Noelle Wilton A, Latulippe DR. An experimental study on sterile filtration of fluorescently labeled nanoparticles – the importance of surfactant concentration. *Sep Purif Technol*. 2019;218:217-226. doi:10.1016/j.seppur.2019.02.038

50. Madsen Jr. RE, Meltzer TH, Jornitz MW. The Relationship among Pore-Size Ratings, Bubble Points, and Porosity. *Pharm Technol*. 31(1):84-100.

51. Peinador RI, Kaabouch M, Ben Aim R, Calvo JI. Non-Destructive Characterization of Industrial Membrane Cartridges by Using Liquid–Liquid Displacement Porosimetry (LLDP). *Membranes*. 2020;10(12):369. doi:10.3390/membranes10120369

52. Aimar P, Bacchin P. Slow colloidal aggregation and membrane fouling. *J Membr Sci*. 2010;360(1-2):70-76. doi:10.1016/j.memsci.2010.05.001

53. Shoaebargh S, Gough I, Fe Medina M, et al. Sterile filtration of oncolytic viruses: An analysis of effects of membrane morphology on fouling and product recovery. *J Membr Sci*. 2018;548:239-246. doi:10.1016/j.memsci.2017.11.022

54. Iritani E. A Review on Modeling of Pore-Blocking Behaviors of Membranes During Pressurized Membrane Filtration. *Dry Technol*. 2013;31(2):146-162. doi:10.1080/07373937.2012.683123

55. Lee JK, Liu BYH. A filtration model of microporous membrane filters in liquids. *KSME J*. 1994;8(1):78-87. doi:10.1007/BF02953246

56. Bowen WR, Jenner F. Theoretical descriptions of membrane filtration of colloids and fine particles: An assessment and review. *Adv Colloid Interface Sci*. 1995;56:141-200. doi:10.1016/0001-8686(94)00232-2

57. Zydney AL, Ho CC. Scale-up of microfiltration systems: fouling phenomena and Vmax analysis. *Desalination*. 2002;146(1):75-81. doi:10.1016/S0011-9164(02)00492-7

6.8. Supplementary Material
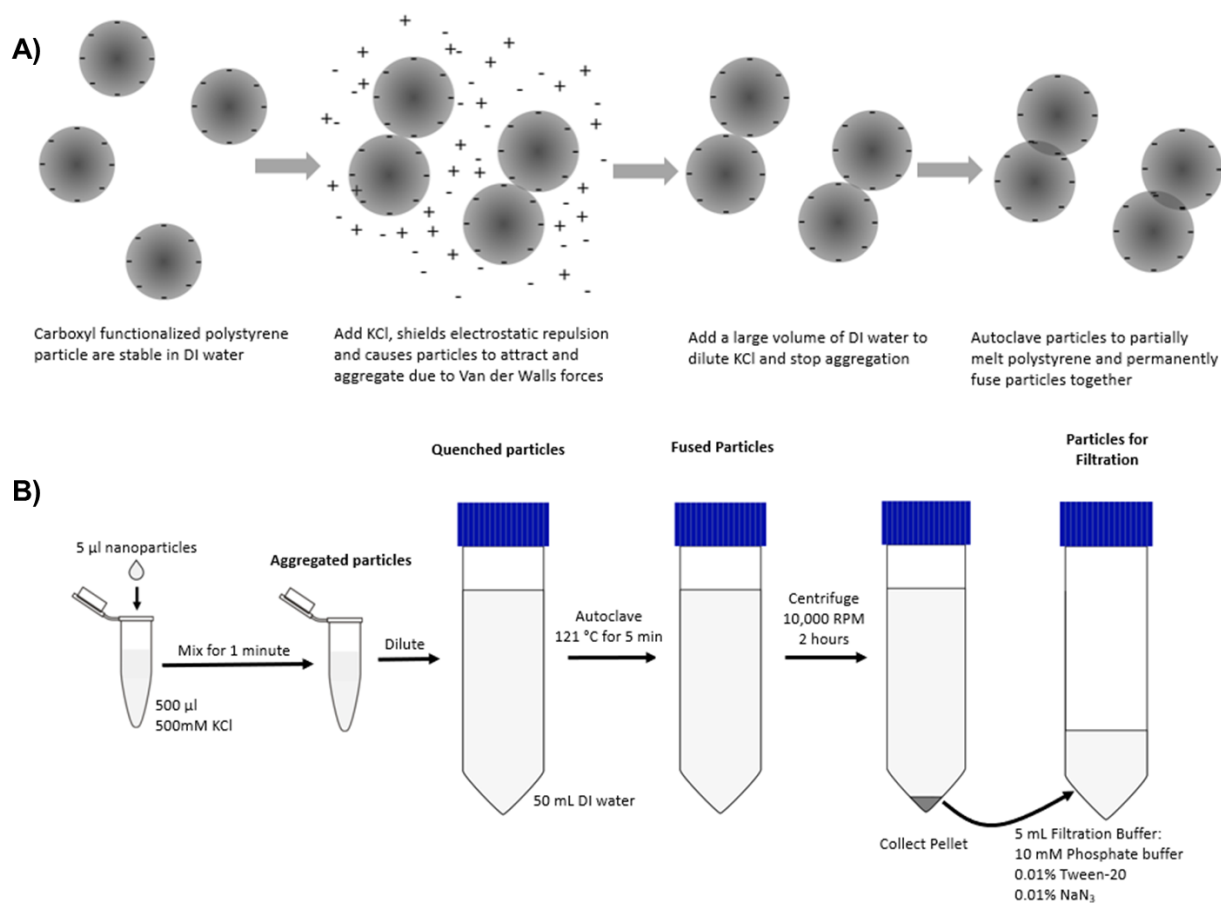
Figure S6.7: Overview of the fused nanoparticle fabrication process. A) Details of the fabrication process on the scale of individual particles, showing the steps of salting out, quenching, and fusing. B) Schematic of the experimental steps for the salting out, quenching and fusing process to create a final fused nanoparticle solution.

Chapter 7

Conclusions and Future Work

7. Conclusions and Future Work

7.1. Conclusions

Therapeutic viruses have played a critical role in modern medicine as vaccine products and promise to be a large part of future medical advancements through the development of gene therapies and cancer treatments. However, efficient manufacturing and downstream processing presents a barrier to the production, testing, and widespread application of these products. Sterile filtration is a critical unit operation in ensuring the safety of therapeutic viruses, however it can result in high product losses and a significant contribution to overall product cost. Little research to date has investigated how the sterile filtration of therapeutic viruses could be improved, and thus this thesis addresses the issue through a variety of approaches. The advancements made here will help elucidate the causes of reduced virus recovery during sterile filtration, aiding others in better optimizing downstream purification and sterile filtration. Furthermore, this work explores various paths which could lead to the development of future technologies to improve sterile filtration.

Chapter 3 provides some of the first available data detailing the transmission of *B. diminuta* bacteria through a variety of commercial microfiltration membranes with varying pore sizes and chemistries. Pore size was clearly correlated to retention, while other membrane characteristics (material, surface zeta potential) showed no clear trend with bacteria retention. Retention by 0.22 µm membranes was independent of any process conditions (increased pressure, added surfactant) and was attributed to purely a size exclusion or sieving effect. Conversely, retention by the large pore size 0.8 µm membrane was independent of pressure, and was theorized to occur through mainly an adsorptive effect. At the intermediate 0.45 µm pore size, retention was highly dependent

on applied pressure for all membranes tested, a phenomena which has been documented before in literature but never for *B. diminuta* through commercial microfiltration membranes. Due to this highly pressure dependent retention, specific 0.45 µm membranes when operated under the appropriate conditions were able to fully retain a challenge test of *B. diminuta* performed in accordance with regulatory standards, signifying that the 0.45 µm membranes could act as sterile filters. The use of a larger pore size membrane in the sterile filtration of therapeutic viruses would be highly desirable, as the tight pore size of many 0.22 µm rated membranes is known to result in reduced recovery of many larger viruses. When challenged head-to-head in the sterile filtration of a VSV preparation (under conditions which had been validated as a sterile filter) the 0.22 µm membranes resulted in only a 61% recovery while the 0.45 µm membrane resulted in an improved 84% recovery. Sterile filtration of VSV was significantly improved by using a 0.45 µm rated membrane, and the process was still validated to be a proper sterile filtration step despite the larger pore size membrane.

Chapter 4 examines what effect small amounts of host cell impurities (DNA and protein) have on the sterile filtration of therapeutic viruses. As demonstrated in Chapter 3, the recovery of VSV through the 0.22 µm membrane was relatively low, and so we sought to examine what conditions may contribute to this. A process was developed through which DNA and protein were selectively purified from Vero cell lysate using anion exchange chromatography and spiked back into highly pure VSV preparations to investigate the effect of elevated host cell protein and DNA alone and in combination. From filtration experiments of spiked and unspiked VSV preparations, it was determined that host cell protein played a significant role in increased membrane fouling and reduced virus recovery. Static adsorption experiments showed that the host cell protein

increased adsorption of virus to the membrane surface, which may be the mechanism for reduced yield in the presence of elevated host cell protein levels. This knowledge is highly valuable in process optimization, as it demonstrates how sterile filtration can be improve by considering the preceding purification steps and how optimizing the removal of host cell protein impurities during chromatography or ultrafiltration could lead to improved sterile filtration. Millipore Durapore 0.22 µm and Millipore Express PLUS 0.22 µm members were compared throughout this study with the Express membrane providing higher recovery and fouling less under all conditions tested, demonstrating how proper selection of the sterile filtration membrane can greatly influence the process performance.

Chapter 5 explores the performance of microfabricated silicon nitride membranes and evaluates their utility in the sterile filtration of therapeutic viruses. In Chapters 3 and 4, and as frequently observed in literature, conventional polymeric membranes result in reduced recovery of virus after sterile filtration, and so an alternative membrane material and structure was explored. Microfabricated silicon nitride membranes were shown to have a hydraulic permeability which is orders of magnitude greater than polymeric membranes, enabling higher throughput processing. The membranes pores showed less than 10% variance in size, as opposed to polymeric membranes where the pore size can vary by an entire order of magnitude. Using nanoparticles and proteins as model foulants, it was demonstrated that slit shaped pores were more resistant to fouling than circular pores, making them more suitable to the filtration of solutions with a high tendency for fouling, such as therapeutic viruses. When slit membranes with 0.2 and 0.5 µm slit widths were challenged with *B. diminuta* the 0.2 µm slit membrane fully retained the bacteria (acting as a sterile filter as discussed in Chapter 3), while the 0.5 µm slit membrane retained only a minimal amount

of the bacteria. The 0.2 µm slit membrane was then compared with a conventional Durapore 0.22 µm membrane in the sterile filtration of both adenovirus and Maraba virus solutions. Contrary to expectations, the 0.2 µm slit membrane showed a similar recovery and even experienced greater fouling for both viruses. In order to both scale up the technology and prevent fouling during filtration, the silicon nitride membranes were implemented in a stirred cell format, with the addition of stirring leading to greatly reduced fouling by model nanoparticle solutions. While this technology shows initial promise, significantly more work is required before it can be considered for use in downstream processing and sterile filtration of viruses.

Some interesting insights can be gained from comparing the retention of *B. diminuta* in Chapters 3 and 5 by polymeric and silicon nitride membrane respectively. While highly variable between membranes, all the polymeric 0.45 µm membranes retained the vast majority (>99.9%) of bacteria in the filtration tests while the silicon nitride membrane retained comparatively little bacteria (<90%). If bacteria retention was purely occurring through size exclusion based on the rated pore size, we would expect to see very similar performance between the two membrane types. From this, it is likely that the high internal surface area of the polymeric membrane is beneficial in allowing adsorption to contribute to bacteria retention. Furthermore, the pore size distribution of the polymeric membrane will mean that some pores are smaller than others, and flow through these more restrictive pores can allow for greater capture of bacteria than expected based simply on the rated 0.45 µm pore size.

Finally, Chapter 6 presents a procedure for creating fused nanoparticles to be used as model foulants in filtration tests. A "salting out – quenching – fusing" was optimized to consistently

create doublets, triplets, and larger aggregates from 0.19 µm diameter nanoparticles at controlled levels. Filtration through 0.22 and 0.45 µm membranes demonstrated a clear relationship between the degree of nanoparticle aggregation and the observed membrane fouling and particle transmission. Thus, the degree of fouling in the filtration process can be tuned by controlling the degree of aggregation. In Chapter 5, nanoparticles were used extensively in filtration tests to rapidly characterize performance without having to perform more complex experiments with virus. However, the fouling behavior of the nanoparticle solutions in Chapter 5 (cake fouling) is not representative of how viruses interact with membranes in many cases. When filtration data for the fused nanoparticles was fit to the pore blocking models, it was revealed that the fused particles followed the intermediate model, just as the Maraba virus in Chapter 5. It was then shown how the fused nanoparticles could be used to evaluate membrane filtration capacity following the Vmax model. This tool would be valuable as an initial test when selecting membranes for sterile filtration applications. For example, only a small number of membranes could be tested in Chapters 3 and 4 due to the limited amount of purified virus available, and initial screening tests on a broader range of membranes could have resulted in a drastically different selection of membranes.

7.2. Future Work

7.2.1. Development of Next Generation Sterile Filtration Membranes

Polymeric membranes produced through a phase inversion process have remained relatively unchanged since the introduction of the 0.22 µm designation and their application to sterile filtration[1]. Current sterile filtration membranes for bioprocessing are largely designed for the processing of protein therapeutics (antibodies, enzymes, blood factors, etc.), with literature from the manufacturers highlighting high throughput, low protein binding, and high transmission of

proteins such as IgG. There is a need for a new generation of membranes which are expressly designed for high recovery of large therapeutic virus products.

As demonstrated in Chapter 3, the 0.22 µm pore size rating is not an absolute requirement, and in fact some 0.45 µm rated membranes were able to fully retain the bacteria challenge test and act as a sterile filter. While the concept of implementing an off the shelf 0.45 µm membrane for sterile filtration in an industrial process is unlikely (industry and regulators being highly risk adverse regarding product safety), there is perhaps room for the design of an intermediate pore size designation. The industry standard phase inversion via immersion precipitation process for the fabrication of microfiltration membranes leads to a pore size distribution and variance in pore size[2] and so achieving such a precise goal may prove challenging. Given that current 0.22 and 0.45 µm designations are defined based on practical filtration challenge tests with bacteria[1], better tools in characterizing membrane pore size and filtration performance may be required in order to properly assess the creation of such a membrane. Potentially, a membrane with properties that lay between the standard 0.22 and 0.45 µm designations could be created which still fully retains bacteria (potentially with specified limitations to operation) while allowing for higher transmission of larger particles, including viruses. Recently, Helling *et al.*[3] reported testing a Sartorius PES membrane with a 0.3 µm pore size designation which fully retained a *B. diminuta* challenge test, acting as a sterile filter. The intention of the 0.3 µm designation, how such a designation is measured or assigned, and the intended application of the membrane was not detailed, however it could potentially be an attempt at an intermediate pore size membrane for sterile filtration.

As detailed in Chapter 5, ultrathin isoporous membranes created through microfabrication techniques show some promise as a new generation of sterile filtration membranes. However, there are multiple barriers to their implementation. Fouling of the membrane was a large issue, which could be mitigated through further investigation into stirred cell filtration or through the design of a cross flow filtration setup. In addition, surface modification of the membrane with anti-fouling coatings, such as PEG or zwitterionic functional groups could aid in reducing fouling due to adsorption of proteins. Processes for attaching these anti-fouling molecules to silicon and silicon-based surfaces have already been demonstrated[4], and could readily be adapted to the silicon nitride membrane surface. Another barrier to the implementation of the silicon nitride membranes is difficulty in scaling up the technology. On an industrial scale, polymeric membranes are available in pleated, spiral wound, and hollow fiber formats[5], all allowing for high membrane surface area with low footprint. Due to the ridged structure of the silicon nitride membranes, these solutions would not be applicable. Therefore, investigations into applying the silicon nitride membranes in a stacked plate or plate and frame format would be necessary.

7.2.2. A Deeper Understanding of Host Cell Proteins in Downstream Purification

In Chapter 4, small amounts of host cell protein were identified as a major factor in membrane fouling and reduced recovery of virus during sterile filtration. This knowledge could be applied by optimizing preceding purification steps to reduce the level of host cell protein, thereby improving sterile filtration. However, the host cell proteins present in downstream processing are a highly complex mixture potentially made up of hundreds of different proteins, all with different physicochemical and functional properties[6,7]. While the total host cell protein amount is often measured, a true risk-based approach would need to consider each of the individual protein species,

and this is an ongoing challenge within the indsutry[8]. If the specific problematic host cell proteins could be identified, then rational design and optimization of purification steps could be performed to specifically target those proteins. Analysis of residual host cell protein using 2 dimensional SDS-PAGE could identify the most abundant proteins and provide information about their relative size and isoelectric point[6], from which design of ultrafiltration (sized based separation) or chromatography (charge based separation) could be improved.

In Chapter 4 anion exchange chromatography was used to produce the host cell proteins for spiking studies, which will inherently select for a subsection of the overall host cell protein population. By implementing a variety of orthogonal methods to produce purified host cell protein subsets, such as cation exchange, hydrophobic interaction, and size exclusion chromatography, the resulting protein could be used in spiking studies to observe relative differences in sterile filtration performance caused by the protein subsets. Coupled with 2D SDS-PAGE or other analytical methods, this could theoretically be used to identify specific problematic proteins. An even more advanced analytical technique such as LC-MS could be used to identify and measure specific proteins and track their relative concentration through different unit operations. In the production and purification of monoclonal antibodies, LC-MS methods have identified and quantified host cell protein profiles[9], and this method could easily be translated to the purification of therapeutic viruses. Applying this methodology will not only help optimize the sterile filtration step, but all downstream processing unit operations.

7.2.3. Discriminating Mechanisms of Bacteria Retention and Membrane Interaction

It is well accepted that sterile filtration membranes retain bacteria through a combination of size exclusion and adsorption effects[1,10]. However, as presented in Chapter 3, it can be difficult to assess the relative contribution of adsorption effects or to investigate which membrane properties result in increased adsorption due to confounding variables such as different membrane structures and unknown pore size distributions. It would be highly beneficial to isolate and test for adsorption of *B. diminuta* to the membrane surface to better understand the mechanisms behind bacteria retention during sterile filtration. One approach to address this would be to perform static adsorption experiments measuring the degree of bacteria adsorption to the membrane surface. Similar work has been performed before for other materials or types of membranes, where the bacteria solution is incubated with the surface of interest (either as a drop on the surface or with the surface immersed in the bacteria solution) and then after a set period of time, potentially with shaking or other gentle agitation, the bacteria adsorbed to the surface can be assessed through a change in the solution cell concentration[11] or through measuring the amount of adsorbed bacteria on the surface with colorimetric[12] or fluorometric assays[13]. Using these methods, isotherms describing the interaction between bacteria and filtration membranes[14] or other materials such as activated carbon[15] have been generated. Furthermore, insights into adsorption of bacteria to novel functionalized surfaces[12,13], the effects of surface charge, hydrophobicity, and texture on bacteria adsorption[16], and the effect of surface charge on adsorption[17] have all been investigated using similar techniques.

Applying this approach to sterile filtration, membranes would be incubated in a solution of *B. diminuta,* then the number of adsorbed bacteria would be assessed and compared between

membranes with differing properties (material, surface charge, hydrophobicity). Performing the experiment using a static adsorption approach would ideally help in eliminating any capture of bacteria from active flow through the membrane and entrapment by pore size exclusion. Data from these studies can be used to generate adsorption isotherms[18] and then applied to kinetic adsorption-filtration models[19] to gain information on the sterile filtration process and what role adsorption plays.

7.2.4. Improved Characterization of Membrane Performance and Structure

MilliporeSigma, Sartorius, Pall, Cytiva, Meissner, and other manufacturers all produce a suite of sterile filtration membranes with varying materials and structures designed for the sterile filtration of biotherapeutics. Given this, how should a researcher or process engineer with the goal of obtaining high recovery of a therapeutic virus approach the selection of a sterile filtration membrane? While some membrane characteristics such as the use of asymmetric or dual-layer membranes are generally understood to improve recovery[20,21], there are no universal properties or standardized measures which can be directly related to the recovery of large biotherapeutic products, such as viruses. The current approach is to simply perform a large number of bench scale experiments, testing each available membrane for recovery of the therapeutic virus of interest. However, this involves significant resources and time, with all the complexities of producing, handling, and analyzing virus solutions.

In other separation operations, many characterization and qualification tests are standardized. In ultrafiltration for example, a filtration test using dextrans spanning a size range of 1-2000 kDa is performed to provide a direct picture of the pore size distribution and membrane sieving

performance[5,22], and this allows for better comparisons between membranes to be made. A similar standardized test to compare sterile filtration membranes would be highly desirable. As discussed in Chapter 6, nanoparticles have been used to assess the performance of sterile filtration membranes, but only nanoparticles of one or two sizes and in inconsistent buffer solutions[21,23]. An ideal characterization test could involve the filtration of a ladder of nanoparticles with varying sizes (e.g $0.1 - 0.3$ µm), potentially with each size having an independent fluorescent absorption and emission to allow for easy analysis. Current nanoparticle synthesis via emulsion polymerization allows for the production of nanoparticles with accurate and precise size[24], which could be applied in filtration tests to help discriminate the pore size distribution and particle sieving of sterile filters.

Alternatively, the pore size and structure of sterile filtration membranes could be elucidated through the use of advanced imaging techniques. Scanning electron microscopy coupled with focused ion beam milling (FIB SEM) allows for a stack of 2D images through the entire depth of the membrane to be acquired, from which an accurate reconstruction the complete 3D structure can be obtained[25,26]. This technique has been applied to ultrafiltration membranes, and has been used to determine the inner pore size and pore distribution, providing novel insights such as the prevalence of dead end pores and quantifying the number of pore sub-structures such as mouths and throats[26]. This detailed information of the membrane structure can then be further applied to better understand particle transmission through applied filtration tests or simulations[27]. To date, this has not been applied to sterile filtration membranes, and could be a powerful tool in characterizing the range of available membranes and understanding their relative capability to achieve high recovery of virus.

7.3. References

1. Meltzer TH, Jornitz MW. The Sterilizing Filter and Its Pore Size Rating. *Am Pharm Rev*. 2003;6:6.

2. Lalia BS, Kochkodan V, Hashaikeh R, Hilal N. A review on membrane fabrication: Structure, properties and performance relationship. *Desalination*. 2013;326:77-95. doi:10.1016/j.desal.2013.06.016

3. Helling A, Grote C, Büning D, et al. Influence of flow alterations on bacteria retention during microfiltration. *J Membr Sci*. 2019;575:147-159. doi:10.1016/j.memsci.2019.01.021

4. Zhang X, Brodus D, Hollimon V, Hu H. A brief review of recent developments in the designs that prevent bio-fouling on silicon and silicon-based materials. *Chem Cent J*. 2017;11(1):18. doi:10.1186/s13065-017-0246-8

5. van Reis R, Zydney A. Bioprocess membrane technology. *J Membr Sci*. 2007;297(1):16-50. doi:10.1016/j.memsci.2007.02.045

6. Kornecki M, Mestmäcker F, Zobel-Roos S, Heikaus de Figueiredo L, Schlüter H, Strube J. Host Cell Proteins in Biologics Manufacturing: The Good, the Bad, and the Ugly. *Antibodies*. 2017;6(3):13. doi:10.3390/antib6030013

7. Bracewell DG, Smith V, Delahaye M, Smales CM. Analytics of host cell proteins (HCPs): lessons from biopharmaceutical mAb analysis for Gene therapy products. *Curr Opin Biotechnol*. 2021;71:98-104. doi:10.1016/j.copbio.2021.06.026

8. Bracewell DG, Francis R, Smales CM. The future of host cell protein (HCP) identification during process development and manufacturing linked to a risk-based management for their control. *Biotechnol Bioeng*. 2015;112(9):1727-1737. doi:10.1002/bit.25628

9. Doneanu C, Xenopoulos A, Fadgen K, et al. Analysis of host-cell proteins in biotherapeutic proteins by comprehensive online two-dimensional liquid chromatography/mass spectrometry. *mAbs*. 2012;4(1):24-44. doi:10.4161/mabs.4.1.18748

10. Mittelman MW, Jornitz MW, Meltzer TH. Bacterial cell size and surface charge characteristics relevant to filter validation studies. *PDA J Pharm Sci Technol*. 1998;52(1):37-42.

11. Bao J, Li H, Xu Y, et al. Multi-functional polyethersulfone nanofibrous membranes with ultra-high adsorption capacity and ultra-fast removal rates for dyes and bacteria. *J Mater Sci Technol*. 2021;78:131-143. doi:10.1016/j.jmst.2020.10.065

12. Orooji Y, Faghih M, Razmjou A, et al. Nanostructured mesoporous carbon polyethersulfone composite ultrafiltration membrane with significantly low protein adsorption and bacterial adhesion. *Carbon*. 2017;111:689-704. doi:10.1016/j.carbon.2016.10.055

13. Wang C, Yang F, Zhang H. Fabrication of non-woven composite membrane by chitosan coating for resisting the adsorption of proteins and the adhesion of bacteria. *Sep Purif Technol*. 2010;75(3):358-365. doi:10.1016/j.seppur.2010.09.005

14. Papaphilippou PC, Vyrides I, Mpekris F, Stylianopoulos T, Papatryfonos CA, Theocharis CR, Krasia-Christoforou T. Evaluation of novel, cationic electrospun microfibrous membranes as adsorbents in bacteria removal. *RSC advances*. 2015;5(83):67617-29.

15. Lupascu L, Petuhov O, Timbaliuc N, Lupascu T. Study of the Adsorption of Bacillus subtilis and Bacillus cereus Bacteria on Enterosorbent Obtained from Apricot Kernels. *C*. 2022;8(3):38.

16. Oh JK, Yegin Y, Yang F, et al. The influence of surface chemistry on the kinetics and thermodynamics of bacterial adhesion. *Sci Rep*. 2018;8(1):17247. doi:10.1038/s41598-018-35343-1

17. Treter J, Bonatto F, Krug C, Soares GV, Baumvol IJR, Macedo AJ. Washing-resistant surfactant coated surface is able to inhibit pathogenic bacteria adhesion. *Appl Surf Sci*. 2014;303:147-154. doi:10.1016/j.apsusc.2014.02.123

18. Borkowski A, Szala M, Cłapa T. Adsorption Studies of the Gram-Negative Bacteria onto Nanostructured Silicon Carbide. *Appl Biochem Biotechnol*. 2015;175(3):1448-1459. doi:10.1007/s12010-014-1374-4

19. Schideman LC, Mariñas BJ, Snoeyink VL, Qi S, Campos C. Three-Component Adsorption Modeling to Evaluate and Improve Integrated Sorption−Membrane Processes. *Environ Sci Technol*. 2007;41(18):6547-6553. doi:10.1021/es070410o

20. Shoaebargh S, Gough I, Fe Medina M, et al. Sterile filtration of oncolytic viruses: An analysis of effects of membrane morphology on fouling and product recovery. *J Membr Sci*. 2018;548:239-246. doi:10.1016/j.memsci.2017.11.022

21. Taylor N, Ma W, Kristopeit A, Wang S, Zydney AL. Evaluation of a sterile filtration process for viral vaccines using a model nanoparticle suspension. *Biotechnol Bioeng*. 2021;118(1):106-115. doi:10.1002/bit.27554

22. Bakhshayeshi M, Kanani DM, Mehta A, et al. Dextran sieving test for characterization of virus filtration membranes. *J Membr Sci*. 2011;379(1):239-248. doi:10.1016/j.memsci.2011.05.067

23. Pazouki M, Noelle Wilton A, Latulippe DR. An experimental study on sterile filtration of fluorescently labeled nanoparticles – the importance of surfactant concentration. *Sep Purif Technol*. 2019;218:217-226. doi:10.1016/j.seppur.2019.02.038

24. Homaeigohar S, Kabir R, Elbahri M. Size-Tailored Physicochemical Properties of Monodisperse Polystyrene Nanoparticles and the Nanocomposites Made Thereof. *Sci Rep*. 2020;10:5191. doi:10.1038/s41598-020-62095-8

25. Roberge H, Moreau P, Couallier E, Abellan P. Determination of the key structural factors affecting permeability and selectivity of PAN and PES polymeric filtration membranes using 3D FIB/SEM. *J Membr Sci*. 2022;653:120530. doi:10.1016/j.memsci.2022.120530

26. Brickey KP, Zydney AL, Gomez ED. FIB-SEM tomography reveals the nanoscale 3D morphology of virus removal filters. *J Membr Sci*. 2021;640:119766. doi:10.1016/j.memsci.2021.119766

27. Sorci M, Woodcock CC, Andersen DJ, et al. "Linking microstructure of membranes and performance." *J Membr Sci*. 2020;594:117419. doi:10.1016/j.memsci.2019.117419